Reconstructions of Late Holocene storminess in Europe and the role of the North Atlantic Oscillation

Submitted by Lisa Claire Orme to the University of Exeter

as a thesis for the degree of

Doctor of Philosophy in Geography

In August 2014

I certify that all material in this thesis which is not my own work has been identified and that no material has previously been submitted and approved for the award of a degree by this or any other University.

Signature: ……..

Abstract

Winter storms can have devastating social and economic impacts in Europe. The severity of storms and the region they influence (southern or northern Europe) is related to the index of the North Atlantic Oscillation (NAO). However recent findings indicate that over the last millennium the relationship between the NAO and storminess varied and the forcings over centennial timescales are debated. Therefore in this research storminess has been reconstructed from NAO-sensitive regions of southern Europe (Galicia, Spain) and northern Europe (Outer Hebrides, Scotland), to investigate the Late Holocene NAO-storminess relationship and the causes of observed variability. Reconstructions were based on measurements of aeolian sand deposits within ombrotrophic peat bogs and a lake sedimentary archive from the Hebrides.

The elemental composition of the lake sediments were analysed (using ITRAX XRF core scanning) to identify aeolian/in-washed sediment resulting from storms, as confirmed by correlations with instrumental data. As this is a relatively new technique there was a methodological focus on assessing its applicability for storm reconstructions and the maximum resolution achievable. It is concluded the reconstruction had a 10-year resolution (equivalent to 2-5 mm sampling resolution).

The peat bog reconstructions span 4000 cal yr BP to present and indicate that there was a Late Holocene northward storm track shift. The results suggest that storminess was high in Galicia between 4000-1800 cal yr BP, after which it decreased and then gradually increased in the Outer Hebrides after 1500 cal yr BP. Comparison with an NAO reconstruction supports a consistent NAO-storm relationship through the Late Holocene. Orbital forcing is suggested as causing a steepening of the latitudinal temperature gradient and increasingly zonal circulation. Superimposed on this trend are centennial variations, which spectral analysis and visual comparisons suggest are primarily the result of solar minima (suggested as causing a weakened latitudinal temperature gradient and meridional circulation patterns), with some additional forcing from volcanic and oceanic changes. Therefore there has been a consistent storm-NAO relationship through the Late Holocene; however there appear to have been millennial and centennial shifts as the result of hemispheric circulation reorganisations.

Contents

Chapter 1: Introduction and Literature Review 12

1.1. Introduction 12

1.2. Storminess and the NAO: instrumental 15

1.2.1. Formation of low pressure systems 15

1.2.2. Meteorology of the North Atlantic Oscillation 18

1.2.3. Causes of NAO and storminess variability 22

1.2.4. Importance of understanding storminess and the NAO 24

1.2.5. Storminess and the NAO: instrumental period 29

1.3. Methodologies of reconstructing storminess and the NAO 34

1.3.1. Storminess reconstruction methods 34

1.3.2. Methods of reconstructing the NAO 36

1.4. Late Holocene climate changes: storminess and the NAO 39

1.4.4. Late Holocene storminess 40

1.4.2. Late Holocene: atmospheric and oceanic circulation 44

1.4.3. Medieval Climate Anomaly 47

1.4.4. Little Ice Age storminess 49

1.4.5. Little Ice Age: atmospheric and oceanic circulation 51

1.4.6. Cyclicity in NAO and storminess reconstructions 53

1.5. Chapter summary 57

Chapter 2: Research design 58

2.1. Introduction 58

2.2. Research Question 1: 59

2.3. Research Question 2: 60

2.4. Research Question 3: 60

2.5. Research Question 4: 63

2.6. Site selection justification 64

2.7. Methodological justification: 68

2.7.1. Peat bogs 69

2.7.2. Lakes 73

2.8. Methods and precision analysis 77

2.8.1. Sand analyses 77

2.8.2. Precision analysis of sand measurements 79

2.8.3. Spectral analysis 81

Chapter 3: Investigating the potential for climate reconstructions using ITRAX XRF analysis: A storminess reconstruction from the Outer Hebrides 83

3.1. Introduction 83
3.2. Study area 86
3.3. Methods 92
3.3.1. Catchment element analysis 92
3.3.2. Sampling 92
3.3.3. Element Analysis 92
3.3.3. Proxy data analysis 94
3.3.4. Chronology 95
3.3.5. Instrumental data comparison 97
3.3.6. Spectral analysis 98
3.4. Results 98
3.5. Comparison with instrumental and proxy climate records 106
3.6. Interpretation 109
3.7. Spectral Analysis 110
3.8. Methodological assessment 114
3.9. Conclusion 116
Chapter 4: Late Holocene storminess in Northwest Scotland - Two peat reconstructions from the Outer Hebrides 118
4.1. Introduction 118
4.2. Study Area 121
4.2.1. General overview 121
4.2.2. Struban Bog 123
4.2.3. Hill Top Bog 125
4.3. Methods 127
4.4. Results 129
4.4.1. Struban Bog results 129
4.4.2. Hill Top Bog results 135
4.4.3. Spectral Analysis 141
4.5. Discussion 144
4.5.1. Intra-bog sand content comparison 144
4.5.2. Inter-bog sand content comparison 145
4.5.3. Comparison with regional Late Holocene climate 148
4.5.4. Storm-NAO relationship 153
4.5.5. Cyclicity 155
4.6. Conclusion 157
Chapter 5: Late Holocene Storminess in Northwest Spain - A Reconstruction from Pedrido Bog, Galicia 158
5.1. Introduction 158

5.2. Study area 161
5.3. Methodology 165
5.4. Results 167
5.5. Discussion 175
5.5.1. Vegetation influence 175
5.5.2. Sand deposition: single or multiple storm events 178
5.5.3. Storminess, the NAO and sand deposition 179
5.5.4. Comparison with Late Holocene Galician Climate 182
5.5.5. Cycles in the Pedrido Record 188
5.6. Conclusion 190
Chapter 6: The patterns and causes of European storminess during the Late Holocene 191
6.1. Introduction 191
6.2. Comparison of the storminess reconstructions 191
6.3. Comparison with storm track reconstructions 195
6.4. Comparison with North Atlantic Oscillation reconstructions 202
6.5. Potential causes of variability in storminess, the storm track and the NAO . 209
6.5.1. Orbital forcing 209
6.5.2. Solar activity 211
6.5.3. Oceanic forcing 218
6.5.4. Volcanic forcing 225
6.5.5. Integration of forcings 227
6.6. Future predictions of storminess 233
6.6.1. Model comparison 233
6.6.2. Future storminess and climate change 236
6.7. Limitations and future research 239
6.8. Chapter summary 240
Chapter 7: Conclusion 242

List of Figures

1.1.	Schematic diagram of the global circulation patterns.	16
1.2.	Schematic diagram of the boundary between the subpolar and subtropical airmasses.	16
1.3.	Ekmans spiral.	18
1.4.	Cluster analysis of the North Atlantic daily pressure data, Winters 1950-2010.	20
1.5.	Pressure anomalies of the extreme negative NAO Winter 2009-2010.	21
1.6.	Schematic illustration of the oceanic and atmospheric circulation patterns related to the NAO.	21
1.7.	Projected future increase in the number of extratropical storms.	28
1.8.	Trends in the geostrophic winds over the North Sea and British Isles for the period 1881–1998.	30
1.9.	Updated instrumental NAO record, 1824-2010.	30
1.10.	Number of cyclones per winter during the period 1958-2000 for winters with positive and negative NAO.	32
1.11.	Proxy NAO reconstruction by Trouet *et al.,* (2009).	37
1.12.	Reconstruction of the mid- to late- Holocene NAO by Olsen *et al.,* (2012).	37
1.13.	Compilation of identified periods of storminess in Europe.	40
1.14.	Summary of ocean circulation proxies.	43
1.15.	Patterns of atmospheric and oceanic circulation in relation to storm intensity and tracks.	44
1.16.	Wavelet spectral analysis of storminess reconstructions.	56
2.1.	Illustration of the NAO pressure centres and the NAO influence on cyclone frequency.	62
2.2.	Map of the location of the study sites in the southern Outer Hebrides	67
2.3.	Map of the location of Pedrido Bog, in Galicia, northwest Spain.	68
2.4.	Graph showing of the influence of wind speed and vegetation cover on sand transport.	72

2.5.	Benthic invertebrate structure in an oligotrophic lake.	75
2.6.	Erosion-transportation-accummulation diagram for Lake Vanern, Sweden.	77
2.7.	Precision analysis measurements of the ignition residue results.	79
2.8.	Precision analysis measurements of the 120-180 μm fraction weight results.	80
2.9.	Precision analysis measurements of the >180 μm fraction weight results.	81
3.1.	Map of Loch Hosta (main) and the sites relation to the NAO pressure centres (inset).	87
3.2.	Box plots of temperature, precipitation and atmospheric pressure at Stornoway, 1873-2012.	88
3.3.	Photo of machair ecosystem lining Loch Hosta.	90
3.4.	Photos of Loch Hosta.	91
3.5.	Age-depth models of Hosta 1 and Hosta 2 cores (left) and plot of sand weight results (right).	100
3.6.	Major elements (%) in the Loch Hosta catchment soil and sand.	102
3.7.	Hosta 1 and Hosta 2 sediment analysis results and ITRAX XRF results.	103
3.8.	Projected numbers of grains in carbonate measurements with changes in grainsize.	105
3.9.	Comparison between Ln(Ca/K) and climate indices.	107
3.10.	Spectral analysis results.	113
4.1.	Summary map of the NAO and the location of the Outer Hebrides (left) and study site locations (right).	123
4.2.	Map of Struban Bog.	124
4.3.	Photo of Struban Bog.	124
4.4.	Satellite image of Struban Bog.	125
4.5.	Map of Hill Top Bog.	125
4.6.	Photos of Hill Top Bog.	126
4.7.	Satellite image of Hill Top Bog showing peat cutting	127
4.8.	Struban Bog raw results and age-depth model.	131
4.9.	Struban Bog results.	133

4.10.	Struban Bog transect results.	135
4.11.	Hill Top Bog raw results and age-depth model.	136
4.12.	Hill Top Bog results.	139
4.13.	Hill Top Bog transect results.	141
4.14.	Lomb-Scargle spectral analysis of Hill Top Bog ignition residue results.	142
4.15.	Wavelet power spectrum analysis of Hill Top Bog ignition residue results.	142
4.16.	Lomb-Scargle spectral analysis of Struban Bog ignition residue results.	143
4.17.	Wavelet power spectrum analysis of Struban Bog ignition residue results.	143
4.18.	Smoothed sand fraction weight results of Hill Top Bog and Struban Bog with marked dating errors.	148
4.19.	Comparison of storminess results with regional storm and precipitation reconstructions.	152
4.20.	Comparison between NAO (Trouet *et al.,* 2009) and storminess reconstructions.	154
4.21.	Comparison between NAO (Olsen *et al*., 2012) and storminess reconstructions.	155
5.1.	Summary diagram of reconstructed climate changes in Spain.	160
5.2.	Location of Pedrido Bog, Galicia.	161
5.3.	Site map of Pedrido Bog.	162
5.4.	Plots of monthly temperature, precipitation and windspeed (1971–2000).	164
5.5.	Age-depth model.	169
5.6.	Results and age-model of Pedrido Bog.	171
5.7.	Lomb-Scargle method spectral analysis of 120-180 μm sand content of Pedrido Bog.	172
5.8.	Wavelet power spectrum analysis of 120-180 μm sand content of Pedrido Bog.	173
5.9.	Comparison between sand, pollen and charcoal results.	174
5.10.	Comparison between NAO (Trouet et al., 2009) and storminess reconstruction.	181

5.11. Comparison between NAO (Olsen et al., 2012) and storminess reconstructions. 182
5.12. Summary diagram of reconstructed climate changes in Spain. 187
6.1. Comparison between storminess reconstructions from northern and southern Europe. 192
6.2. North-South index of European storminess. 194
6.3. Spectral analysis of the north-south index. 194
6.4. Location map of key storminess reconstructions. 199
6.5. Comparison between reconstructions of storminess and storm track position. 200
6.6. Comparison between NAO reconstruction and peat bog storminess reconstructions. 204
6.7. Cross-spectral analysis between the NAO and storminess 207
6.8. Late Holocene winter insolation receipt at different latitudes and seasonal insolation pattern. 211
6.9. Comparison between storminess reconstructions, Total Solar Irradiance and north-south storm index. 214
6.10. Comparison between Loch Hosta Ln(Ca/K) storminess reconstruction and Total Solar Irradiance. 215
6.11. Cross-spectral analysis between storminess and Total Solar Irradiance 217
6.12. Cross-spectral analysis between the NAO and Total Solar Irradiance 218
6.13. Comparison between ocean circulation and storminess reconstructions. 220
6.14. Cross-spectral analysis between storminess and ice-rafting debris reconstructions. 222
6.15. Cross-spectral analysis between NAO and ice-rafting debris reconstructions. 223
6.16. Comparison between Loch Hosta storminess and Atlantic Multidecadal Oscillation reconstructions. 225
6.17. Comparison between Loch Hosta storminess reconstructions and a volcanic proxy reconstruction (based on stratospheric aerosol optical depth). 226

6.18. Comparison between peat bog storminess reconstructions and a volcanic proxy reconstruction (based on GISP2 sulphate measurements). 227
6.19. Comparison between storminess reconstructions, the north-south storm index and reconstructions of ice-rafting, TSI, Greenland temperatures and 60ºN insolation receipt. 232
6.20. Comparison of the Pedrido Bog storminess reconstruction and modelled wind speed. 235
6.21. Comparison of the Hill Top Bog and Struban Bog storminess reconstructions and modelled wind speed. 235
6.22. Comparison of the Loch Hosta storminess reconstruction and modelled precipitation. 236

List of Tables

1.1. Summary of NAO cycles..... 54
3.1. ^{210}Pb and radiocarbon dating results..... 99
4.1. Radiocarbon dating results from Struban Bog..... 132
4.2. Radiocarbon dating results from Hill Top Bog..... 137
5.1. ^{210}Pb dates from Pedrido Bog..... 167
5.2. Radiocarbon dates and calibrated ages from Pedrido Bog. 168
6.1. Correlations between NAO and storminess reconstructions 203
6.2. Summary of cycles in storminess reconstructions, the NAO and solar/oceanic reconstructions..... 208

Acknowledgments

I would firstly like to sincerely thank my supervisors Dr Liam Reinhardt, Dr Richard Jones, Professor Dan Charman, Dr Andy Barkwith and Dr Michael Ellis for their advice and support throughtout my PhD. I have been lucky to have had supervisors that are each generous with their time and with a range of expertise. I would particularly like to thank Liam, Richard and Dan for their day-to-day support.

The research would not have been possible without the kind donation of the Pedrido Bog core, which was sampled as part of the EU FP5 ACCROTELM project; so many thanks are due to Professor Fraser Mitchell and Dr Bettina Stefanini. Thanks also to Professor Ian Croudace for advice and assistance with the ITRAX element analysis.

Thanks to the academic and research staff in the Geography department at the University of Exeter, including Dr Tim Barrows for advice on sedimentary element analysis and assistance with ^{210}Pb dating and the Environmental Change research group for helpful feedback and cake. I would also like to thank the research technicians for their help and friendliness. Particularly Sue Franklin, Angela Elliot, Neville England and Jim Grapes for kindly giving laboratory advice and assistance as well as Mandy Lee for sharing her sinks and making sieving enjoyable!

My fieldwork in the Outer Hebrides would not have been possible without a number of people. Thank you to my supervisors Liam and Richard, as well as Rachel Smedley, Hannah Bailey and Rose Ferraby for being amazing coring partners. Many thanks to Dr Fraser Sturt, Dr Duncan Garrow and the other archaeologists who welcomed me onto their field season, assisted me with coring and transported my cores. Finally thank you to Dr Rebecca Rennell and Dr Kate MacDonald for their generosity and assistance in collecting sediment samples from Loch Hosta.

Finally I would like to thank my friends and family for their support during the last four years. Those in my office have been a constant source of encouragement, advice and entertainment, in particular Zoë Thomas, Rose Ferraby and Mark Grosvenor. Finally I would like to thank my family and especially my mum Claire Orme for always listening and caring.

Chapter 1: Introduction and Literature Review

1.1. Introduction

Late Holocene storminess is investigated in this study using reconstructions from sites in northern and southern Europe. Storminess is a word that encompasses both the *intensity* and *frequency* of storms in a given period. In palaeoclimatic research this is a necessary term because it is often difficult to separate the environmental signatures of multiple storms of medium magnitude from fewer high magnitude storms. Here storminess reconstructions are made for regions under the influence of an important atmospheric circulation pattern, the North Atlantic Oscillation (NAO), in order to improve our understanding of the temporal relationship between the NAO, storminess and storm track positions. Therefore the research has two main **aims**:

1) To create and compare Late Holocene storminess reconstructions from northern and southern Europe

2) To assess the causes of storminess variability during the Late Holocene, in particular the role of the North Atlantic Oscillation

To help achieve these aims four **research questions** have been determined:

1) What are the temporal patterns of storminess during the Late Holocene in northern and southern Europe?

2) Do the storminess reconstructions from northern and southern Europe show storm track changes or widespread, synchronous storminess variations?

3) What do the patterns of storminess and inferred storm track changes tell us about the storm-NAO relationship?

4) What do the results tell us about the causes of storminess variability?

These research questions will be further outlined and justified in the Research Design chapter (Chapter 2). The outline of this thesis is described below:

Chapter 1: Introduction and literature review. This chapter will include a summary of the atmospheric circulation systems with a focus on storm development and the NAO. Following this is a literature review of the current understanding of storminess and the NAO during the instrumental period, the methods of reconstructing storminess from the pre-instrumental period and a summary of current understanding of the NAO and storminess during the Late Holocene.

Chapter 2: Research design. The aims and research questions of this research are outlined. The selected study sites of Galicia and the Outer Hebrides are justified. The chosen methodologies are explained, with consideration of issues relating to peat bog and lake environments. Finally the precision of the method used to measure sand content in the peat bogs and lake is assessed.

Chapters 3 to 5 are results chapters, which are structured in the form of papers. These therefore each include literature review, methods, study area, results, discussion and conclusion sections. These chapters are focussed on the research carried out at the site(s) in question, with a regional focus for the literature review and discussion, as well as consideration of methodological limitations. The discussion chapter (Chapter 6) links the findings of the sites and discusses these within the broader European-wide storminess and NAO literature.

Chapter 3: Investigating the potential for climate reconstructions using ITRAX XRF analysis: A storminess reconstruction from the Outer Hebrides. The results from Loch Hosta in the Outer Hebrides are presented. This chapter investigates the potential for ITRAX XRF core-scanning analysis of elements as a method of reconstructing storminess. This is assessed by comparison of the ITRAX data with core sediment analyses and comparison with instrumental climate data. The ITRAX method has the potential to provide very high (annual-to-decadal) resolution reconstructions, so using spectral analysis and comparison with instrumental data the optimum resolution of the ITRAX method in Loch Hosta is assessed.

Chapter 4: Late Holocene storminess in Northwest Scotland: Two peat reconstructions from the Outer Hebrides. The results of two storminess reconstructions from peat bogs in the Outer Hebrides are presented in this chapter. The issues of intra- and inter- bog variation are investigated through comparisons between transects of cores on each bog. The storminess reconstructions are then compared with others from Scotland and northern Ireland. The results are compared with regional storminess and NAO reconstructions and the cycles are analysed.

Chapter 5: Late Holocene storminess in Northwest Spain: A reconstruction from Pedrido Bog, Galicia. A reconstruction of storminess from a Spanish peat bog (Pedrido Bog) is presented in this chapter. The results are compared with previously measured pollen analysis to assess the influence of vegetation change on the sand influx. The results are compared with the NAO reconstructions and the cyclical changes are analysed.

The storminess reconstructions are compared and discussed in Chapter 6:

Chapter 6: The patterns and causes of European storminess during the Late Holocene. The results from the four sites are compared and synthesised into a north-south storm index. The results are compared with reconstructions of storm track changes and storminess from Europe and the NAO-storm relationship is discussed. Following this the causes of storminess variability are considered. Finally the implications of the findings for future climate changes are outlined.

Chapter 7: Conclusions. In this chapter the conclusions in relation to the aims and research questions are summarised.

1.2. Storminess and the NAO: instrumental

1.2.1. Formation of low pressure systems

Clear explanations of how low pressure systems and storms are formed have been given by Bjerknes and Solberg (1922) and Lamb (1995), and more recently by Aguado and Burt (2013), and these are summarised here. The atmospheric circulation (illustrated in Figure 1.1) is driven by the imbalance of solar radiation between high and low latitudes: thermal gradients drive the circulation of the Hadley Cell in the low latitudes and the Polar Cell in the high latitudes. Between the Hadley and Polar Cells lies the Ferrell Cell, which influences the climate of the mid-latitudes. The circulation of the Hadley Cell creates subtropical high pressures, for example the Azores High pressure, while the Polar Cell creates sub-polar low pressures, for example the Icelandic Low.

Above the boundary layer the pressure gradient between the high and low pressures draws air away from the equator, while the Earth's rotation pushes the air towards the east (the Coriolis Effect), resulting in westerly airflow in the mid-latitudes of the northern hemisphere. The polar high pressure is caused by cooling, increasingly dense air that sinks thus increasing the surface air pressure, however the descending isobaric levels result in low pressure forming above the 500 hPa level and up to 20 km high in the atmosphere, which is called the circumpolar vortex (Girs, 1974; Veretenenko and Ogurtsov, 2012). The pressure and temperature differences associated with this boundary are illustrated in Figure 1.2. The circumpolar vortex of each hemisphere are manifested as meandering bands of air moving from west to east over the mid-latitudes. If the temperature difference between the mid- and high- latitudes is strong (weak) there are high (low) zonal wind velocities and longer (shorter) wavelengths of the circumpolar vortex (Barry and Chorley. 2010; Lamb, 1995). This has implications for the locations of storm tracks and the NAO, as shown by studies of the circumpolar vortex and weather using reanalysis data (Walter and Graf, 2005; Graf and Walter, 2005; Baldwin and Dunkerton, 2001).

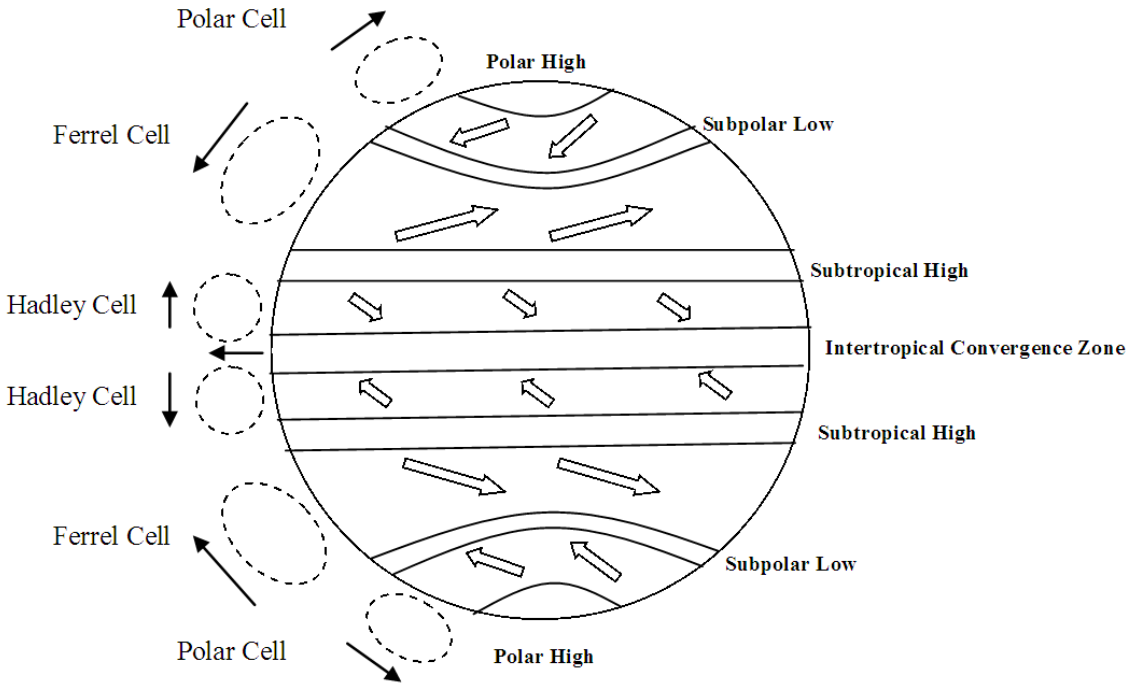

Figure 1.1: Schematic diagram of the global circulation patterns (adapted from Aguado and Burt, 2013, Pg 217)

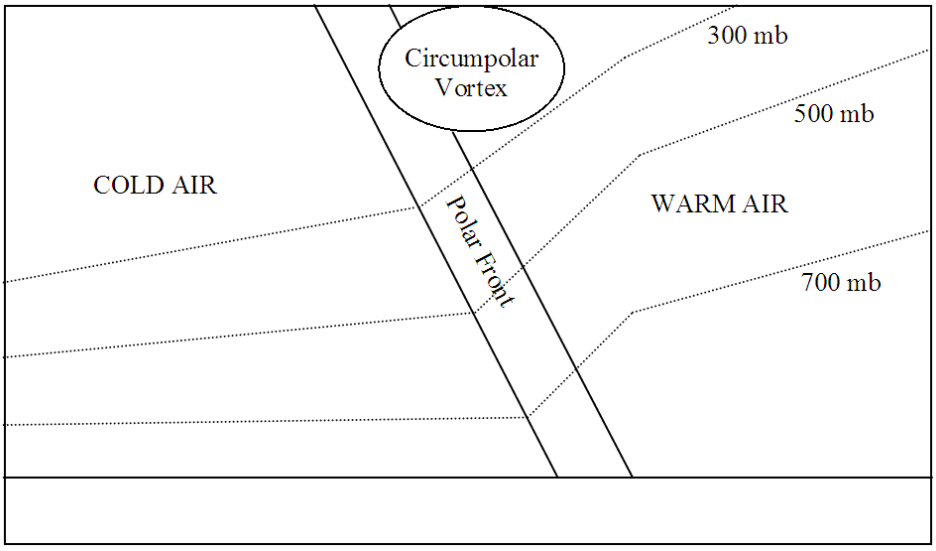

Figure 1.2: Schematic diagram of the boundary between the subpolar and subtropical air masses. Cold air associated with the subpolar low pressures and warm air is associated with the subtropical high pressures. Adapted from Aguado and Burt (2013, pg 225).

Where the circumpolar vortex has pressure imbalances or changes direction air can converge or diverge, leading to the formation of high and low pressure systems. The formation and development of low pressure systems, or storms, is termed cyclogenesis. Generally high pressure systems form on the equator-side of the vortex and low pressures on the polar-side. When warm and cold air collide in a depression (also referred to as an extratropical cyclone, low pressure system or storm), the warm air is forced upwards creating a warm front on the leading side and a cold front behind, and on these fronts precipitation forms. Within depressions the winds circulate in an anti-clockwise direction, with the wind strength varying with the steepness of the pressure gradient.

Storms are usually steered along by the westerly movement of the circumpolar vortex above, however within the boundary layer the circulation is much more variable, so winds can occur from all directions in the mid-latitudes. The higher frictional drag from the earth's surface causes the westerly winds to slow down, so that pressure differences tend to exert more of a control on wind direction than the Coriolis Effect, as described by *Ekmans Spiral* (Ekman, 1905, Figure 1.3). European climate is therefore highly variable as a result of the depth and location of pressure centres around Eurasia and the North Atlantic, which are connected with the strength and position of the circumpolar vortex. These pressure patterns control the direction and strength of airflow across Europe so have an influence on spatial and temporal patterns of temperature, precipitation and storminess.

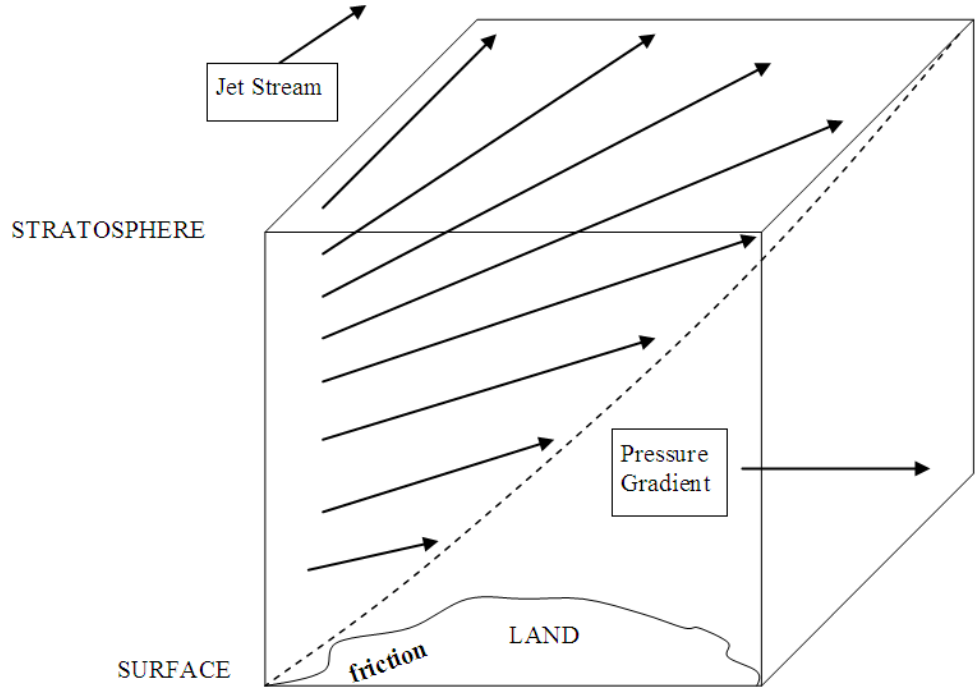

Figure 1.3: Ekmans Spiral. Adapted (for atmosphere) from Aquado and Burt (2013, pg 231).

1.2.2. Meteorology of the North Atlantic Oscillation

The high and low pressures associated with global circulation occupy characteristic positions, for example the Azores High in the Tropical Atlantic and the Icelandic Low in the Atlantic Arctic (Figure 1.4). The pressure difference between these is captured by the NAO index, which is the most frequently occurring North Atlantic weather circulation pattern and exerts a strong influence on wind speeds, temperature and precipitation across the North Atlantic and surrounding continents (Hurrell and Deser, 2010; Trigo *et al*., 2002; Walker and Bliss, 1932; Hurrell, 1995; O'Hare *et al*., 2005; Van Loon and Rogers, 1978). The NAO is scaled using an 'anomaly' index, which in terms of climate variability refers to the difference between the instantaneous NAO state and that of the mean state over a long period (Hurrell *et al.*, 2003). The NAO pressure characteristics control the strength of the westerly airflow, the position of the tropospheric jet stream and therefore the pathway of extratropical cyclones crossing the Atlantic (Hurrell *et al.*, 2003; Serreze *et al.*, 1997; Trigo *et al.*, 2002).

When the circumpolar vortex is strong and contracted a positive NAO index is caused (Angell, 2006; Baldwin and Dunkerton, 2001). A deeper Icelandic Low pressure and higher Azores High pressure create a steep pressure gradient, causing stronger westerly airflow across northern Europe (Hurrell 1995, Hurrell *et al.,* 2003). The stronger westerly airflow between the NAO pressure centres prevents the jet stream from meandering and leads to a high frequency of moderate intensity storms to cross Europe (Figure 1.6; Van Vliet-Lanoë *et al*., 2014). Precipitation, storminess and temperatures across north-west Europe are increased, while storminess and precipitation are decreased in southern Europe and parts of the Middle East and North Africa (Alexander *et al.*, 2005; Alexandersson *et al.*, 1998; Hurrell, 1995, 1996; Hurrell *et al.*, 2003; Hurrell and VanLoon, 1997; Pinto *et al.*, 2009; Visbeck *et al.*, 2001).

When the circumpolar vortex is weak and meandering the NAO is negative (Angell, 2006; Baldwin and Dunkerton, 2001). These situations have a smaller pressure difference between the Icelandic Low and Azores High (Figure 1.4), and during extreme negative anomalies there is a pressure reversal, as shown in Figure 1.5 (D'Arrigo *et al.*, 1993). As the jet stream is able to meander more when the pressure difference is weak, this can result in the storm track crossing southern Europe (Figure 1.6; Van Vliet-Lanoë *et al*., 2014). During negative NAO's, storminess and precipitation across areas of southern Europe are increased, with decreases across northwest Europe (Andrade *et al.* 2008; Serreze *et al.*, 1997; Trigo *et al.*, 2002). Although as the pressure gradient is reduced during negative NAO winters, there are weaker westerlies (O'Hare *et al.*, 2005; Serreze *et al.*, 1997). Across northern Europe the reduced zonal (westerly) airflow allows cold air to move southwards or eastwards, so the weather is calm, cold and dry (Trigo *et al.*, 2002).

Although the NAO is the most dominant pressure pattern of the North Atlantic in winter, occuring approximately 47% of the time, there are other pressure patterns that can occur (Figure 1.4; Hurrell and Deser, 2010). A blocking regime, also termed the Scandinavian Blocking regime, occurs 29% of the time and has a high pressure situated over mainland Europe causing easterly winds and cold, dry conditions (Michelangeli *et al*., 1995; Hurrell and Deser, 2010; Yiou and Nogai, 2004; Figure 1.4.). The Atlantic Ridge regime, otherwise called the East Atlantic Pattern, has two dipoles (one over Western

Europe and the other over North Africa and the Mediterranean) and can influence precipitation patterns over Southern Europe (Barnston and Livezey, 1987; Michelangeli *et al*., 1995; Hurrell and Deser, 2010; Krichak and Alpert, 2005). Therefore in addition to the NAO, storminess in Europe can be influenced by the Scandinavian Blocking regime (causing lower storminess) and the East Atlantic Pattern.

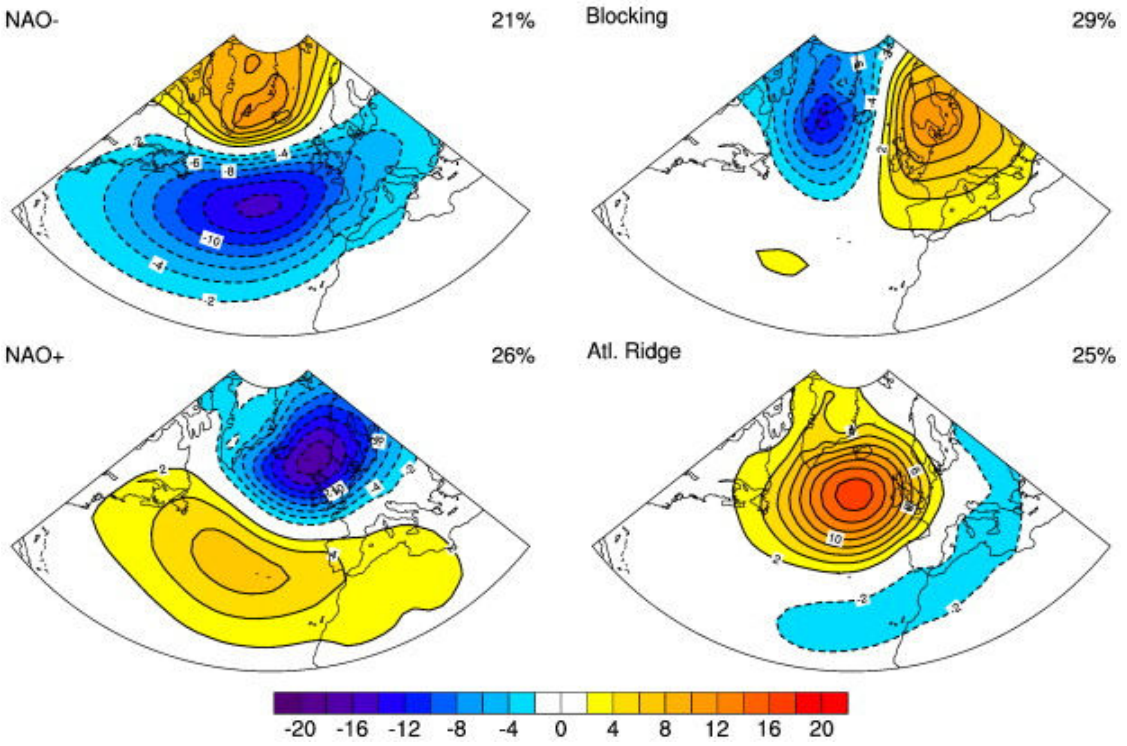

Figure 1.4: Clustering analysis of North Atlantic daily pressure data (hPa) for winters (Dec-March) for the period 1950-2010. Shows (anticlockwise from top left) the negative NAO, positive NAO, Atlantic Ridge regime (also termed the East Atlantic Pattern) and the Blocking regime (also termed the Scandinavian Blocking regime). Numbers refer to the percentage of time these regimes were dominant (Hurrell and Deser, 2010, pg 238)

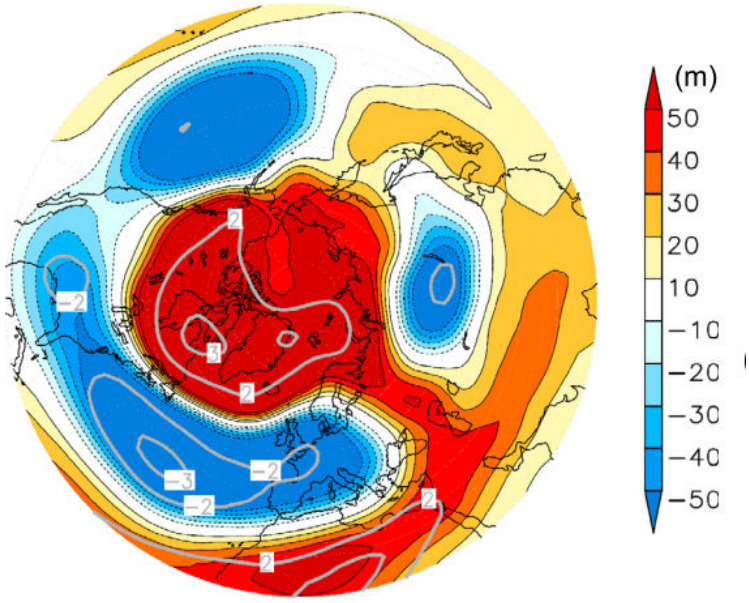

Figure 1.5: Pressure anomalies of the extreme negative NAO Winter 2009-2010, with high pressure over Arctic and low pressure over the Azores (Cattiaux *et al.*, 2010, pg L20704/2). This was made using averaged 500 mb geopotential height data. Grey contours are standard deviation levels.

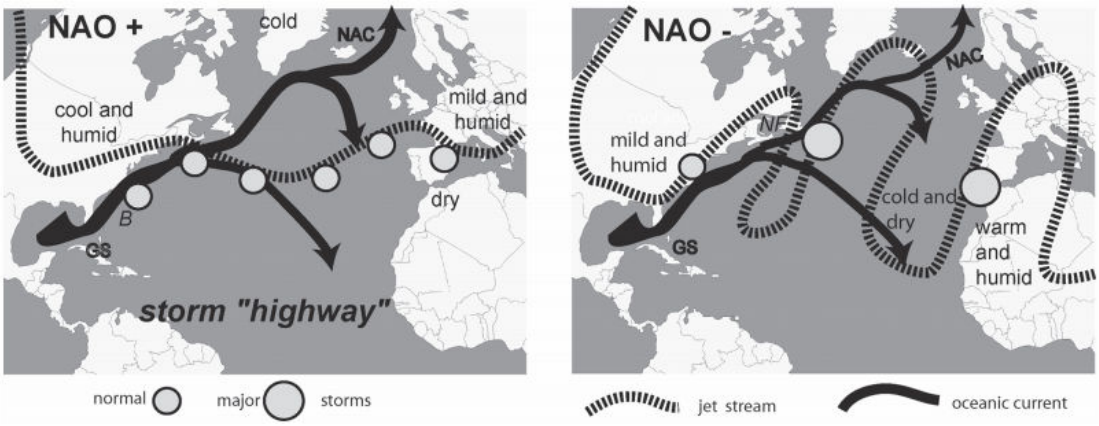

Figure 1.6: Schematic illustration of the oceanic and atmospheric circulation patterns related to the NAO, including the jet stream position, North Atlantic Current (NAC) position, Gulf Stream (GS) strength and storm frequency and size (Van Vliet-Lanoë *et al.*, 2014, pg 442)

1.2.3. Causes of NAO and storminess variability

The NAO during the instrumental period (since c.1820 A.D.) has varied temporally at a number of timescales, which will be outlined in section 1.2.5. In this section the causes of NAO and storminess variability will be outlined. It has been considered that the atmospheric dynamics governing the NAO are 'quasi-random' (Cassou, 2010), so the potential for predicting its changes are limited. Nevertheless there are a number of global teleconnections that influence the North Atlantic climate and circulation patterns. It is thought changes are also caused by external forcings, such as solar variability and volcanic eruptions.

As outlined above the stratosphere has been found to influence the patterns of the NAO and storms, in particular the behaviour of the circumpolar vortex. Twentieth century trends of expansion and contraction of the circumpolar vortex in winter have been found to significantly correlate with negative and positive NAO trends respectively (Angell, 2006). Furthermore anomalous changes in the strength of the stratospheric circulation have been found to propagate downwards, causing the tropospheric atmospheric circulation to become locked into a regime for extended periods of up to 60 days, which affects the NAO sign and storm track position (Baldwin and Dunkerton, 2001). A weakening of the circumpolar vortex can result in a reversal from westerly to easterly airflow and a persistent negative NAO situation (e.g. Baldwin and Dunkerton, 1999; Limpasuvan *et al.*, 2004; Zhou *et al.*, 2002), while a strengthening of the circumpolar vortex can result in persistent positive NAO anomalies (Baldwin and Dunkerton, 2001). However other studies of the circumpolar vortex have found less relation to the NAO. Walter and Graf (2005) found that weak circumpolar vortex circulation results in an atmospheric circulation pattern that resembles the NAO, but that the stronger circumpolar vortex created a circulation pattern resembling the southward shifted NAO (much like the East Atlantic Pattern, described in section 1.2.2 and shown in Figure 1.4), which resulted in the storm track crossing the British Isles. Finally cyclogenesis is increased by the southward intrusion of the jet stream across the Atlantic, as this increases the temperature gradients that lead to storm formation and deepening (Betts *et al.*, 2004).

Therefore the strength of the circumpolar vortex can have a large influence on the NAO and storminess, over weekly to monthly timescales.

The North Atlantic changes in sea surface temperature (SST) have been suggested as causing NAO index changes (Mehta *et al.*, 2000; Rodwell *et al.*, 1999), with oceans holding a 'memory' of temperature anomalies from the preceding year (the re-emergence mechanism) (Alexander and Deser, 1995; Cassou *et al.*, 2007; Hurrell and Deser, 2010). An example of this is the negative NAO winter of 2009-2010, which is thought to have caused the negative NAO winter of 2010-2011 (Taws *et al.*, 2011). A model simulation suggests that this mechanism represents a weak (15-20%) positive feedback (Cassou *et* al., 2007). Tropical SST's are another suggested cause of NAO trends (Cassou *et al.*, 2004a; Hoerling *et al.*, 2001; Robertson *et al.*, 2000). However, others have questioned the role that oceans play (Bretherton and Battisti, 2000), for example Cohen and Barlow (2005) found a divergence between tropical SST's and the NAO in recent years, as SST's increased due to global warming while the NAO decreased.

Ocean temperatures have also been suggested as an influence on storm intensity. North Atlantic SST's have been associated with increased storm intensity, as years with a high storm index in the British Isles occur when there is a 'tripole' of SST anomalies (Allan *et al.*, 2009). Similarly Betts *et al.* (2004) suggested that a west-east oceanic temperature gradient in the Atlantic is the most important factor causing extreme storm events in the South-Western Approaches (northwest France and southwest Britain). In addition, the Atlantic Multidecadal Oscillation (AMO) is a measure of North Atlantic temperatures that appear to influence sea level pressures and precipitation in Europe, particularly during autumn (Knight *et al*., 2006). Therefore these indicate that ocean temperatures can play an important role in the intensity and frequency of storms in Europe.

External forcings have been suggested as causing storminess and NAO variability. Solar minima are thought to cause negative NAO anomalies along with contraction of the Ferrell cells and an equator-ward shift of atmospheric jets and storm tracks (Ineson *et al*., 2011; Haigh *et al*., 2005; Gleisner and Thejll, 2003; Martin-Puertas *et al*., 2012). Conversely solar maxima are thought to cause positive NAO anomalies, a weakened and expanded Ferrell Cell with

pole-ward shifted and weaker atmospheric jets and storm tracks (Boberg and Lundstedt, 2002; Kuroda and Kodera, 2002; Haigh *et al*., 2005; Gleisner and Thejll, 2003).

Volcanic eruptions are also thought to influence the NAO and storminess. Model results and observations have indicated that large volcanic eruptions that inject aerosols into the stratosphere cause a strong circumpolar vortex circulation, positive NAO anomalies and wetter conditions in northern Europe in successive years (Fischer *et al*., 2007; Stenchikov *et al*., 2006; Kodera, 1994; Jones *et al*., 2005). Therefore large volcanic eruptions may force the climate over relatively short timescales, while clusterings of eruptions may have a stronger influence on climate in Europe.

These forcings and others are still under investigation; however those described here demonstrate that the NAO and storminess are likely to be controlled by a combination of factors. These may be the result of internal circulation patterns within the oceans and atmosphere, or from external sources such as volcanic and solar forcing.

1.2.4. Importance of understanding storminess and the NAO

Research into past patterns and causes of storminess and NAO variability are important for a number of reasons. The impacts on society and the environment from the NAO and storms are described here, to demonstrate the need for further research into these climate variables. Furthermore the benefits of improved understanding for predictions of future climate changes are outlined.

Storminess and NAO impacts

The NAO can bring both benefits and disadvantages to the countries under its influence. For example in the winter 2009-2010 there was an extremely negative NAO index (-1.18) (Figure 1.5) and a southerly position of the jet stream (c. 30-50 ºN), which caused severely low temperatures across

northern and western Europe, with detrimental economic and social impacts (Moore and Renfrew, 2012; Cattiaux *et al.*, 2010; Guirguis *et al.*, 2011; Santos *et al.*, 2013). In southern Europe the southerly storm track brought successive low pressure systems to the region: in the Iberian Peninsula this caused flooding, with implications for transport, dwellings and livelihoods, and thus economic costs (Vicente Serrano *et al.*, 2011). On the other hand the high precipitation in places like Portugal led to the refilling of reservoirs, which had been on a downward trend, and 30% increased hydroelectric power production (Andrade *et al.*, 2011).

The winter 2011-2012 is an example of a year with an extremely positive NAO (+1.35), which steered the storm track poleward of 50ºN, causing dry weather in southern Europe and warm weather in northern Europe (Santos *et al.*, 2013). The detrimental impacts of this positive NAO anomaly appear to have been minimal, however when positive NAO periods are associated with high storminess there can be greater disadvantages. For example the severe storm of October 1987 affecting northern Europe occurred during a period with particularly positive NAO anomalies; the extensive damage of this storm cost insurers $2.6 billion (Association of British Insurers, 2003; Alexander *et al.*, 2005), which today is the equivalent of £5 billion (Hewston and Dorling, 2011). This shows the huge impact that positive NAO conditions bringing severe storms can have. More recently the December 2013 to February 2014 period had a persistently positive NAO and a anomalous southward excursion of the storm track across North America; this created atmospheric temperature contrasts that accelerated the jet stream and caused increased cyclogenesis (Slingo *et al.*, 2014). The result was high precipitation, gale force winds and storm surges, causing flooding and damage to properties and infrastructure, particularly in coastal areas, with the economic cost yet to be calculated. It is also clear from these extreme winters that there is a social and economic incentive for better understanding of the NAO and its relationship with storminess and the storm track.

Understanding the variability of the NAO and storminess can help long-range forecasting, allowing preparations by authorities prior to periods that may be expected to have lower temperatures or higher storminess than usual. The NAO demonstrates high bi-annual and multi-annual variability (with cycles of 2

and 6-10 years) but also has longer decadal variations (Hurrell and Van Loon, 1997). Better understanding of these longer cycles can give authorities more time to prepare, particularly for changes that may have a greater impact over successive years. For example, it would be more effective to strengthen sea defences *before* predicted periods with high storminess rather than experience the disruption and expense of flooding from successive storms. The shortness of the instrumental records of the NAO and storminess, which extend back to the end of the 19th century at most, prevent the longer cycles being fully understood.

The NAO also has various influences on the earth system, inducing changes in the oceans, land system and ecology among others. The impacts of the NAO on the oceans include an Atlantic tripole of sea-surface temperature anomalies, changes to vertical mixing depths and altered rates of deepwater formation (Hurrell and Deser, 2010; Seager *et al.*, 2000; Visbeck *et al.*, 2001). The NAO wind-stress on the oceans is also known to influence the strength of circulation of the subpolar gyre and the subtropical gyre; these are oceanic circulation patterns that reflect the atmospheric pressure centres of the NAO, and strengthen in anti-phase as the westerly winds shift latitudinally with NAO changes (Curry and McCartney, 2001). The temperature anomalies and wind-driven circulation patterns affect the strength of the Atlantic Meridional Overturning Circulation (AMOC) and northward heat transport in the Atlantic (Curry and McCartney, 2001; Hurrell, 1995; Hurrell and Deser, 2010; Visbeck *et al.*, 2001). Furthermore the NAO wind-stress has been shown in the instrumental period to have a strong influence on the amount of Atlantic Water Inflow (AWI) into the Nordic Sea (Orvik *et al.*, 2001). Therefore the NAO directly alters the circulation of the ocean.

Examples of NAO influence on the land system are precipitation changes controlling glacier mass balances in Scandinavia (Nesje *et al.*, 2000), river flow in northwest Europe and northeast USA (Kingston *et al.*, 2006) and landslide occurrence in Spain and the Azores (Marques *et al.*, 2008; Zezere *et al.*, 2008). NAO driven variations in wind have been linked to Danube delta advances and retreats (Vespremeanu-Stroe *et al.*, 2007) and Mediterranean Sea beach ridge formation (Goy *et al.*, 2003; Rodríguez-Ramírez *et al.*, 2003). Ecologically the NAO can alter the onset of the growing season, affecting herbivores and then

carnivores (D'Odorico *et al.*, 2002; Ottersen *et al.*, 2001) as well as behavioural changes in fauna, such as bird migration timings and deer behaviour (Forchhammer *et al.*, 2002; Ottersen *et al.*, 2001). Therefore there are climatic, oceanic, societal and environmental impacts of NAO variability.

Future changes

One of the most important reasons for increasing understanding of the NAO and storminess is to support predictions of future climate changes. The Intergovernmental Panel on Climate Change (IPCC) 2013 report gives projections that by 2050 and 2100 A.D. the storm track will have shifted northwards in the northern hemisphere, with the storm tracks extending further eastwards across Europe, along with a more positive NAO (Stocker *et al.*, 2013 and references therein, including Pinto *et al.*, 2007; Bengtsson *et al.*, 2006). Many projections of future storminess agree that storm intensity will increase in the future (Feser *et al.*, 2014 and references therein). The British Isles in particular are predicted to have a higher frequency of storm occurrence (Figure 1.7), which it is thought will result from an intensified jet stream (Pinto *et al.*, 2009). In contrast it has recently been suggested that polar amplification of warming is causing the latitudinal temperature gradient to reduce, resulting in slower zonal circulation, large meanders of the circumpolar vortex and therefore persistent extremes of weather (Francis and Vavrus, 2012). The IPCC report makes it clear that there is low to medium confidence in the predictions of future storm track positions and NAO patterns particularly for the North Atlantic, in part due to the projected changes being within the range of internal variability (Stocker et al., 2013). Furthermore model simulations of storminess have been found to have overly-high stability in comparison with palaeoclimate data (Valdes, 2011; Braconnot *et al.*, 2012), suggesting that future predictions of storminess may be underestimated.

In section 1.2.3., the oceanic and solar forcings on the NAO and storminess were described. The IPCC report observed that processes like sea ice loss and changes in SST could influence the response of the NAO, storm track and storm intensity to warming (Stocker *et al.*, 2013; Kvamsto *et al.*, 2004; Graff and LaCasce, 2012). As well as this, a projected weakening of the North Atlantic ocean circulation may cause the southern North Atlantic to have a reduction in temperature thus increasing the meridional temperature gradient,

leading to increases in storm intensity and activity (Stocker *et al*., 2013; Catto *et al*., 2011; Woolings *et al*., 2012). Furthermore it is observed that a solar minima may influence the NAO over coming decades (Stocker *et al*, 2013; Lockwood *et al*., 2012). Therefore the ocean forcing of the NAO and storminess may be enhanced by anthropogenic climate change, which are superimposed on natural, external forcing.

The IPCC report demonstrates a need for better understanding of the causes of NAO and storminess changes, including the underlying natural forcing from solar variability, as well as the effects of ocean circulation changes and alterations of the temperature gradients (Stocker *et al*., 2013). By reconstructing past changes in the NAO and storminess, palaeoclimate research (such as this project) can contribute to climate change research by showing the influence of natural factors such as solar variability, as well as the climatic response to past changes in the oceans.

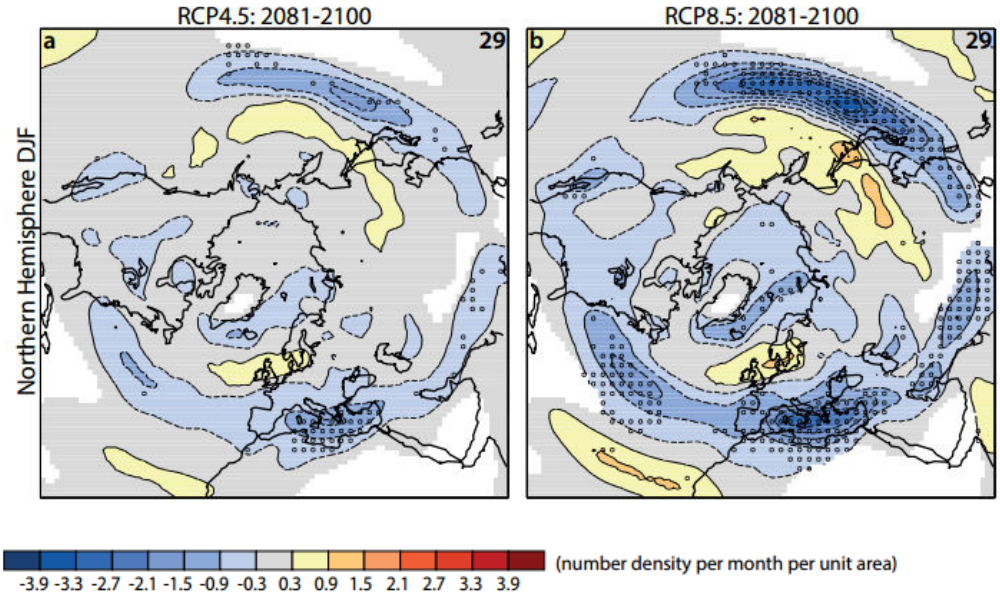

Figure 1.7: Projected future increase in number of extratropical storms; the period 2081-2100 compared to the period 1986-2005 (Stocker *et al*., 2013, pg 1075).

1.2.5. Storminess and the NAO: instrumental period

As described in section 1.2.4. there are a number of important reasons for improving our understanding of the patterns of storminess and NAO variability, as well as the climate forcings. The period with instrumental records provides detailed data for analysis of the NAO and storms. Twentieth century storminess is well understood, due to high quality pressure records since c.1950 A.D (Alexandersson *et al.*, 1998; Kaas *et al.*, 1996; Schmith *et al.*, 1998) and the Beaufort Scale (Clarke and Rendell, 2009; Schmith *et al.*, 1998). Understanding is also based on counts of annual numbers of gale days since 1770 A.D. (Dawson *et al.*, 2004). Records show there was a decreasing trend in storminess from 1920-1980 A.D. before an increasing trend peaked around 1990 A.D., as shown in Figure 1.8 (Alexandersson *et al.*, 2000; Bärring and Fortuniak, 2009; Dawson *et al.*, 2004; Hanna *et al.*, 2008; Schmith *et al.*, 1998). The overall storminess trend is generally agreed to have been one of large inter-annual and decadal variability but with no overall change (Bärring and Fortuniak, 2009; Hanna *et al.*, 2008; Kaas *et al.*, 1996; Lozano *et al.*, 2004; Schmith *et al.*, 1998; WASA_Group, 1998).

Instrumental records of the NAO extend as far back as 1823 A.D. through the station pressure measurements from Gibralter and Reykjavik (Jones *et al.*, 1997) (Figure 1.9). These records show decadal variations through the 19th century, more positive NAO from c.1900-1930 A.D., becoming more negative from c.1940-1970 A.D. then increasingly positive until the mid-1990s (Hurrell, 1995). This positive NAO trend peaked in the years 1983, 1989 and 1990 A.D.; the highest positive NAO values of the pressure record as they were > +4 (Hurrell, 1995). Since the early 1990's A.D. the NAO was more neutral and negative (Cattiaux *et al.,* 2010). The two most negative NAO anomalies on record occurred in the severe winters of 1995-1996 A.D. (Jones *et al.*, 1997) and 2009-2010 A.D. (Cattiaux *et al.*, 2010) as shown in Figure 1.9.

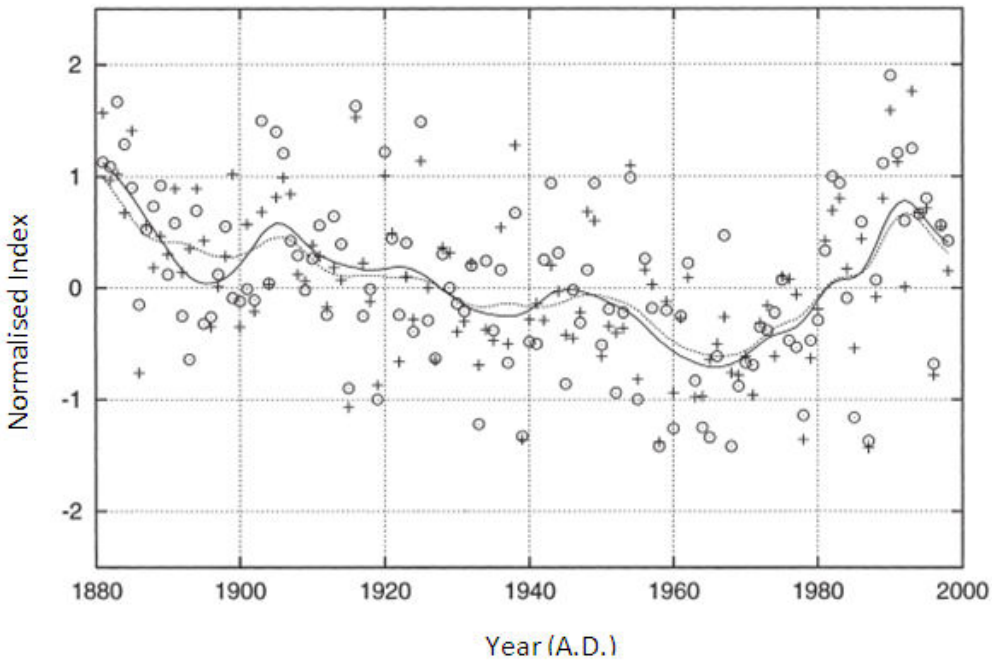

Figure 1.8: Trends in the geostrophic winds over the North Sea and British Isles for the period 1881-1998 A.D. (Alexandersson *et al.*, 2000, pg 72). For each year 95th percentiles (+ and solid lines) and 99% percentiles (o and dashed lines) were calculated.

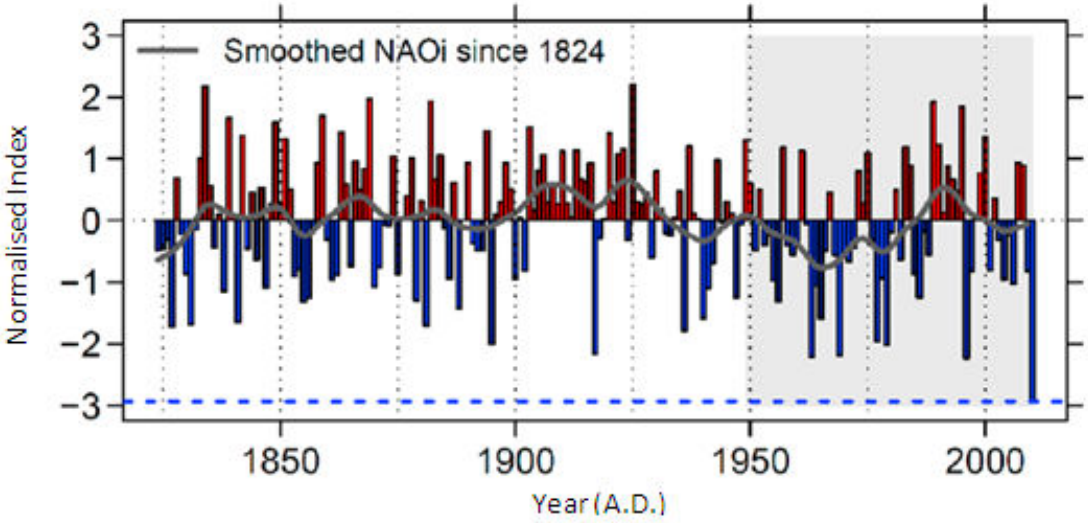

Figure 1.9: Updated instrumental NAO record, 1824-2010 A.D., calculated by the difference between the normalised pressure from Gibralter and the normalised pressure from southwest Iceland (Cattiaux *et al.*, 2010, pg L20704/2; Jones *et al.*, 1997)

Variations in storminess in northern Europe during the instrumental period are similar to the general trends of the NAO, as shown in Figures 1.8 and 1.9. For example, storm activity was at a minimum in the 1960's A.D. in accordance with negative NAO anomalies, before storminess increased towards the early 1990's A.D. as the NAO became more positive (Pinto and Raible, 2012; Alexandersson *et al.*, 2000). The trends in the NAO and storminess also correspond to long term trends in the circumpolar vortex: the circumpolar vortex expanded up until 1968 A.D. before contracting up until the year 2000 A.D., and has also had a steeper geopotential gradient after 1970 A.D. which explains the increase in storminess (Frauenfeld and Davis, 2003; Angell, 2006). This illustrates how the circulation patterns occurring in the North Atlantic are part of global scale circulation systems.

Although the relationship between storms and the NAO is clear for some regions using records since 1950 A.D., some longer instrumental records suggest that the relationship is not constant through time. Station pressure data from across the United Kingdom shows a strong correlation between the NAO and storms from 1940-1960 A.D. (R = 0.5) and 1970-1990 A.D. (R = 0.6), but a weaker correlation from 1920-1940 A.D. (R = 0.2) and no correlation from 1960-1970 A.D. (Allan *et al.*, 2009). Similarly a station record from Aberdeen (from 1871 to 2005 A.D.) had a significant correlation between storms and the NAO over the full period, however closer inspection showed it was insignificant from 1871-1930 A.D. (Hanna *et al.*, 2008). Therefore, to correctly interpret storm records and pre-instrumental reconstructions, it needs to be considered that the NAO may not have consistently been the dominant influence on storminess.

The spatial influence on storminess from the NAO can be investigated using minima in gridded geopotential height measurements to identify cyclones; with data available from 1958 A.D. (see Trigo, 2006 for methodology). Studies using this method have shown that negative NAO events result in a reduction in the numbers of cyclones compared to positive NAO events, as well as a reduction in cyclone intensity (Andrade *et al.*, 2008; Serreze *et al.*, 1997; Trigo *et al.*, 2002; Zezere *et al.*, 2005). Figure 1.10 illustrates the correlation between cyclone frequency and NAO phases (Andrade *et al.*, 2008), and shows that northwest Scotland and coastal sections of Norway have the strongest positive correlation between cyclone numbers and the NAO, while there is a negative

correlation in Portugal, northwest Spain and southern France. Precipitation changes in response to the NAO show similar differences between northern and southern Europe: the UK, northern France and Scandinavia have higher precipitation during positive NAO's and the Iberian Peninsula and southern Europe have lower (Trigo *et al.*, 2002). Based on these results there should be contrasting patterns between storminess reconstructions from northern and southern Europe. These findings have helped to inform the choice of study sites in this project.

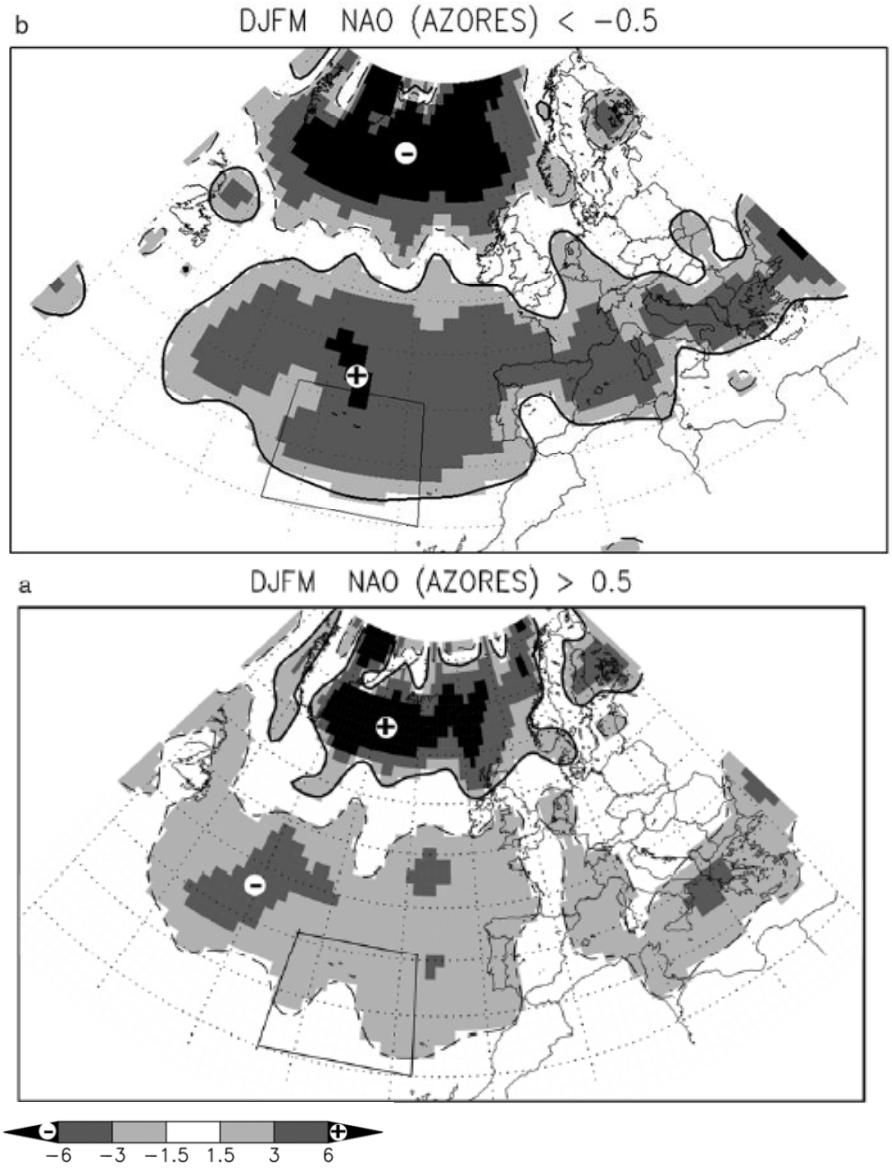

Figure 1.10: Number of cyclones per winter (DJFM) during the period 1958-2000, for winters with positive NAO (a) and negative NAO (b), data normalised for 50ºN (Andrade *et al*, 2008, pg 751).

Cluster analysis has allowed the identification of pressure regimes; reoccurring periods with an enduring atmospheric circulation pattern (Cassou, 2010; Palmer, 1999; Vautard, 1990; Woollings *et al.*, 2010). For example, Raible *et al.* (2001) identified two regimes: an *active regional regime* (where the NAO is dominant within the North Atlantic) and a *passive global regime* (with influences from the El Nino-Southern Oscillation and the Tropics). Other studies have categorised four regimes: including the positive and negative NAO states (occurring approximately 52% of the time) but also the Atlantic Ridge and Scandinavian Blocking regimes, as explained in section 1.2.3. (Cassou, 2010; Cassou *et al*., 2004b). Since 2001 A.D., cluster analysis suggests Atlantic Ridge or Blocking regimes have been dominant, rather than the NAO (Hurrell and Deser, 2010) and similarly other regimes are thought to have been dominant from 1900-1925 A.D. (Cassou *et al.*, 2004b). The 'blocking' regime is thought to cause a negative NAO index, as it did during the 1960's (Croci-Maspoli *et al.*, 2007; Greatbatch, 2000; Hurrell, 1996). Finally Allan *et al.* (2009) found that in the British Isles in winter the NAO is the dominant driver of storm events but the East Atlantic pattern is the second driver, with a significant correlation with October-December storms of R = 0.33. A strong polar vortex has been found to result in an atmospheric circulation pattern very similar to the East Atlantic pattern, which results in the storm track crossing north and west Europe (Walter and Graf, 2005). Therefore the instrumental data implies that care needs to be taken when interpreting climate proxy reconstructions, as other regimes may be causing climate variations at times.

1.3. Methodologies of reconstructing storminess and the NAO

Studies have sought to reconstruct pre-instrumental changes in storminess and the NAO because the instrumental data is too short to capture the low-frequency variability of these and does not span periods of non-anthropogenic climatic change (Hegerl *et al*., 2007). There are also benefits for modelling research, as longer climate reconstructions can be used to assess the ability of models to simulate past climate, and thus to predict future climate (e.g. Anderson *et al*., 2006; Kohfeld and Harrison, 2000; Hegerl *et al*., 2006). Pre-instrumental storminess reconstructions will be created in this research, so initially the methods used to make these and NAO reconstructions will be outlined, before their findings are described in section 1.4.

1.3.1. Storminess reconstruction methods

The reconstruction of storminess prior to the instrumental record has been done using documentary evidence such as journals, ship logbooks and others (Lamb, 1991; 1995; Dawson *et al.,* 2004; Wheeler *et al.,* 2010). Proxy data reconstructions of storminess have included: dated layers within sand dunes using Optically Stimulated Luminescence (OSL) (Jackson *et al.*, 2005; Sommerville *et al.*, 2003), dated cliff-top storm deposits (boulders, gravel and sand) (Hansom and Hall, 2009), geochemical analysis of the GISP2 ice core on Greenland to identify aerosols originating from sea-spray (Meeker and Mayewski, 2002; O'Brien *et al.*, 1995), sedimentological analysis of marine and estuarine cores to identify changes in the strength of ocean currents and marine influence (Andresen *et al.*, 2005; Hass, 1996; Sorrel *et al.*, 2009) and over-washed sand deposits in lagoons (Sabatier *et al.*, 2010). Additionally some reconstructions have identified low pressure occurrence through the deposition of in-washed sediment layers within lake deposits, as these represent the high precipitation events that accompany storms (Noren *et al.*, 2002; Page *et al.*, 2009).

Each method of reconstructing storminess has different levels of sensitivity and bias. Some of these methods, such as cliff-top storm deposits, record extreme events while others such as coastal over-wash deposits may be destroyed by subsequent events so only show the most recent (Haslett and

Bryant, 2007). Those that rely on wind-blown sand may be more sensitive during dry periods. For example, on sand dunes when evapo-transpiration exceeds precipitation vegetation is reduced, allowing sand to be more easily entrained (Lancaster, 1989). There may also be an influence from human activities, for example sand dunes can either be stabilized (e.g. Gilbertson *et al.*, 1999) or disturbed (e.g. Pye, 1990) by human actions altering the vegetation cover, causing misleading results if interpreted solely as a storminess proxy. All these factors need to be considered when using windblown sand as a proxy for storminess, because although it is shown that wind is a dominant factor for sand transport, it is clear that there are other factors that can enhance or reduce the amount of sand being transported.

Studies in Scandinavia have used variations in the quantity of windblown sand in ombrotrophic peat bogs as a proxy for storminess, with higher sand quantities within the peat used to identify periods when more sand was blown inland and therefore higher storminess (Björck and Clemmensen, 2004; De Jong *et al*., 2006; De Jong *et al*., 2007). Peat bogs can be used to produce long, continuous reconstructions of storminess with decadal resolution, so are more sensitive than some other terrestrial proxies and can allow relatively short term changes to be seen. Such records are needed if storminess is to be compared with continuous records from oceanic cores and NAO reconstructions, so therefore this method is used in this research.

High resolution reconstructions have also been created using ITRAX XRF analysis (Croudace *et al.,* 2006), a method that measures the elemental composition of lake sediment, which can reflect sediment that has been washed or blown into lakes during storms (e.g. Martin-Puertas *et al.,* 2012; Giguet-Covex *et al.,* 2012). Although the method provides relative elemental measurements, which may be influenced by the sediment composition and other elements (Löwemark *et al.,* 2010), the extremely high resolution of the records mean that there is potential for annual and multiannual resolution climate reconstructions to be created. As such this method will also be used in this research, to create a storminess reconstruction and to test the potential and limits of this method.

1.3.2. Methods of reconstructing the NAO

Pre-instrumental reconstructions of the NAO do not use pressure measurements but infer past changes using documentary evidence or climate proxies for precipitation and temperature, which are influenced by the NAO. Using documentary observations of ice, snow and biological features, as well as tree-ring data, Luterbacher *et al.* (1999) created an NAO record back to 1675 A.D.. Luterbacher *et al.* (2002) then extended this record back to 1500 A.D. with a seasonal resolution, again using environmental observations. Documentary evidence of precipitation in Andalusia (Spain), which is strongly related to NAO variability in the instrumental period, was also used by Rodrigo *et al.* (2001) to create a record back to 1501 A.D.

Proxy reconstructions of the NAO have used records of tree ring band width (Cook *et al*., 1998; Glueck and Stockton, 2001; Trouet *et al.*, 2009), speleothem band width (Proctor *et al.*, 2000; Trouet *et al.*, 2009), ice accumulation rates from cores and $\delta^{18}O$ measurements (Appenzeler *et al.*, 1998; Glueck and Stockton, 2001). Some reconstructions have used a combination of sites (Cook *et al.*, 1998) or the opposite behaviour of climate reconstructions from sites that are oppositely influenced by the NAO (Glueck and Stockton, 2001; Trouet *et al*., 2009). Initial reconstructions extended the record back to 1650 A.D. and 1701 A.D. (Appenzeler *et al.*, 1998; Cook *et al.*, 1998), while later reconstructions have extended it to 1429 A.D. (Glueck and Stockton, 2001), 1049 A.D. (Trouet *et al.*, 2009; Figure 1.11) and 900 A.D. (Proctor *et al.*, 2000). Most recently, proxies for hypolimnic anoxia in a Greenland lake have been used, because the NAO controls temperature and precipitation here, which influences lake stratification (Olsen *et al.*, 2012; Figure 1.12). This is the longest NAO record to date and spans 5200 cal yr BP to present (Olsen *et al.*, 2012).

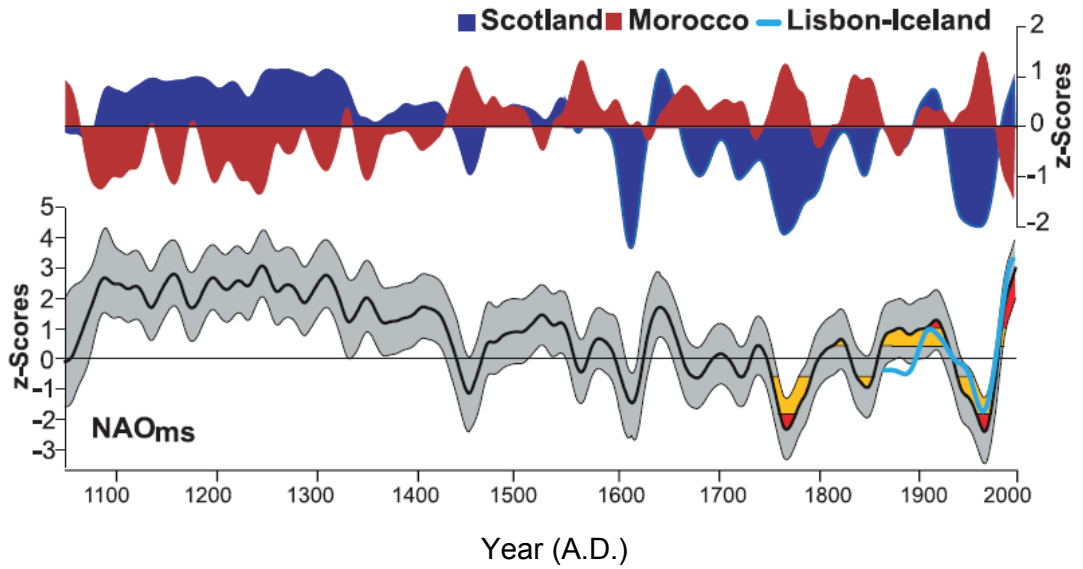

Figure 1.11: Proxy NAO reconstruction by Trouet *et al.* (2009, pg 78). Based on the opposite changes between a speleothem reconstruction of precipitation from Scotland (Proctor *et al*., 2000) and a Moroccon tree-ring drought reconstruction (Esper *et al*., 2007).

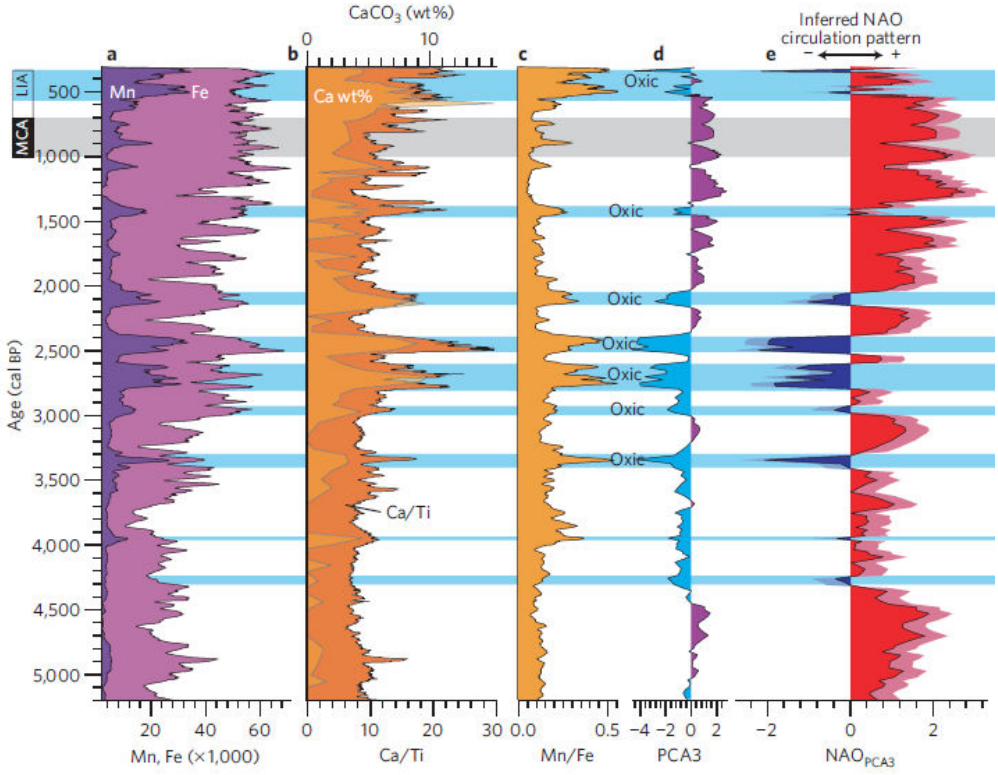

Figure 1.12: Reconstruction of the mid-to-late Holocene NAO using proxies for lake hypolimnoxia from southwest Greenland (Olsen *et al*., 2012, pg 810)

NAO reconstructions have some contrasting results, particularly the higher resolution records that span the past millennium. Schmutz *et al.* (2000) compared three NAO reconstructions (Appenzeller *et al.*, 1998; Cook *et al.*, 1998; Glueck and Stockton, 2001) with the instrumental/documentary records of Jones *et al.* (1997) and Luterbacher *et al.* (1999) and found that only the Cook *et al.* (1998) and Stockton and Glueck (1999) reconstructions significantly correlated, which was probably because these were both from the same location. Another similar study showed better agreement between the records between 1620 and 1720 A.D. but strong disagreement in the 15th, 16th and 18th to early 19th centuries (Pinto and Raible, 2012). Therefore there are poor correlations between NAO reconstructions during the past millenium, suggesting some of these are erroneous.

The lack of correlation could be the result of non-stationarity in the NAO teleconnection (Luterbacher *et al.*, 2002). Frequent spatial variations have been demonstrated, for example evidence suggests that the NAO pressure cells exhibit spatial variation seasonally and have different positions during positive and negative NAO phases (Cassou *et al.*, 2004b; Hurrell *et al.*, 2003; Portis *et al.*, 2001). Therefore spatial variations in the NAO and periods when the NAO is not a dominant regime are likely to have changed the impact on proxies in different locations (Schmutz *et al*., 2000; Pinto and Raible, 2012). The validation period used can also make a difference to the perceived skill of an NAO reconstruction. Schmutz *et al.* (2000) suggested that the Cook *et al.* (1998) and Glueck and Stockton (2001) reconstructions could be verified using the Jones *et al.* (1997) dataset in the second half of the 19th century and from 1920-1970 AD, but not in the intervening period and since 1970 AD. Similarly comparison of the Trouet *et al*. (2009) reconstruction with longer instrumental records of the NAO has shown that the southern dipole Moroccan site only correlates with the NAO after 1914, and reduces the skill of the NAO reconstruction before this (Lehner *et al.,* 2012). These illustrate that the NAO influence on climatic proxies varies temporally.

In summary, errors in NAO reconstructions can be caused by NAO non-stationarity, different regimes (such as atmospheric blocking), the validation period used, as well as changes in the relationship between proxies and the NAO (Lehner *et al.*, 2012; Pinto and Raible, 2012; Schmutz *et al.*, 2000). As

such, changes to the NAO influence on climatic proxies needs to be considered when using NAO reconstructions, but also when interpreting changes in climatic reconstructions that are under the influence of the NAO.

1.4. Late Holocene climate changes: storminess and the NAO

This study will focus on the Late Holocene, which is here defined as 4500 cal yr BP to present. During this time climatic conditions were similar to the present and more climatic and oceanic reconstructions exist for this period than any other, which makes it the most suitable period to investigate long-term, natural climate variability (Wanner *et al*., 2008). In this section the identified storminess and NAO patterns during the Late Holocene (4500-1000 cal yr BP), Medieval Climate Anomaly (MCA, ~950-1400 A.D.) and Little Ice Age (LIA, ~1400-1850 A.D.) are described in turn. This separation was undertaken as the LIA and MCA are frequently identified as periods when different climates and circulation patterns occurred in the North Atlantic region and Europe (Lamb, 1965; 1995; Meeker and Mayewski, 2002). The Late Holocene before the MCA has less distinct climate events and is spanned by fewer storminess and NAO reconstructions, thus the period from around 4500-1000 cal yr BP is described in one section. Within each section the evidence for storminess is described in terms of location. Reconstructed storm events from sites in Europe are summarised in Figure 1.13 and proxies for changes in ocean and atmospheric circulation are shown in Figure 1.14. In each section the relationship between the NAO, storm intensity and storm track position are discussed. As well as this cycles that have been identified are discussed in section 1.4.6.

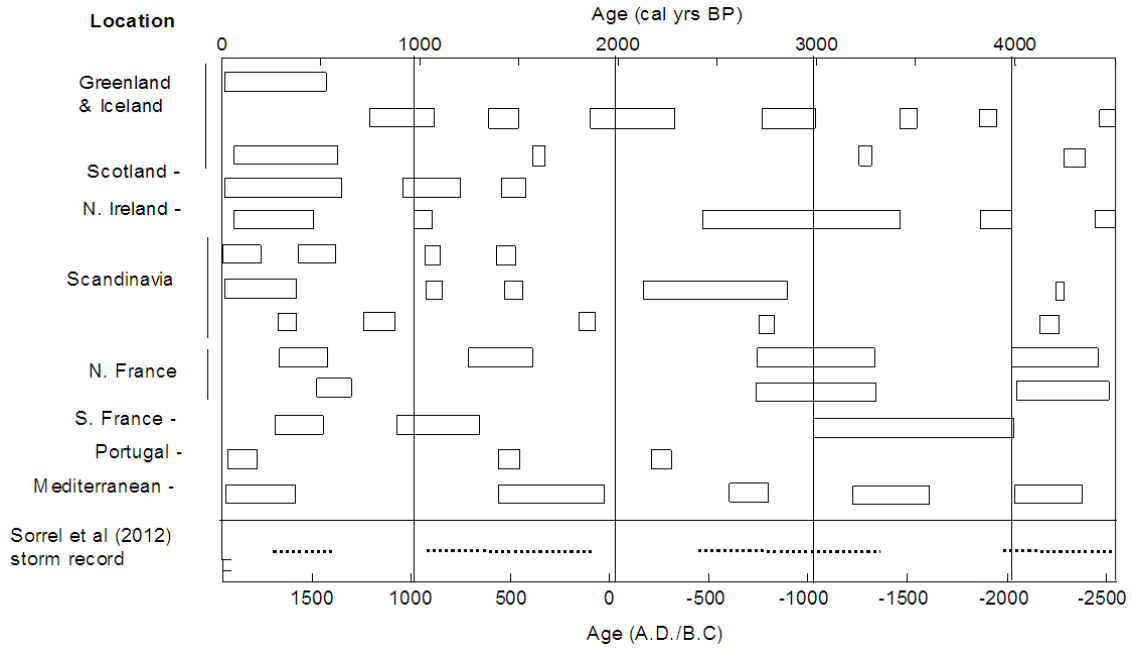

Figure 1.13: Compilation of identified periods of storminess in Europe, as mentioned during section 1.4. Sites (from top): Greenland (Meeker and Mayewski, 2002), Iceland (basalt/plagioclase ratio) (Andresen *et al.*, 2005), Iceland (Jackson *et al.*, 2005), Scotland (Hansom and Hall, 2009), northern Ireland (Wilson *et al.*, 2004), Skagerrak Sea (Hass, 1996), Halland Coast, Sweden (De Jong *et al.*, 2006), Denmark (Clemmensen *et al.*, 2009), Seine Estuary, France (Sorrel *et al.*, 2009), Mont-Saint-Michel Bay, France (Billeaud *et al.*, 2009) Aquitaine coast, France (Clarke *et al.*, 2002), Portugal (Clarke and Rendell, 2006), French Mediterranean coast (Sabatier *et al.*, 2010).

1.4.4. Late Holocene storminess

The ages are expressed for the Late Holocene period in calibrated years before present (cal yr BP) rather than the Gregorian calendar (AD/BC) as for the LIA and MCA sections. This is because the Late Holocene storminess and oceanic reconstructions are typically expressed in cal yr BP and the period is not spanned by historical records of climate, which are expressed in calendar years. Longer records of storminess that span the Holocene have indicated that there was a number of periods when storminess was higher, although there are differences between the timings of these, as illustrated in Figure 1.13.

From high latitudes a GISP2 reconstruction indicates that there was greater storminess at 3100-2400 cal yr BP (O'Brien *et al.*, 1995). In Iceland glacier advances at 4700, 4200, 3200-3000, 2000 and 1500 cal yr BP have been interpreted as being caused by temperature, but with precipitation and therefore storms having some influence as well (Stotter *et al.*, 1999). Five similar events have also been identified in records showing surface mixing offshore of Iceland, leading to the interpretation that the glacier advances are caused by cyclonic activity also affecting the marine conditions (Witak *et al.*, 2003). Similar timings have been found in an Icelandic loess formation proxy record, which it is suggested reflects greater storminess at 4300, 3300 and 1600 cal yr BP (Jackson *et al.*, 2005) and a proxy of storminess from a marine core offshore of Iceland indicates there was high storminess from a westerly and northerly direction at approximately 4500-4400, 3500, 3000-2600, 2200-1900 and 1500-1400 cal yr BP (Andresen *et al.*, 2005). These high latitude records show some similar, but also some different, storm events during the Late Holocene.

In the British Isles, sand dune movements have occurred on the Western Isles at 3800-3300 and 1700-1300 cal yrs BP (Gilbertson *et al.*, 1999) and in Northern Ireland at 3100-2400 cal yrs BP (Wilson *et al.*, 2003). Cliff-top storm deposits formed in Scotland at 1550-1400 cal yrs BP (Hansom and Hall, 2009). The records from Scotland support the finding by Lamb (1995) using documentary evidence that storminess was high in the 6th century A.D. around the North Sea region. The position of these sites in the northwest of the British Isles mean they are likely to have been affected by the same storms.

In Scandinavia a pulse in the wind-driven currents occurred in the Skaggerak Sea at c.1450 cal yr BP (Hass, 1996), storm blown sand was deposited in a Swedish bog at 4800, 4200, 2800-2200 and 1500 cal yr BP (De Jong *et al.*, 2006) and sand dune developed was initiated in Denmark at 4150, 2750 and 1850 (Clemmensen *et al.*, 2009). There is some similarity between these records, with storm events at approximately 1450, 2800 and 4200 cal yr BP.

A study from France suggests high storminess occurred in the English Channel at Mont-Saint-Micheal Bay at 4500-4000 and 3000 cal yr BP (Billeaud *et al.*, 2009) while in southern France sand dune movements occurred on the

Aquitaine coast, France, at 4000-3000 yrs BP (Clarke *et al.*, 2002). In southern France a lagoon system indicates storm activity was highest at 4400-4050, 3650-3200, 2800-2600 and 1950-1400 cal yr BP (Sabatier *et al.*, 2011). These records show quite different results, perhaps due to the distance between sites; however the latter records periods of high storminess perhaps similar to those seen in Scandinavia, centred around 1450, 2800 and 4200 cal yr BP.

In Portugal there were sand dune accretions at 2200 and 1500 yrs BP (Clarke and Rendell, 2006). A reconstruction from a lagoon environment indicates that between 5700-2900 cal yr BP storminess was higher than after 2900 cal yr BP (Bao *et al.*, 2007). Other evidence points to there having been strong storm currents at 2850 cal yr BP in the Ría de Vigo, northwest Spain (González -Alvarez *et al.*, 2004).

The above storm reconstructions show a variety of timings for storm events, which could be the result of spatial differences in storminess, but also because some reconstructions only show local or extreme events (Haslett and Bryant, 2007). The above described reconstructions perhaps show common storm events at approximately 1450, 2800 and 4200 yrs BP. A compilation of reconstructions by Sorrel *et al.* (2012) inferred periods of high storminess at 4500-3950, 3300-2400 and 1900-1050 cal yr BP, which are similar but much broader periods of storminess than those identified here.

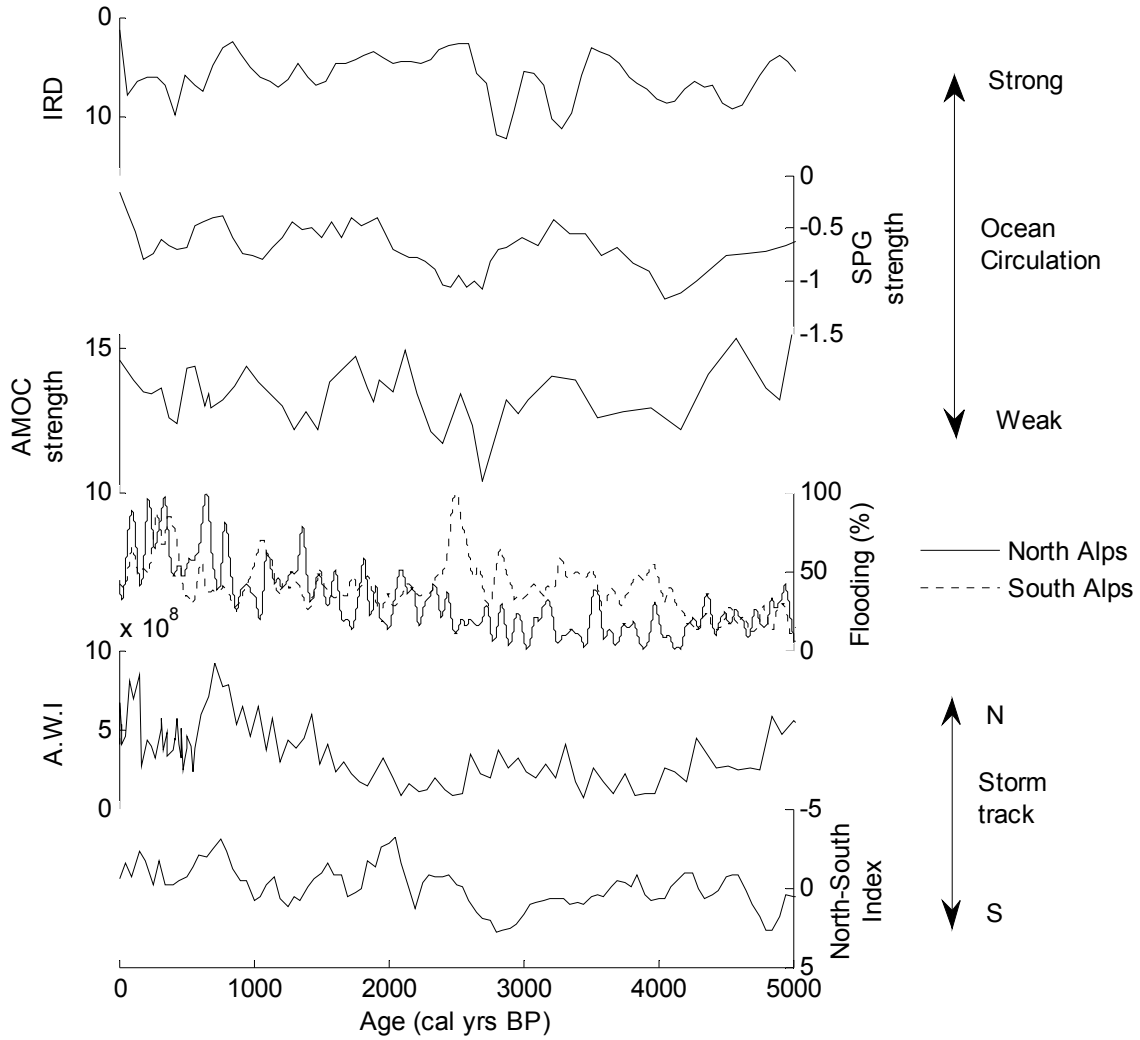

Figure 1.14: Summary of the ocean circulation proxies. From top: Ice Rafted Debris (IRD) proxy measured by percentage of Haematite Stained Grains (HSG) from 4-stacked records from North Atlantic (Bond *et al.,*2001); Sub-Polar Gyre (SPG) strength measured using the density difference (Thornalley *et al.,*2009); Atlantic Meridional Overturning Circulation (AMOC) current strength measured using mean sortable silt (10-63μm) terrigenous fraction weight (Bianchi and McCave, 1999); percentages of flood events from stacked lake reconstructions from the northern and southern Alps (Wirth *et al.*, 2013); proxy for the strength of Atlantic Water Inflow (AWI) into the Nordic seas measured using G.Muellerae concentrations (coccoliths/g dry sediment) (Giraudeau *et al.*, 2010); North-South Index of westerly airflow based on the opposite precipitation reconstructions from Folgafonna and Lyngen glaciers in Norway (Bakke *et al.*, 2008).

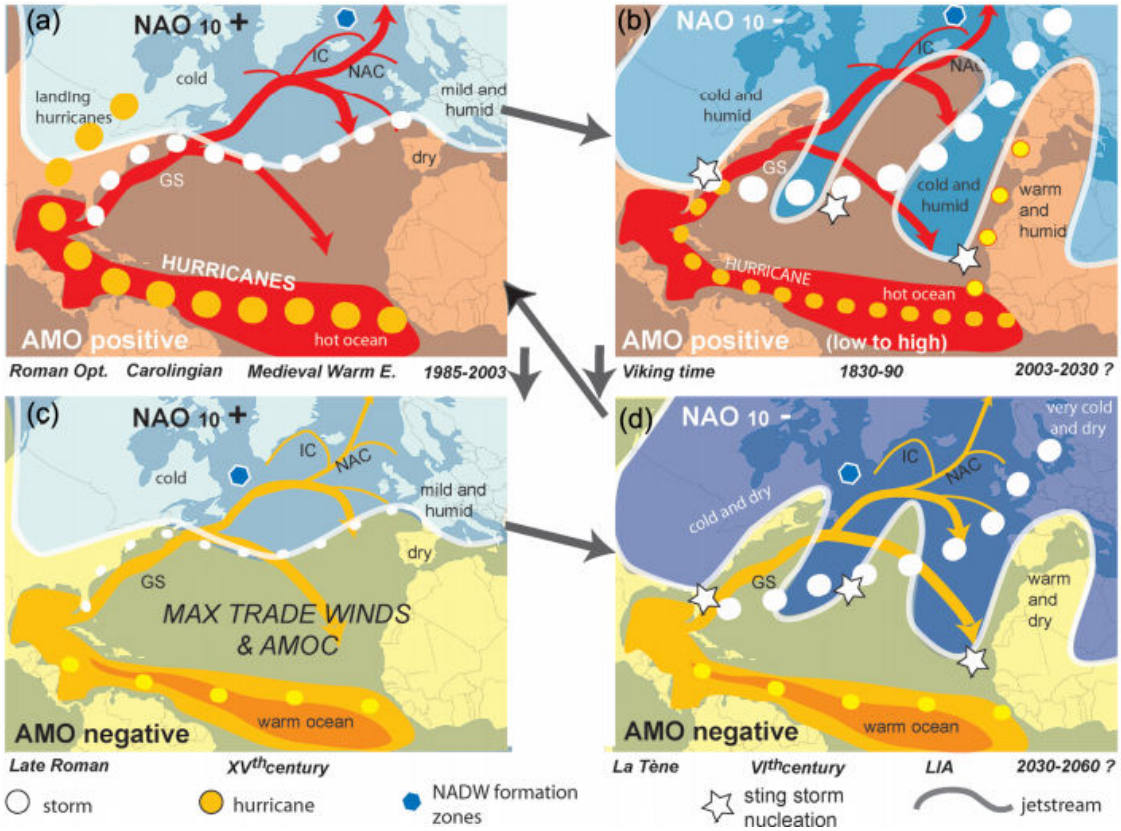

Figure 1.15: Summary of patterns of oceanic and atmospheric circulation, including the circumpolar vortex and North Atlantic Current (NAC) in relation to the NAO and AMO indices, including the influence these have on storm intensity and storm tracks (Van Vliet-Lanoë *et al.*, 2014, pg 449).

1.4.2. Late Holocene: atmospheric and oceanic circulation

Understanding the long-term patterns of the NAO is made difficult by only one reconstruction spanning the Late Holocene. The most detailed reconstruction was compiled by Olsen *et al.* (2012) (Figure 1.12) and suggests that before 4300 cal yrs BP the NAO was strongly positive, between 4300-2000 cal yr BP the NAO was more negative (particularly between 3500-2000 cal yr BP) before becoming positive after 2000 cal yr BP. Another reconstruction has inferred broad changes in NAO variability from changes in oceanic proxies. Rimbu *et al.* (2003) compared alkenone-based sea-surface temperature reconstructions between sites in the Atlantic; the trends suggest that the NAO was increasingly negative up until c.2000 cal yr BP before becoming moderately more positive (Wanner *et al.*, 2008; Rimbu *et al.*, 2003). There is therefore good agreement between the NAO reconstructions available.

Evidence has been gathered that indicate that the Holocene has been punctuated by abrupt oceanic reorganisations (initially shown by increased ice rafting in the North Atlantic), which have occurred approximately every 1470 ± 500 yrs and lasted for several centuries at c.4200, 2800 and 1400 cal yr BP (Bond *et al.*, 1997). A c.1500 year cycle has also been found in the Iceland-Scotland Overflow Water proxy (Bianchi and McCave, 1999), in proxies used to infer the strength of the sub-polar gyre (Thornally *et al.*, 2009; Copard *et al.*, 2012) and in southerly movements of colder water further south than the Iberian Peninsula (Pena *et al.*, 2010).

Some reconstructions suggest that these ocean circulation changes influenced storminess in Europe. This is supported by the timings of high European storminess described in section 1.4.1. Fletcher *et al.* (2012) compiled a transect of reconstructions from western Europe, between Iceland and Morocco, which appear to show storm tracks were further south between 4500-3700 and 2900-1900 cal yr BP. These were linked with oceanic circulation changes that were suggested as being the result of changes in the strength of the Atlantic Meridional Overturning Circulation (Fletcher *et al*., 2012). A shift in the storm track to the south of northwest Spain accompanied by southward shifts in oceanic fronts has been reconstructed for the periods 3800-3000, 2200-1800, c.1000 and since 600 cal yr BP (Pena *et al*., 2010). Storminess increased in the Mediterranean at 4400-4050, 3650-3200, 2800-2600 and 1950-1400 cal yr BP, and these changes are similarly linked with a southward displacement of the storm track as a result of cold ocean temperatures at high latitudes, causing a steepened temperature gradient (Sabatier *et al*., 2011). Finally widespread storminess increases in northern Europe at 4500-2950, 3300-2400, 1900-1050 and 600-50 cal yr BP have been linked with ocean-atmosphere reorganisations (Sorrel *et al*., 2012). Therefore these reconstructions all include the c.1500-1700 cal yr BP cycle that is thought to be an internal oceanic cycle, however there are differences in the timings of the inferred southward storm track shifts. These periods of storminess do not resemble the negative NAO events during the Late Holocene (Olsen *et al.*, 2012; Figure 1.12), suggesting there was a change in storminess, but not as the result of NAO circulation changes.

Conversly warm ocean temperatures may also be a factor increasing storminess. A recent storminess reconstruction from France by Van Vliet-Lanoë *et al*. (2014) indicates that the most intense storms are generated when positive AMO conditions (warm Atlantic temperatures) coincide with negative NAO anomalies (cool atmospheric conditions), as this encourages vertical temperature exchanges and cyclogenesis (illustrated in Figure 1.15 B).

Other reconstructions of storminess, particularly those that are based on precipitation proxies, show different patterns through the Late Holocene. In northern Europe a North-South Index of precipitation along Norway's coast (using the fluctuations of two glaciers from northern and southern Norway) suggests that there were more southerly storm tracks at 2800, 1200 and 400 cal yr BP, superimposed on a transition from southward to northward storm tracks at c.2000 cal yr BP (Bakke *et al.,* 2008). The centennial variations are proposed as being due to ocean circulation changes in the North Atlantic, while the transition is considered as resulting from a strengthening of the circumpolar vortex resulting from orbital changes (Bakke *et al*., 2008; Figure 1.14). A southward storm track between 4200-2400 cal yr BP has also been inferred by the contrasting patterns of flooding reconstructions from the northern and southern Alps (Wirth *et al.*, 2013; Figure 1.14). Finally a northward storm track transition is also indicated by increasing Atlantic Water Inflow in the Norwegian Sea after 2000 cal yr BP, which is driven by wind-stress (Giraudeau *et al*., 2010; Figure 1.14). These reconstructions resemble the reconstructed negative NAO period around 4300-2000 cal yr BP (Olsen *et al.*, 2012) indicating a NAO-driven storm track change through the Late Holocene. The results above demonstrate that some reconstructions show long-term trends and others cyclical variability in storminess; therefore further research is needed to explain these contrasting results.

Finally some research indicates that storminess and atmospheric circulation patterns are the result, at least in part, of solar activity changes. This has been suggested by Sabatier *et al.* (2011) who found that some, but not all, storm events coincided with periods of solar minima. Storminess reconstructions highlight that solar activity are linked to low and unsteady NAO values that allow jet stream fluctuations and enhanced cyclogenesis (Van Vliet-Lanoë *et al*., 2014; Wirth *et al.,* 2013). Finally the solar minimum c.2800 cal yrs

BP has been linked with an increase in storminess in Germany, which models suggest was the result of an abrupt change in atmospheric circulation (Martin-Puertas *et al.,* 2012). Therefore solar variability may be an external forcing for atmospheric and oceanic reorganisations, although this forcing is disputed by some storminess research (Sorrel *et al*., 2012; Fletcher *et al*., 2012).

In summary some European storminess reconstructions show centennial variability and others long-term trends that resemble the transition from negative to positive NAO. Some studies link these changes to internal oceanic circulation variability (Sorrel *et al*., 2012; Pena *et al*., 2010; Fletcher *et al*., 2012) and others to external forcing from insolation changes as the result of orbital and solar variability (Bakke *et al*., 2008; Sabatier *et al*., 2010). Therefore both the patterns and causes of storminess variability require further research.

1.4.3. Medieval Climate Anomaly

The MCA (~950-1400 A.D.; Diaz *et al*., 2011) was a period that in Europe is thought to have had warmer temperatures than the following LIA, with evidence of higher precipitation in northern Europe (Diaz *et al*., 2011; Hughes and Diaz, 1994; Lamb, 1965; Mann *et al*., 2009). There is some evidence that storminess was lower during the MCA, for example windblown sea salt (Na^+) measurements from the GISP2 ice core are thought to show less intense atmospheric circulation during the MCA (Meeker and Mayewski, 2002). This is also supported by reduced erosion of the Seine Estuary (Sorrel *et al*., 2009) and low windblown current strength in the Skagerrak Sea (Hass, 1996).

However there is also evidence of increased storminess at points during the MCA, for example at 850 A.D.. At this time enhanced storminess is suggested by: sand movement on the Aquitaine coast, France, from 650-1050 A.D. (Clarke *et al*., 2002), evidence of storms in estuarine cores in northern France at 750-950 A.D. (Billeaud *et al*., 2009), wind-blown sand to a Swedish peat bog at 850 A.D. (De Jong *et al*., 2006), higher wind-driven current strength in the Skagerrak Sea at 900 A.D. (Hass, 1996) and documentary evidence of high storminess in the North Sea in the 9th century (Lamb, 1995).

Other records show later MCA storminess at approximately 1050 A.D.. In Iceland evidence from an ocean core indicates heightened storminess at 850-

1250 A.D. (Andreson *et al.*, 2005) and the combination of an Icelandic glacier advance record with a marine record has also provided evidence supporting increased cyclonic activity around 950 A.D. (Stotter *et al.*, 1999; Witak *et al.*, 2003). This is similar to the timing of Scandinavian sand dune development at 1000-1200 A.D. (Clemmensen *et al.*, 2009) and widespread sand drift from c.1000 to 1300 A.D. across Europe (Janotta *et al.*, 1997). Both the periods of storminess at approximately 850 A.D. and 1050 A.D. are perhaps represented by cliff-top storm deposits in Scotland dated to 700-1050 A.D. (Hansom and Hall, 2009).

Finally there is some evidence of high storminess just prior to the LIA, from 1200 A.D. onwards. This has been recognised in documentary evidence (Lamb 1967), Swedish peat records (De Jong *et al.*, 2007, 2009), in sand dune development between 1200-1400 A.D. at Liverpool and Southport (Pye and Neal, 1993) and in marshland sand deposits from Brittany and western Ireland (Haslett and Bryant, 2007).

As these sites are mostly in northern Europe it may show that the storm track was in a northerly position. This would support that during the MCA there was a positive NAO (Trouet *et al.*, 2009). A north-south index of glaciers supports that there was a northerly storm track (Figure 1.14; Bakke *et al.*, 2008). There is also evidence of strengthened circulation of the Atlantic Meridional Overturning Circulation (Bianchi and McCave, 1999), Atlantic Water Inflow into the Nordic Seas (Giraudeau *et al.*, 2010), sub-polar gyre circulation (Thornalley *et al.*, 2009; Curry and McCartney, 2001) and less southerly extent of ice-rafted debris in the North Atlantic (Bond *et al.*, 2001). The oceanic circulation is in part influenced by the storm track position and oceanic wind stress caused by NAO changes, so the results support that there was a positive NAO during this time (Trouet *et al.*, 2009; Olsen *et al.*, 2012). This situation of strong ocean circulation and warm ocean temperatures (positive AMO) at a time of positive NAO has been hypothesised as occurring during the MCA (Figure 1.15 A; Van Vliet-Lanoë *et al.*, 2014). It is thought to have caused low intensity but frequent storms as a result of a low thermal contrast between the warm oceans and the warm atmospheric conditions (Van Vliet-Lanoë *et al.*, 2014). Further reconstructions of storminess, particularly for southern Europe, are required to confirm that the storm track was further north in this time. They are

also needed to establish the relative storm intensity compared to the LIA, as based on the NAO index higher storminess would be expected in northern Europe.

1.4.4. Little Ice Age storminess

The LIA occurred between approximately 1400-1850 A.D. and was a period that in Europe is thought to have had lower temperatures and higher storminess than the proceeding medieval period (section 1.4.3) and the twentieth century (Lamb, 1965; Mann *et al*., 2009; Matthews and Briffa, 2005). In the high latitudes increased storminess at 1400 A.D. is indicated in the GISP2 record by increased Na^+ values (reflecting increased sea-spray caused by storms) and by episodes of Icelandic loess formation between 600-100 cal yr BP (Jackson *et al.*, 2005).

On the British Isles increased storminess is suggested by cliff-top storm deposits on the Shetland Islands, deposited at 1300-1900 A.D. (Hansom and Hall, 2009) and on the Outer Hebrides (St Kilda) by the expansion of a maritime vegetation community (Walker, 1984). Along the coast of the Outer Hebrides sand movements created inland sand wedges in the early LIA between around 1400-1600 A.D. (Dawson *et al.*, 2004; Gilbertson *et al.*, 1999) and in Northern Ireland sand dune development occurred from 1450-1850 A.D. (Wilson *et al.*, 2004). On the Aran Islands, Ireland, large boulders were deposited onto cliff-tops and moved several metres during severe storms (Williams and Hall, 2004). In addition sand deposits within marshes in South Wales are loosely dated to the second half of the LIA from around 1600 A.D. onwards (Haslett and Bryant, 2007). However there were also variations within the LIA. Reconstructions using documentary evidence show that there were weak westerly winds between 1560 and 1700 A.D. and stronger westerlies in the early 1500's and c.1730 A.D., with 6 of the most severe storms at 1690-1720 A.D. and 1790-1840 A.D. (Lamb, 1967; 1991; Clarke and Rendell, 2009). Records of the numbers of gale days since 1770 A.D. from Edinburgh show lower numbers of gale days at 1770-1815 A.D. and 1845-1880 A.D. but higher numbers of gale days during the periods 1815-1845 A.D. and 1880-1918 A.D. (Dawson *et al.*, 2004). Therefore some records capture a general increase in LIA storminess, while others show more decadal variability.

The Maunder Minimum (1645-1715 A.D.) was the coldest time in the LIA as atmospheric blocking situations caused severe winters; however there were also documented severe storms and frequent gales especially in Spring and Autumn (Lamb, 1967; 1995; Luterbacher *et al*., 2001; Wheeler *et al*., 2010). For example, the September 1697 A.D. storm overwhelmed the site of Udal, Outer Hebrides, with sand and one of the historically most severe storms occurred in December 1703 A.D. affecting southern Britain (Defoe, 1704; Lamb, 1979; Lamb, 1991; Gilbertson *et al.*, 1999). On the Outer Hebrides severe storms also occurred after the Maunder Minimum in 1756 A.D., when Baleshare (North Uist) was buried in sand and in 1764 A.D. when a storm breached the Eoligarry Isthmus (Gilbertson *et al.*, 1999). Therefore the Maunder Minimum at the peak of the LIA was a time of extreme storms.

A different pattern has been shown by a reconstruction of wind-driven current strength in the Skagerrak Sea; it shows increased strength at the onset of the LIA c.1350-1550 A.D. and the end of the LIA from c.1750-1900 A.D., with a slower current during the intermediate period (Hass, 1996). It was suggested that the LIA transitions were a time when general westerly airflow in northern Europe increased (Hass, 1996). However other records from Scandinavia contradict this: a record of windblown sand into a peat bog has indicated that there was high storminess spanning the intervening time from 1550-1900 A.D. (De Jong *et al.*, 2006) and sand dune development occurred between 1550 and 1650 A.D. (Clemmensen *et al.*, 2008). Within this time storm surge frequency appears to have increased at 1600-1630, 1690-1720 and 1820-1850 A.D. (Aagaard *et al.*, 2007), with coastal flooding events in continental Europe at 1634, 1671, 1682, 1686 and 1717 A.D. (Lamb, 1995). Therefore as in the UK, Scandinavia appears to have had severe storms at the peak of the LIA, particularly during the Maunder Minimum.

In France a reconstruction from the Seine Estuary has indicated high storminess in the LIA between 1350 and 1650 A.D. (Sorrel *et al.*, 2009). Similarly a reconstruction of dune development from the southwest of France (the Aquitaine Coast) suggests storminess increased in the early LIA between 1400 and 1700 A.D. (Clarke *et al.*, 2002). However in a compilation of reconstructions from western Brittany it has been found that storminess was low in the early LIA (c. 1420-1530 A.D.) and was high particularly after 1700 A.D.

(Van Vliet-Lanoë *et al.*, 2014). Therefore the evidence from this region shows some conflicting timings.

Reconstructions of storminess in southern Europe show temporal variations during the LIA (Figure 1.13): a lagoon reconstruction from the northwest Mediterranean implies that there was high storminess during the mid-LIA from 1550 A.D. onwards (Sabatier *et al.*, 2012), a sand dune based reconstruction in Portugal may indicate high storminess from 1770 A.D. onwards (Clarke and Rendell, 2006) but also at 1550 and 1650 A.D. (Costas *et al.*, 2012), while in northwest Spain sand in-wash into a lagoon indicates that there was a severe period of storminess between 1680 and 1760 A.D. (Bao *et al.*, 2007). Additionally a marine record from northwest Portugal provides evidence of stronger hydrodynamic conditions during the LIA and therefore potentially higher storminess and precipitation (Martins *et al.*, 2012). However a reconstruction from the Bay of Biscay suggests only a small increase in storminess during the LIA (Mojtahid *et al.*, 2012). In southern Europe there is therefore some evidence of increased storminess during the LIA, but the magnitude and timing of increases vary between records.

1.4.5. Little Ice Age: atmospheric and oceanic circulation

There is some evidence that there has been a different relationship between the NAO and storminess during the LIA compared to the instrumental period. Broadly the understanding is that storminess during the LIA was higher than the present day (Sorrel *et al.*, 2012; Sabatier *et al.*, 2011; Lamb, 1995) and that the NAO during the LIA was frequently negative and neutral (Trouet *et al.*, 2009). The negative NAO would be expected to have directed the storm track across southern Europe, however as described above, storminess increased during the LIA in both northern and southern Europe. Temporal variations in the NAO-storm relationship have also been shown by documentary records. Dawson *et al.* (2002) compared the NAO with gale-day frequency in Scotland and Ireland during two periods (1885-1898 and 1983-1996 A.D.). In the latter period the highest gale-day frequencies occurred in years with positive NAO, supporting the positive correlation observed in the instrumental period (section 1.2.5); however, the earlier period had higher storminess when there was only slightly positive or even negative NAO values, something that is suggested as

being due to the influence of sea ice directing the storm tracks to the south (Dawson *et al.*, 2002). Therefore the NAO-storminess relationship has not been constant during the pre-instrumental period.

A similar explanation for the contradiction of high storminess across northern Europe when there were negative NAO conditions has been provided by Trouet *et al.* (2012). It has been hypothesised that during the LIA a steeper meridional temperature gradient caused intensified storms in the North Atlantic (Trouet *et al.*, 2012; Raible *et al.*, 2007; Lamb., 1995; Sorrel *et al.*, 2012), with some attributing this to steeper sea surface temperature gradients and sea ice at high latitudes (Sabatier *et al*., 2012; Bakke *et al*., 2008; Betts *et al*., 2004). This is a similar suggestion to the proposal by Dawson *et al.* (2002), except that Trouet *et al.* (2012) emphasise the importance of the NAO through the LIA, in directing the storm tracks more frequently south but suggest that storms when they infrequently crossed northern Europe were more intense.

These hypotheses are supported by much evidence of an altered North Atlantic Ocean circulation (Figure 1.14), which is likely to have changed the latitudinal temperature distribution. Documentary evidence supports that during the LIA polar waters moved further south, as there were frequent failures of cod fisheries in the Faroe Islands and Norway and southern extension of sea ice from 1600-1830 A.D. (Lamb, 1979). In addition sea ice proxy reconstructions suggest that sea ice increased from 1300 A.D., in the late 1400's A.D. and between 1600 and 1900 A.D. (Masse *et al* 2008) and ice-rafting reached further south in the North Atlantic between 1350-1850 A.D. (Bond *et al.*, 1997). The northward progression of the Gulf Stream is thought to have been limited, instead only reaching as far north as the Iberian Peninsula (Lamb, 1979; Mörner, 2010), which is also shown by reduced Atlantic Water Inflow into the Nordic Sea (Giraudeau *et al.*, 2010). Furthermore the weakening of the thermohaline circulation is supported by evidence indicating there was a reduced Iceland-Scotland Overflow Water intensity (Bianchi and McCave, 1999) and weakened subpolar gyre circulation (Thornalley *et al.*, 2009). During the instrumental period the reduced strength of the Atlantic Water Inflow and subpolar gyre circulation are associated with *negative* NAO conditions (Giraudeau *et al.*, 2010; Thornalley *et al.*, 2009; Copard *et al.*, 2012; Orvik *et al*., 2001; Curry and McCartney, 2001). Therefore it appears that the weaker ocean

circulation during the LIA was reflecting the negative NAO circulation pattern, and may explain the increased temperature gradient thought to have increased storm intensities.

Precipitation proxies are less affected by changes in storm intensity and have supported that the storm track during the LIA was in a more southerly position in accordance with the negative NAO. In northern Europe, the North-South Index of precipitation along Norway's western coast supports that there was a more southerly storm track at c.1350-1550 A.D. (Bakke *et al*., 2008). Higher flooding in the southern Alps compared to the northern Alps also indicates that the storm track was in a more southerly position during the LIA (Wirth *et al.*, 2013). Therefore in ocean and precipitation proxies there is evidence that during the LIA there were more southerly storm tracks as would be expected during times with negative NAO conditions.

1.4.6. Cyclicity in NAO and storminess reconstructions

Spectral frequency analysis of the instrumental and reconstructed NAO has been done to assess periodicity (Table 1.1) as identification of cycles is a method that can improve predictability and allow causes to be identified (e.g. Debret *et al.,* 2007; Gray *et al.,* 2010). From the reconstructed NAO indices Cook *et al.* (1998), Appenzeler *et al.* (1998), Glueck and Stockton (2001), Luterbacher *et al.* (1999) and Olsen *et al.* (2012) all identified spectral powers between 58 and 90, which are perhaps comparable to each other. Wavelet analysis allows changes in variability through time to be assessed; this method has indicated that NAO cycles between 2-32 years have had no persistent mode of oscillation (Rodrigo *et al.* 2001; Appenzeler *et al.*, 1998). However Luterbacher *et al.* (1999) and Appenzeler *et al.* (1998) found periods of enhanced and reduced variability. The longest NAO record by Olsen *et al.* (2012) has allowed the identification of longer NAO cycles of ~170 and ~300 years. Therefore there is evidence of multi-annual, multi-decadal and multi-centennial trends in the NAO, which are likely to have produced changes in the European climate and storminess.

Table 1.1: Summary of cycles identified in proxy and instrumental NAO data using spectral analysis.

Journal Article	Method	Cycles/Powers (years)
Instrumental NAO Records		
Rogers (1984)	Instrumental pressure reconstruction	7.3-8,0
Schneider and Schonwiese (1989)	Instrumental pressure reconstruction	1.7, 2.2
Hurrell and Van Loon (1997)	Instrumental reconstruction	2.5, 6-10
Proxy NAO Reconstructions		
Cook *et al.* (1998)	Multiproxy reconstruction, including dendrochronological and ice core data	2.1, 3, 8, 23, 70 (latter in last 120 yrs)
Appenzeler *et al.* (1998)	Proxy reconstruction: ice core accumulation record	5-7, 9-11, 12-14, 80-90 (since 1850 AD)
Luterbacher *et al.* (1999)	Documentary observations and dendrochronology	54-68
Proctor *et al.* (2000)	Proxy reconstruction based on speleothem band width	6-9
Glueck and Stockton (2001)	Proxy reconstruction: dendrochronology, GISP2 $\delta^{18}O$ and accumulation records	2.4, 6.5, 20.9-29.3, 60
Cullen *et al.* (2001)	Composite reconstruction using proxy and instrumental records	2.3 (2.3, 7-8, 12.5)
Olsen *et al.* (2012)	Proxy reconstruction of lake hypolimnic anoxia	~20, 50-70, ~170, ~300

Most storminess reconstructions have not been analysed for cycles, partly due to the discontinuous nature of the data (e.g. dated sand dune units), however spectral analysis has been used on some of the continuous storm reconstructions and have indicated long, multi-centennial cycles. A cycle of 1500-1700 years has been observed in the GISP2 sodium reconstruction, which is thought to reflect sea-spray and atmospheric circulation in the North Atlantic, and similarly a 1700 year cycle has been identified in a loess reconstruction from Iceland (Figure 1.16; Debret *et al.*, 2007; O'Brien *et al.*, 1995; Jackson *et al.*, 2005). Furthermore in southern Europe a 1750 year cycle has been identified in a proxy for westerly airflow in the Mediterranean, which it has been suggested is the result of fluctuations between weak and zonal airflow (Fletcher *et al.*, 2013). This 1500-1700 year cycle therefore appears to reflect atmospheric circulation changes in Europe, and as this cycle is present in ocean circulation records it is considered to be the product of an ocean-atmospheric linkage (Debret *et al.*, 2007). A similar cycle of 1500 years has been identified in a number of climate and ocean reconstructions (e.g. Bond *et al.*, 1997; Bianchi and McCave, 1999; Pena *et al.*, 2010) and this pacing has also been identified in a compilation of storminess reconstructions from northern Europe (Sorrel *et al.*, 2012). This may support the link between storminess and the ocean, which was described during section 1.4.

Centennial and decadal cycles have also been identified in a couple of reconstructions. Flooding in the Alps during the Holocene had cycles of 500, 350 and 250 years as well as cycles between 150-70 years (Wirth *et al.*, 2013), which are likely to have been the result of low pressures. Spectral analysis of the GISP2 sodium reconstruction for the last 1000 years has also identified cycles of 62 and 10 years (Fischer and Mieding, 2005). Therefore, although not widely assessed, it is apparent that there are decadal and centennial scale cycles causing variations in atmospheric circulation.

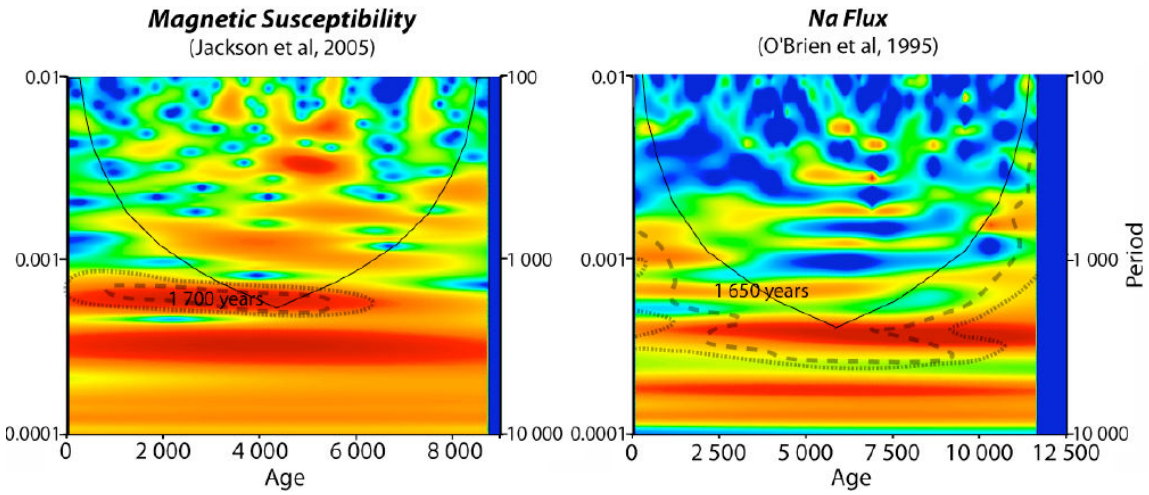

Figure 1.16: Wavelet spectral analysis of storminess reconstructions: the loess magnetic susceptibility reconstruction from Iceland (Jackson *et al.*, 2005) and the GISP2 sodium flux (O'Brien *et al.*, 1995), both calculated by Debret *et al* (2007, pg 572). The occurrence of cycles with respect to time is shown by the yellow and red, with the dashed line showing the cycles over the 95% significance level. The continuous line is the cone of influence: as the timeseries are finite in length and therefore padded by zeros during analysis the cycles outside the cone are likely to be underestimated.

1.5. Chapter summary

This chapter has summarised the connection between the NAO and storminess during the instrumental period and the Late Holocene. The NAO during the instrumental period causes opposite patterns of winter storminess between northern and southern Europe by its influence on the storm track, with storm intensity also increased during positive NAO periods. Over the instrumental period it is also clear that a number of multi-annual and multi-decadal cycles occur.

For the pre-instrumental period storminess and the NAO have been reconstructed using various methods, with the results showing complex and often contradictory patterns. Some storminess reconstructions indicate long-term storm track shifts while others provide evidence supporting multicentennial peaks in storminess. Findings suggest that there has been variability in the NAO-storm relationship over long timescales, with the LIA used as an example of a time when storminess was apparently high across much of Europe, despite a negative NAO. The recent hypothesis suggesting that increased storminess was due to a steeper temperature gradient during the LIA (Trouet *et al*., 2012) means that the storm-NAO relationship requires investigation. Studies have also speculated about storminess forcings, which include internal oceanic, solar and orbital changes.

In the following chapter the research design will be outlined, which will show how this project will investigate past storminess and seek to improve our understanding of the NAO-storm relationship during the Late Holocene. The chapter will include justification of the key aims and research questions that this study will be addressing. It will also outline and justify the study sites and methods that have been chosen.

Chapter 2: Research design

2.1. Introduction

Research into past climatic change requires not only reconstructions from single locations, but spatially distributed reconstructions that are of a high enough temporal resolution to capture changes in atmospheric circulation patterns, such as the NAO. This research investigates past storminess from two locations in northern and southern Europe, to better understand past storminess changes and storm track shifts. As these locations are in NAO-sensitive regions the storminess reconstructions from here will be used to investigate the relationship between the past NAO and storminess. As was made clear in Chapter 1, there is a contrast between the NAO-storminess relationship during the instrumental period and during climatic 'events' such as the Little Ice Age, which has raised questions over the importance of the NAO in the past.

The project has two overriding **aims**:

1) To create and compare Late Holocene storminess reconstructions from northern and southern Europe

2) To assess the causes of storminess variability during the Late Holocene, in particular the role of the North Atlantic Oscillation

To help achieve these aims four **research questions** have been determined:

1) What are the temporal patterns of storminess during the Late Holocene in northern and southern Europe?

2) Do the storminess reconstructions from northern and southern Europe show storm track changes or widespread, synchronous storminess variations?

3) What do the patterns of storminess and inferred storm track changes tell us about the storm-NAO relationship?

4) What do the results tell us about the causes of storminess variability?

In the following section these research questions will be described and justified. After the research questions have been explained, the methodology and chosen study sites are then justified. These outline why the study sites were chosen, and why the methods used to create the reconstructions were selected. Finally the methodological precision is investigated.

2.2. Research Question 1:

What are the temporal patterns of storminess during the Late Holocene in northern and southern Europe?

In this project aeolian deposits in lake and peat sedimentary archives are used to create reconstructions of Late Holocene storminess. These will complement the growing collection of storm reconstructions that span the Late Holocene. Long reconstructions with annual to multi-decadal resolution have been made from various regions, in particular from Scandinavia, France and the high latitudes (e.g. De Jong *et al.*, 2006; Sabatier *et al.*, 2011; O'Brien *et al.*, 1995), however such detailed reconstructions are lacking from many areas. This research will focus on northwest Scotland and northwest Spain (see section 2.6), which are two locations exposed to high storminess from the North Atlantic but are currently lacking high resolution storm reconstructions. The period of interest is the last 4500 cal yr BP: as explained in Chapter 1 reconstructions provide evidence that the Late Holocene had oceanic and atmospheric circulation variability at decadal and centennial resolutions, which have been related to storminess changes in Europe. Further reconstructions will help to disentangle the spatial and temporal patterns of storminess in Europe during these circulation alterations.

Spectral analysis will be carried out on the storminess reconstructions to identify cycles within these (described in section 2.8.3.). In the IPCC report (2013) low-medium confidence in projections of future changes in the northern hemispheres storm track and the NAO were partly attributed to poor understanding of the internal variability of these (Stocker *et al*., 2013), therefore understanding this variability is key. Currently few reconstructions of storminess have looked at the decadal cyclicity present in their records, so this is an area requiring further research. Therefore cycles in Late Holocene climate will be

investigated using spectral analysis, which may enable greater predictability of storminess changes.

2.3. Research Question 2:

Do the storminess reconstructions from northern and southern Europe show storm track changes or widespread, synchronous storminess variability?

The contradiction between storminess reconstructions from the LIA that suggest widespread storminess variability and others that suggest storm track shifts has been outlined in Chapter 1. By analysing storminess from both north and south Europe, the intension is that latitudinal storm track shifts or widespread increases in storminess can be detected, which can help show whether storm intensity or storm track changes have caused regional storminess changes during the Late Holocene.

2.4. Research Question 3:

What do the patterns of storminess and inferred storm track changes tell us about the storm-NAO relationship?

In this project the locations of the Outer Hebrides and Galicia have been chosen as these sites are sensitive to the NAO changes in precipitation and wind (Figure 2.1), based on data from the instrumental period (Andrade *et al.*, 2008; Trigo *et al.*, 2002; Pirazzoli *et al.*, 2010). Therefore these sites are well placed to capture the changes in storminess that are related to the changes in the NAO, with increased storminess in the Outer Hebrides during positive NAO anomalies and in Galicia during negative NAO anomalies. Discussions in the literature have focused on the unexpected NAO-storm relationship during the LIA, as there was high storminess in northern Europe when the NAO was negative (which would under modern conditions cause lower storminess), something which it is suggested was the result of a steeper latitudinal temperature gradient causing more intense storms (Trouet *et al.*, 2012; Lamb, 1995; Raible *et al.*, 2007; Sorrel *et al.*, 2012). Research into the storm-NAO

relationship over the whole Late Holocene is enabled by a recent NAO reconstruction, which spans from 5000 cal yr BP to present (Olsen *et al.*, 2012), which in this research will be compared against long storminess reconstructions from northern and southern Europe. These are used to investigate whether periods with persistent negative NAO during the Late Holocene have, like the LIA, been associated with higher storminess across Europe. The assessment of the relationship between the NAO and storminess is further enabled by the analysis of cycles in the storminess reconstructions, which allows comparison with cycles typically identified in the NAO (see sections 1.4.6), as similar cyclicity may show if the modern NAO-storm relationship has been consistent through the Late Holocene.

The strong influence from the NAO on the climate of the selected regions and the debates surrounding the NAO-storminess relationship are key reasons for carrying out this research. As the results chapters are structured as papers, these debates are reviewed in the introductions and considered in the short discussion sections of these chapters. In the discussion chapter (chapter 6) these debates are considered in much greater detail, considering not only the results from both the Outer Hebrides and Galicia, but also results from elsewhere in Europe and the North Atlantic.

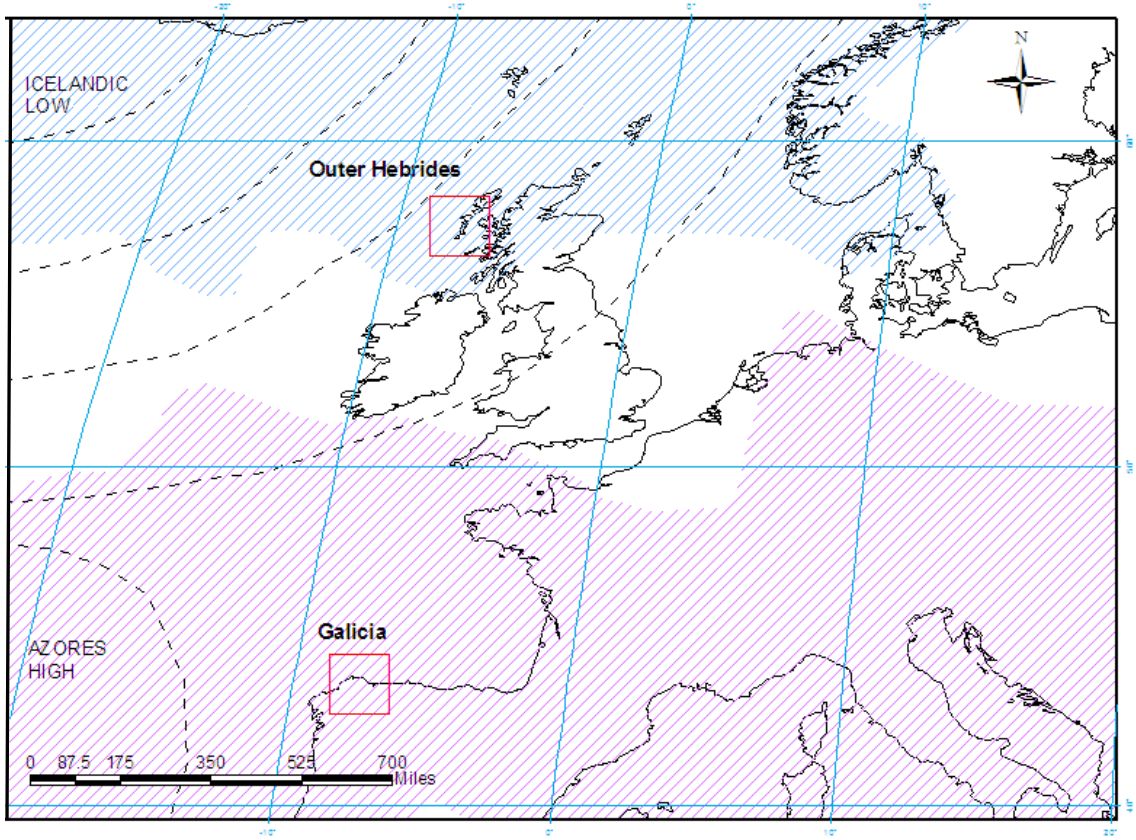

Figure 2.1: Illustration of the locations of the Icelandic Low pressure and Azores High pressure (dashed lines) and the influence on cyclone frequency in Europe. The blue and red shaded regions are where there are significantly increased cyclone numbers in years with positive (>1) and negative (<1) NAO indices respectively (based on the analysis of instrumental data by Andrade *et al.*, 2008, pg 751). Red rectangles show the location of the chosen study sites in the Outer Hebrides (Scotland) and Galicia (northwest Spain).

2.5. Research Question 4:

What do the results tell us about the causes of storminess variability?

The causes of storminess variations over the Late Holocene have been debated; with the question investigated by comparison of storminess reconstructions with solar, oceanic and orbital reconstructions. Some support that there has been oceanic forcing of storminess and storm tracks (e.g. Sorrel *et al*., 2012; Sabatier *et al*., 2011; Pena *et al*., 2010; Fletcher *et al*., 2012), others orbital forcing through changes to the latitudinal insolation receipt (e.g. Bakke *et al*., 2008; Wirth *et al*., 2013) and others solar forcing (e.g. Van Vliet-Lanoë *et al*., 2014; Sabatier *et al*., 2011). An alternative method has been used by Debret *et al.* (2007), who compared the spectral frequencies of storminess, solar and oceanic reconstructions, and concluded that there were oceanic-like cycles (of 1500-1700 years) present in the storminess reconstructions. The contrasting findings of these studies show that further research is required. In this research the storminess reconstructions will be compared with reconstructions that are proxies for solar and oceanic changes, as well as the known orbital changes, in addition to spectral analysis. These methods will provide the basis for inferring the causes of storminess variability.

The understanding of what causes storminess variability is important for determining how storminess may increase or decrease in response to future climate change. As explained in section 1.2.4., it has been predicted that changes to the temperature gradient through oceanic warming and Arctic cooling may increase European storminess (Stocker *et al.*, 2013; Catto *et al.*, 2011; Woolings *et al.*, 2012; Francis and Vavrus, 2012). Investigation of the effect on storminess from changes to the latitudinal temperature gradient during the Late Holocene may therefore allow greater confidence in predictions of future storminess.

2.6. Site selection justification

Full site descriptions will be given within the results chapters (3-5), however here the choices of study sites are justified. In this chapter the decisions underpinning the site selection are described, so that it is clear how the four sites complement each other, address the research questions and share site selection criteria. As the results chapters are structured as papers these include Study Area sections, which reiterate some of the reasons for site selection described here, but provide greater detail and are more focused on the local site or region. As described above, the Outer Hebrides and Galicia were selected as locations that under modern climate conditions are influenced by the storm track during positive and negative NAO anomalies respectively (Figure 2.1), so storminess reconstructions from these locations are appropriate for investigating the influence of the NAO on storminess.

The premise of the research therefore is that sand deposition onto the studied peatbogs or lakes will increase when there are more frequent or intense storms. However it must be considered that storm track changes will not necessarily cause an increase in sand deposition onto the sites: for example a storm crossing to the north or south of a location will cause winds from the west or east respectively. The sand source in the Outer Hebrides is the machair and beaches which are along the western side of the islands; therefore storms may not transport sand if they pass to the south causing easterly winds. Therefore it is noted that low sand deposition onto the study sites may not always signify that there were weak storms, but may indicate that the storms were not passing to the north.

The Outer Hebrides and Galicia were considered suitable as they contained terrestrial sedimentary archives in the form of peat bogs and lakes, from which continuous records of storminess can be produced. The choice of peat bogs was determined by two factors. Firstly the peat bogs were required to be ombrotrophic, so deposited sediment has originated from the atmosphere and has had to undergo aeolian transportation (de Vleeschower *et al.*, 2010; Allan *et al.*, 2013). Secondly the peat bogs were required to be close to sand or sediment sources, to provide material for aeolian entrainment and transport during storms. In the Outer Hebrides the high annual precipitation and low evapo-transpiration means there is excess surface water that has allowed peat

lands to form extensively at low levels (Boyd and Boyd, 1990). Much of the peat covered area is blanket bog however a number of ombrotrophic, raised peat bogs are situated in natural depressions in the underlying bedrock (Angus *et al.*, 1997). Therefore in the Outer Hebrides there was the ideal situation of slowly accreting ombrotrophic peat bogs in close proximity to abundant sand sources.

To identify peat bog sites in the Outer Hebrides multiple sites were initially identified using satellite images. These were visited and the depth of peat tested using rods, as deeper peat indicates faster sediment accumulation rates that show the potential of the site for high resolution records. Two deep (6m), ombrotrophic and previously uncored bogs were identified; one on North Uist and the other on South Uist (Figure 2.2). The selected peat bogs on the Outer Hebrides formed to the east of the machair sand ecosystem, which lines the Outer Hebrides west coast, so during storms with westerly winds sand does not need to travel more than 2 km to reach the selected bogs.

Due to financial and time constraints during the research, fieldwork could not be carried out in Galicia as it had in the Outer Hebrides. However a core with a highly resolved chronology from a suitable bog in Galicia was donated to this research by the ACCROTELM project (EU FP5 ACCROTELM project, Prof. Fraser Mitchell, TCD). As only a single site was assessed in Southern Europe, the resulting reconstruction of storminess from southern Europe is less certain than those from the Outer Hebrides, as multiple sites provide a more cohesive picture of regional climate and limit local factors.

In Galicia the blanket bogs are the southernmost in Europe (Díaz Varela *et al.*, 2008) and include ombrotrophic bogs. The peat lands form in the higher altitude mountains where there is higher precipitation and cooler temperatures than the lower altitude coastal areas (Martínez-Cortizas *et al.*, 1997). As the peat bogs form in high altitudes in Galicia these were not located near sea level and beaches, therefore a compromise was required. The Galician ombrotrophic peat bog is therefore a distance of around 25 km away from the nearest beaches, which are to the northeast. As sand (62.5 – 2000 μm) travels through saltation, and only rarely through suspension (Bagnold, 1937) it seems unlikely that sand can travel 25 km during storms, and therefore it is considered more likely that eroded soil has been entrained during storms and blown onto the bog.

The site selection was also influenced by other considerations. It has been suggested that sand influx (or dust influx) to peat bogs can be caused by human land disturbance around the sites (Martínez-Cortizas *et al.*, 2005). In the Outer Hebrides multiple sites were used to reduce the effect of human influence on the reconstructions. As both North and South Uist will be affected by the same storms, the records would be expected to show similar patterns, so influxes of sand only present in single sites are more likely to have resulted from human disturbance. The Pedrido Bog core was analysed prior to the start of this project using various proxies including pollen analysis. Therefore these results are used to allow assessment of the past human disturbance of the area surrounding the bog. Despite these steps to separate the human and climatic influence on sand influx to the study sites, it is likely that there has been a complex relationship between these factors. For example, in the Outer Hebrides climate deteriorations accompanied by heightened storminess may have caused people to rely on the resources provided by the dune system (e.g. marram grass for thatch, sand for fertiliser), which may have destabilised the fragile dune environment and led to enhanced windblown sand (Angus and Elliot, 1992; Gilbertson *et al*., 1999; Sommerville *et al.,* 2007). Similarly in Galicia harsh climates may have caused additional human pressure on vegetation (Martinez Cortizas *et al.,* 2009). Furthermore volcanic eruptions are thought to cause higher storminess in northern Europe (e.g. Fischer *et al*., 2007) however some eruptions such as the 1783 Laki eruption caused acid deposition, causing damage to crops and other vegetation (Grattan and Charman, 1994), This may have influenced sand erosion if dune vegetation was damaged or increased peoples reliance on marginal land following crop failure. Therefore climatic or environmental changes may have at times led to changes in human activities that enhanced the amount of sand being blown by storms.

In the Outer Hebrides a number of lakes were visited however only one, Loch Hosta (North Uist), was considered suitable based on physical characteristics and location. Loch Hosta was directly adjacent to the machair and within 0.7 km of the beaches, providing sediment sources for aeolian transport of sand during storms. It was also required that the lake was deep enough to limit the resuspension of sediments by wind mixing and to have limited bioturbation. The other investigated lakes were around one to two metres deep as they have formed on low lying, relatively flat land behind the

machair. Loch Hosta was the deepest lake investigated with a maximum depth of 11 m on its eastern side. In Galicia coastal lagoons were considered as an option for creating storm reconstructions however previous studies on these showed that they had stratigraphical complexity (Bao *et al.*, 2007; González - Villanueva *et al.*, 2009; Santos *et al.*, 2001), which made them unsuitable for creating the high-resolution and continuous reconstructions of storminess that were aimed for in this project.

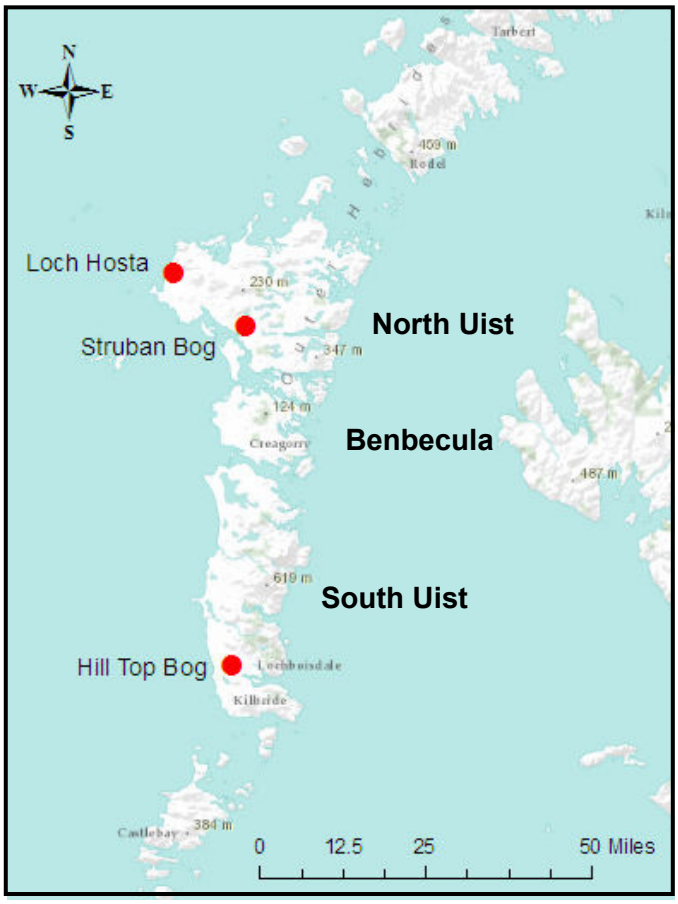

Figure 2.2: Map of the location of the study sites in the southern Outer Hebrides. Red points show the study sites of Loch Hosta, Struban Bog and Hill Top Bog.

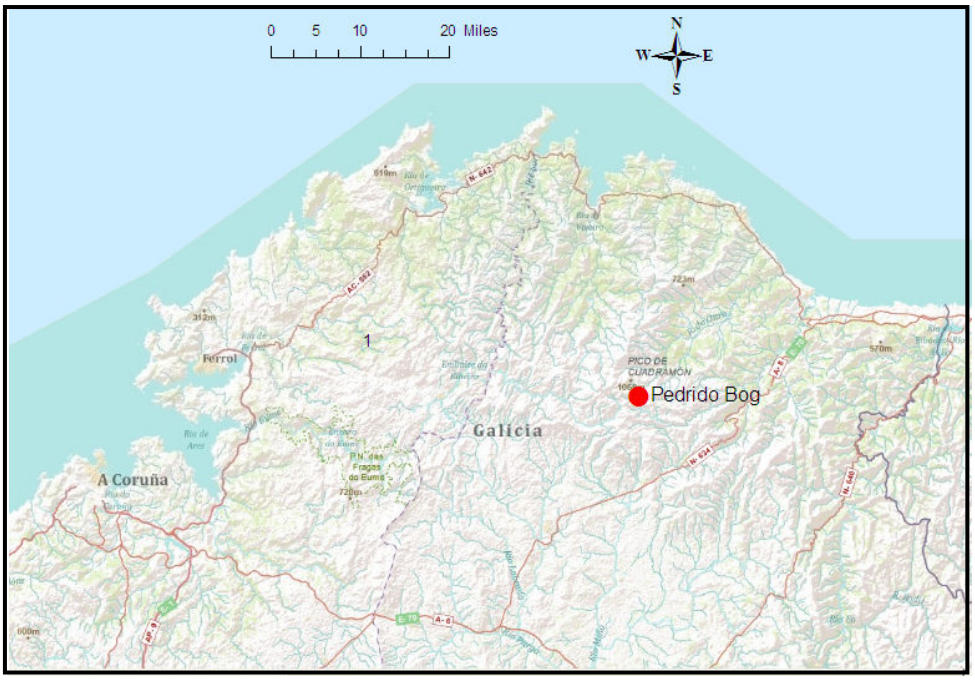

Figure 2.3: Map of the location of Pedrido Bog (red point) in Galicia, northwest Spain.

2.7. Methodological justification:

In this section the methods used to identify aeolian sand in peat bogs and lakes will be described and justified. The issues surrounding climatic reconstructions from these environments will also be considered and any measures taken to mitigate these will be outlined. The focus here is on the methods used at every site and the central concept that storms can be identified by aeolian sand deposits. However the results chapters also include detailed methods sections, because these chapters are structured as papers and there are some differences in the methods used at each site, particularly in the reconstruction from Loch Hosta (Chapter 3). Furthermore potential limitations of using lake and peat bog environments are described here, as these considerations were important for site selection and coring procedures, but are also discussed within the results chapters, as some of these may have influenced the results.

2.7.1. Peat bogs

Ombrotrophic peat bogs contain archives of atmospherically derived material, including aerosols and dust (deVleeschower *et al.*, 2010; Allan *et al.*, 2013). The dust flux to bogs has been identified using analysis of the elements present, which reflects the source of sediments (e.g. Allan *et al.*, 2013; Martínez-Cortizas *et al.*, 2005; Le Roux *et al.*, 2006) and using the ash (or ignition residue) of the peat, which reflects the total inorganic material present (e.g. Björck and Clemmensen, 2004; Zaccone *et al.*, 2012). The dust reaching bogs can originate from deserts, for example Saharan dust has been identified in the Pyrenees (Bücher and Lucus, 1984; Goudie and Middleton, 2001); from volcanic eruptions, for example Icelandic eruptions frequently deposit tephra across northern Europe (e.g. Dugmore *et al.*, 1995); and finally from local and regional soils and beaches (Allan *et al.*, 2013; De Jong *et al.*, 2006). The entrainment of dust is frequently related to vegetation cover, both local and regional, as a response to climatic changes (such as aridity) or human activities (Lawrence and Neff, 2009; Martínez-Cortizas *et al.*, 2005; Marx *et al.*, 2011; Allan *et al.*, 2013). The processes that have been found to be important for the transport and deposition of dust include wind speed, wind direction and storms (Bao *et al.*, 2012; Marx *et al.*, 2011; Fábregas Valcarce *et al.*, 2003), so dust reconstructions are also used as proxies for these. There are therefore complex interpretations of dust within peat bogs, as the content can be influenced by changes to the source or transport pathway. In this research the sediment of interest is that transported from local sources, which means focusing on the sand rather than the dust fraction.

As mentioned above dust in Europe can include Saharan long-range dust, which is 5-30 μm in size (Bücher and Lucas, 1984), and Icelandic tephra found in Great Britain that is around 10-100 μm in size (Hall and Pilcher, 2002). Therefore in this research the sand >100 μm in size are measured as long-distance dust and tephra transport would otherwise interfere with the signal of locally derived sediment being transported onto the bog during storms. Unlike dust, sand sized particles (62.5-2000 μm) are rarely carried in suspension (Bagnold, 1937). Sand between 70-500 μm predominantly travels by saltation: particles are carried along a trajectory through the air, for distances greater than 8 m in some instances, before returning to the surface and either settling, saltating again or dislodging other grains that saltate (Bagnold, 1937; Kok *et al.*,

2012). Sand >500 μm travels more often by reptation (jumps short distances < 1cm; Anderson, 1987) or creep (grains rolled or splashed by saltating grains; Bagnold, 1937; Kok *et al.*, 2012). The saltating grains are therefore the most mobile and likely to have been deposited on the bog surface. Although these grains are likely to be between 100-500 μm in size, it has been noted that the size fractions of the transportation modes are not fixed, and that stronger winds could potentially transport sand >500 μm through saltation (Kok *et al.*, 2011). The chosen measured sand fractions were therefore the 120-180 μm and >180 μm fractions. The lower boundary excludes the dust fraction, which may confuse the interpretation. The division of these two fractions is rather arbituary, however the larger grains are likely to have required more intense winds to have transported them onto the study sites, so was defined to separate between periods with moderate and intense storminess.

In peat bogs the methodology of analysing non-visible sand layers was developed by Björck and Clemmensen (2004) and De Jong *et al.* (2006) using peat bogs from Sweden; the analysis of sand content was done using the ignition residue and Aeolian Sand Influx (ASI), which is a measure of the number of grains above a certain size threshold. This method has not currently been used outside of Sweden; however it allows high resolution and continuous reconstructions of storminess, so this methodology, with some minor adaptations, has been used in this research. A difficulty with this method is that a frequent number of medium-magnitude storms could result in more coarse grains being deposited than a single extremely severe storm. The method used here of *weighing* rather than counting the sand grains over a certain size (as used by Björck and Clemmensen, 2004) mitigates this problem slightly, as large sand grains deposited by severe storms will weigh more and thus increase the measurement, compared to the counting method where within the size brackets each grain is considered equal. This method is outlined in section 2.8.1.

Considerations

The deposition of sand can be influenced by factors such as precipitation. Precipitation can prevent the aeolian entrainment of sand as moisture creates inter-particle forces that inhibit saltation (Kok *et al.*, 2012; Chepil, 1956; McKenna-Neuman and Nickling, 1989). Experiments have found wet sand requires a higher threshold sheer velocity to initiate transport than dry sand, however once the threshold has been exceeded the wet and dry sand are transported equally (Hotta *et al.*, 1984). On beaches in the Netherlands this finding was supported, and furthermore it was found that days with moderate rainfall such as showers were able to transport greater amounts of sand than dry days with similar winds, as raindrops encourage sediment transport by dislodging sand grains (Arens, 1996). However when the sand was saturated under prolonged rainfall, the transport of sand was close to zero regardless of the wind speed (Arens, 1996). As such it was concluded that extreme events, often accompanied by high rainfall and high seas (which cover the sand) are less important for total sand transport than moderate events with strong winds and less rainfall (Arens, 1996). Furthermore it has previously been found that the cumulative effects of moderate aeolian events are more responsible for the majority of sand movement than rare, extreme events (Wolman and Miller, 1960). Therefore the inland transport of sand during storms onto the study sites may be reduced by storms with continuous precipitation, but otherwise will reflect patterns of storminess.

Vegetation is another factor that can influence the amount of sand transported during storms, as there is an exponential increase in sand transport when vegetation is reduced (Wasson and Nanninga, 1986; Lancaster and Bass, 1998). Figure 2.4 illustrates the relationship between vegetation cover, wind speed and sand transport; when vegetation cover is greater than 30% sand transport is low, however as vegetation cover is reduced below 30% there is a steep increase in sand transport, particularly at high wind speeds (Wasson and Nanninga, 1986). Therefore in both Galicia and the Outer Hebrides the amount of sediment being transported may at times have been related to land cover changes, rather than storminess changes, so this will need to be considered in the interpretation of the results.

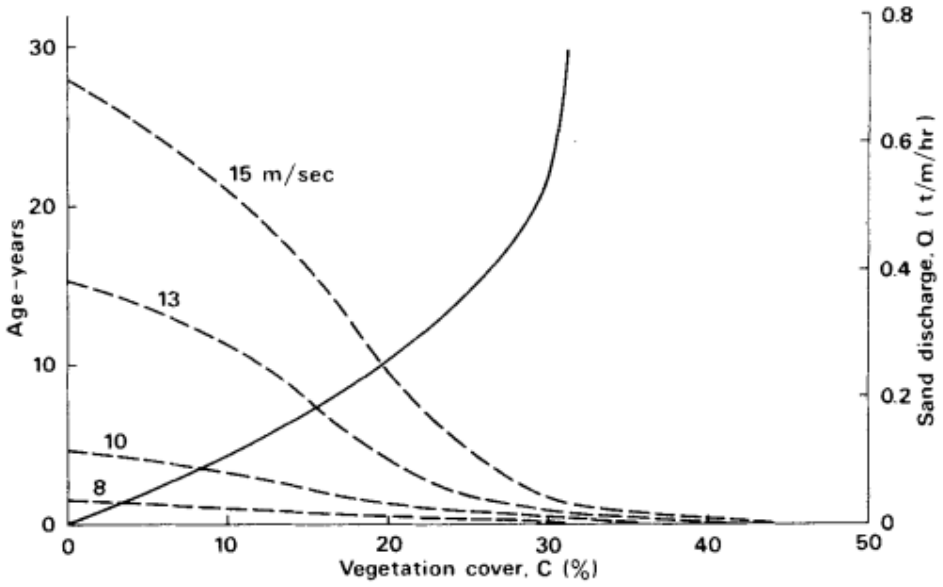

Figure 2.4.: Graph illustrating changes in the sand transport rate (or discharge) at different wind velocities (dashed lines) as vegetation cover changes. Based on changes in Spinifex cover in an arid Australian environment (Wasson and Nanninga, 1986, pg 509)

There is also an issue of intra-bog differences in peat bogs. Previous research that has compared reconstructions of heavy metals and testate amoebae within ombrotrophic bogs have found that broad changes or trends are captured in multiple cores but often there are differences in short term variations (Coggins *et al*., 2006; Bindler *et al*., 2004; Mauquoy *et al*., 2002; Hendon *et al*., 2001). These are thought to be due to microform variability (for example coring of hummocks or hollows) that influence the trapping of heavy metals, vegetation type and accumulation rates (Bindler *et al*., 2004; Coggins *et al*., 2006; Robinson and Moore, 1999) or the result of coring bog margins (Hendon *et al*., 2001). To investigate this influence the peat bogs from the Outer Hebrides were cored in 4 locations: a main core from a central bog location, and a transect of 3 short cores from across the bog.

Finally another factor that can influence the dust content of peat is post-depositional weathering due to acidic bog conditions; research found acidity can destroy some rock types, such as calcite, below the surface (Le Roux *et al.*, 2006). In the Outer Hebrides there are abundant sources of shell sand, consisting of both quartz grains and calcium carbonate shells, so therefore it

was considered that the acidity of the peat bogs may dissolve the shell sand at depth. To remove the possibility of higher measurements of sand in the upper sediments, as the result of incomplete dissolution of calcium carbonate, the peat samples were treated with acid prior to analysis to remove any remnants of calcium carbonate from the samples (as described in section 2.8.1.).

2.7.2. Lakes

In lake sediments the processes controlling sediment accumulation are more complex, as soil and sand entering the lake can be from both aeolian transport (particularly from smaller suspended grains as sand cannot saltate across water) and fluvial transport. In the literature many studies of lake sediment have focused on in-washing of sediment as the result of high precipitation events (e.g. Noren *et al.*, 2002, Page *et al.*, 2009). In coastal lagoons and lakes storminess has been identified using sand deposits washed in by large waves (e.g. Dezileau *et al.*, 2011; Yu *et al.*, 2009; Sabatier *et al.*, 2012). As low pressure systems and storms in Europe are associated with both stronger winds and higher precipitation, which both correlate similarly with the NAO (Serreze *et al.*, 1997; Andrade *et al.*, 2008; Marques *et al.*, 2008), the separation of sediment that has been in-washed or in-blown may be irrelevant, with lake sediment reconstructions providing a low-pressure proxy rather than a wind strength proxy.

In this project multiple methods have been used to better understand the complex lake system. These methods are explained in detail within the methods section of the Loch Hosta results chapter (section 3.3). To detect sand layers within the lake sediment the elemental composition was analysed using an ITRAX XRF core scanner, which was calibrated using traditional XRF measurements along the core (and the calibration method of Weltje and Tjallingi, 2008). The element analysis of the lake sediment is complimented by traditional XRF analysis of samples from the lake catchment (nearby hillslopes and rivers) to support the interpretation of the sources of elements present in the lake. As on the peat bogs, the sand content of the lake sediment was analysed by sieving the sand sized fractions; similar methods have been used by Yu *et al.* (2009) and Parris *et al.* (2010). The carbon:nitrogen content of organic matter in lakes is controlled by its source: organic matter from terrestrial

plants has abundant cellulose causing high C:N ratios (>20), while organic matter from lake algae are without cellulose, causing low C:N ratios (4-10) (Meyers, 1994). Therefore by assessment of the C:N content of the lake sediment the source of organic material to the lake (both allochthonous and autochthonous) can be measured. This method has previously been used in lakes to indicate changes in precipitation (e.g. Mayr *et al*., 2007) and human activity (e.g. Rosenmeier *et al.,* 2004). Therefore the C:N analysis combined with the sand-fraction analysis was designed to support that the elemental signature of sand was reflecting in-washed or aeolian deposition of sand.

Considerations

Here the influences of biological activity and wave driven disturbance are explained in detail, as these factors are considered as likely to have influenced the sediment, and the methodological considerations relating to these are explained.

Bioturbation by lakes flora (such as root growth) and fauna (burrowing or movements) are likely to disturb lake sediment to depths between 3 and 20 cm (Krantzberg, 1985; Lee, 1970; Liu and Fearn, 1993), so is one of the primary considerations in the interpretation of the lake data. Bioturbation can introduce noise and smooth elemental data (Lee, 1970), which can disguise climatic signatures. A detailed study on present day benthos and their sedimentary traces determined that most faunal activity occurs in the sublittoral zone, above the thermocline and below the 1% light level (Figure 2.5; White and Miller, 2008). In most lakes the zone where faunal activities are concentrated is between 2 and 4 m (White and Miller, 2008), so therefore Loch Hosta was cored below 4 m in the profundal zone. It seems likely that, given the high resolution of the ITRAX data, bioturbation will have introduced some noise to the data. Therefore this research seeks to establish the extent of noise introduced, from sources such as bioturbation, to the high resolution sediment reconstructions. The methods for doing this are explained in Chapter 3.

Biological activity also contributes to the sedimentary deposits in the lake, as faunal skeletons and shells are calcium carbonate rich. Enhanced temperatures or light levels (reduced cloudiness) particularly in summer may

cause greater biological productivity and therefore calcium carbonate deposition (Leng *et al.,* 2001). Similarly temperature has been found to influence direct $CaCO_3$ precipitation from the water in some lakes, with increasing precipitation as temperatures both increase and decrease from 15 ºC (Krumbein, 1979). Furthermore biological processes (such as photosynthesis and decomposition) change the CO_2 levels in lakes, which also has an influence on $CaCO_3$ precipitation (Wetzel, 1975; Krumbein, 1979; Müller *et al*., 2003). These latter processes are likely to only occur in lakes where the water is saturated in $CaCO_3$, and as the geology of the lake catchment is gneissic (Weaver and Tarney, 1981) it is not considered likely that this carbonate precipitation has contributed $CaCO_3$ to the sediment. Nevertheless autochthonous sediment from biological remains must be considered in the interpretation of the lake sediment, as concentrations might vary with temperature rather than storminess.

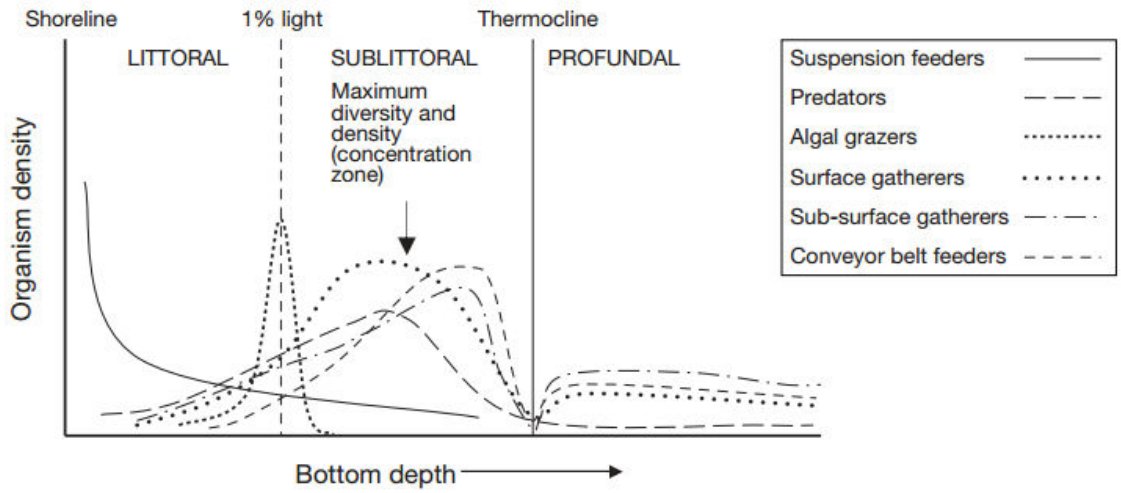

Figure 2.5.: Benthic invertebrate structure in oligotrophic Lake Michigan (White and Miller, 2008, pg 270; after White *et al.*, 1986), illustrating the density of fauna in the littoral, sublittoral and profundal zones of the lake.

There have been ten lake sediment distribution mechanisms described by Hilton *et al.* (1986), including deposits from river inputs (forming deltas and plumes), intermittent/continuous mixing, wave erosion, slope processes and movements associated with currents. These influence the distribution and redistribution of sediment. In an exposed lake such as Loch Hosta the wind is likely to disturb sediment, particularly in the shallower areas of the lake. The disturbance can occur from wind driven bottom water currents and direct wave action (Bengtsson *et al.*, 1990). For all sediment grain sizes the bottom currents are only erosive above 0.3-0.4 m/s, which requires winds stronger than 67 mph, however the wave action can be much more erosive (Bengtsson *et al.*, 1990). The size of waves depend on the fetch (i.e. the lake size), and wind velocity and duration, while their effect on lake sediment depends on the depth of water (Hakanson, 1977). This relationship between wave fetch and water depth is summarised in Figure 2.6, which is based on data from the large Lake Vanern (Hakanson, 1977). Loch Hosta is a relatively small lake so does not experience large wave fetches (at most 0.7 km), so Figure 2.6 indicates that erosion from waves is likely to occur only in waters <2 m deep. Coring was therefore carried out in the deepest section of the lake where the wind influence was minimal.

As described in section 2.6, changes in storm latitude will influence the amount of sediment being blown and entering the lake; however the wind direction will also influence the wave direction within the lake and potentially the current strength, and therefore alter the erosion of lake margins or shallow areas. As these are situated along the southwestern edge of the lake, enhanced easterly winds when the storm track is situated further south may cause enhanced erosion of sand within the lake. Alternatively when the storm track is to the north bringing westerly winds this is more condusive to aeolian sand transport. Therefore it is speculated that storms both to the north and south of the Outer Hebrides may cause enhanced sand to reach the centre of the lake, although through different mechanisms.

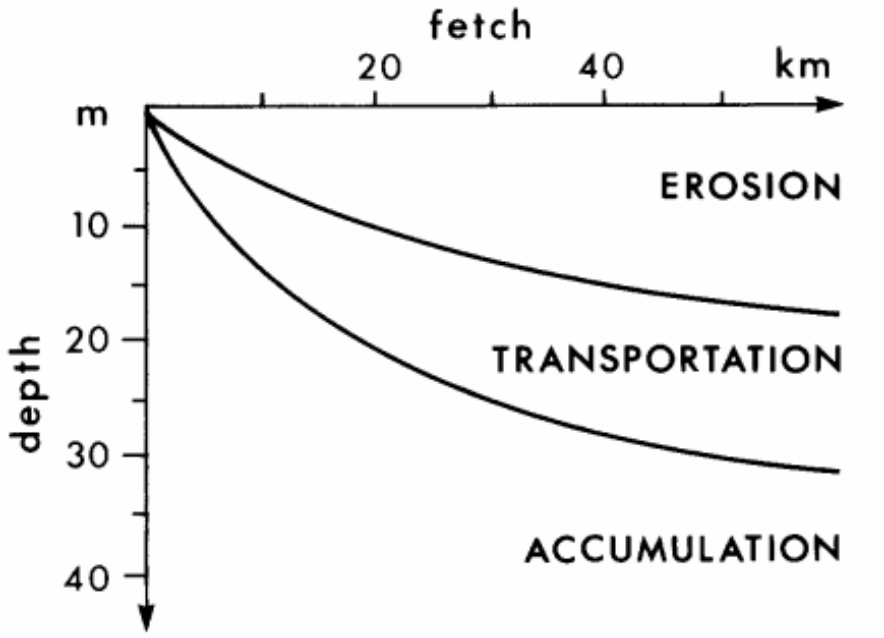

Figure 2.6.: Erosion-transportation-Accumulation (ETA) diagram for Lake Vanern, Sweden (Hakanson, 1977, pg 406; Bengtsson *et al.*, 1990, pg 168). The diagram indicates that increasing wave magnitude (shown by fetch distance) increases the depth at which sediment is eroded and transported in lakes.

2.8. Methods and precision analysis

2.8.1. Sand analyses

The methods used at each site vary, particularly at the Loch Hosta site (Chapter 3), so the methods specific to these sites will be described within each results chapter. The techniques used for analysing the sand content and the spectral analysis methods were used at each site, so are outlined here.The sand content of the peat bogs and lake sediment has been analysed by three stages. Initially loss-on-ignition was carried out to show the inorganic content (also called ignition residue or ash). To separate the inorganic material, loss-on-ignition was carried out following the methods of Dean (1974) and Heiri *et al.* (2001). Samples were dried in an oven overnight at 102ºC and then ignited at 550ºC for 4 hours. Between each stage the samples were cooled in a dessicator and weighed. This allowed the water, organic and inorganic content to be calculated.

Secondly this material was sieved to 120-180 μm and >180 μm to identify the medium and coarse sand weights. Before being sieved the IR samples were left in 10% hydrochloric acid overnight: acidic peat bogs are likely to have dissolved $CaCO_3$ shell sand over time, so to prevent a decrease in sand with depth the carbonate sand was removed from all samples before sieving. Following this 10 ml of 30% hydrogen peroxide was added, at which point they were heated gently for 4 hours to stimulate a reaction. After wet sieving, to separate the 120-180 μm and >180 μm fractions, these were washed with distilled water into beakers and dried in an oven, before being cooled in dessicators. The beaker and sand fractions were weighed, then the fractions were swept using a brush from the beakers, and the empty beakers reweighed. The weight of the sand was calculated by the beakers weight subtracted from the sample and beaker weight. This method minimised the loss of sand grains during the process and, as all the weighing for each sample was done in immediate succession, any variations through time of the scales were minimised.

Finally in the dated cores the sand weight values were converted to sand influx. The changes in peat accumulation can potentially cause enhanced or reduced sand accumulation in a given layer. For example, 1 cm^3 of peat might accumulate over 10 years and a different 1 cm^3 sample might accumulate over 50 years, which would most likely result in higher sand content in the latter sample. To account for this, the known wet volume and approximate accumulation rate of the peat were used to calculate the sand influx per year:

Sand Influx (g cm^{-3} yr^{-1}) = sand weight / wet volume / time span of sample

The same loss-on-ignition and sieving methods were used on the lake sediment, although the shell sand was not removed before sieving as unlike peat bogs the lake sediments are not acidic. Instead prior to sieving the inorganic material was disaggregated by being put in 0.4% sodium hexametaphosphate (Bamber, 1982), left for 24 hours and then put in the ultrasonic bath for two minutes.

2.8.2. Precision analysis of sand measurements

As the storminess reconstructions from the peat bogs were based entirely on the measurement of sand concentrations, the results of repeat measurements will next be used to test the methods precision and limitations. As the same sieving method was also used on the lake sediment, the precision analysis performed below is applicable to the analyses of sand content in both the lake and peat bogs. To assess the precision of this method, repeat measurements over a depth of 20 cm were made. High numbers of repeat measurements were desirable to assess the range of measurements possible, however due to a lack of sediment only three measurements could be made at each depth. The precision of the inorganic content, or ignition residue (IR), and the sieved sand fraction weights were calculated by finding the mean of the three samples and the difference from this of the maximum and minimum values at each depth. The results of the IR repeat measurements are shown in Figure 2.7. The IR measurements are highly repeatable, with an average precision of 0.26%. Therefore it is considered that even small peaks in the range of ~1% can be considered in the interpretation of the IR results.

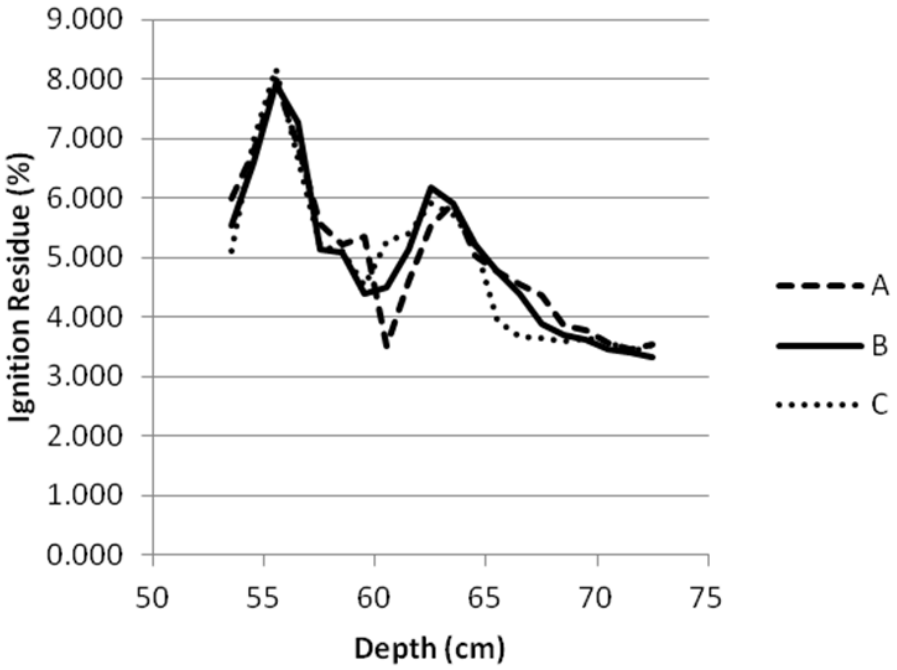

Figure 2.7: Precision analysis measurements of the ignition residue results. Three repeat measurements were taken over a 20cm section of core from Hill Top Bog (transect core 1).

Precision analysis for the measurements of the 120-180 and >180 μm sand weights are shown in Figures 2.8 and 2.9. The precision of 0.0009 g and 0.0004 g for the 120-180 and >180 fraction weight measurements respectively support that there is good precision. However if expressed as a percentage of the mean measurements the sieving results show lower precision: the 120-180 μm fraction vary by 15.5% and the >180 μm fraction by 17.4%, compared to the precision for the IR results of 5.3%. The sieving results therefore have lower precision than the IR results, which suggest that not all the differences in measurements were the result of differences in sand content. As the samples being measured are small it is likely that there is some machine error from the scales as well as human error, for example a loss of sand grains during the sieving method. However the precision analysis has shown that repeat measurements show the same trends. This gives confidence that the variations in the sieved fractions can be considered meaningful.

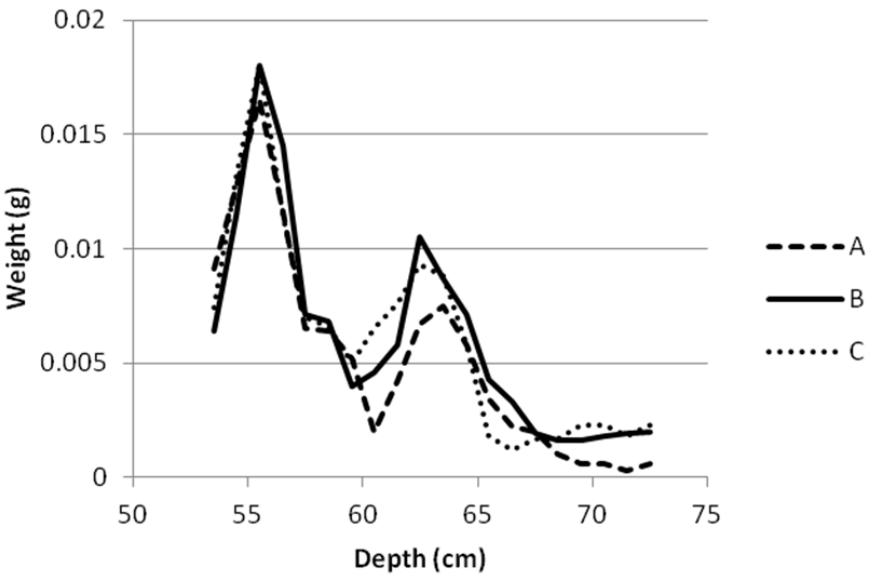

Figure 2.8: Precision analysis measurements for the 120-180 μm fraction weights. The same section of core shown in Figure 2.7 was analysed.

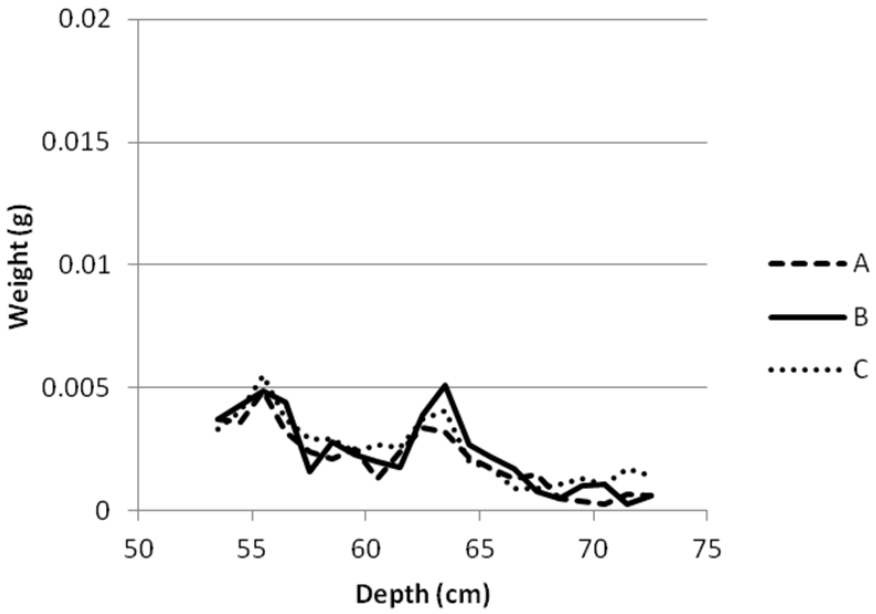

Figure 2.9: Precision analysis measurements for the >180 μm fraction weights. . The same section of core shown in Figure 2.7 was analysed.

2.8.3. Spectral analysis

To investigate how storminess varies through time spectral analysis was carried out on the results from each study area. Three methods of spectral analysis were used, each with different outputs, benefits and disadvantages.

The first method was the Lomb-Scargle spectral analysis, which is advantageous as it can be applied to unevenly spaced data (Lomb, 1976; Press and Rybicki, 1989; Scargle, 1982). As storminess reconstructions are not evenly spaced (due to changes in sediment accumulation rate) this method is appropriate as it does not require interpolation of the data, which can lead to underestimation of the high frequency cycles (Schulz and Stattegger, 1997). This method of spectral analysis including the 95th percentile of significance was carried out using a Matlab code (Shoelson, 2001).

The second method of spectral analysis carried out was wavelet analysis, a method introduced by Morlet (1983) and applied to climate timeseries by Lau and Weng (1995). This method was used as it allows changes in cycles through time to be identified, as previous research gives evidence for non-stationary variability in storminess (Debret *et al*., 2007). This method uses a mother wavelet that is stretched or compressed to represent

different frequencies and passed over the dataset, in order to assess the cyclicity through time. This method requires evenly spaced data, so the results were interpolated and then smoothed and re-sampled to the time interval representing the 90th percentile of the time interval distribution. In other words the resolution was re-sampled to the typical age resolution of the data. The Wavelet analysis was then carried out in Matlab using software provided by C.Torrence and G.Compo, which used a Morlet mother wavelet and calculated the 95% significance levels (Torrence and Compo, 1998). A disadvantage of this method is that it requires evenly spaced data, so as described above there is a possibility that high frequency cycles may be underestimated. Furthermore the method requires zeros to be added to the start and end of the reconstructions, as the wavelets overrun onto these as they pass over the record. This leads to underestimation of the cycles at the start and end of the reconstructions, particularly the low frequency cycles (Debret *et al*., 2007). The parts of the record influenced by this effect are highlighted on the diagrams by the cone of influence.

Finally cross-spectral analysis (Chatfield, 2004) was carried out between various reconstructions to identify shared spectral frequencies, for example this method was used to infer the periodicities at which the NAO was driving storminess by identifying shared cycles in each record. For the cross-spectral analysis, the two records being compared were interpolated and sampled to the same resolution and the cross-spectral analysis was calculated using a Matlab function. The significance level was calculated as follows: for 5000 iterations the storm record and forcing datasets (e.g. the NAO, solar reconstruction) were randomised and cross-spectral analysis carried out, in order to capture the range of spectral magnitudes at each frequency that can occur randomly, i.e. significant results are those that arise <5% of the time after random mixing of the data (Jones *et al.,* 2013). The 95th percentile of these results provided the 95th percent significance level.

In summary the Lomb-Scargle method of spectral analysis was selected because it is the most reliable method of analysis for unevenly spaced records, while the wavelet analysis was also selected as it provides more information about the changes in cyclicity through time. The cross-spectral analysis was chosen to investigate climate-forcing linkages.

Chapter 3: Investigating the potential for climate reconstructions using ITRAX XRF analysis: A storminess reconstruction from the Outer Hebrides

This chapter is based on the paper:

Orme, L. Reinhardt, L. Jones, R, T. Charman, D. Dawson, A. Croudace, A. Ellis, M. Barkwith, A. (*submitted*) Investigating the potential for climate reconstructions using ITRAX XRF analysis: A storminess reconstruction from the Outer Hebrides. *The Holocene.*

3.1. Introduction

Rapid, very high (sub-millimetre) resolution element analysis on sediment cores can be achieved non-destructively using an ITRAX XRF core scanner (Croudace *et al*., 2006). The scanner focuses an intense X-ray beam onto a split core surface to irradiate the sediment; a detector captures the response of fluorescence energy and wavelength spectra, which reflects the element composition (Croudace *et al.*, 2006; Weltje and Tjallingii, 2008). This method has been used to create reconstructions of past climate from lake sediment deposits (e.g. Metcalfe *et al*., 2010; Moreno *et al*., 2008; Yancheva *et al*., 2007; Giguet-Covex *et al*., 2012; Martin-Puertas *et al.,* 2012). However due to methodological limitations it is not clear how reliable such high-resolution data are for non-varved lake sediments.

A methodological limitation of ITRAX analysis is that it produces *relative* element concentrations, and therefore the measurements can be influenced by changes in sediment composition and other elements. Changes in the organic or carbonate content can result in an increase in undetectable light elements (carbon, oxygen and nitrogen), causing lower counts of the heavy elements, which is termed the 'dilution effect' (Löwemark *et al*., 2010). Similarly, changes in one element can cause detection of other elements to increase or decrease, which is termed the 'matrix effect' (Löwemark *et al*., 2010). In this chapter ITRAX data is calibrated using the log-ratio calibration equation method of Weltje and Tjallingii (2008), which expresses the ITRAX results as natural log-

ratios. This method includes the normalisation of elements against an abundant, conservative element, to solve the dilution effect, as calculated relative changes between two elements removes the methodological error influencing both (Guyard *et al*., 2007; Löwemark *et al*., 2010; Weltje and Tjallingii, 2008). Furthermore, the calibration of normalised ratios against absolute compositional down-core measurements using XRF analysis allow parameters to be determined that account for the matrix effect and detection efficiency, and in practise also reflect changes in core surface, grain size and water content (Weltje and Tjallingii, 2008). Using these methods there is a demonstrated correspondence between the ITRAX results and the traditional XRF analysis results (Weltje and Tjallingii, 2008), indicating that the limitations of the ITRAX core scanning method are reduced.

A benefit of ITRAX XRF analysis is that it produces high resolution data; however it is uncertain whether climatic signatures are preserved in the sediment at sub-centimetre resolutions. Bioturbation (mixing) of benthic sediment occurs through the movements of flora and fauna: this has been found to occur over depths of 3-20 cm (Krantzberg, 1985; Lee, 1970). However these effects are unevenly distributed within lakes (White and Miller, 2008) and the level of degradation of environmental signals in lake sediment is uncertain. Furthermore sediment disturbance can occur from re-deposition by currents and sediment slumping (Hilton *et al*., 1986). Therefore, even using traditional methods of sediment analysis (typically at 1 cm resolution) the climatic signal may not have been preserved, and at the sub-millimetre resolution of ITRAX analysis the influence of disturbance is likely to be enhanced. Some studies using ITRAX analysis have dealt with the issue by using varved and laminated lake sediment sections only, as the influence of bioturbation on these can be shown to be minimal, and these therefore allow annually resolved climate records to be produced (e.g. Metcalfe *et al*., 2010; Giguet-Covex *et al*., 2012). However on homogenous lake sediment the extent of bioturbation is less clear, and is often an issue unaddressed by studies using ITRAX analysis.

To investigate the maximum resolution of ITRAX analysis and the potential of this method for creating reconstructions of climatic changes, analysis was carried out on two cores from a lake on North Uist, an island in the Outer Hebrides, western Scotland. This location was selected as an

environment likely to be sensitive to variations in the NAO, which is a measure of the pressure difference between the Azores High and the Icelandic Low (Van Loon and Rogers, 1978; Hurrell, 1995). The calibrated ITRAX XRF data, specifically the Ln(Ca/K) results, have been used to produce a Late Holocene palaeo-storminess reconstruction. This ratio was selected as calcium-rich sediment is dominant in the beach sand, which is likely to be deposited across the catchment and in the lake by both aeolian and fluvial transport pathways, therefore capturing both 'wet' and 'dry' storm events. Previous climate reconstructions from the Outer Hebrides have supported that there was high storminess particularly since 1400 A.D. (Dawson *et al*., 2004; Gilbertson *et al*., 1999), and during severe storms sand inundated the settlements of Udal in 1697 A.D. and Baleshare in 1756 A.D. (Gilbertson *et al*., 1999; Lamb, 1984; 1991).

Sedimentological analysis, comparison with instrumental climate data and elemental analysis of catchment sediment sources provide the basis for interpretation of the element changes within the lake sediment. By correlating with climate records and assessing cyclicity in the record, the climate influence on the lake sediment will be inferred. Reconstructions of the NAO have identified cycles of c. 20, 40, 60 and 70-90 years (Glueck and Stockton, 2001; Luterbacher *et al*., 1999; Wanner *et al*., 2001; Higuchi *et al*., 1999; Cook *et al*., 1998; Appenzeler *et al*., 1998), and in a 5200 year reconstruction cycles of 170 and 350 years were identified (Olsen *et al*., 2012). Similar cycles have also been found in a Greenland reconstruction of storminess (Fischer and Mieding, 2005) and in 40-100 year cycles of the Atlantic Multidecadal Oscillation (AMO), which is a measure of Atlantic Ocean temperatures (Kerr, 2000; Enfield *et al*., 2001; Knudsen *et al*., 2011; Gray *et al*., 2004). As it has been suggested that coupled atmosphere-ocean interactions control climate in the North Atlantic region (Higuchi *et al*., 1999; Olsen *et al*., 2012; Yang and Myers, 2007), detection of these cycles within the data is a way of confirming the climatic influence on the lake sediment. Finally comparison of the elemental results with instrumental climate data at a range of resolutions, as well as detection of the highest frequency cycles present in the data, allow an assessment of the resolution at which the ITRAX results are unaffected by noise from sources such as bioturbation.

3.2. Study area

Loch Hosta (57º37”30’N 7º29”8’W) is a low lying lake (measuring 0.27 km^2, up to 11m deep and at an altitude of 10 m) on the west coast of the Outer Hebridean island of North Uist (Figure 3.1). The climate of the Outer Hebrides (based on Stornoway station measurements, 1981-2010 A.D.) is mild, wet and windy, with an average annual precipitation of 1250 mm, temperatures between 6 - 11 ºC and on average winds around 11 knots (Met Office, 2014). The winter months are when the lowest temperatures and highest precipitation occurs, with more extremes of atmospheric pressure (Figure 3.2). The NAO is a strong control on storms here, as shown by the positive correlation between the NAO and wind speed, gale days, precipitation and cyclone occurrence since 1950 A.D. (Pirazzoli *et al*., 2010; Marques *et al*., 2008; Andrade *et al*., 2008). Severe storms at times influence the Outer Hebrides, for example hurricane force winds in January 2005 A.D. caused sand dune retreat, flooding and coastal erosion, however this was not a unique event as records show two other storms of greater magnitude have occurred since 1980 A.D. (Dawson *et al*., 2007). The exposed situation of Loch Hosta mean it is likely to be particularly affected by the high winds and precipitation brought by severe storms, and these are likely to cause the erosion, transport and deposition of sediment into the lake.

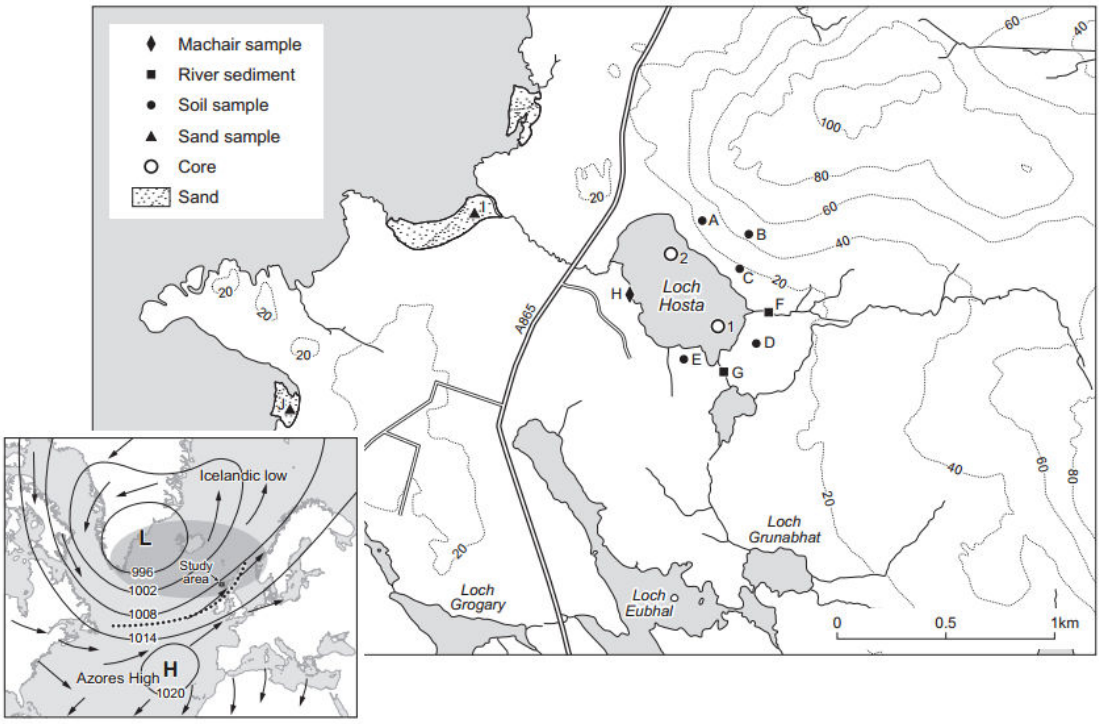

Figure 3.1: Map of Loch Hosta, situated at 57º37”30’N 7º29”8’W on North Uist (Outer Hebrides). Labels 1 and 2 represent the coring locations of the sediment cores Hosta 1 and Hosta 2 respectively. Labels A-J represent sampling locations of soil and sand from the catchment. *Inset:* Schematic diagram of the location of the Outer Hebrides, and the North Atlantic Oscillation pressure centres (Azores High and Iceland Low). The shaded area is the region with increased cyclone numbers when there is a positive NAO index (>1) (based on results of Andrade *et al*., 2008).

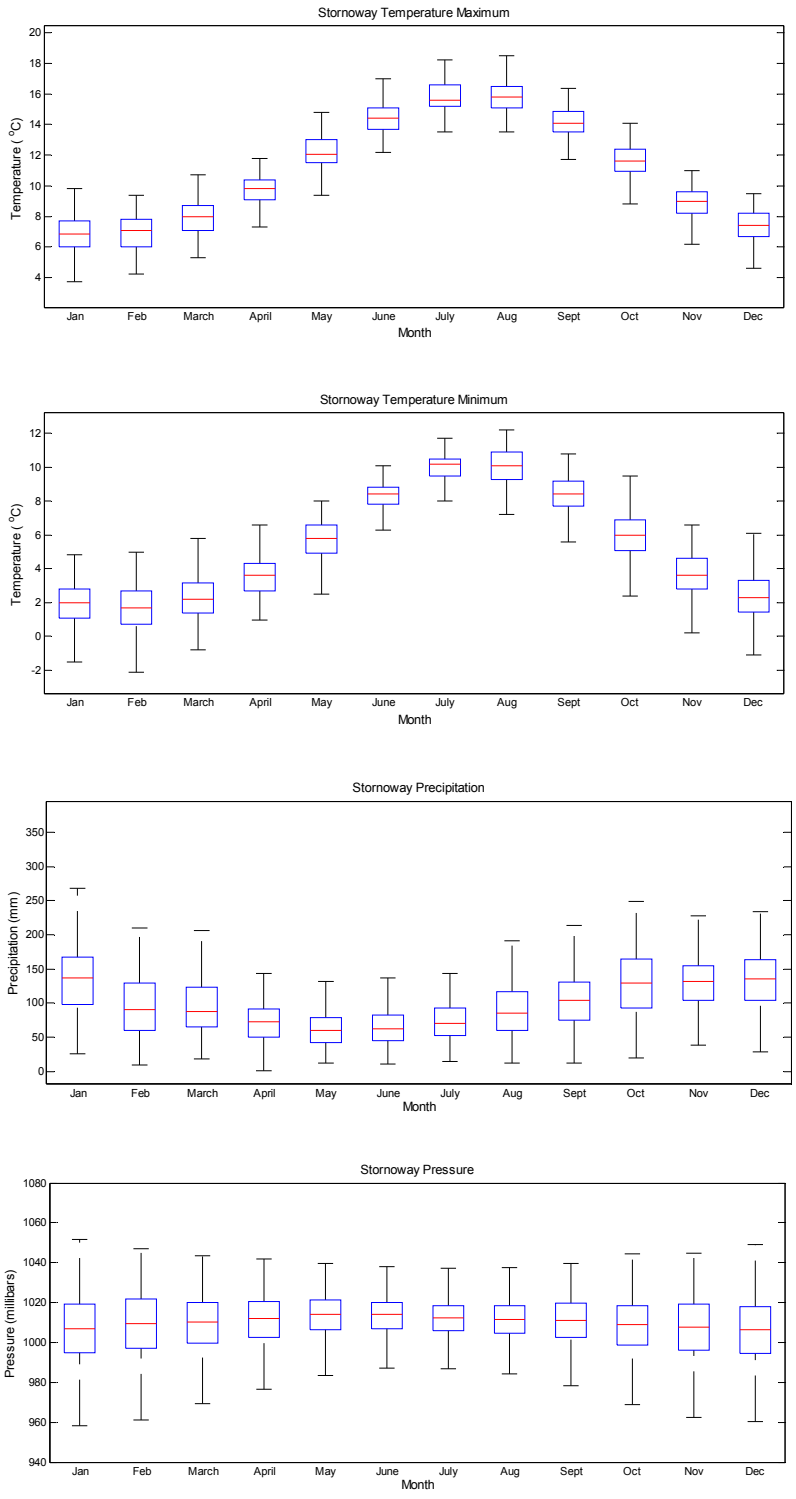

Figure 3.2: Box plots of (from top) maximum temperature, minimum temperature, precipitation and atmospheric pressure at Stornoway for the period 1873-2012 A.D.. Atmospheric pressure measurements were collected by A.Dawson from the Met Office archives in Edinburgh and kindly donated. Temperature and precipitation measurements were obtained from the Met Office online records (Met Office, 2014).

Loch Hosta was selected as it is surrounded by sources of Ca rich sand, which may be entrained either by aeolian or fluvial processes during storms. Sources of calcium carbonate-rich shell sand, for aeolian transport, include the nearby beaches, and the machair; a rare, sand-based, grassland ecosystem adjacent to Loch Hosta (Angus, 1997). The coastal location of the lake may also mean that sea-spray is blown into the lake during storms, although the concentration of Ca in sea water is small (0.04 %) (Kirk and Moberg, 1933). Ca deposition is also likely to occur by overland flow from the hill bounding the north eastern side of Loch Hosta and from two tributary streams that enter the lake at the southern end. The catchment bedrock is Lewisian grey gneiss, which is typically formed of quartz, plagioclase feldspar, biotite and hornblende, with Ca concentrations of 3-7% (Weaver and Tarney, 1981; Angus, 1997; Smith and Fettes, 1979). Sediment originating from such bedrock contains low Ca; as we show later catchment soil does contain Ca (<10%) most likely originating from both the bedrock as well as from windblown carbonate sand. Ca can precipitate in some lakes due to biological processes (Leng *et al*., 2001; Stabel, 1986; Dittrich and Obst, 2004), however these are most often where Ca saturation has occurred, which is unlikely in a grey gneiss bedrock catchment. Therefore the dominant source of Ca in Loch Hosta sediments are wind driven beach deposits that either blow directly into the lake or first onto adjacent hill slopes, which thereafter wash down into the lake during rainfall.

Changes to the catchment in the past by either human or natural processes may have influenced sediment sources of the lake. At present the land around Loch Hosta is predominantly grazing pasture for cattle but includes a few houses. The adjacent hill slope is known to once have had a settlement called Baleloch (consisting of a number of buildings), which was probably in existence between 1666 A.D. until depopulation around 1815 A.D. (canmore.rcahms, 2014; Moisley, 1961). The distance between the coastline (sand sources) and the lake may also have varied due to relative sea level changes: a reconstruction from the Outer Hebridean island of Harris indicated <0.5 m of sea level rise over the last two millenia (Jordan *et al*., 2010), however even with stable sea level coastal changes can occur depending on the offshore topography and sand supply (Cattaneo and Steel, 2003; Hansom, 2001). These anthropogenic and geomorphic changes are necessary considerations in the interpretation of changes in the lake sedimentology.

Figure 3.3.: Machair ecosystem and eroded bank lining the south-western edge of Loch Hosta

Figure 3.4: View of Loch Hosta from south-western bank looking (from top) towards the northern, middle and southern end of the lake.

3.3. Methods

3.3.1. Catchment element analysis

To confirm the element composition of abiotic sediment entering Loch Hosta, nine sand and soil samples were collected from the adjacent machair, beaches, rivers and fields, at the locations shown on Figure 3.1. These samples were treated using hydrogen peroxide to remove organic material and sieved to separate the <500 μm fraction, as this is the size fraction most easily transported by aeolian and fluvial processes (Kok *et al.*, 2012). The samples were subject to XRF analysis at X-ray Mineral Services (Colwyn Bay, Wales), where they were dried at 105°C, crushed into a fine powder, blended with lithium metaborate and then fused at 1080°C into a glass "bead". XRF analysis was performed on the beads using a Spectro X-Lab Energy Dispersive (polarised) XRF Spectrometer.

3.3.2. Sampling

Coring of Loch Hosta was undertaken in September 2011 using a short (1 m) Mackereth corer (Mackereth, 1969) at two locations shown in Figure 3.1. To minimise the influence of bioturbation cores were taken from depths >5 m, as in most lakes faunal activities are concentrated between 2 and 4 m in the photic zone (White and Miller, 2008). Cores were extracted within plastic tubes and transported vertically. Once in the laboratory excess water was removed and the cores were extruded from their tubes, split into two along their length and put into semi-circular plastic tubes, which were wrapped with plastic film. The cores were stored in a cold store.

3.3.3. Element Analysis

High resolution elemental measurements were taken by an ITRAX XRF core scanner (Croudace *et al*., 2006) at the National Oceanography Centre, Southampton, using a voltage of 50 kV, current of 50 mA, exposure time of 200 milliseconds and a step size of 200 μm. The ITRAX results were calibrated using sixteen XRF samples, each 1 cm thick, which were taken from points along the cores selected to represent the extremes of the ITRAX data (as

recommended by Weltje and Tjallingii, 2008). These samples were mixed with lithium tetraborate and fused at 1100 ºC before casting into glass disks, which were analysed using a Philips Magix-Pro wavelength dispersive XRF spectrometer (also at Southampton National Oceanography Centre).

To investigate the sand content within the cores the Ln(Ca/K) ratio was selected. As described above and shown in the following sections (Figure 3.6.), Ca is present in high concentrations within the catchment sand on the beaches and machair, so the deposition of Ca into the lake and across the catchment is likely to occur during storms. An element present in the catchment soil was used as a denominator as the intention was to identify the aeolian signature of storms, so higher ratios would indicate that an increased amount of sand had been deposited into the lake or across the catchment relative to the constant levels present in the soil. The selection of the major element to use as denominator was partly dependant on the ITRAX detection: aluminium is a conservative element so is often suggested as a good element to use for this (Löwemark *et al.,* 2011), however aluminium had low levels of detection by the ITRAX machine, as did silica, magnesium, phosphorous, sodium and sulphur. Iron and manganese could not be used as these are highly influenced by redox conditions, even in shallow lakes within the sediment (Davison, 1993). The remaining elements were titanium and potassium, both of which were present in the catchment soil and well detected by the core scanner. The Ln(Ca/K) and Ln(Ca/Ti) results were both calibrated using the method described below: the Ln(Ca/K) calibrated much more successfully than the Ln(Ca/Ti) results (as indicated by the Goodness of Fit statistic) so was selected as the most suitable ratio. One limitation of using a ratio is that the values may change as the result of K rather than Ca variations. As both Ca and K are present in the catchment bedrock and therefore soil, the changes resulting from only sediment inwash should not influence the ratio, however this may not be the case if either Ca or K are more easily eroded or transported.

The calibration method of Weltje and Tjallingii (2008) was followed. In brief, the measured Ln(Ca/K) ratio of the 16 calibration (XRF) samples were compared with the Ln(Ca/K) of the ITRAX data (averaged over the equivalent 1 cm depth) and the relationship between these expressed as a Log Ratio Calibration Equation (LRCE):

$$\ln\left(\frac{W\_Ca}{W\_K}\right) = \alpha \ln\left(\frac{I\_Ca}{I\_K}\right) + \beta$$

where I_Ca and I_K are the ITRAX intensity values and Ln(W_Ca/W_K) is the calibrated ITRAX results expressed as natural log ratio's. The Ln(Ca/K) calibration gave parameters of α = 0.309 and β = 0.794. The success of the LRCE was confirmed using a Goodness of Fit (R^2) equation (Weltje and Tjallingii, 2008), with R^2=0.86 between the calibrated ITRAX Ln(Ca/K) and the XRF measured Ln(Ca/K) samples.

3.3.3. Proxy data analysis

A number of sediment analyses were carried out to support the interpretation of the ITRAX data. The loss-on-ignition and sieving methods outlined in section 2.8.1. were carried out to assess the organic and inorganic content of the sediment.

Further sediment was sampled at the 1 cm resolution for the Carbon:Nitrogen (C:N) analysis, to identify the sources of organic matter, from allochonthonous sources (>20 C:N) or autochonthonous sources such as algae (4-10 C:N), which can be related to catchment runoff and lake productivity (Meyers, 1994; Silliman *et al*., 1996). Sediment was freeze-dried, ground and weighed to 4-12 mg using a Sartorius Supermicro Balance machine. Analysis of the C:N content was done in a Flash 2000 Organic Element Analyzer.

Following the above analyses the carbonate content was measured. Given the abundant calcium carbonate shell sources surrounding the lake, carbonate measurements were considered likely to resemble sand concentrations, and so may also reflect changes in the Ln(Ca/K). Sediment was exhausted at some depths, particularly where sampling for the XRF calibration and ^{210}Pb dating had been carried out, so measurements are discontinuous. Analysis was done by repeating the loss-on-ignition method outlined above and then following it with ignition of the samples at 1050ºC for two hours to remove the carbonate, before reweighing (Dean, 1974; Heiri *et al*., 2001).

To compare measurements both the Ln(Ca/K) results and proxy datasets had to be re-sampled to the same resolution, because they were measured at

0.2 mm and 1 cm resolution respectively. The sampling interval was chosen by finding the 90th percentile age interval of the 1 cm resolution age-depth models for each core. Both the proxy and Ln(Ca/K) results were re-sampled to this resolution, by interpolating, smoothing and down- (or up-) sampling the data.

3.3.4. Chronology

^{210}Pb analysis was used to date the upper sediment of each core. Samples taken every 2-3 cm were dried, ground gently, sealed in plastic tubes and left for 21 days to achieve radioactive equilibrium. Analysis was made by gamma assay (measuring activity of ^{210}Pb, ^{226}Ra and ^{137}Cs). To convert the ^{210}Pb activity to ages the Constant Rate of Supply (CRS) model was used because the unsupported ^{210}Pb was not linearly associated with depth when plotted logarithmically, as would be expected if sediment accumulation in the lake had been continuous (Appleby and Oldfield, 1978; Goldberg, 1963; Appleby, 2001). Analysis was carried out with inputs of the unsupported ^{210}Pb activity (calculated by the ^{226}Ra activity subtracted from the initial ^{210}Pb activity), the samples dry bulk density and depths. The samples datable using ^{210}Pb were those above the equilibrium depth (the point at which the ^{210}Pb and ^{226}Ra are in equilibrium; Appleby *et al*., 2001). The cumulative unsupported ^{210}Pb above this depth was calculated using a trapezoidal integration. This allowed the cumulative amount of ^{210}Pb in the full profile (A(0)) to be calculated and thus the cumulative sum of ^{210}Pb below the sample in question (A) and above the sample in question (Â). Using Â and A as well as the ^{210}Pb radioactive decay constant (λ), which is 0.03114 y^{-1}, the age of the samples was calculated with the following equation:

$$t = \frac{1}{\lambda}\ln\left(1 + \frac{\hat{A}}{A}\right)$$

To ascertain dating accuracy the ^{210}Pb ages were compared against increased levels of ^{137}Cs in the cores, caused by nuclear weapons tests between 1953 and 1963, and the 1986 Chernobyl nuclear disaster (Pennington

et al., 1973; Ritchie *et al*., 1973). The standard errors were calculated following the method outlined in Appleby (2001) and the following equation:

$$\sigma_t = \frac{1}{\lambda}\left[\left(\frac{\sigma A(0)}{A(0)}\right)^2 + \left(1 - \frac{2A}{A(0)}\right)\left(\frac{\sigma A}{A}\right)^2\right]^{0.5}$$

One sample near the base of each core was AMS radiocarbon dated using bulk sediment, as above-ground plant macrofossils were not present. These were dated at Queens University Belfast's ^{14}CHRONO centre. The radiocarbon dates were calibrated using OxCal version 4.2.3, which uses the IntCal13 calibration curve (Ramsey and Lee, 2013; Reimer *et al*., 2009; Ramsey 2009a).

Age-depth models for each core were produced using Bayesian analysis by OxCal version 4.2.3, which used the IntCal13 calibration curve (Bronk Ramsey, 2013; Reimer *et al*., 2009; Bronk Ramsey 2009a). The median of the 2-sigma age range was used to estimate the age for individual samples down the core. However as the age-depth models in this study were poorly constrained, and to some extent 'all age-depth models are wrong' (Telford *et al*., 2004), how the subtle variations in the age-depth models influence the results was explored. This was done by selecting age-depth curves that produced the best correlations between the measured sand content of both cores within the age-errors, as a way of tuning the two records to common environmental signals.

To do this, 3000 age-depth power-law curves were randomly fitted to each core, with each fit lying within the 2-sigma dating error bars. The power-law fits were chosen with the assumption that the deposition rate is steady and increasing sediment compaction is expected with depth (e.g. Christensen, 1982). The best 100 age-depth fits from each core were then used to calculate the mid-point age of each 1 cm section of measured down-core sand mass. The variability in sand deposition through time was then correlated between the two cores for all 100 pairs of possible age depth fits. 10,000 possible combinations were explored and the best correlation was selected. Thus the selected age-depth fits a) meet the physical constraints of deposition and compaction, b) fit within assigned age error bars, and c) tune the age-depth data to common

environmental signals experienced at both core locations. It is important to note that the age depth fits were calibrated using the sand-fraction weight results to avoid circularity, i.e. sand weight is used to calibrate the best age-depth fits and these fits are then applied to independently measured ITRAX Ln(Ca/K) ratio data. The Matlab code used to calculate the age-depth models was designed and written by L. Reinhardt and will be outlined fully in forthcoming papers. Dated ITRAX results were then independently tested against instrumental climate data over the past c.130 years to ascertain how well the common environmental lake-core signals correlate with historical climate variability, as described in the following section.

3.3.5. Instrumental data comparison

To assess the climatic influences on the Loch Hosta sediment, instrumental weather records from Stornoway in the Outer Hebrides were correlated with the Ln(Ca/K) ITRAX results, using Spearman's rank correlation method. As correlations with high resolution data are likely to be sensitive to small errors in the age model, the correlation was done with the Ln(Ca/K) results, dated using the age models with the 500 strongest between-core correlations and the OxCal age model. The climate records that the results were compared against included temperature and precipitation measurements (1873-2012 A.D.; Met Office, 2014) and the lowest 10^{th} percentile of atmospheric pressure from Stornoway (1867-2010 A.D.). In addition the Ln(Ca/K) data was correlated against a winter (NDJF) NAO index for the period 1823-2012 A.D. (Jones *et al*., 1997; Climate Research Unit, 2004). To test the highest resolution at which ITRAX is useful, the comparison with instrumental data was carried out at a range of age resolutions (between 1 and 20 years). Re-sampling was carried out by smoothing then downsampling each dataset to the chosen age resolution. Finally the Ln(Ca/K) was correlated against a millennial length NAO reconstruction spanning 1049 to 1995 A.D. (Trouet *et al*., 2009) to investigate the long-term influence of this circulation pattern on the climate of the Outer Hebrides.

3.3.6. Spectral analysis

Cycles within the record were analysed using the Lomb-Scargle spectral analysis method for unevenly spaced data (Lomb, 1976; Press and Rybicki, 1989; Scargle, 1982; described in section 2.8.3.). The sensitivity of the results to age model selection was assessed by analysing the spectral frequency using the OxCal age model, as well as those that showed strong between-core correlations in sand content. This was another method used to infer the highest resolution achievable using ITRAX data: noise from the ITRAX scanner and sediment will not exhibit cyclicity, so therefore it is suggested that the highest-frequency, significant cycle present in the raw ITRAX data provides an indication of the maximum resolution of the method. Cycles can only be identified when they are twice the sampling resolution, also called the Nyquist frequency (Grenander, 1959). For example, 20 year cycles would support that the climate signal at the 10 year resolution had been preserved. The spectral cycles were also used to support the cause of Ln(Ca/K) variations. Finally cross-spectral analysis (Chatfield, 2004) between the Ln(Ca/K) record and the Trouet *et al.* (2009) NAO reconstruction was carried out to identify shared spectral frequencies (see section 2.8.3.). This method was used to infer the periodicities at which the NAO was driving storminess over the last millennium.

3.4. Results

^{210}Pb dating of the cores offers little constraint in age-depth modelling due to the large analytical errors (Table 3.1). Furthermore in Hosta 1 ^{210}Pb activity was only detected in the upper 2 cm of sediment. Nonetheless a wide range of plausible fits were produced that allowed the sensitivity of the final results to the age-depth model used to be explored: models with the strongest significant correlation between the sand fraction results are shown in Figure 3.5.. The best of these had a correlation of R = 0.59 between the two cores sand fractions. Selection of the top-500 correlations between pairs of age models resulted in many duplicate age models for each core, so that there were in fact only 26 unique age models for Hosta 1 and nine for Hosta 2, as well as the OxCal age-model. These age model outputs are used to assess the sensitivity of the results to age model selection. The resulting age models of Hosta 1 and 2 span the period since 260 and 820 A.D. respectively.

Table 3.1: Results of ^{210}Pb and radiocarbon dating of samples from Hosta 1 and Hosta 2. Note: the ^{210}Pb date at 1-2 cm in Hosta 1 was not used to create the age model due to the large errors associated with this date.

Core and sample depth (cm)	Dating Method (Lab. code)	$\delta^{13}C$ (‰)	Radiocarbon Age(^{14}C yr BP ± 1 σ)	Age (A.D.) (2σ error)	Calibrated Age (A.D.) (2σ range)
Hosta 1: 0-1	^{210}Pb	--	--	2001 ± 90	--
Hosta 1: 1-2	^{210}Pb	--	--	1964 ± 434	--
Hosta 1: 43-44	Radiocarbon (UBA-20599)	-32.3	1379 ± 30	--	652 (607-681)
Hosta 2: 0-1	^{210}Pb	--	--	2006 ± 33	--
Hosta 2: 1-2	^{210}Pb	--	--	1995 ± 37.8	--
Hosta 2: 3-4	^{210}Pb	--	--	1968 ± 60.2	--
Hosta 2: 5-6	^{210}Pb	--	--	1939 ± 129.2	--
Hosta 2: 47-48	Radiocarbon (UBA-20600)	-30.6	1071 ± 33	--	975 (895-1021)

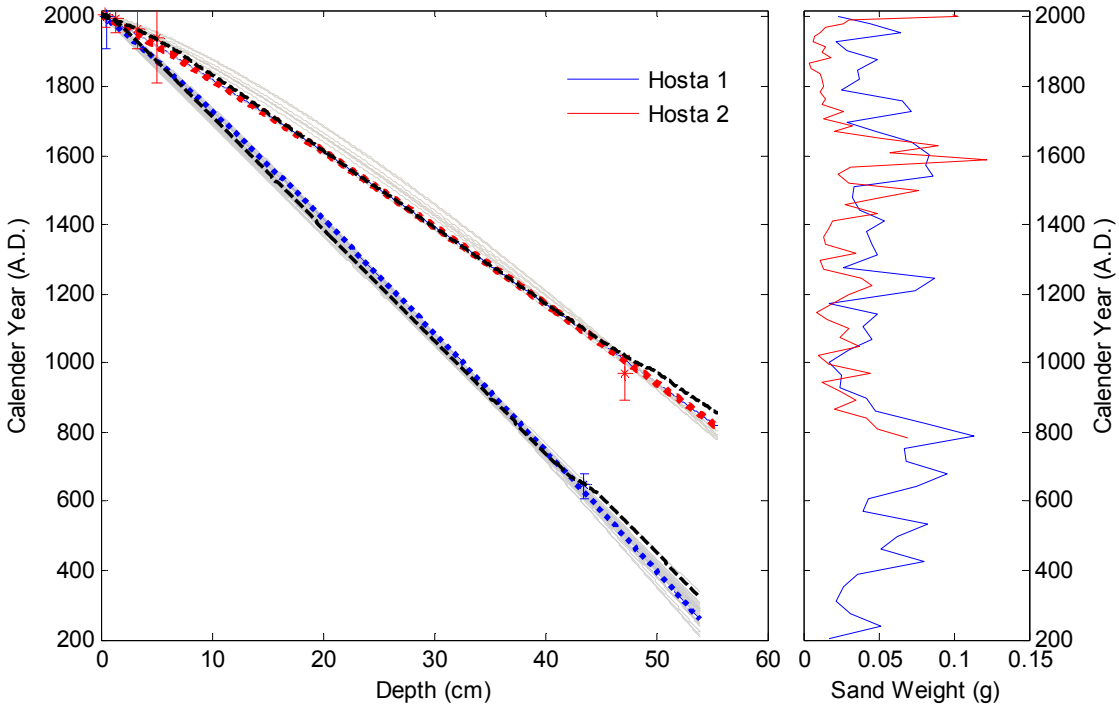

Figure 3.5: *Left* Dated horizons and age-depth models considered within this chapter. Error bars show horizons dated using ^{210}Pb and radiocarbon methods, with the 2-sigma error bars for Hosta 1 (blue) and Hosta 2 (red). The age models selected are those with the strongest correlation between the two cores sand weight results, using the method described in section 3.3.4. Coloured dashed lines are the age models with the strongest correlations between the Hosta 1 (blue) and Hosta 2 (red) results, as illustrated in the *right* graph. Grey lines are the other multiple age-fit curves considered, which had weaker correlations between the sand weight results. The black lines show the age models calculated using the OxCal software.

The two cores were stratigraphically homogenous, black to very dark brown in colour and consisted of organic lake mud with silt/sand. The organic content of the cores showed little variation, particularly Hosta 1 (Figure 3.7, B and I). The Ln(Ca/K) results (Figure 3.7, E and F) show an increase in Ln(Ca/K) prior to c.1000 A.D. and after 1600 A.D., with low values between 1000-1400 A.D.. After 1900 A.D. the Ln(Ca/K) results decrease until 1950 A.D. when they again increase. The cores show highly similar trends, supporting the contention that the results are capturing common environmental changes in the lake. A difference between the cores is that Hosta 2 has increasing values of Ln(Ca/K) between 1400 A.D. and 1900 A.D. while in Hosta 1 the values only increase after 1600 A.D.

The elemental composition of catchment sediment sources were assessed to support the interpretation of the Ln(Ca/K) results (Figure 3.6). The XRF results from the catchment have been grouped and averaged into sand samples from the beach and machair, which are sources of sediment for aeolian transport, and soil-sediment samples from the hillslopes and tributaries, which will reflect sediment that may be washed or flow into the lake. The sand samples were composed primarily of Ca (29-43%) and Si (14-35%), while the soil from the catchment and rivers had high Si (55-67%) as well as Fe (4-8%), Al (13-15%) and Ca (4-9%). Therefore there is distinctly more Ca present in the catchment sand than the soil. The Ca in the catchment soil may have been derived from two sources; the first is the slowly eroding Lewisian gneiss bedrock, and the second is from aeolian transport of sand onto the soil inland. Variations in storminess are likely to influence the amount of sand in the catchment soil over multi-annual timescales, which will then alter the Ca content of sediment being washed into the lake. Therefore there are three transport pathways for Ca into the lake; aeolian, fluvial and a combined aeolian-then-fluvial (or sheet wash) process. Both catchment sand and soil are likely to be mobilised by high winds and/or precipitation from storms over the multi-year periods studied here, raising confidence in the association between storms and pulses of calcium sediment deposition into the lake.

To investigate if fluvial changes were an important influence on the sediments Ca content the Ln(Ca/K) and C:N ratio results were compared, as the C:N ratio can vary with changes in terrestrial carbon deposition and

therefore runoff. The results are uncertain as C:N values of 10-18 are between the levels considered as representing algal (4-10) and terrestrial carbon (>20) (Figure 3.7 A and J; Meyers, 1994). Furthermore the correlation between the Ln(Ca/K) and the C:N is significantly negative with Hosta 1 (R = -0.43) and insignificantly positive with Hosta 2 (R = 0.29). Positive correlations would be expected if runoff was the dominant factor influencing both the C:N and Ln(Ca/K) content of the cores, therefore these results suggest that either the C:N is influenced by lake productivity or calcium sediment is not deposited by runoff from the catchment.

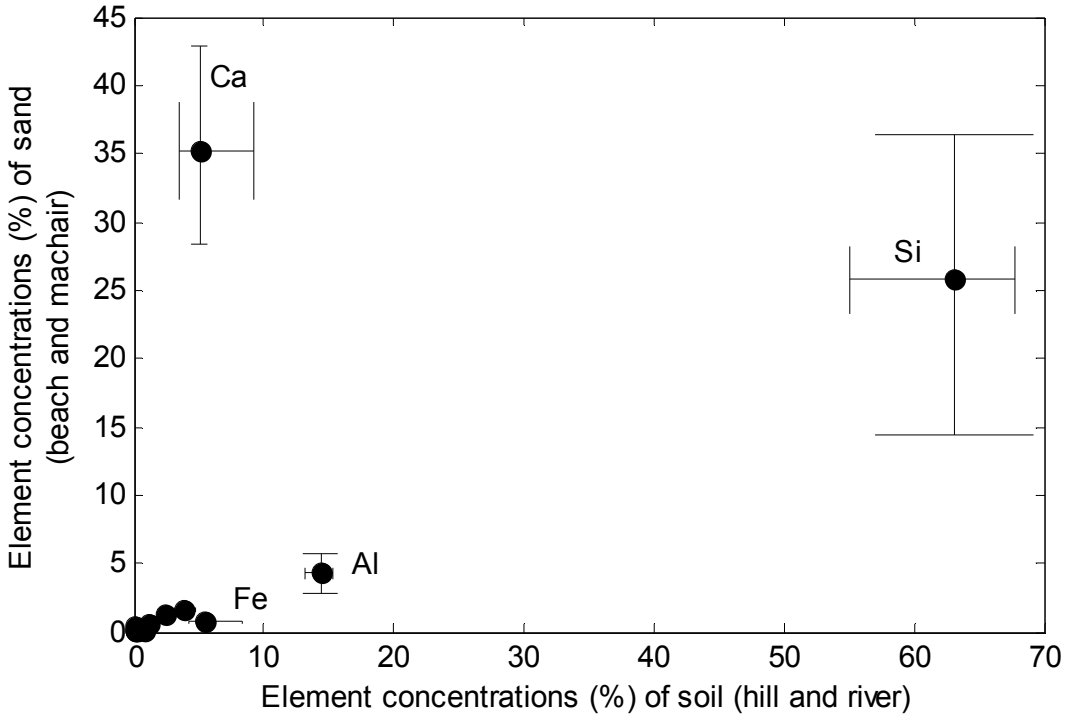

Figure 3.6: Composition of the major elements present in the Loch Hosta catchment soil (based on the average of 6 soil and river sediment samples: Figure 3.1) and sand (from an average of 3 samples from the machair and beaches). The error bars show the range of element concentrations for both sand and soil samples.

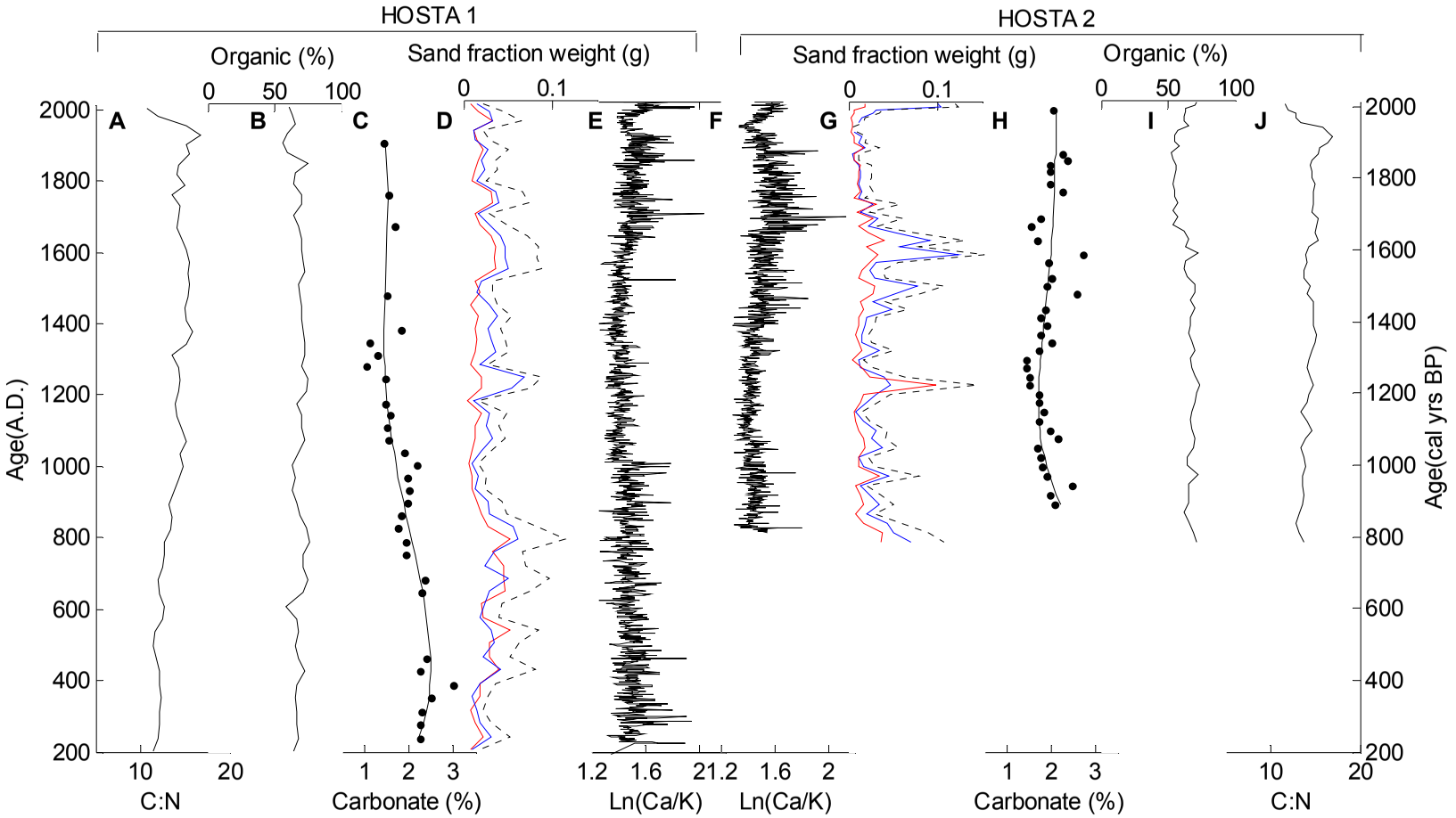

Figure 3.7: Hosta 1 and Hosta 2 sediment analysis results and ITRAX XRF Ln(Ca/K) results. The ITRAX XRF Ln(Ca/K) results (E and F) are smoothed and down-sampled to 1-year resolution for Hosta 1 and 2. Other proxies are the C:N analysis (A and J), organic percentage found using loss-on-ignition (B and I), carbonate percentage found using loss-on-ignition, including polynomial trend lines (C and H) and the sand fraction weights (D and G) in 5 cm^3 wet volume of sediment (red line = 120-180 µm fraction, blue line = >180 µm fraction, dashed line = 120-180 and>180 µm fractions combined).

Next the Ln(Ca/K) ratios down core were compared with known sand concentrations (Figure 3.7, D and G). Logically there should be a 1:1 relationship, but the resolution differences and grain size effects make such comparisons non-trivial. To compare the high resolution Ln(Ca/K) results with the low resolution sand fraction results each record had to be re-sampled to the same resolution, which for Hosta 1 was 40 years and Hosta 2 was 30 years. The Ln(Ca/K) results did not correlate positively with the sand fraction weights as expected; for example the combined 120-180 and >180 μm fraction weights had a significant correlation of R= -0.39 with Hosta 1 Ln(Ca/K) and an insignificant correlation of R = 0.19 with Hosta 2 Ln(Ca/K). An explanation for the lack of correlation may be that the sediment smaller than 120 μm was not measured by the sieving method, and may have had more of an influence on the ITRAX measurements than the coarser fractions. This is visually supported by the available carbonate measurements (Figure 3.7, C and H), which are likely to reflect the total $CaCO_3$ shell fraction of the sediment. These vary between 1-3% of the dried weight, and show some similar changes to the Ln(Ca/K) results. As the ITRAX method only measures the surface of the sediment, to a maximum depth of 1 mm (Löwemark at al., 2010; Weltje and Tjallingii, 2008), it is suggested that coarse sand distributed through the sediment was less likely to be present on the core surface than the fine sand.

The ITRAX scanning method may therefore influence the results, as fine particles are more likely to be present on the core surface than sand-sized particles. The typical number of sand grains analysed by the ITRAX core scanner was estimated using the average sand weight measurements, the density of $CaCO_3$ and the volume of scanned sediment. As the laser that scans the surface of a split core is 0.4 cm wide and penetrates to a maximum depth of 0.1 cm, only 0.04 cm^3 of sediment is scanned over 1 cm depth. The average volume of sand within this layer was calculated from the averaged sand fraction weight measurements and the density of $CaCO_3$, and the number of grains was inferred by dividing the total sand volume by the estimated volume of individual grains (assuming spherical grains with 120 μm and 180 μm diameters). These calculations showed an estimated 93 fine grains (120 μm diameter) and 20 coarse grains (180 μm diameter) are scanned over 1 cm depth, however this is likely to be an overestimation due to the sand consisting of Si (~25%) as well as

Ca (~35%) and the smallest possible grain size in each fraction used. These calculations indicate that coarse grains in particular may not be well distributed through the sediment and therefore not captured by the ITRAX results. To illustrate the grain size effect the same calculations were repeated, this time using the average carbonate weights of Hosta 1, but assuming that it is composed of homogenous, equal-sized grains. Figure 3.8 shows the number of grains that would be expected if the carbonate content consisted of spheres with 0-150 µm diameters. It is shown that there is an exponential increase in number of sand grains as the grain size decreases. Therefore the smaller grain sizes, particularly below 50 µm, are more likely to be present on the core surface and, due to their abundance, are more likely to be spread through the sediment than the same amount of $CaCO_3$ concentrated in larger sand grains. For this reason it is suggested that grain size may play an important role in the element detection of the ITRAX scanner; a corollary is that by ignoring the very finest sand fraction the sand percentage measurements may have been made inadvertently biased.

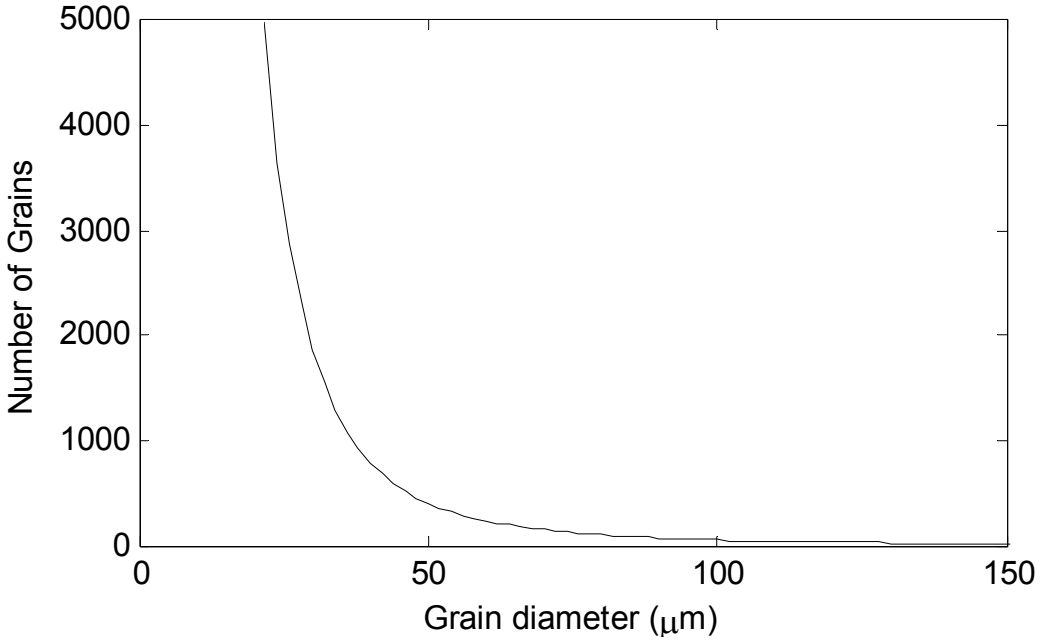

Figure 3.8: Projected numbers of grains in the average carbonate volume of Hosta 1 if identical grain sizes are assumed. The average volume of carbonate measured was estimated using the volume scanned by the ITRAX scanner, the average weight of carbonate (as determined by loss-on-ignition) and the known density of carbonate. This carbonate volume was then divided by the volume of spheres of different sizes to estimate the number of grains this would result in.

3.5. Comparison with instrumental and proxy climate records

To assess whether elemental ITRAX data may be used as a climate proxy the results were compared with instrumental climate data from Stornoway and the NAO index. The first step in this task was to determine the optimum sample resolution for this comparison, as sediment mixing in the lake bed might have introduced noise that will degrade the climate signal at high, annual resolutions. This was done by correlating with instrumental precipitation data at different resolutions (between 1 and 20 years). To assess the sensitivity of the results to the choice of age model, this process was carried out not only on the Ln(Ca/K) results using the 'best' age model produced but using the multiple versions of the record produced from the different age models, as well as the OxCal age model.

The Hosta 1 results (Figure 3.9 B) demonstrate that both the optimum age-depth model and the standard OxCal age-depth model produce significant correlations between Ln(Ca/K) and precipitation at almost all resolutions. Notably not all of the plausible age-depth solutions produce Ln(Ca/K) results that correlate with the precipitation data, which implies that the interpretation of proxy data is highly dependent on obtaining a reliable age model. The second core (Hosta 2; Figure 3.9 C) does not correlate significantly with precipitation when using any of the age models, indicating that precipitation driven changes in runoff are not influencing this coring location, at least during the instrumental period. As Hosta 1 was sampled from nearest to the tributaries (Figure 3.1), the sediment may be recording changes in precipitation resulting from riverine plumes of sediment being deposited (Hilton *et al*., 1986), which may not have reached the furthest end of the lake from which Hosta 2 was sampled. This in some respects contradicts the visual similarity between the two cores; the reason may be that the changes seen in both cores were the result of large magnitude storminess changes influencing both coring sites, whereas the low magnitude variability of the instrumental period only influenced the Hosta 1 coring site closest to the tributaries, which thus can be considered a more sensitive reconstruction.

The changes in correlation (using Hosta 1) can be used to infer the optimum resolution of the data, where the influence of bioturbation and other (noisy) mixing processes are minimised. The correlations between the selected

Hosta 1 Ln(Ca/K) record and annual precipitation correlate significantly at all resolutions up to 10 years, but are at times insignificant at resolutions greater than 10, therefore the correlation of R = 0.62 at 10 years is taken as the maximum correlation achievable, which is equivalent to 3-5 mm sediment depth (Figure 3.9 D). Other versions of the age model, including the OxCal age model, correlate more strongly with precipitation, however it is encouraging that each of these reach the maximum correlation at approximately the same resolution.

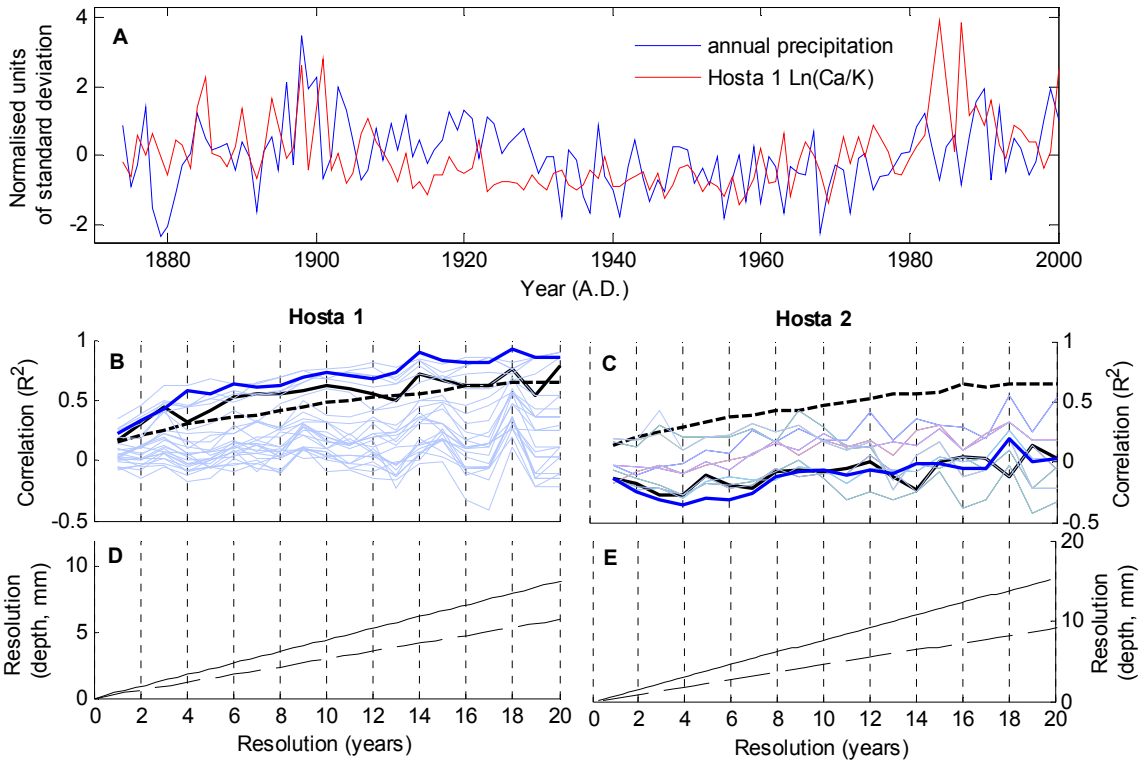

Figure 3.9: Comparison between Ln(Ca/K) and climate indices. A: normalised Stornoway annual precipitation plotted against the Hosta 1 normalised Ln(Ca/K) from 1870-2000 A.D.. B and C: correlation between annual precipitation and the Hosta 1 Ln(Ca/K) (*B*) and Hosta 2 Ln(Ca/K) (*C)* at resolutions between 1 and 20 years, using the selected age model (thick black line), the OxCal age model (thick blue line) and the alternative age models shown in Figure 3.5 (light blue lines). The dashed line indicates the 95% significance level. D and E: conversion between the average depth and resolution for the instrumental period (black line) and full core (dashed line) for Hosta 1 (*D*) and Hosta 2 (*E*).

Having determined the optimum resolution, the Ln(Ca/K) records of both cores, as well as all of the climate indices, were smoothed and downsampled to the 10 year resolution and the correlations between these calculated. Hosta 1 correlated significantly with annual precipitation (R = 0.76; n = 13) and low pressures (R = -0.63, n = 14), which supports that low pressure storms bring sand into the lake, however the correlation with the winter NAO (R = 0.22; n = 18) was insignificant. Hosta 2 did not correlate significantly with precipitation, low pressures or the NAO, however the correlation with annual temperature was negative and significant (R = -0.68, n = 22). This result indicates that different climatic conditions control sediment deposition in different sections of the lake, although the reason for this correlation with temperature is unclear.

The correlation with the instrumental records has supported that storms are influencing the Ln(Ca/K) content of the lake sediment at the site of Hosta 1. By correlating with the Trouet *et al.* (2009) NAO reconstruction the climatic influence on the lake over the past millennium can be investigated. The correlation of the Ln(Ca/K) results (at the 10 year optimum resolution) with the NAO reconstruction of Trouet *et al.* (2009) is significant in both Hosta 1 (R = -0.49, n = 95) and Hosta 2 (R = -0.62, n = 95). The negative correlations contrast with the positive correlation between precipitation/storms and the NAO observed in the instrumental period (Hurrell and Van Loon, 1995). This may indicate that there has been long-term discontinuity of the storm-NAO relationship; for example the Little Ice Age (1400-1850 A.D.) would be expected to have had calm and dry conditions in northwest Scotland given the reconstructed negative NAO (Trouet *et al*., 2009), however the increased Ln(Ca/K) indicates that storminess was higher. Other research supports these findings, suggesting increased Little Ice Age storminess across Europe including the Outer Hebrides (Sorrel *et al*., 2012; Gilbertson *et al*., 1999; Dawson *et al*., 2004), and it has been hypothesised as being the result of intensified storms (Trouet *et al*., 2012). The Ln(Ca/K) reconstruction may therefore be capturing the climate deterioration associated with the Little Ice Age.

3.6. Interpretation

The above correlations of Ln(Ca/K) with precipitation and low pressure instrumental data perhaps indicate that storminess changes resulted in sand deposition into the lake. However human-climate interactions, sea level changes and alternative processes of $CaCO_3$ deposition are necessary considerations in the interpretation of the results presented here.

It is possible that human activities in the vicinity of the lake may have increased the amount of sediment deposited by increasing catchment erosion. The nearby small settlement of Baleloch was in existence between 1666-1815 A.D. (canmore.rcahms, 2014; Moisley, 1961), during the period when the Ln(Ca/K) results indicate greater sand deposition. Furthermore it is suggested that during the coldest periods of the LIA a more severe climate (both cold and stormy) led to people harvesting marram grass for fuel from the sand dunes as well as overgrazing land, removing sand to use as a soil fertilizer and other activities that resulted in sand dune destabilisation (Sommerville *et al.,* 2007; Gilbertson *et al.,* 1999; Angus and Elliot, 1992). The climatically driven human activities may therefore have resulted in more sand entering the lake catchment, so this may have been an indirect way that increased storminess (combined with lower temperatures) caused changes in sand content.

Similarly changes through time of sediment availability could be caused by sea level changes, influencing the distance between the coastline and sand sources. Despite relative sea level in the Outer Hebrides having changed by <0.5m since c. 1 A.D. (Jordan *et al*., 2010), the offshore topography and variable sediment availability may have caused local transgressions (Cattaneo and Steel, 2003; Hansom, 2001). As sand is abundant along this coastline however, and the lake is in close proximity to the machair and dunes, it is not considered that this is a dominant cause of the observed variability in sand content.

Changes in Ln(Ca/K) may also have resulted from a number of autochthonous processes, in addition to the inwashed or aeolian sediment during storms. Along the southwestern edge of the lake there are sandy machair banks (Figure 3.3.), which are likely to be eroded by waves during storms, with sand then transported to the centre of the lake by currents (Hilton *et al*., 1986). This may provide an additional transport pathway for sediment

deposition during storms (particularly for storms with easterly winds). Further investigation of this as well as the extent of the riverine plume around the tributaries would be benefited by geomorphological mapping of the lake bed, to assess the locations of the cores in relation to these deposits.

As described in section 3.2. direct $CaCO_3$ precipitation from the water is considered unlikely given the gneissic bedrock in the catchment, however it is possible that calciferous fauna in the lake may have left remains in the sediment that have varied with lake productivity and therefore temperature or sunlight (Leng *et al.,* 2001). The Hosta 2 core had a significant correlation with temperature; however this was a negative correlation, which is not the expected response between temperature, productivity and $CaCO_3$ deposition. To better understand the composition of the sediment and the possible contributions from shell sand, fauna or even $CaCO_3$ precipitates, it would be beneficial to use SEM elemental mapping (Kotula *et al.,* 2003).

Despite these uncertainties, the above correlations with the long NAO reconstruction and the instrumental climate indices support that the Loch Hosta Ln(Ca/K) reconstruction is capturing a climatic signal. The contributions of sand however may have been somewhat influenced by climatically-induced human changes or bank erosion.

3.7. Spectral Analysis

The variability of the Hosta 1 Ln(Ca/K) has been assessed through spectral analysis, as it is considered that this core contains the strongest storminess signal. An aim of this chapter was to identify the highest resolution of ITRAX analysis: as it is unlikely that noise in the data will have significant cyclical changes, the identification of the highest frequency cycle present may potentially show the resolution at which the climate signal has been preserved. Again, each of the Hosta 1 age models were used in the analysis of periodicities, as a means of assessing the sensitivity of the results to age-depth model selection.

The Lomb-Scargle spectral analysis (Figure 3.10) indicated that many centennial-scale cycles were present, including those of c.860, 250-200, 153-

139 and 105-95 years, which are significant in all or most of the age models. Shorter cycles of 77-87 and 50-58 are also identified in many of the age models. The shortest cycle of 16-20 years is only significant in the results of one age model, although many show an insignificant peak at this frequency. This is potentially a real cycle therefore, however the detection of this and other high frequency cycles is clearly highly dependent on the skill of the age model, as small errors in the dating would distort the cycle greatly. The comparison with instrumental climate data indicated that the optimum resolution of Hosta 1 was 10 years, and the identification of the 16-20 year cycle, which has a Nyquist frequency between 8 and 10 years, supports that this is the case. Finally cross-spectral analysis of the main Hosta 1 Ln(Ca/K) record with the Trouet *et al* .(2009) NAO reconstruction showed shared cycles of 256 and 60 years, which implies an NAO influence on the Ln(Ca/K). This supports that the positive correlation between the NAO and storminess and precipitation during the instrumental period (Hurrell and Van Loon, 1997) has been consistent over the last millennium.

Many of the cycles identified are similar to those identified in NAO reconstructions. The 16-20 year cycle is similar to a ~20 year cycle that has been identified in previous NAO reconstructions (Olsen *et al*., 2012; Glueck and Stockton, 2001; Cook *et al*., 1998; Luterbacher *et al*., 1999). The cycle of 50-58 years, and the 60-year cycle identified by the cross-spectral analysis, is similar to a c.60 year cycle often identified in NAO reconstructions (Glueck and Stockton, 2001; Luterbacher *et al*., 1999; Olsen *et al*., 2012; Wanner *et al*., 2001; Cook *et al*., 1998) as well as in the GISP2 sodium reconstruction of storminess spanning the last 1000 years (Fischer and Mieding, 2005). Cycles around this length are also features of the AMO index of North Atlantic temperatures (Kerr, 2000): the 50-58 year and 77-87 year cycles identified in Loch Hosta resemble the dominant 60-80 year cyclicity of the AMO (Wanner *et al*., 2001; Higuchi *et al*., 1999; Enfield *et al*., 2001; Kerr, 2000; Gray *et al*., 2004; Knudsen *et al*., 2011). The results indicate that there may be an ocean-atmosphere climate link controlling storminess and precipitation patterns over multi-decadal timescales. A link with the NAO is not supported however by the longer cycles present in the reconstruction (95-105, 139-153, and 200-250 years), as the longest NAO reconstruction included cycles of c.170 and 300

years (Olsen *et al*., 2012). The cause of these cycles are therefore unclear, although the 200-250 year cycle resembles the c.220 year solar cycle (e.g. Stuiver and Braziunas, 1989), indicating solar changes are a possible external climate forcing.

Overall the spectral analysis results provide some support that the maximum resolution of the Hosta 1 Ln(Ca/K) record is around 10-years, as implied by the occurrence, albeit weakly, of the 16-20 year cycle in the record. The presence of cycles of 16-20, 50-58 and 77-87 years support that changes in the NAO and AMO are influencing temporal precipitation patterns in this region. The influence on storminess from the NAO and AMO will be discussed further in Chapter 6, as here the results will be combined with those from the studied peat bogs (Chapters 4 and 5) as well as others from Europe and the North Atlantic.

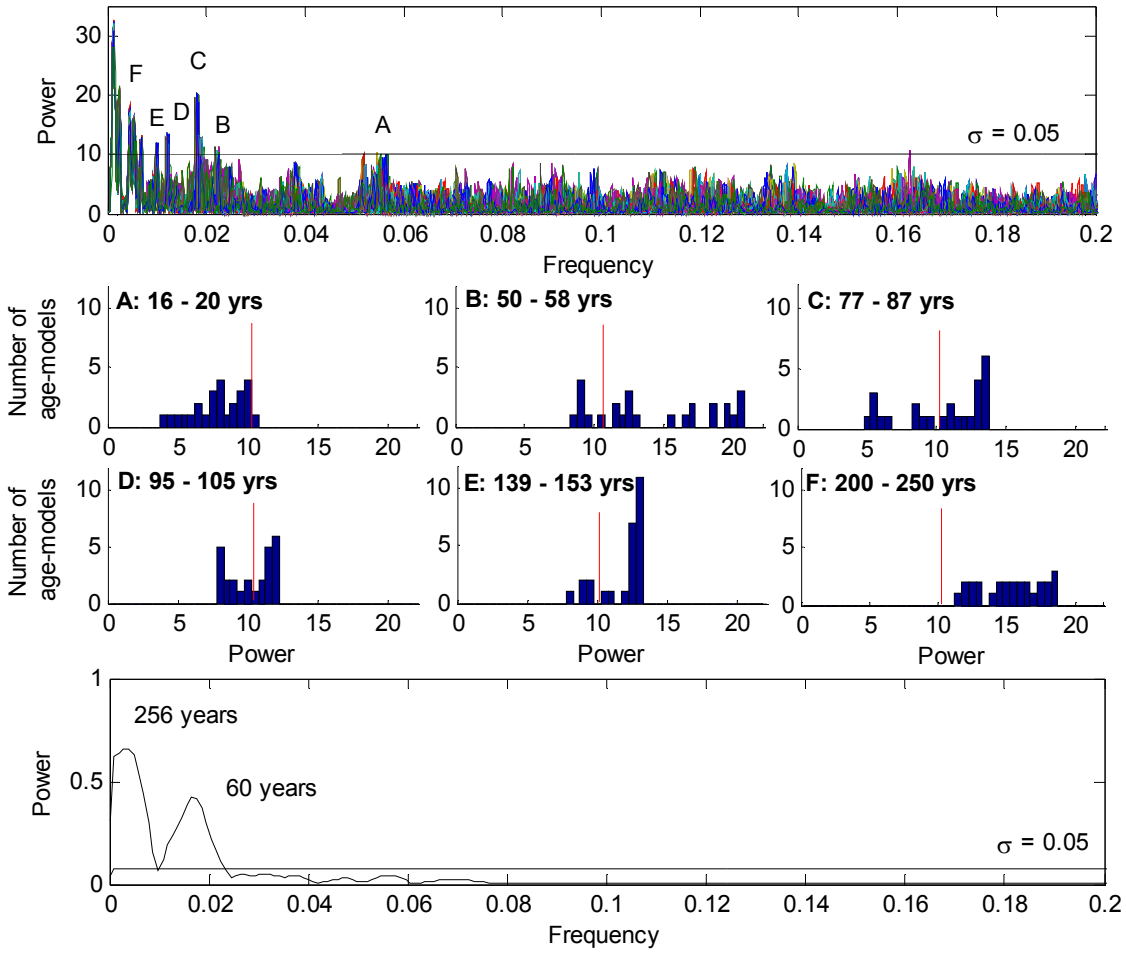

Figure 3.10: *Top:* The Lomb-Scargle spectral analysis of the Hosta 1 Ln(Ca/K) using the many age models shown in Figure 3.5. The black line illustrates the σ=0.05 significance level and labels A-F show the significant peaks, which correspond to histograms A-F. *Middle:* Histograms showing the number of spectral peaks at specified periods produced from the different iterations of age-depth fits: note that many of the randomly generated age-depth fit lines overlap, so while there were 500 fits modelled many of them overlap. Results to the right of the red line are statistically significant at the 95% confidence level. There is a high degree of confidence in the cycle identified if most of the modelled age-depth solutions produce cycles lying to the right of the significance line, and vice-versa where most results lie to the left. *Bottom:* cross-spectral analysis results between the Hosta 1 Ln(Ca/K) results and the Trouet *et al.,* (2009) NAO reconstruction (using method outlined in section 2.8.3.; Chatfield, 2004). The black line indicates the σ=0.05 significance level.

3.8. Methodological assessment

One of the aims of this research was to investigate the potential of ITRAX XRF analysis as a method of creating high resolution climate reconstructions. To maximise the skill of the ITRAX data the age-depth models were tuned and the results calibrated. The potential for climate reconstructions has been assessed by comparisons with climate indices, measurements of the sedimentology of the core and spectral analysis, as well as testing the sensitivity of the data to the choice of age model. Using these methods it has been demonstrated that there is a climatic influence on the Ln(Ca/K) content of the lake, with storm driven changes in sedimentation in the core from closest to the tributaries. In this section the ITRAX methods potential will be discussed further.

The method of Weltje and Tjallingi (2008) was used to calibrate the data, which was expressed as a natural-log ratio to reduce the influence of matrix and dilution effects, and factors relating to sediment composition that have proved problematic in previous research (e.g. Löwemark *et al*., 2010). The significance testing following calibration was a useful confirmation of its success, and supported that the chosen ratio was reflecting real element concentrations.

In addition to the standard OxCal age-depth model a tuning-technique was also used: multiple age-depth curves were calculated within the age errors, and following this the 'best' age-depth curves of the two cores were selected, based on the strength of correlation between each cores sand weight results, i.e. their common environmental signal. When performing the spectral analysis and correlation with climate data, to address the sensitivity of the results to age-model selection, the results of the other possible age models and the OxCal age model were also looked at. The correlation with instrumental climate data gave some indication that the results are sensitive to the chosen age model, presumably because the size of the age errors (and therefore the potential range of ages for each sample) are large compared to the length and resolution of the instrumental data. On cores with better dating constraints this problem may be limited. Nevertheless the Hosta 1 age model created by the tuning-method, and the OxCal age model, correlated well with the precipitation data, which demonstrates that carefully selected element ratios of ITRAX data can be used to make palaeoclimatic reconstructions. The spectral analysis of the

results indicated that the detection of low-frequency cycles was less sensitive to the age-model selection; the higher frequency cycles appeared to be much more sensitive, for example the 16-20 year cycle was only significant in one age model. This could be because the errors in the dating were in some cases larger than the cycles being detected, causing the age models to distort the cycle. Therefore the choice of age model is an important factor influencing whether or not high-frequency cycles are detectable. These results highlight an issue with ITRAX XRF analysis, as although the method allows high sub-millimetre resolution data to be produced (Weltje and Tjallingi, 2008; Croudace *et al*., 2006), the results are sensitive to age errors.

An aim of this research was to assess the maximum resolution, given possible sediment disturbance from bioturbation and basal lake currents among other causes (Krantzberg, 1985; Lee, 1970). This was achieved by correlating Ln(Ca/K) with precipitation data at different resolutions and spectral analysis. In Hosta 1 both these methods indicated the optimum resolution was reached at ~10 years resolution (representing 3-5 mm), however even at higher resolutions the correlations were significant, which suggests that the sediment mixing has degraded rather than destroyed the climatic signal in the sediment (Lee, 1970; White and Miller, 2008). At this 10-year resolution, results are the average of measurements from a 3 mm sample thickness, across a 4 mm wide scanning cross-section and to x-ray penetration depths of 1 mm (Croudace *et al*., 2006). Therefore the averaging of the element measurements over both width and depth may reduce the influence of sediment mixing and enable the ITRAX analysis results to correlate with instrumental data at high resolutions. Overall the evidence suggests that bioturbation in the deepest part of Loch Hosta is minimal, so in similar lakes the ITRAX XRF method could potenially provide sub-centimetre resolution results.

Finally, the results indicated that ITRAX elemental analysis may be most sensitive at detecting fine sediment changes, as coarser sand fractions were found to not correlate positively with the Ln(Ca/K) measurements. Similarly a lake precipitation reconstruction from the Alps found low correlations between coarse sand and ITRAX calcium results, which was suggested as being the result of the analyses being carried out on different sediment from the same depth and sediment deformation during coring (Giguet-Covex *et al*., 2012).

However here it is alternatively suggested that fine-scale ITRAX measurements may be capturing changes in the amount of very fine Ca silt and sand rather than the coarser sand. This was suggested because there was a similarity between the Ln(Ca/K) and the carbonate measurements, which reflect grains of all sizes. The calculations demonstrated an exponential increase in the number of particles in the sediment as the grain size decreases, which supports that the finer sediments will be more dispersed within the sediment, so are more likely to be detected by the ITRAX scan of the surface sediment.

The evidence given here goes some way to showing that ITRAX XRF core scanning can be used to make palaeo-climate reconstructions using sub-centimetre resolution measurements, as in Loch Hosta it appears to produce a multi-annual resolution record. Proxies that offer annual resolution results, such as speleothem reconstructions or varved lake sediments, are not present in many regions; therefore the ITRAX method provides a widely applicable alternative for high resolution terrestrial climate reconstructions.

3.9. Conclusion

Past changes in storminess in the Outer Hebrides (since 200 A.D.) have been reconstructed with high-resolution ITRAX elemental analysis. The Ln(Ca/K) ratio in a core sampled from close to a tributary correlated with instrumental records of precipitation and low-pressures, indicating that storms deliver pulses of sediment into the lake. The presented storminess reconstruction has distinct centennial-scale changes, which can be related to the higher storminess during the Little Ice Age. The results support previous findings that the LIA had high storminess, despite a negative NAO and southerly storm track, something which has been suggested as being due to higher storm intensity (Trouet *et al*., 2012). Spectral analysis, and cross-spectral analysis with a long NAO reconstruction (Trouet *et al*., 2009), supported an influence of the NAO and oceanic temperature on climate, particularly as c.50-80 year cycles were identified. These results demonstrate that there is a strong climatic influence on Loch Hosta resulting from regional storminess.

The research in this chapter aimed to assess whether sub-millimetre resolution ITRAX data can be useful for producing high resolution climate

records. This chapter has investigated the optimum resolution of the ITRAX data in this location, given possible disturbance from bioturbation and other sediment mixing processes. This was done by comparing the ITRAX results with instrumental data at different resolutions, as well as establishing the highest frequency cycles present in the raw ITRAX data. Both methods gave some indication that the optimum resolution was reached at 10 years, which in Loch Hosta corresponds to 0.3-0.5 cm. Therefore it is suggested that meaningful sub-centimetre sampling resolutions can be attained using ITRAX analysis.

The results imply that the correlation with instrumental data, and the identification of high frequency cycles in particular, are highly sensitive to the age model used; the standard OxCal age-model offered one of the most robust solutions, while low frequency cycles were identified using most age models. This is thought to be due to the relatively large dating errors (and therefore the range of possible ages for each sample depth) compared to the frequency of the short cycles and the resolution and length of the instrumental data.

Finally the comparison of the results with traditional analyses of sediment composition indicated that the Ln(Ca/K) was reflecting changes in the carbonate content rather than the sand fraction. This is suggested as being the result of a much greater distribution of fine sand within the sediment, meaning it is more likely to be measured by the high resolution ITRAX laser, which analyses only a small quantity of sediment compared to traditional methods.

Chapter 4: Late Holocene storminess in Northwest Scotland - Two peat reconstructions from the Outer Hebrides

4.1. Introduction

In this chapter the results from two peat bog reconstructions of storminess from the Outer Hebrides in western Scotland will be presented. Future climate change predictions indicate that Atlantic storm tracks will shift northwards and bring more frequent storms to Britain and Scandinavia by 2100 A.D. (Stocker *et al.*, 2013), suggesting that the current levels of storminess are likely to increase in the near-future. Currently storms have the potential to cause widespread damage. The 2011 National Flood Risk Assessment showed that in Scotland 125,000 properties were at risk of flooding, with 17% of floods caused by the sea when there are high winds and low atmospheric pressures (SEPA, 2011). However flooding is only one aspect of storms, as high winds can cause infrastructural damage inland. A recent example of a severe storm was the January 2005 storm, which caused hurricane-strength winds, coastal flooding, erosion and loss of life on the Outer Hebrides. Storms of this magnitude are relatively frequent as there have been two other storms of greater severity since 1980 (Wolf 2007, Dawson *et al*. 2007). If the predictions of increased storminess in the British Isles in the future are realised, the vulnerability to storms in the Outer Hebrides and Scotland is likely to increase, which could have economic and social impacts on many communities. Reconstructions allow better understanding of storminess patterns, recurrence intervals, potential storm intensity and insight into the causes of storminess, so enable authorities to better prepare for increasing storminess.

The NAO is a dominant influence on storminess across northern Europe. There is a strong positive correlation in the Outer Hebrides between the NAO and storminess during the instrumental period (Pirazzoli *et al*., 2010; Andrade *et al*., 2008). However it has been suggested that the storm-NAO relationship is not constant, both within the instrumental period (Dawson *et al.,* 2002) and during the Little Ice Age (Trouet *et al.*, 2012; Raible *et al.*, 2007; Lamb., 1995). The longest NAO reconstruction spanning the Late Holocene suggests the NAO was often negative between 4300-2000 cal yr BP, and persistently positive between 2000 and 600 cal yr BP (Olsen *et al*., 2012). However this contrasts

with evidence of cyclical storminess changes (1500-1800 year pacing) through the Late Holocene (Sorrell *et al*., 2012, Debret *et al*., 2007; Fletcher *et al*., 2012), which also suggest that there are inconsistencies in the long-term NAO-storm relationship. Storminess reconstructions that span the Late Holocene will help determine how far the NAO influences storminess over centennial timescales. Furthermore centennial cycles of 170 and 300 years have been identified in the NAO (Olsen *et al*., 2012), which if also present in storminess reconstructions can indicate long-term continuity of the NAO-storminess relationship. Similarly the presence in the storminess reconstructions of solar cycles of c.3300-2500, 2200-2100, 1050-830, 710, 520, 420, 350, 300, 230-200 and 150-140 years (Debret *et al*., 2007; Damon and Sonett, 1991; Stuiver and Braziunas, 1989; 1993; Stuiver *et al*., 1995; Steinhilber *et al*., 2012; Wirth *et al*., 2013) and oceanic circulation cycles of c.1370 ± 500 (Bond *et al*., 1997; Bianchi and McCave, 1999; Debret *et al*., 2007) can also give an indication of what is forcing storminess variability.

A number of methods have been used to create storminess reconstructions in Scotland. On the Outer Hebrides reconstructions have been made by dating wedges of sand that have blown inland during periods of high storminess (Dawson *et al*., 2004) and by dating sand dune movements (Gilbertson *et al*., 1999). Additionally a pollen reconstruction from St Kilda shows increases in maritime plant communities during times of higher sea spray (Walker, 1984). However no continuous and decadal resolution reconstructions of storminess have been made from the Outer Hebrides, which means that only broad comparisons can be made between suggested periods of high storminess and other proxy reconstructions. Storminess elsewhere in Scotland has been investigated using documentary evidence, which describes temporal variations as well as individual severe storms (Hickey, 1997; Lamb, 1984; 1991). Longer reconstructions of storminess in Scotland and northern Ireland have been made by dating periods of sand dune activity and buried sand layers (Wilson, 2002; Wilson *et al*., 2004; Sommerville *et al*., 2003; 2007; Tisdall *et al*., 2013) and dating cliff-top storm deposits (Hansom and Hall, 2009; Hall *et al*., 2006). High precipitation accompanies storm events and is also positively correlated with the NAO (Trigo *et al*., 2002); precipitation reconstructions have been created using various methods. These include reconstructions of

allochthonous material deposited into lakes (Oldfield *et al*., 2010) and speleothem characteristics (Proctor *et al*., 2000; 2002; Charman *et al*., 2001). Comparison between these is somewhat limited by the nature of the reconstructions, as it is likely that they are influenced to varying degrees by seasonality, storm intensity and direction, temperature, human activities and sea level changes. Therefore interpretation and inter-comparison of storminess reconstructions requires consideration of these factors.

The aim of this chapter is to present two Late Holocene storminess reconstructions from the Outer Hebrides, as a means of improving understanding of storminess in northern Europe. During storms in the Outer Hebrides the wind blows sand from the machair and beaches, situated on the west coasts of the islands, across the peatland inland. Analysis of the sand content within two continually-accreting peat bogs provides a decadal-resolution and continuous reconstruction of past storminess (Björck and Clemmensen, 2004; De Jong *et al*., 2006). To confirm that reconstructions are reflecting storminess a number of factors must be considered, for example the Late Holocene increase in relative sea level (Jordan *et al*., 2010) and the long history of human occupation of the Outer Hebrides (Sharples and Pearson, 1999; Bennet *et al*., 1990; Henley, 2003; Garrow and Sturt, 2011; Ashmore *et al*., 2000). The effect of sediment disturbance due to local human impact is limited by using two sites, as shared storminess patterns are likely to influence both sites, whereas human impacts are not. The two reconstructions will then be compared with other storminess and precipitation reconstructions from the region. It has also been found that reconstructions of aerosols from bogs may be influenced by micro-topography (which affects vegetation species, surface wetness variations and accumulation rate) and marginal effects (Coggins *et al*., 2006; Bindler *et al*., 2004; Mauquoy *et al*., 2002; Hendon *et al*., 2001). Therefore in addition to a main core from each bog, a transect of three shorter cores across the bogs are also analysed to allow intra-bog variations in sand deposition to be assessed. Therefore in this chapter the two peat bog reconstructions of storminess from the Outer Hebrides are presented and supported by intra-bog, inter-bog and regional comparisons. The focus is on the local environments of the bogs and regional climate of northwest Europe, as the broader patterns of European storminess will be discussed in Chapter 6.

4.2. Study Area

4.2.1. General overview

The location of the Outer Hebrides in the eastern Atlantic Ocean means that the islands have a hyperoceanic climate, with mild, wet and windy weather (see Figure 3.2; Birse, 1971; Langdon *et al*., 2005). The Outer Hebrides are situated to the south of a major storm track, so storms often bring gales from the south and west (Angus, 1997). During the instrumental period the weather of the region has been more strongly influenced by the NAO than much of the rest of Europe (Figure 4.1; Andrade *et al*., 2008), as there is a positive correlation between the NAO and precipitation, gale days and wind speed (Pirazzoli *et al*., 2010; Corbel *et al*., 2007; Marques *et al*., 2008). These are the result of the storm track crossing northern Europe and intensifying when there is a positive NAO index (Hurrell and Van Loon, 1997; Hurrell, 1995). As the NAO is a dominant control on the climate of the Outer Hebrides it is an ideal location from which to reconstruct storminess and investigate the influence of the NAO during the Late Holocene.

In this research storminess is reconstructed using sand deposits in ombrotrophic peat bogs. This method requires firstly that there are ombrotrophic peat bogs that have developed over the period of interest, and secondly that there is an abundant sand supply for aeolian entrainment and transport during storms. The sand source in the Outer Hebrides is the unique machair ecosystem, which encompasses beaches, sand dunes, machair grassland, machair lochs, blackland (machair-peat transition), saltmarshes and sandflats (Boorman, 1993). The machair formation was the result of rising sea levels following the last glacial; a transgression first transported material from the continental shelf onto the shore and then pushed it further inland (Ritchie and Whittington, 1994). To the east of the machair are soils consisting of peaty gleys, peaty podzols and importantly raised peat bogs (Angus 1997, Hudson 1991). The conditions are favourable for peat growth on the Outer Hebrides as there is an iron pan horizon in the soil and high precipitation, which cause water-logging and acidity (Glentworth 1979; Moore, 1987; Bragg, 2002). Localised peat bogs are thought to have been in existence on the Outer Hebrides from as early as 9100 cal yr BP (Ritchie, 1985) and were more extensive after the reduction of forests, which occurred between 5200-3800 cal

yr BP due to human pressure and a more oceanic climate (Bennet *et al*., 1990; Fossitt, 1996). Therefore an abundant sand supply in close proximity to raised peat bogs, which have been in existence over the Late Holocene, make this a suitable location to develop reconstructions of past storminess.

The amount of sand being blown onto the bogs in the past may have been influenced by sea level change altering the proximity of the sand sources. Jordan *et al.* (2010) has carried out the only fieldwork-based reconstruction of sea level from the Outer Hebrides, from the Isle of Harris. The results indicate that relative sea level gradually increased from around 2 m below present after 4000 cal yr BP, with the rate of increase slowing through time, until present levels were reached at approximately 3100-2000 cal yr BP (Jordan *et al*., 2010). These results suggest that through time a transgression may have occurred changing the positions of the coastline and sand sources. On the other hand, Ritchie (1966) suggested that sea level changes were insufficient to influence the coastline after 5700 cal yr BP, which would indicate the distance between the coastline (sand sources) and the bogs was unaffected by the sea-level changes over the Late Holocene.

The Outer Hebrides have been inhabited by humans through the Late Holocene (Henley, 2003; Garrow and Sturt, 2011; Sharples and Pearson, 1999), which could have caused disturbance in the catchment. Between c.2500-600 cal yr BP people lived on the machair, as shown by archaeological evidence and the deposition of anthropogenic organic layers (Sharples and Pearson, 1999; Gilbertson *et al*., 1999) and people may also have been responsible for gradual deforestation (Ashmore *et al*., 2000; Bennet *et al*., 1990). After 600 cal yr BP settlements moved eastwards onto the peat lands, potentially as a result of sand dune instability from a climate deterioration or grazing pressure (Sharples and Pearson, 1999; Bennet *et al*., 1990). There is a risk therefore that human activities could have disturbed sediment, leading to increased aeolian entrainment and transport of sand during storms.

Two peat bogs have been cored during this investigation: Struban Bog on North Uist and Hill Top Bog on South Uist (Figure 4.1). These sites are both situated on the west coast of the Outer Hebrides, in exposed locations close to sand sources (the beaches and machair). The two sites are approximately 40

km apart and were selected to separate the regional storminess signal, expected to be present in each core, from local climate, environmental and human changes.

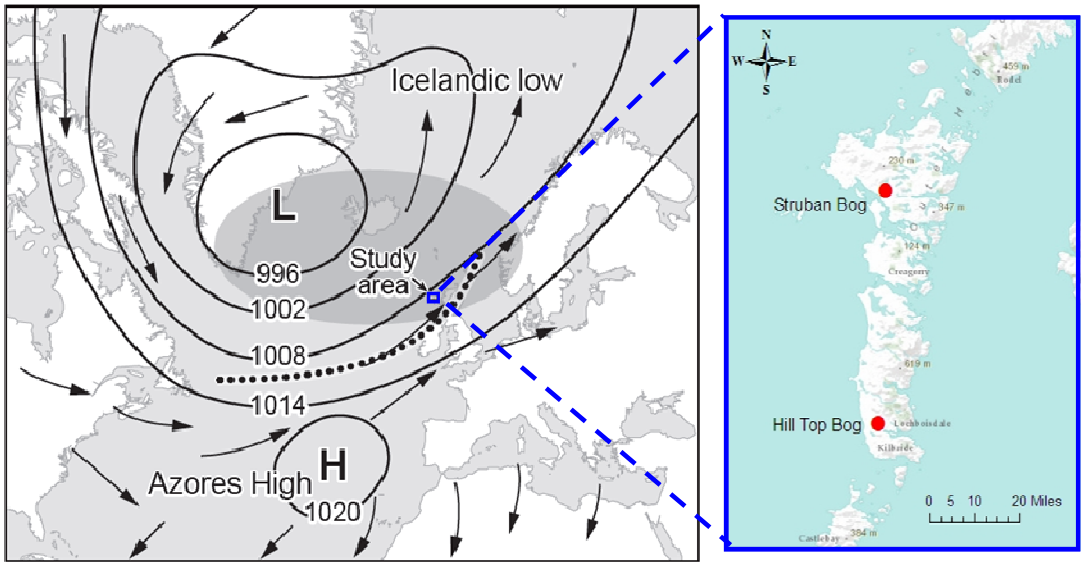

Figure 4.1.: Summary map of the pressure pattern of the North Atlantic Oscillation and the location of the Outer Hebrides, Scotland. Shaded area is the approximate region of increased cyclone frequency during positive NAO (>1) index years (based on Andrade *et al.*, 2008). *Right:* map of the Outer Hebrides including the location of Struban Bog on North Uist and Hill Top Bog on South Uist.

4.2.2. Struban Bog

Struban Bog (Figures 4.2, 4.3 and 4.4) is a raised peat bog located on the west coast of North Uist at 57°33'35"N, 7°20'45"W, around 1 km from the tidal sands that separate North Uist from the island of Baleshare. The bog is on an outcrop of bedrock surrounded by four lochs, which are connected by streams and form an “island” (Figure 4.4). Much of this is covered by blanket peat that has exposures of rock in places, however towards the western, seaward end there is a large depression in the bedrock, in which Struban Bog has formed. As the peat bog is surrounded by lochs, with only small rock outcrops around its edges, inflow from surrounding areas is minimal, and therefore the bog is ombrotrophic. The peat bog extends over an area of approximately 0.05 km^2 and has a maximum depth of 6 m.

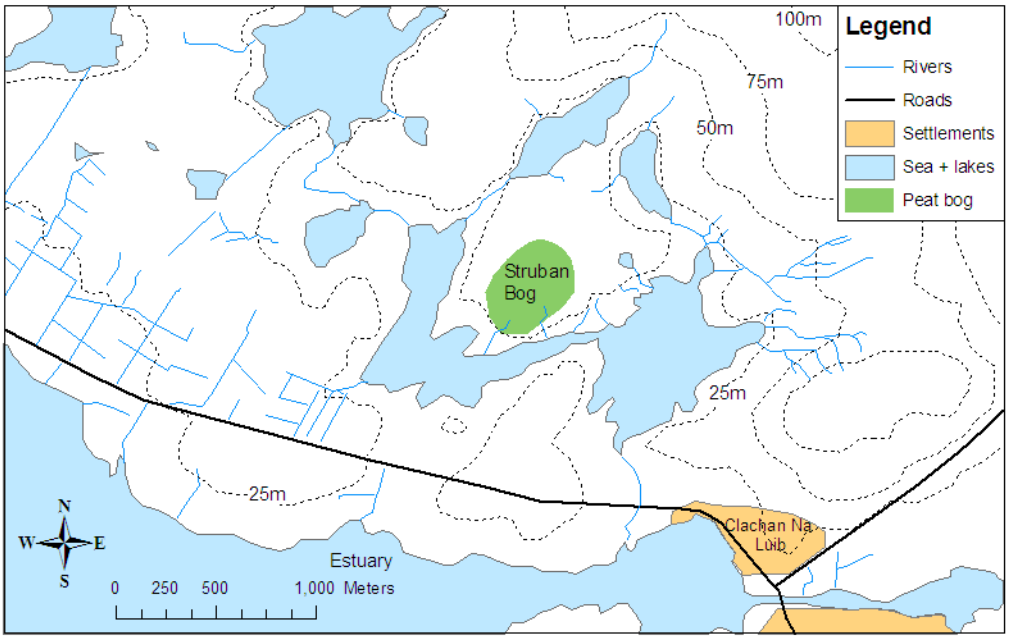

Figure 4.2.: Map showing the location of Struban Bog, North Uist, in relation to the coast, settlements, roads, waterways and topography.

Figure 4.3: View of Struban Bog from the southeast.

Figure 4.4: Satellite image of Struban Bog showing the coring locations (transect cores 1-3 and the main core).

4.2.3. Hill Top Bog

Hill Top Bog (Figures 4.5 and 4.6), on the western side of South Uist at 57°10'5"N, 7°20'52"W, is a peat bog around 3 km from the sea. The bog sits on top of an exposed hill with no higher ground adjacent; therefore there is minimal drainage of groundwater into the bog. Towards the nearby road (the A865) and Dalabrog the peat has been cut in the past, however the central peat bog appears in satellite images to have been untouched (Figure 4.7). The area of the bog is approximately 0.03 km^2 and it reaches a maximum depth of 6.1 m.

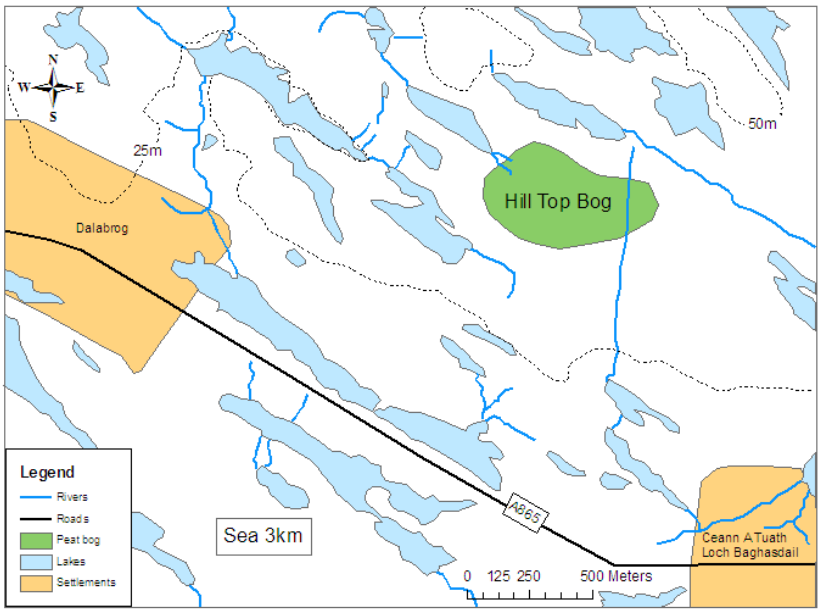

Figure 4.5: Map of Hill Top Bog, South Uist, showing the surrounding settlements, roads, lochs and rivers.

Figure 4.6: View from Hill Top Bog, looking to the north east (top) and south west (bottom)

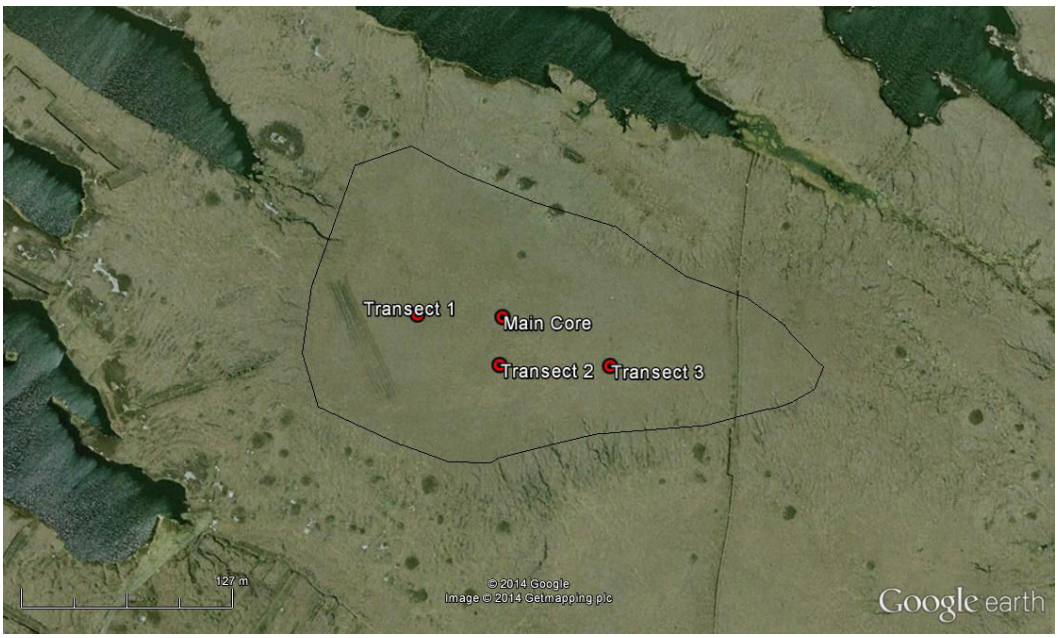

Figure 4.7: Satellite image of Hill Top Bog showing the positions of transect cores 1-3 and the main core as well as areas of peat cutting.

4.3. Methods

A 3 m long core was sampled from the centre of each bog in September 2011; these were to provide long storm reconstructions with chronological control. Cores were extracted using two drives, so that there could be 10 cm overlaps between segments of core, in order to limit the disturbance at the ends of the segments. Following this, in June 2012, three-core transects were taken across each peat bog from the seaward side going inland, to assess intra-bog variations. The shorter transect cores were taken using one continuous drive, meaning there is a possibility of some sediment disturbance at the ends of core segments. Coring of the peat bogs was carried out using a Russian Corer with a barrel length of 50 cm. Peat cores were transferred to plastic tubing and wrapped securely in plastic film in the field. The cores were transported horizontally to limit water movement, and stored in a cold store following fieldwork.

The main core chronologies were constructed using radiocarbon dating (AMS ^{14}C). Dated samples were taken from 1 cm depths of the core, unless there was insufficient material for dating, in which case 2 cm of sediment was used. Under the microscope above-ground plant material (such as leaves, twigs

and seeds) were collected for dating, to prevent roots being dated as these originate from younger plants (Piotrowska *et al*., 2011, Kilian *et al*., 1995). Radiocarbon dating on most samples was carried out by the NERC Radiocarbon Facility and the SUERC AMS Laboratory; however a sample from each core was dated by the radiocarbon facility (^{14}CHRONO) at Queens University, Belfast. Age-depth models were produced using Bayesian analysis by OxCal version 4.2.3, using the IntCal13 calibration curve (Ramsey, 2013; Reimer *et al*., 2009; Ramsey, 2009a). The median of the modelled 2-sigma age range was used to estimate the age for individual samples down the core.

As explained in sections 2.7.1 and 2.8 the sand content of the cores was assessed by analysis of the inorganic content, and the 120-180 μm and >180 μm fractions. The IR, sand fraction analysis and sand influx results together can be used to show peaks in sand content in the peat, and are therefore proxies for storminess. The IR and sand fraction analysis have been done on the main cores as well as the transects, however the lack of age control on the transect cores mean that the sand influx cannot be calculated.

Using the results from the loss-on-ignition method the Organic Bulk Density (OBD) was calculated as follows:

Organic bulk density (g cm^{-3}) = (dry weight – ignited weight)/wet volume

Some authors have shown that low organic bulk density values are associated with poorly humified peat, suggesting high moss production and/or a high water table (Yu *et al*., 2003; Björck and Clemmensen, 2004; Chambers *et al*., 2011).

As described in section 2.8.3. cycles within the sand influx records were analysed using the Lomb-Scargle spectral analysis method (Lomb, 1976; Press and Rybicki, 1989; Scargle, 1982) and wavelet analysis (Morlet, 1983; Lau and Weng, 1995; Torrence and Compo, 1998).

4.4. Results

4.4.1. Struban Bog results

The upper 16 cm of peat from the Struban Bog main core, corresponding to the modern active peat (acrotelm), was not preserved during coring. Therefore the Struban Bog core spans from 16-300 cm depth. The peat is humified and sedge dominated, with rather little *Sphagnum* content. The OBD (Figure 4.8) has small variations through most of the core before a gradual increase between 100 and 40 cm. The values are typically less than 0.1 g cm^{-3}, indicating that humification was low and is typical of ombrotrophic bog conditions (De Jong *et al*., 2009). The IR has values of around 2-4% through much of the core (between 300-70 cm), however both the IR and sand content show four distinct peaks above 70 cm. The similarity between the IR and sand weight results shows that the IR is dominated by changes in the sand sized particles within the peat, especially those between 120-180 µm.

The 3 m main core was dated using seven radiocarbon dates, which are displayed in Table 4.1. A full 6 m core to the base of the bog was sampled during a preliminary visit, and a single sample from just above the underlying bedrock/clay (at a depth of 597-599 cm) was radiocarbon dated, which shows the bog developed at c.10,640 cal yr BP. The full 6 m peat core has not been analysed here, as the period of interest is the Late Holocene, however this radiocarbon date shows the potential for reconstructions spanning the entire Holocene from this site. The modelled age-depth curve for the 3 m core, along with the 2-sigma errors, is shown in Figure 4.8. The core spans the period from 4200 to 200 cal yr BP and shows there has been a fairly constant peat accumulation rate through this time. This is beneficial to storminess reconstructions, as sand accumulation will not be influenced by changes in the peat accumulation rate.

On Struban Bog the sand deposition is shown by the IR, sand weight and sand influx results (Figure 4.9). As a result of the constant peat accumulation rate, the sand influx results are very similar to the sand weight results. Sand deposition onto the bog was relatively low between 4200-1500 cal yr BP, although the magnitude of sand peaks increased through this time. After 1000 cal yr BP sand deposition abruptly increased, with four peaks centred at c.800,

700, 500 and 300 cal yr BP. The results show that the 120-180 μm sand content varies more than the >180 μm fraction. The smaller sand will have been more easily transported, so reflects lower magnitude storms; more medium than coarse sand was deposited at c.2500, 1500, 500 and 300 cal yr BP and may show frequent but low magnitude storms around these times. There are other periods when there are peaks in coarse sand, for example at c.2900 and 1300 cal yr BP and during the period 1000-700 cal yr BP, so it can be inferred that there were more severe storms capable of transporting large sand particles during these times.

The OBD values are low but variable between 4200 and 1500 cal yr BP, indicating low humification, and therefore summer conditions on the bog were wetter (causing less decomposition) and/or more productive (more moss production) (Chambers *et al*., 2011; Yu *et al*., 2003; De Jong *et al*., 2006). After 1500 cal yr BP the increasing organic density values suggest drier summer conditions and/or less productivity, as low water tables on the bog would cause more peat decomposition and high humification (Yu *et al*., 2003; De Jong *et al*., 2006). Overall the change in peat humification resembles the sand content changes, perhaps indicating a climatic change after 1500 cal yr BP.

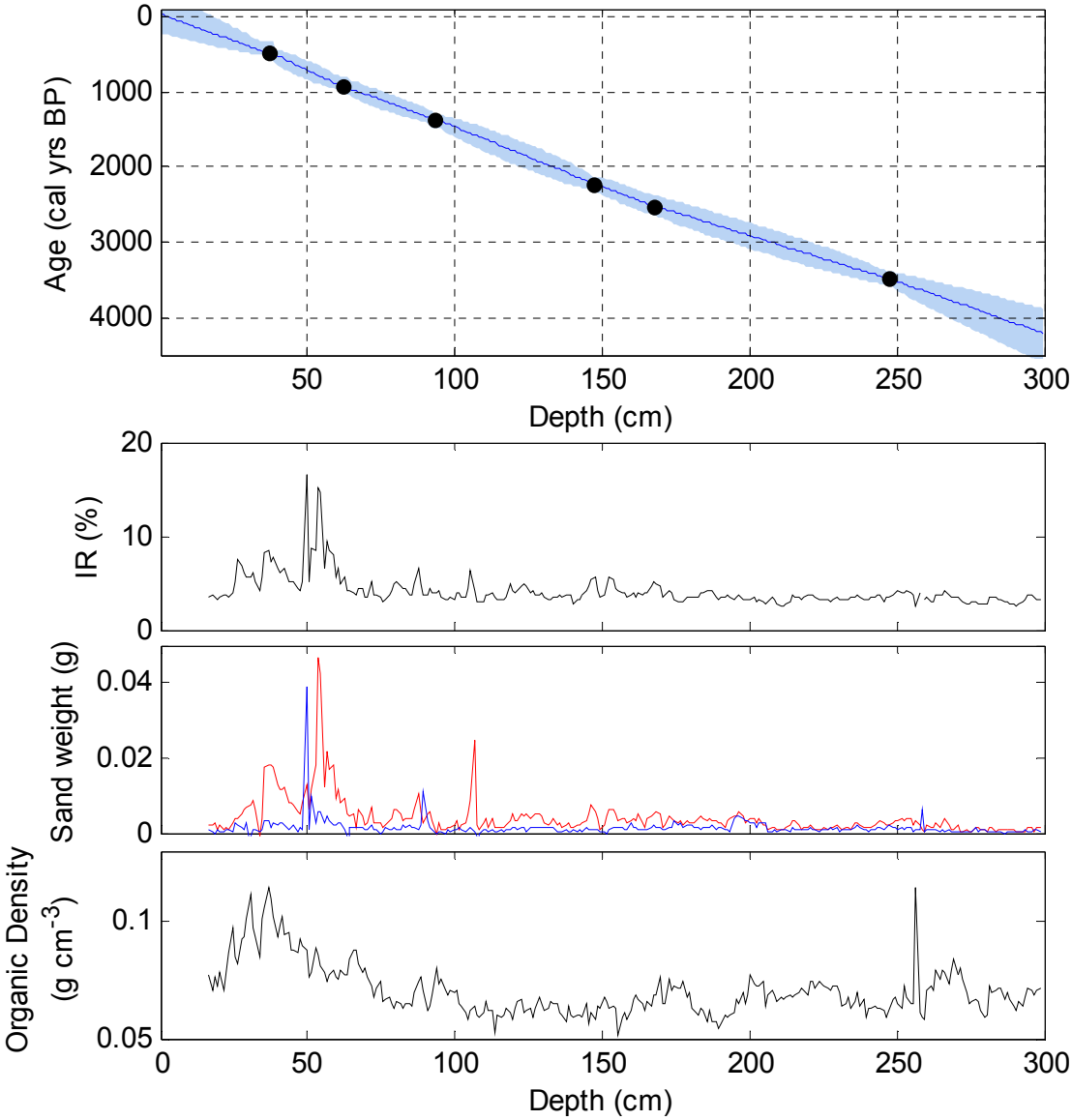

Figure 4.8: Struban Bog raw results and age-depth model (*from top*): age-depth model including dated horizons (black points) and 2-sigma error (shaded blue area), ignition residue, sand weight and organic bulk density results. Red line shows the 120-180 µm sand fraction and the blue line shows the >180 µm fraction.

Table 4.1: Radiocarbon dating results from Struban Bog main core

Sample Depth (cm)	Laboratory Code	$\delta^{13}C$ (‰)	Radiocarbon Age (^{14}C yr BP ± 1σ)	Median calibrated age (cal yr BP) and 2σ range
37-38	SUERC-51107	-29.4	417 ± 35	492 (340-530)
62-63	SUERC-51108	-29.4	1024 ± 35	938 (801-987)
93-94	SUERC-51109	-30.0	1447 ± 35	1364 (1301-1474)
147-148	SUERC-41801	-26.8	2201 ± 37	2225 (2129-2314)
167-168	SUERC-41802	-29.4	2488 ± 37	2512 (2369-2639)
247-248	SUERC-41803	-29.4	3249 ± 37	3483 (3398-3568)
597-599	UBA-18149	-27.7	9410 ± 41	10 639 (10523 – 10743)

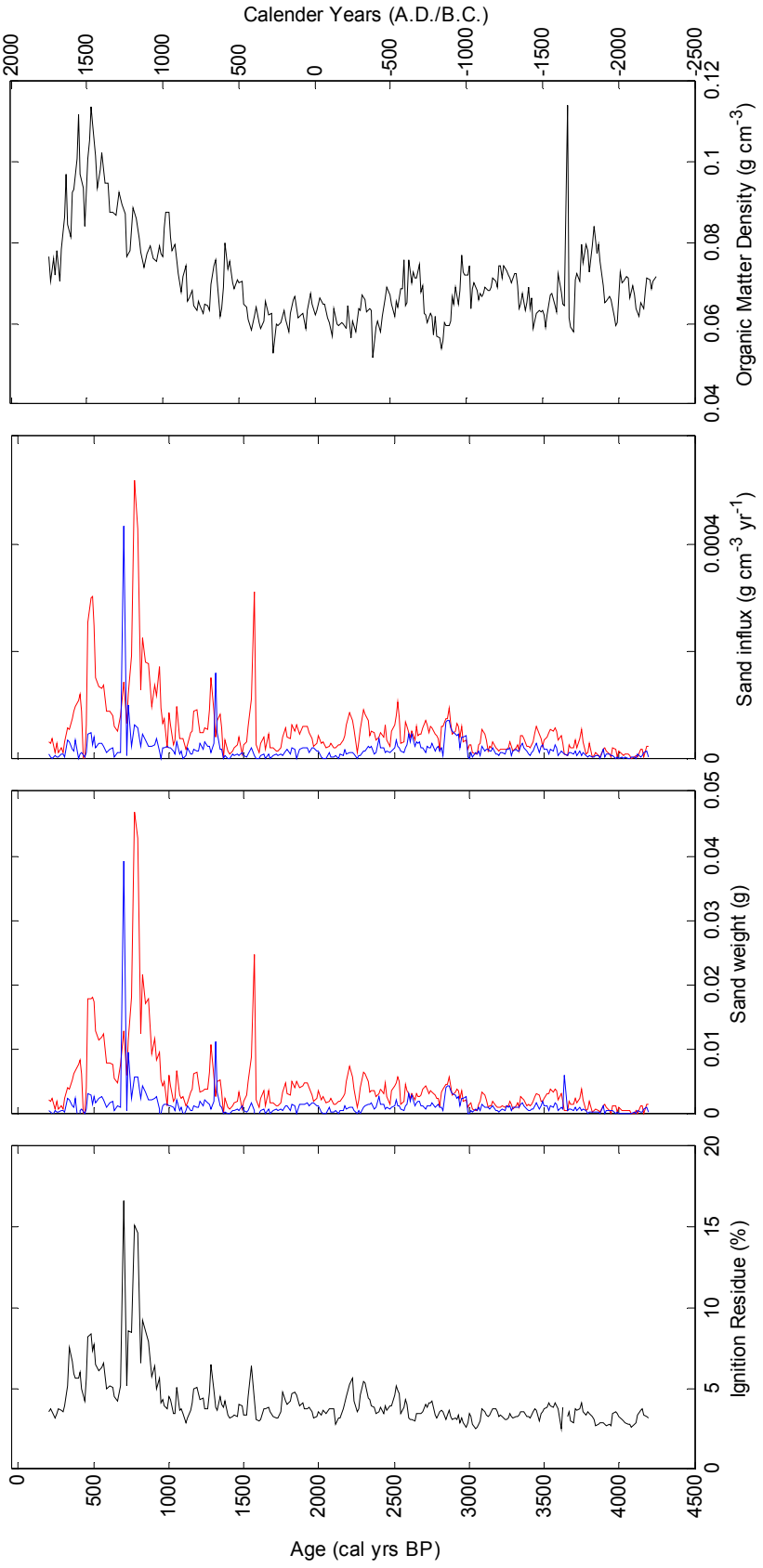

Figure 4.9: Struban Bog results (*from left to right*): ignition residue, sand weight, sand influx and organic bulk density. Red lines indicate the 120-180 µm sand results and blue lines the >180 µm sand results.

The transects were sampled from across Struban Bog (from the southwest to the northeast: transect 1 to 3) to assess changes in the sand content across the bog. The results show that the IR, sand content and organic bulk density vary (Figure 4.10), although this may be the result of no chronological control on these cores. Transect cores 2 and 3 and the main core have the largest peak in sand content around 50 cm depth, however this peak is absent (or at least smaller) in transect core 1. Many of the smaller variations in sand content cannot easily be compared between the cores, so it is unclear whether contrasting patterns are the result of different accumulation rates across the bog or different patterns of sand influx.

The mean and maximum values of the IR results are greater in the transect 3 core furthest from the coast than the other transect cores; the mean is 4.45% compared to 4.08% and 4.12% and the maximum value is 10.46% compared to 7.66% and 8.45%. This could suggest that storms have caused larger amounts of sand to enter the bog from the eastern side furthest from the sand dunes and machair. There are 3 possible reasons for this: 1) severe storms had easterly winds, 2) transect 3 and the main core were sampled from the leeside of a raised section of bog, where sand deposition may occur as the wind weakens, or 3) the lochs to the southwest and southeast of the bog minimised sand influx from these directions, so sand was blown more easily across land from the north and east.

Finally the organic bulk density results also show some differences between the transect cores. The main core and transect 3 have similar changes, with high organic bulk density values above 50 cm depth, however transect 1 and 2 display a steadily increasing trend towards the bogs surface sediment. Again the reasons for these differences are unclear without having dated tie-points between the cores. As we sampled the main core from the central dome of the bog we have maximised the likelihood that the peat accumulated consistently through time, as supported by the age-depth model, however the apparent differences between the organic density results of the main core and transect 3 with transect 1 and 2 suggest intra-bog variability.

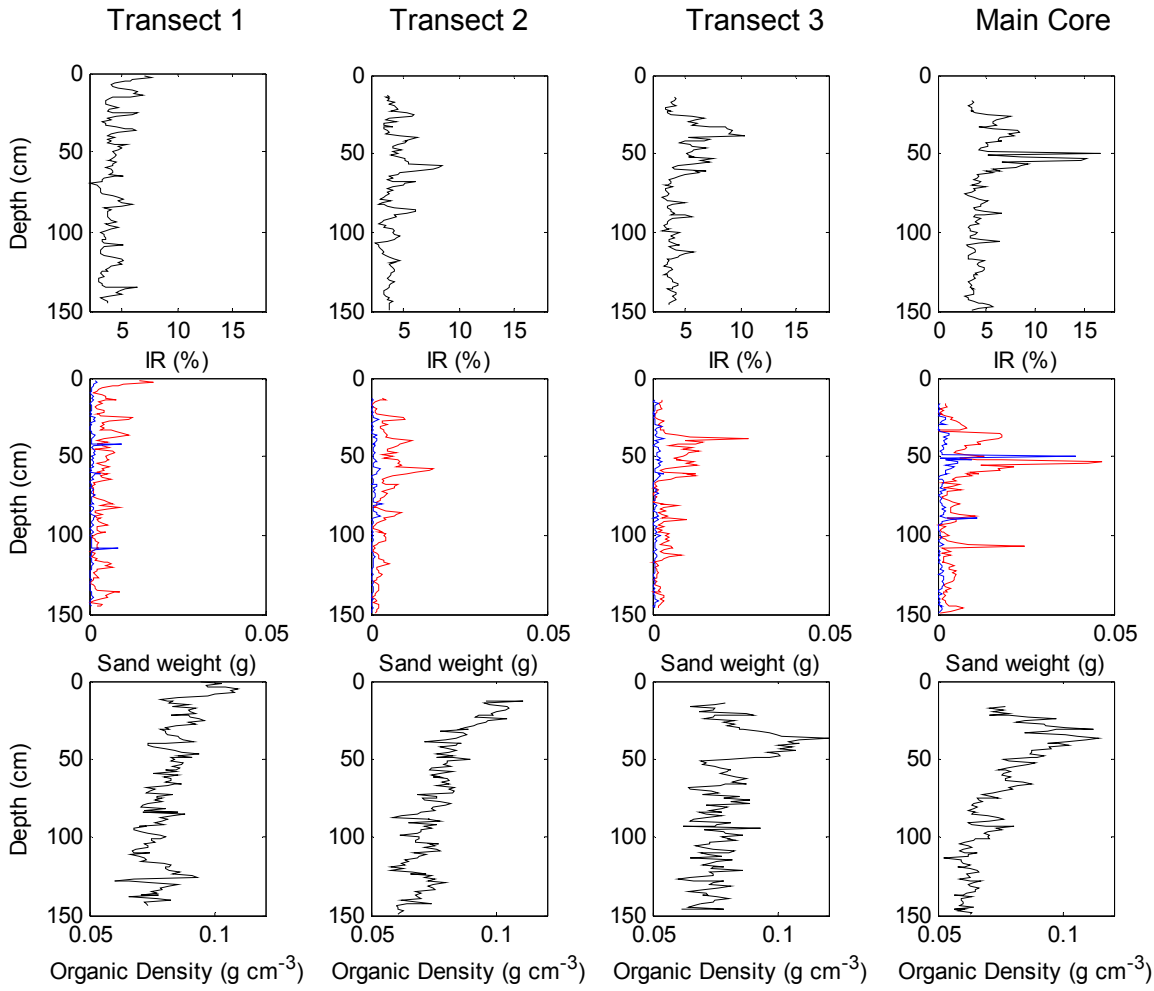

Figure 4.10: Struban Bog ignition residue (top), sand fraction weight (middle) and Organic Bulk Density (bottom) results for transects 1-3 and the main core. Red lines show the 120-180 µm sand and blue lines the >180 µm sand.

4.4.2. Hill Top Bog results

The upper 5 cm of peat from the Hill Top Bog core, which is within the modern active peat (acrotelm), was not preserved during coring. Therefore the Hill Top Bog main core spans from 5-330 cm depth. The peat is a humified sedge dominated peat with rather little *Sphagnum* content. The organic bulk density results (Figure 4.11) indicate that the humification of the peat varies through the core with small peaks, for example at 40 cm depth. The ash content of the peat (IR) has values of around 3% through much of the core (between 330-150cm) and fairly low but variable sand content. Above 150 cm the IR and sand content values gradually increase towards a peak between 50 and 30 cm. As in Struban Bog the similarity between the IR and sand weight results shows that the IR is dominated by changes in the sand sized particles within the peat.

The results of the eight radiocarbon dates are displayed in Table 4.2. The modelled age-depth curve for the main core, along with the 2-sigma errors, is shown in Figure 4.11. The core spans the period from -13 to 4000 cal yr BP and shows there has been a fairly constant peat accumulation rate through this time, with a slightly faster accumulation rate having occurred before c.3000 cal yr BP and after c.1000 cal yr BP.

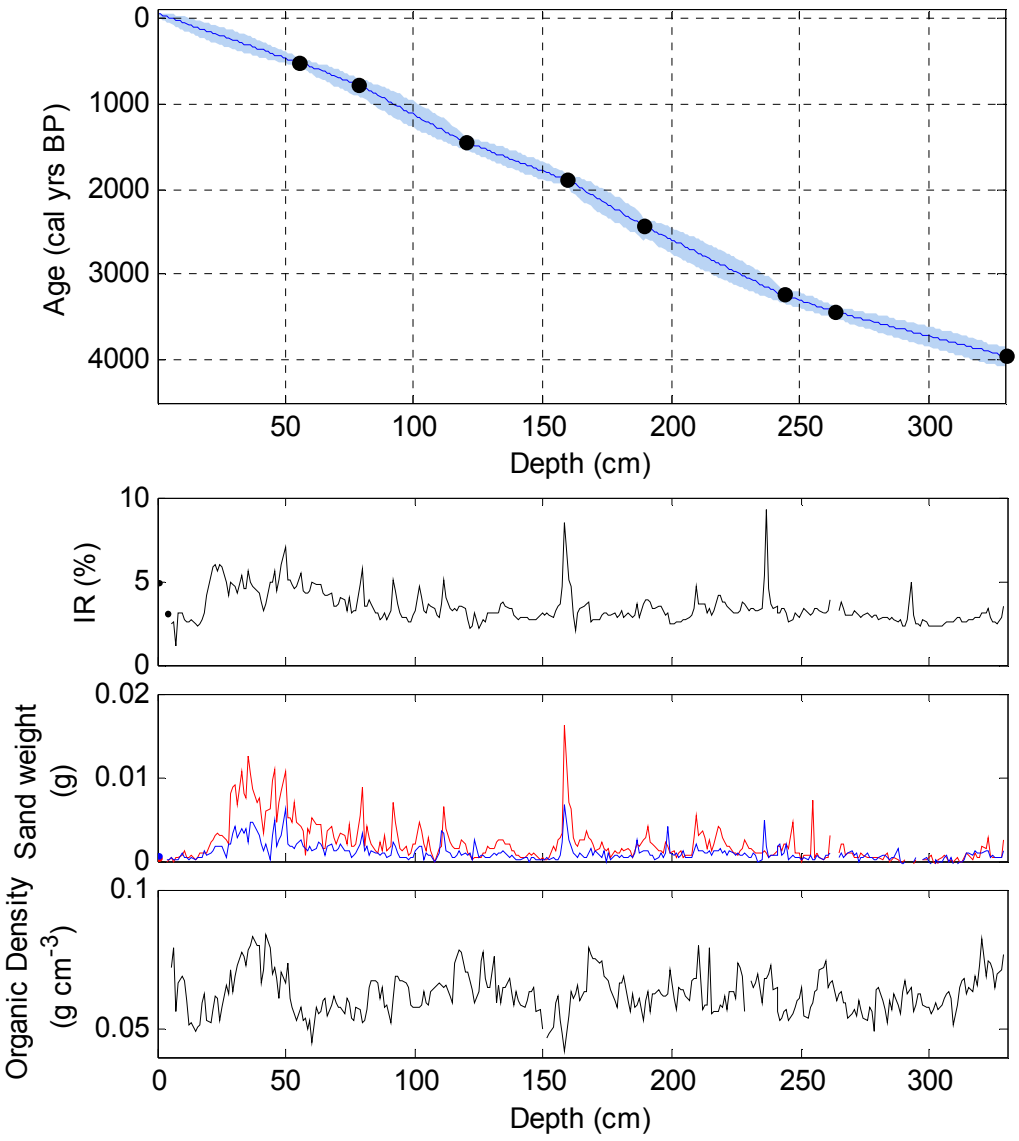

Figure 4.11: Hill Top Bog raw results and age-depth model (*from top*): age-depth model including dated horizons (black points) and 2-sigma error (shaded blue area) and ignition residue, sand weight and organic bulk density results. Red lines indicate the 120-180 µm sand results and blue lines the >180 µm sand results.

Table 4.2: Radiocarbon dating results from Hill Top Bog main core.

Sample Depth (cm)	Laboratory Code	$\delta^{13}C$ (‰)	Radiocarbon Age (^{14}C yr BP ± 1σ)	Median calibrated age (cal yr BP) and 2σ range
55-56	SUERC-51102	-22.8	449 ± 37	508 (446-540)
78-79	SUERC-51103	-25.2	845 ± 37	768 (693-903)
120-121	SUERC-51106	-26.8	1585 ± 35	1442 (1386-1530)
159-160	SUERC-41797	-27.7	1913 ± 35	1881 (1817-1970)
189-190	SUERC-41798	-28.6	2439 ± 37	2421 (2350-2606)
242-244	SUERC-41804	-25.8	3063 ± 37	3239 (3157-3326)
263-264	SUERC-43068	-26.0	3243 ± 35	3434 (3376-3507)
329-330	UB-No 19468	-24.7	3579 ± 37	3954 (3848-4083)

The sand deposition onto Hill Top Bog is shown by the IR, sand weight and sand influx measurements (Figure 4.12). As on Struban Bog, the constant rate of peat accumulation means that the sand influx results are very similar to the sand weight measurements, therefore increased concentrations of sand have not been caused by periods of slower peat formation. The only apparent difference in the influx results is that the sand content peaks between 1500 and 500 cal yr BP are slightly smaller relative to the peaks in sand content after this time. Nevertheless all proxies support that sand deposition on the bog was relatively low between 4000 and 1500 cal yr BP aside from a few large magnitude peaks, particularly at 1870 cal yr BP. After 1500 cal yr BP sand deposition appears to have gradually increased and was interspersed with four peaks in sand content at c.1300, 1150, 1000 and 800 cal yr BP. The results indicate that the maximum sand deposition occurred between c.500 and 200 cal yr BP. The sand weight results show that the 120-180 μm sand content is more

variable than the >180 μm fraction, as was also observed in Struban Bog. In the earliest section of the record before c.2000 cal yr BP the medium 120-180 μm sand at times increases when the >180 μm sand fraction remains low, for example between 3500 and 3200 cal yr BP. However in the younger parts of the record, the overall increasing trend in sand is mirrored in the >180 μm fraction.

The organic bulk density of Hill Top Bog does not have any long-term trends through the period, instead showing high centennial and sub-centennial variability. High organic density values occur at c.2800, 2000, 1500 and 600-250 cal yr BP, and may indicate that peat humification was higher at these times, suggesting drier summer conditions and/or less productivity (Chambers *et al*., 2011; Yu *et al*., 2003). Lower organic density values such as at c.1900 cal yr BP and c.800-500 cal yr BP suggest the opposite: wetter summers and/or more productivity (Chambers *et al*., 2011; Yu *et al*., 2003).

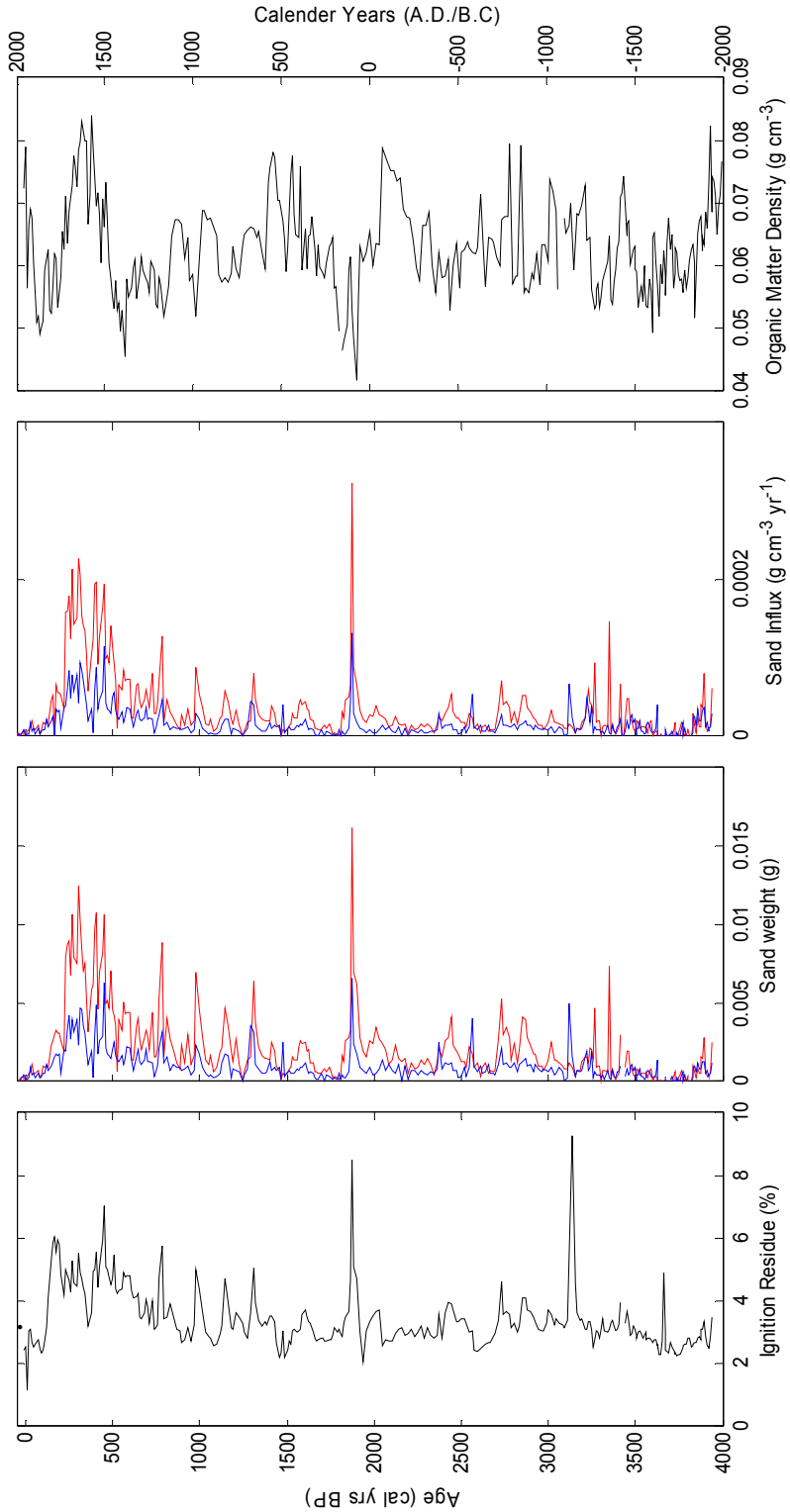

Figure 4.12: Hill Top Bog results (*from left to right*): ignition residue, sand weight, sand influx and organic bulk density. Red lines indicate the 120-180 µm sand results and blue lines the >180 µm sand results.

The transect of cores from Hill Top Bog (Figure 4.13) show similar trends in sand content (IR and sand fraction weights). However, there are some dissimilarities in the peak depths and also in the smaller sand peaks. The sand content in each core increases towards a maximum around 50 cm, although in transect core 3 this is at c.30 cm. A small peak is also apparent in the transect cores between depths of 100-150 cm. The results indicate that accumulation rates have differed across the bog but the broad patterns of sand influx are similar.

As on Struban Bog, the maximum and mean IR values are greater on the eastward side of the peat bog. From transect cores 1 to 3 the maximum IR values are 7.98%, 8.6% and 13.73%, and the mean IR values are 3.88%, 3.91% and 4.05%, although it is likely that the large peaks in transect core 3 in the upper sections are responsible for these results. As on Struban Bog it may be that the most severe storms arrived with easterly winds, or that sand was deposited on the leeside of the bog dome.

Finally the organic bulk density results also show some differences between the transect cores, but have similar trends. The transect cores and main core all show the highest organic bulk density values in the upper 50 cm of sediment. The main core differs from the transect cores as it also has high density values between 150 and 100 cm depths, while the transect cores steadily increase from low values around 130 cm depth towards higher values in the upper sections.

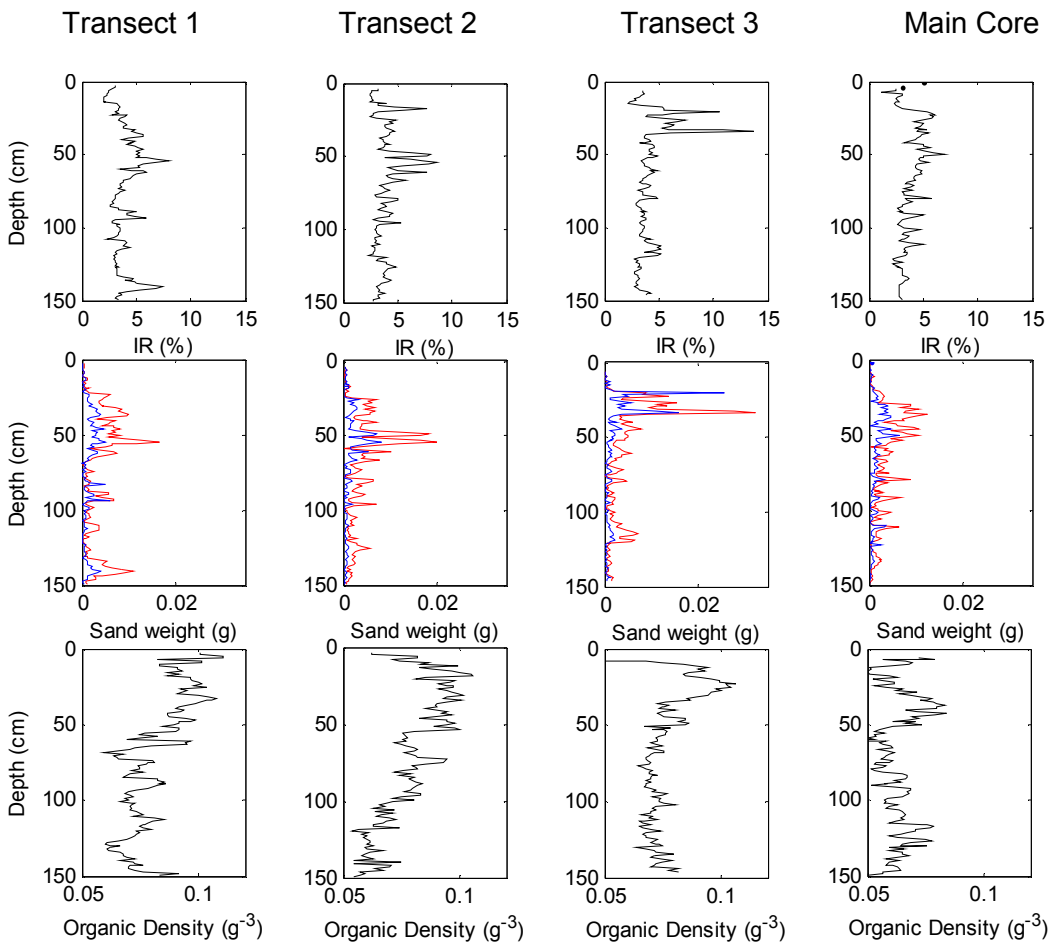

Figure 4.13: Hill Top Bog ignition residue (top), sand fraction weight (middle) and Organic Bulk Density (bottom) results for the transects 1 to 3 and the main core (left to right). Red lines indicate the 120-180 µm sand results and blue lines the >180 µm sand results.

4.4.3. Spectral Analysis

The main core IR results have been analysed using spectral analysis to identify any cycles. The Lomb-Scargle spectral analysis of the Hill Top Bog reconstruction identified significant cycles at 2287 (range of 2670-2040), 1334 (1460-1180), 889 (1000-870), 728 (750-700), 326 and 291 (295-280) years (Figure 4.14). The wavelet analysis (Figure 4.15), which looks at cyclicity through time, did not find any significant centennial cycles aside from two short periods c.3200 and 1800 cal yr BP when c.100 year cycles occurred.

The Lomb-Scargle spectral analysis on the Struban Bog reconstruction indicates that there are only two significant centennial length cycles, with

periods of 1453 (range of 1610-1230) and 940 (1000-910) years (Figure 4.16). The wavelet analysis (Figure 4.17) suggests that centennial cycles became more pervasive after c.2500 cal yr BP, when the c.1500, 1000 and 500 year cycles were significant (although these could be multiples of the same 500-year cycle). Finally in the last 1000 years there appear to have been decadal cycles.

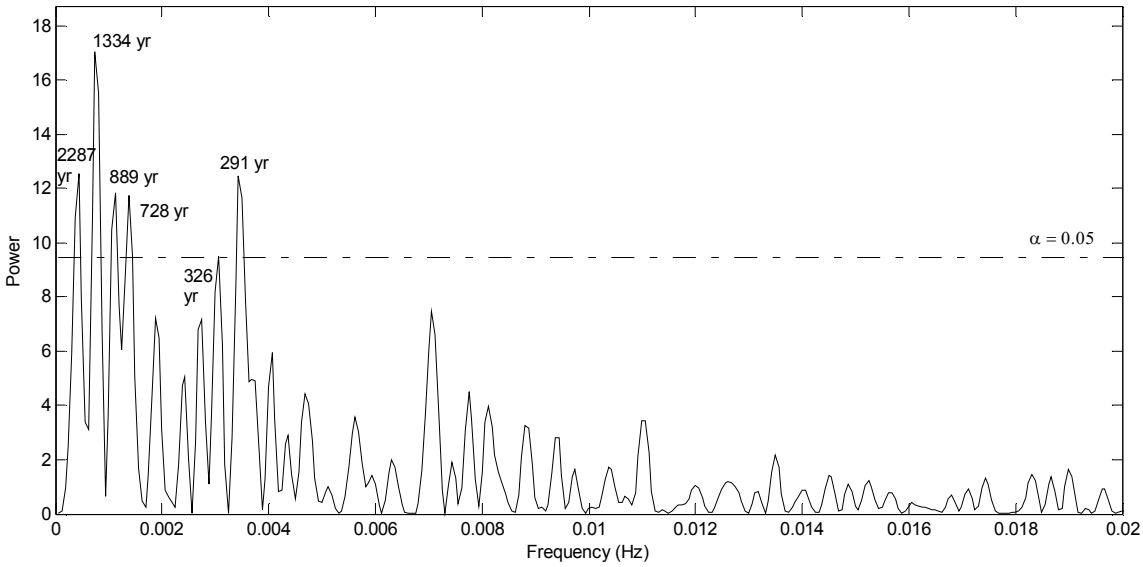

Figure 4.14: Lomb-Scargle spectral analysis of Hill Top Bog ignition residue results. The dashed line shows the 95% significance level.

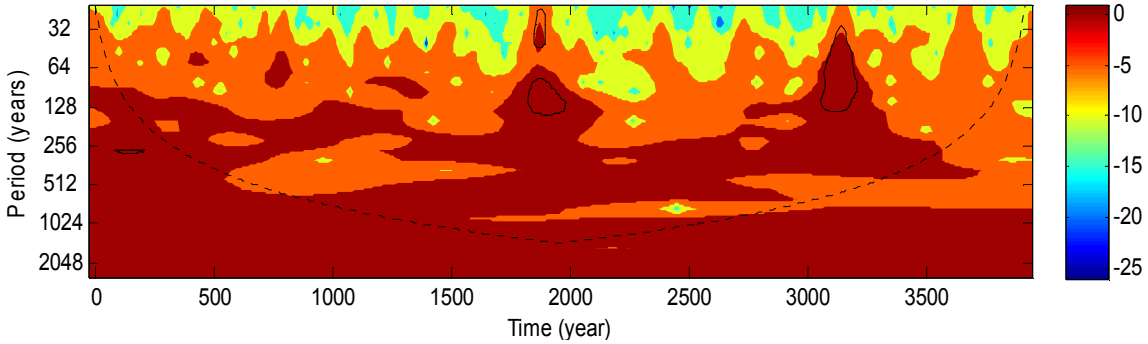

Figure 4.15: Wavelet power spectrum analysis of the Hill Top Bog ignition residue results. The colours show the magnitude of the cycles and illustrate the cyclical variability through time. Black continuous lines encompass cycles over the 95th percent significance level. The dashed line shows the cone of influence: as the timeseries is finite in length, and therefore padded by zeros during analysis, the cycles outside the cone are likely to be underestimated.

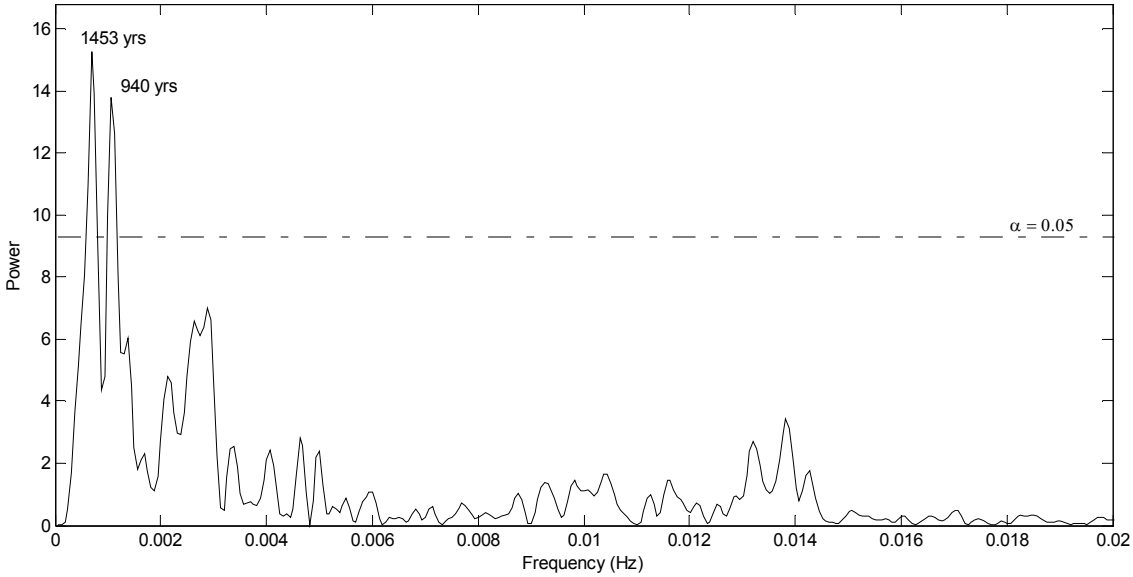

Figure 4.16: Lomb-Scargle spectral analysis of Struban Bog ignition residue results. The dashed line shows the 95% significance level.

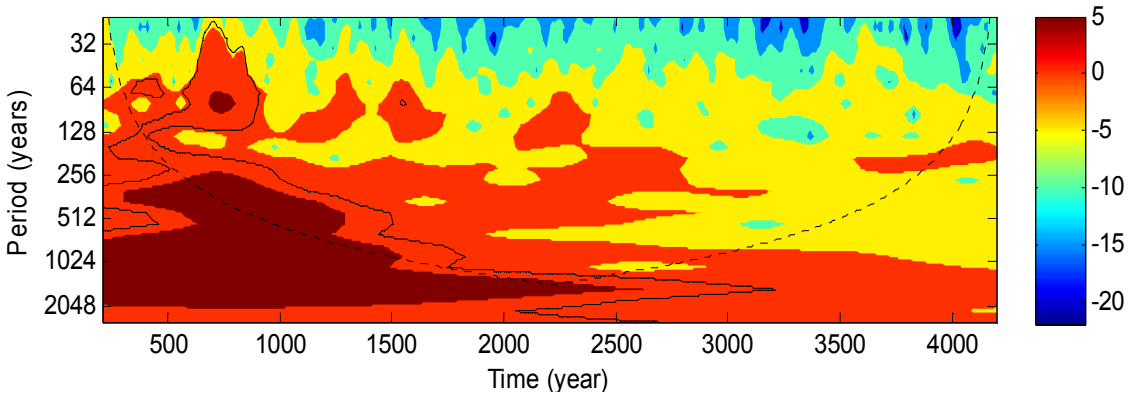

Figure 4.17: Wavelet power spectrum analysis of the Struban Bog ignition residue results. See Figure 4.15 for explanation.

4.5. Discussion

4.5.1. Intra-bog sand content comparison

The analysis of the peat bog transects showed that, although the trends are shared between cores, there were differences in the depths of these changes and the small magnitude variability. As the cores were not dated it was difficult to assess whether these findings were the result of different accumulation rates across the bog or real differences in sand influx/humification. Struban Bog transect core 1 in particular differed from the other cores from this bog.

Previous palaeoclimatic reconstructions using multiple cores from ombrotrophic peat bogs have found similar differences (using proxies such as heavy metals and testate amoebae), with differences in the variability but the same general trends (e.g. Coggins *et al*., 2006; Bindler *et al*., 2004; Mauquoy *et al*., 2002). Intra-bog differences have been suggested as being due to microform variability (such as hummocks/hollows/lawns), as the level of water logging or the vegetation type of these features may influence the trapping of heavy metals, or sand in this case (Bindler *et al*., 2004; Coggins *et al*., 2006). Furthermore it has been found that accumulation rates are higher for hollows than hummocks (Robinson and Moore, 1999), so this is another way that the bog micro-topography may have influenced the depths of sand peaks in the transect cores. Finally the core margins have been found to produce less accurate reconstructions than central bog cores (Hendon *et al*., 2001), which could explain why the Struban transect core 1 is different.

Therefore, in agreement with other studies, the transect cores indicate that the trends are captured by cores from ombrotrophic bogs, but that short-term variations are more influenced by local factors (Bindler *et al*., 2004; Hendon *et al*., 2001). As such the short-term variations will not be considered as meaningful hereafter.

4.5.2. Inter-bog sand content comparison

The inter-bog comparison using two sites allows the variability produced by local factors, such as sediment disturbance caused by human activities, to be separated from the regional storminess signal. To remove the high frequency variability caused by intra-bog heterogeneity (section 4.5.1) the results were smoothed using a 100-year window before comparison. There are similar timings of peaks in sand content between the two sites within the age-errors (Figure 4.18). Peaks in storminess observed in both sites occurred at approximately 3500, 2800, 2400, 1900, 1600, 1300-1100, 800 and 500 cal yrs BP. The reconstructions imply that storminess was higher in the last 1000 cal yrs BP; however there is a difference in the timing of the maximum sand content at each site. The Hill Top Bog reconstruction indicates maximum storminess after 500 cal yrs BP, whereas the maximum sand influx to Struban Bog occurred c.800 cal yrs BP.

There are two possible causes for the inter-site differences in peak magnitude, which will be discussed. The first is that amplification of peaks in sand influx were the result of non-climatic factors, such as human disturbance or volcanic eruptions. People have lived on the Outer Hebrides throughout the Late Holocene (Henley, 2003; Garrow and Sturt, 2011), settlements have been situated on the machair between the middle of the first millennium B.C. until the 14th century (c.2500-600 cal yrs BP) (Sharples and Pearson, 1999). On the machair between Hill Top Bog and the coastline there was the settlement of Cladh Hallan from the Late Bronze Age to the Iron Age (Pearson *et al*., 2005). After the 14th century the settlements were moved inland onto the peat lands (Sharples and Pearson, 1999). This coincides with the time when sand content increased in Hill Top Bog in particular, so this peak could be a reflection of changing settlement and farming activity. However it has been speculated that the reason for the settlement move was a climate deterioration, which destabilised the sand dunes (Sharples and Pearson, 1999), which if correct indicates that storminess was a cause of both the human changes and the observed sand influx to the bogs.

Furthermore, human activities rather than settlements may have had a greater influence on sand disturbance. The beaches, dunes and machair in the past have been harvested for marram grass (for thatch and bedding), kelp, plant

roots (for dye) as well as for the sand itself (for soil fertiliser) and has been used for agriculture (Angus and Elliot, 1992; Gilbertson *et al*., 1999). However as with the settlement patterns, these actions may have been prompted by a climate deterioration, leading to difficult conditions and increased use of marginal land that destabilised these environments (Sommerville *et al.,* 2007). Sand entering the bog may therefore not only be a direct result of increased storminess, but may also be caused by difficult climate conditions that led to the disturbance of sediment sources. At other times human artifacts and waste within sediment layers in the machair support that human activities locally stabilised the machair (Gilbertson *et al.,* 1999). Furthermore palaeo-environmental studies from Barra and South Uist have suggested that the landscape became increasingly tree-less through the Bronze Age and since 4000 cal yrs BP respectively (Ashmore *et al*., 2000; Bennet *et al*., 1990). The more open landscape may have made sand more easily blown across the islands and onto the bogs. Therefore it is difficult to separate whether the changes in aeolian sand are driven by climatic or human factors, or a combination of both.

The environmental impact from volcanic eruptions in Iceland is another factor to consider, as vegetation changes may have made sand more easily blown. For example, the 1783 Laki eruption is documented as causing widespread acid deposition in Europe, which damaged crops and other vegetation (Grattan and Charman, 1994). This could potentially lead to increased marginalisation of environments causing sediment erosion, however the calcerous sand in the Outer Hebrides are alkali and are therefore less vulnerable to acid deposition (Sommerville *et al.,* 2007; Grattan *et al.,* 1999), This suggests that volcanic eruptions are not a factor causing environmental changes that increase sand deposition within the bogs, although the climatic influence from eruptions is not discounted and is discussed in Chapter 6.

The second explanation for the different magnitudes of the sand peaks is the position of each bog, in relation to the coastline and sand sources, as well as obstacles such as lakes, which may have influenced the transport of sand onto each bog. Possible factors influencing sand transport include the greater distance of Hill Top Bog than Struban Bog from the coastline and the aspect of the coastlines (Hill Top Bog is located on a west-facing coast whereas Struban Bog is located on a south-west facing coast). Additionally, surrounding lochs

may have acted as barriers to aeolian sand transport. There are lochs to the south-east and south-west of Struban Bog and as sand 70-500 μm in size travels by saltation (Kok *et al.*, 2012; Bagnold *et al.*, 1937), which cannot occur on water, it is possible that there is a bias towards storms with northerly winds. Alternatively warmer periods may have resulted in lower lake-levels, thus reducing the barrier. Finally sea-level changes may have influenced the magnitude of sand peaks. The relative sea level reconstruction from Harris has suggested that close to present sea levels were reached after 3100-2100 cal yrs BP (Jordan *et al*., 2010), which may explain the trend towards higher sand content in the most recent sections of peat. However studies that cored the present day machair have shown the stratigraphy consists of many Late Holocene sand wedges extending inland (Gilbertson *et al*., 1999; Dawson *et al*., 2004), so despite a steady trend in sea-level through the Late Holocene, the inland extent of sand has varied.

In summary the inter-site comparison supports that the reconstructions are capturing regional storminess. It is considered likely that the different magnitudes of peaks in sand content between the two bogs is related to local factors (such as human activity and sensitivity to storm direction). However the relative importance of the discussed factors is difficult to determine, as human activities may change in response to climate deteriorations and increased storminess, leading to increased marginalisation of the land, with this as a cause of increased aeolian sand activity.

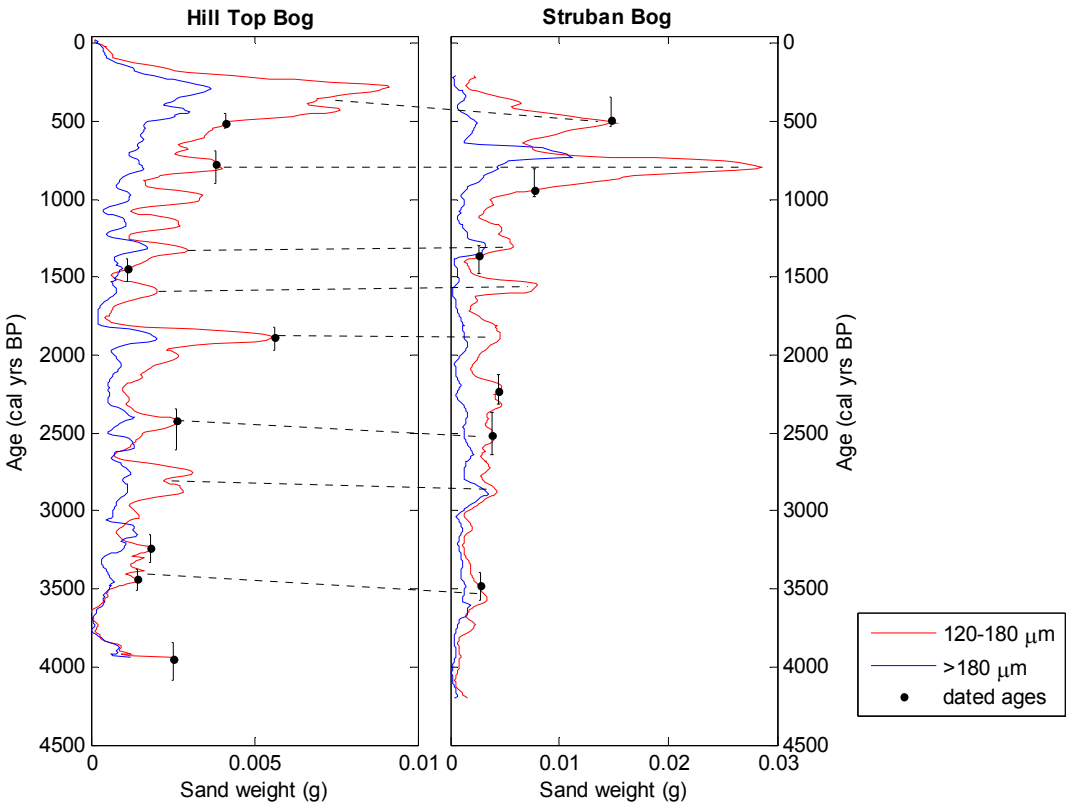

Figure 4.18: Sand fraction weight results of Hill Top Bog and Struban Bog, smoothed using a 100-year moving window. Dated horizons and 2-sigma error bars are plotted to demonstrate the potential range of ages at these points. Corresponding peaks between the two reconstructions are suggested by the dashed lines. Red lines indicate the 120-180 μm sand results and blue lines the >180 μm sand results.

4.5.3. Comparison with regional Late Holocene climate

The storminess reconstructions from the two bogs will next be compared with other regional climate reconstructions, as illustrated in Figure 4.19. The uppermost peaks at c.500-200 cal yrs BP may have been deposited during historically documented severe storms that buried in sand the Outer Hebridean settlements of Udal in 1697 A.D. and Baleshare in 1756 A.D. (Gilbertson *et al*., 1999; Lamb, 1984; 1991; Figure 4.19A). Sand wedges are interpreted as signifying periods with high storminess, and dating of these has indicated that during the LIA they formed locally (Gilbertson *et al.,* 1999; Figure 4.19B) and particularly at the LIA onset c.500 cal yrs BP (Dawson *et al.,* 2004; Figure 4.19C). Furthermore increases in maritime plant communities on St Kilda during

the LIA may show there was high storminess and saline conditions caused by sea-spray (Walker, 1984). Therefore the reconstructions from the Outer Hebrides support the common assertion that the LIA had high storminess.

Prior to the LIA the Struban Bog reconstruction indicates high storminess during the Medieval Climate Anomaly at c.780 cal yrs BP. This event may be synchronous with sand deposition phases on South Uist and Barra, as dating of the base of sand wedges gives ages of 940 ± 40 and 670 ± 130 cal yrs BP respectively (Dawson *et al*., 2004). Few storminess reconstructions are available from earlier in the Holocene from the Outer Hebrides. Localised sand movements occurred at 1300-1700 and 3300-3800 cal yrs BP (Gilbertson *et al*., 1999), however these are not clearly identified as periods of high storminess in the reconstructions from this research. Therefore the evidence of storminess changes during the last 1000 years from the Outer Hebrides support that storminess increased at c.800 cal yrs BP and after 500 cal yrs BP, however there is little comparator data from earlier than the last millennium.

Additional reconstructions allowing regional storminess comparisons spanning the Late Holocene are available from elsewhere in Scotland and northern Ireland, and are based on the dating of episodes of sand dune formation, sand wedges as well as cliff-top storm deposits. Most support that storminess during the LIA was high (Figure 4.19; Wilson, 2002; Wilson *et al*., 2004; Sommerville *et al*., 2003; 2004; Hansom and Hall, 2009; Hall *et al*., 2006), but there are contradictions in the timings of earlier periods. Sand dune development at 3100-2400 cal yrs BP (Wilson *et al*., 2004; Figure 4.19E) and 2470 and 920 cal yrs BP (Wilson, 2002; Figure 4.19D) were synchronous with small peaks in storminess indicated by the Hill Top Bog reconstruction but not the Struban Bog reconstruction. Furthermore peaks of similar magnitude occur in the Outer Hebrides reconstructions with no corresponding episodes of sand dune development recorded. As sand dunes can be influenced by factors such as sea-level fluctuations and land-use changes (Wilson, 2004; Gilbertson *et al*., 1999) and the preservation of sand dune deposits may be dependent on subsequent phases of erosion, methodological limitations may explain the differences between the reconstructions.

The dating of sand wedges on Orkney and Shetland point to high storminess at c. 1150 and 850 cal yrs BP (Sommerville *et al*., 2003; Figure 4.19F), 2965 cal yrs BP (Sommerville *et al*., 2007) and 3400-3100 and 2800-2260 cal yrs BP (Tisdall *et al*., 2013; Figure 4.19G). There is agreement with the Outer Hebrides reconstructions that suggest storminess increased at c.850 cal yrs BP; however there is dissimilarity between the periods of high storminess inferred from before this time.

A reconstruction of severe storms created by dating cliff-top storm deposits on the Shetland Islands indicated that there was heightened storminess at 1550-1400 and 1250-900 cal yrs BP (Hansom and Hall, 2009; Figure 4.19H). These severe storm events may be contemporaneous with the three peaks in storminess suggested by the Hill Top Bog reconstruction between 1400-900 cal yrs BP, and possibly the peaks at 1550 and 1300-1100 cal yrs BP in the Struban Bog reconstruction.

This regional synthesis has focused on the dating of sediments resulting from aeolian and wave mechanisms. Further comparison is possible using precipitation reconstructions from the region, as storms bring both strong winds and high precipitation. A reconstruction thought to be reflecting detrital input into a remote lake in the Cairngorms has peaks at c.2950, 1620-1470, c.700 and since c.450 cal yrs BP (Oldfield *et al*., 2010; Figure 4.19I). These peaks are seen in one or both bogs, supporting that these were periods with severe storms in Scotland. Furthermore the reconstruction suggests a long-term trend of increasing catchment input (Oldfield *et al*., 2010), which resembles the gradual increase in sand peak magnitude and supports that an increase in storminess was producing this long-term trend. Many precipitation reconstructions from the region, such as bog surface wetness reconstructions, are biased towards summer precipitation and influenced by temperature; however a speleothem reconstruction from northwest Scotland is considered as a winter precipitation proxy (Charman, 2010; Proctor *et al*., 2000; 2002; Figure 4.19J). This reconstruction indicates that there were drier conditions at 3600-2000, 1400-1200 and 600-0 cal yrs BP and wetter conditions at 2000-1400 and 1200-600 cal yrs BP (Proctor *et al*., 2000; 2002). Although these wet periods coincide with peaks in inferred Outer Hebridean storminess at c.1850 and 800 cal yrs BP there is otherwise little similarity between the reconstructions and this

contradicts that the LIA was stormy. This dissimilarity may be due to the speleothem capturing seasonal averages rather than extreme events.

This regional synthesis of storminess and precipitation reconstructions support that storminess increased during the LIA and at c.800 cal yrs BP, with potentially increased storminess episodically during the period 1500-800 cal yrs BP. Prior to 1500 cal yrs BP there are differences in the timings of storm events between the reconstructions compared here. The cliff-top storm deposit reconstruction (Hansom and Hall, 2009) and the reconstruction of detrital input into a lake in the Cairngorms (Oldfield *et al*., 2010) most strongly resemble the reconstructions of storminess from the Outer Hebrides. These are considered insensitive to human activities (due to the nature of deposition and location respectively), which support that the Outer Hebrides storminess reconstructions are climatically driven. Furthermore as the cliff-top storm deposits are only deposited by severe storms, this implies that the Outer Hebrides reconstructions are sensitive to extreme events.

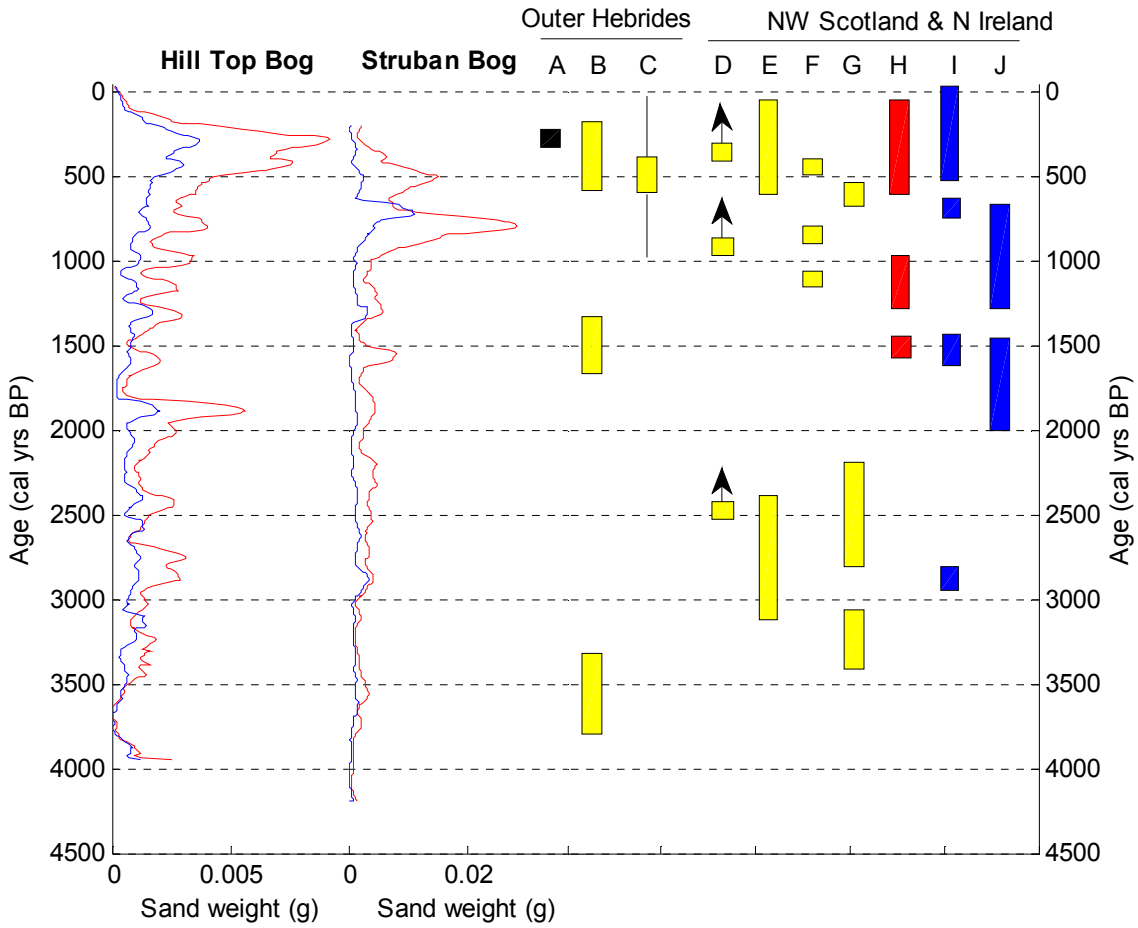

Figure 4.19: Reconstructions of storminess from Hill Top Bog and Struban Bog: red line is 120-180 µm sand weight and blue line is >180 µm sand weight. Rectangles show other storm and precipitation reconstructions. A: historical records of severe storms in 1697 and 1756 A.D. (Lamb 1984; 1991; Gilbertson *et al*., 1999). B and C: local sand movements on the Outer Hebrides (B: Gilbertson *et al*., 1999, C: Dawson *et al*., 2004). D: onset of sand dune formation of two dunes in northwest Scotland (Wilson, 2002). E: dune instability in northern Ireland (Wilson *et al*., 2004). F and G: sand layers representing periods of sand inundation and storminess on Orkney (F: Sommerville *et al*., 2003. G: Tisdall *et al*., 2013). H: dated cliff-top storm deposits on the Shetland Islands (Hansom and Hall, 2009). I: minerogenic input into a remote lake in the Cairngorms (Oldfield *et al*., 2010). J: precipitation reconstruction based on speleothem band width from northwest Scotland (Proctor *et al*., 2000; 2002).

4.5.4. Storm-NAO relationship

The storminess reconstructions from the Outer Hebrides are next compared with reconstructions of the NAO, in order to understand how this circulation pattern has influenced storminess. This comparison will only be briefly discussed here, as it is discussed further in Chapter 6.

During the last millennium the NAO and storminess reconstructions show conflicting results (Figure 4.20). Struban Bog correlates positively and significantly with the Trouet *et al.* (2009) NAO reconstruction (R = 0.55, n=70), while the Hill Top Bog reconstruction has no correlation (R = -0.06, n=93). Visual assessment of the results suggests that storminess variations over the last millenium occurred during times with both a positive and negative NAO index: the storm reconstructions indicate that there was high storminess at c.800 cal yrs BP during the MCA when the NAO is thought to have been positive, as well as c. 500 cal yrs BP during the LIA when the NAO was more frequently negative (as shown in Figure 4.20). Therefore other factors may be driving storminess in northern Europe. It has been hypothesised that during the LIA storminess increased as a result of a steepened latitudinal temperature gradient despite a frequent negative NAO (Trouet *et al.*, 2009; 2012; Raible *et al.*, 2007; Lamb., 1995; Sorrel *et al.*, 2012). Therefore the high storminess in the MCA inferred by the Struban Bog reconstruction may have been the result of the positive NAO index, whereas the high storminess indicated particularly by the Hill Top Bog reconstruction during the LIA may have been caused by infrequent storms of high intensity, caused by the steeper temperature gradient.

The NAO-storm relationship over the Late Holocene can be assessed by comparison of the storm reconstructions with the Olsen *et al.* (2012) NAO reconstruction (Figure 4.21). The Olsen *et al.* (2012) NAO reconstruction, as well as an NAO reconstruction based on Atlantic sea-surface temperature reconstructions (Rimbu *et al*., 2003; Wanner *et al*., 2008) suggest that the NAO was negative until around 2000 cal yr BP, before becoming increasingly positive towards 1500 cal yr BP. The Hebrides reconstructions indicate increasingly large magnitude peaks in storminess from around 1500 cal yr BP. This reflects the transition towards more positive NAO values in the last 1500 years, implying that a more frequent positive NAO caused the storm tracks to cross northwest

Europe, although the reconstructed transition from negative to positive NAO is earlier and more abrupt than the change in storminess.

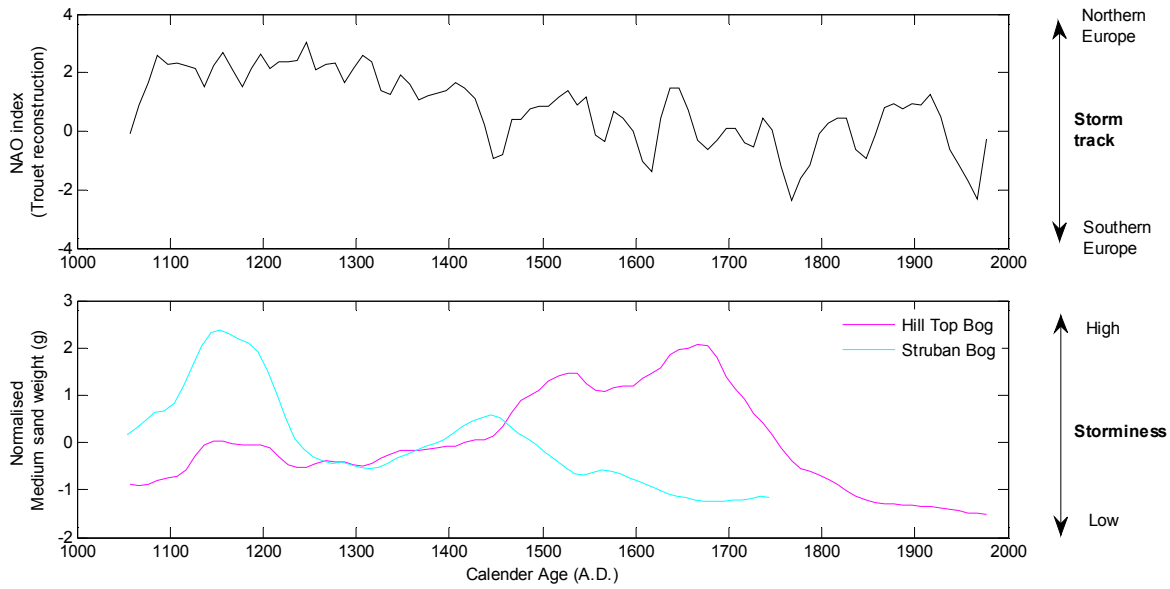

Figure 4.20: Comparison between an NAO reconstruction since 1049 A.D. (Trouet *et al*., 2009) and reconstructed storminess from Struban Bog and Hill Top Bog for this period.

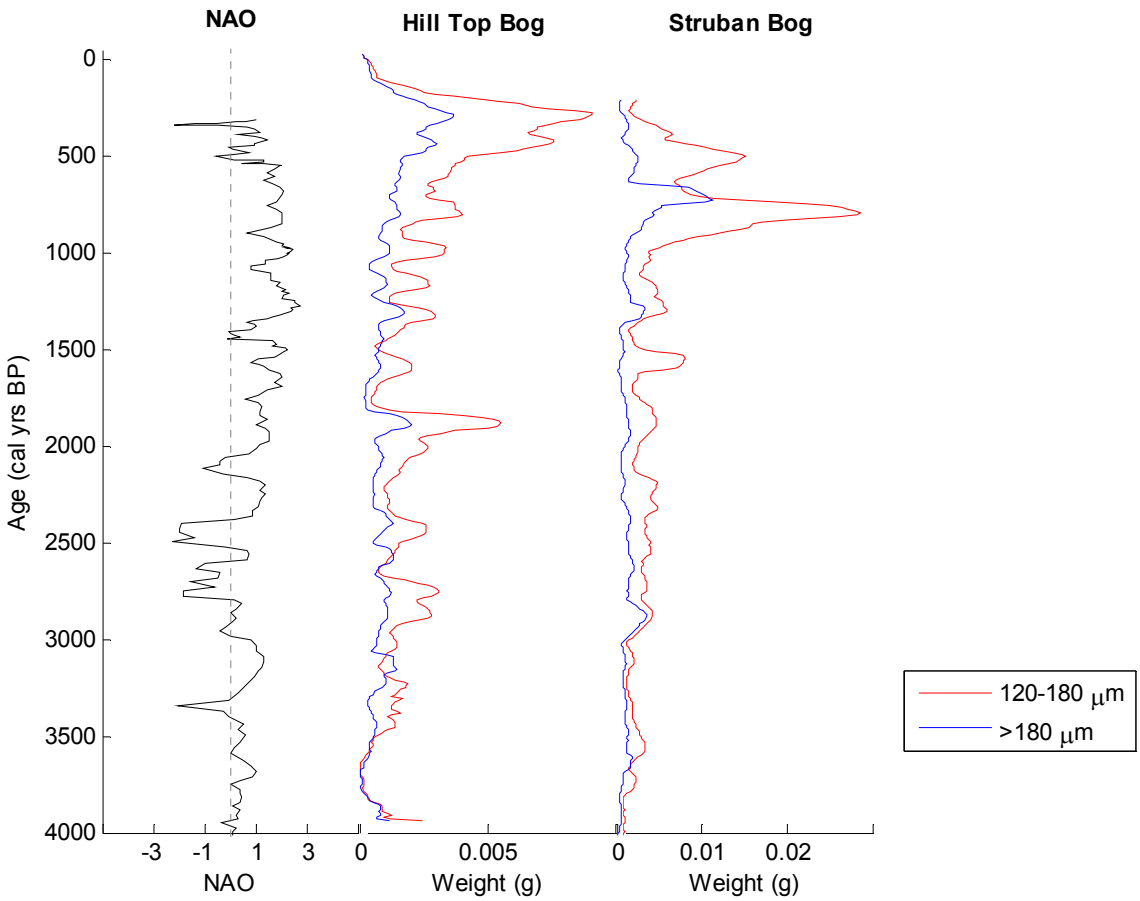

Figure 4.21: Comparison between the Hill Top Bog and Struban Bog storminess reconstructions from the Outer Hebrides and a reconstruction of the NAO (Olsen *et al.*, 2012).

4.5.5. Cyclicity

Analysis of the cycles present within the bog records can allow inference of the drivers of storminess variability in this region. The findings are briefly outlined here and discussed further in Chapter 6, as this chapter will synthesise the results chapters and focus more on the causes of storminess.

A millennial-length cycle of 2290 years was identified on Hill Top Bog (Figure 4.14), however given that the full record only spans c.4000 years it is not clear how reliable this result is. Nevertheless this cycle may be a reflection of the 2500 year solar cycle (Debret *et al.*, 2007) or the c.2100 year Hallstatt solar cycle (Damon and Sonett, 1991), supporting a solar influence on storminess.

Struban Bog has a cycle centred on 1450 years and Hill Top Bog a cycle centred on 1330 years (Figures 4.14 and 4.16). Similar length cycles have been identified in reconstructions of North Atlantic storminess and moisture transport previously (Sorrel *et al*., 2012; Turney *et al*., 2005; O'Brien *et al*, 1995; Debret *et al*., 2007). Furthermore an oceanic-climate connection is indicated by a similar 1370±500 year periodicity in the North Atlantic reconstructions of ice-rafting (Bond *et al*., 1997) as well as a 1500 year cycle observed in a reconstruction of Iceland-Scotland Overflow Water strength (Bianchi and McCave, 1999).

The reconstructions also suggest centennial-length cycles in storminess: Struban Bog has a cycle of c.940 years and Hill Top Bog a cycle of c.890 years (Figures 4.14 and 4.16). This resembles a c.900 year cycle identified in the Greenland $\delta^{18}O$ storminess reconstruction suggested as being the result of the NAO (Schulz and Paul, 2002), and a c.800 years cycle in a reconstruction of Irish precipitation, thought to reflect variations in westerly airflow (Turney *et al*., 2005). This cycle may have been due to changing solar activity, which shows periodicities between 830-1050 years (Stuiver and Braziunas, 1993; Stuiver *et al*., 1995).

Shorter cycles are seen in Hill Top Bog with periodicities of 730, 330 and 290 years (Figure 4.14), and a significant c.500 year cycle was identified using wavelet analysis after 1500 cal yr BP on Struban Bog (Figure 4.17). This latter cycle resembles a 478-year cycle of westerly airflow from northern Ireland (Turney *et al*., 2005), while the 290 and 330 year cycles are similar to a 300-year cycle identified in the Late Holocene NAO reconstruction (Olsen *et al*., 2012). The cycles also resemble identified solar cycles with lengths of c.510, 350 and 300 years (Stuiver and Braziunas, 1989; Turney *et al*., 2005; Steinhilber *et al*., 2012), which it has been suggested may have influenced oceanic circulation, as a 550 year cycle has been identified in a North Atlantic Deep Water formation reconstruction (Chapman and Shackleton, 2000).

In this section some of the identified storminess cycles have been shown to correlate with the available reconstructions of the NAO and Atlantic storminess, which span the Late Holocene. Cycles are similar to solar cycles, which support previous findings that there is a strong solar forcing on climate (e.g. Van Geel *et al*., 1999; Shindell *et al*., 2003; Mayewski *et al.,* 2004).

4.6. Conclusion

Reconstructions of storminess have been made by analysing changes through time of aeolian sand content in two ombrotrophic peat bogs from the Outer Hebrides: Hill Top Bog on South Uist and Struban Bog on North Uist. Multiple, but undated, cores from each bog indicate that the trends in sand content are consistent across the bog but that there is intra-site variability in the high-frequency, low-magnitude sand content. As such the focus is on centennial-resolution variations in sand content.

The main cores from each site span the period since 4000 cal yr BP and show gradually increasing sand content after c.1500 cal yr BP. Maximum peaks in sand content occur in Hill Top Bog c.400 cal yr BP during the Little Ice Age and in Struban Bog at c.800 cal yr BP during the Medieval Climate Anomaly. The difference in peak magnitude between the two bogs is suggested as being the result of the different bog localities and potentially increased human use of marginal land, such as the sand dunes, during periods with more severe climates. By comparing the two reconstructions it is considered that storminess in the Outer Hebrides increased at c.3500, 2800, 2400, 1900, 1600, 1300-1100, 800 and 500 cal yrs BP.

Comparison of the storminess reconstructions with proxies for the NAO, suggest that increasing storminess in the Outer Hebrides after c.1500 cal yr BP was the result of the transition from predominantly negative to positive NAO indices. The storminess maximum in Struban Bog during the MCA coincides with the maximum positive NAO index, however the Hill Top Bog storminess maxima during the LIA coincides with more negative NAO conditions. Therefore in northern Europe the NAO is not the sole driver of storminess changes, as peaks occur in periods of both positive and negative NAO. Finally, the presence of solar and oceanic cycles within the storminess reconstructions indicates that these may be driving the atmospheric circulation patterns during the Late Holocene.

Chapter 5: Late Holocene Storminess in Northwest Spain - A Reconstruction from Pedrido Bog, Galicia

5.1. Introduction

A small pressure gradient between the Icelandic Low pressure and the Azores high pressure causes the storm track to be positioned across southern Europe when there is a negative NAO index (e.g. Hurrell, 1995; Serreze *et al*., 1997; Trigo *et al*., 2002). The passage of low pressures across southern Europe as a result of the NAO is important for water provision in the arid climate of southern Europe, as in mountainous regions precipitation is stored in reservoirs (López -Moreno *et al*., 2011). However the NAO can also have detrimental impacts, as negative NAO anomalies can cause flooding or storm damage if there are severe or frequent low pressures, as occurred during the extremely negative NAO winter of 2009-2010 (Vicente-Serrano *et al*., 2011). Therefore understanding the natural variability of the NAO and storminess in southern Europe has important implications for the region.

In this chapter a Late Holocene storm reconstruction from a peat bog in the Cantabrian Mountains, Galicia, is presented. Galicia, in the northwest corner of Spain, is a region particularly influenced by storm tracks from the Atlantic during negative NAO anomalies. Instrumental records have shown that in winter there is a negative correlation between storms and the NAO in this region (Andrade *et al.,* 2008; Zezere *et al.,* 2005). The NAO controlled storm track position also affects temperature and precipitation: on the Iberian Peninsula river runoff in winter is negatively correlated to the NAO, with successive cyclones causing flooding events during negative NAO phases (Trigo *et al*., 2002; 2004; Benito *et al*., 2008; García *et al.*, 2005). In the Cantabrian Mountains, which extend into Galicia, the NAO is significantly negatively correlated with precipitation (R= -0.6) and significantly positively correlated with temperature (R= 0.4) (López-Moreno *et al*., 2011). The presented storminess reconstruction from Galicia will address the project aim of reconstructing storminess from southern Europe. As such this chapter will focus on the environmental changes in Galicia and the regional climatic changes in the northwest Iberian Peninsula. Furthermore by comparison with proxy reconstructions and analysis of cycles the second project aim of researching the

causes of storminess variability will be addressed. As this region is strongly influenced by the NAO this research will help investigate whether storminess was driven by changes in the NAO over long timescales and during different climatic periods. The NAO-influence on storminess will be briefly discussed here, with a more in-depth discussion in Chapter 6.

Storminess changes in southern Europe before the instrumental record have been inferred from proxy records of over-washed sand in lagoon deposits (Bao *et al*., 2007), by dating sedimentary units within sand dunes (Costas *et al*., 2012) and from various proxies in marine cores (Gonzales-Alvarez *et al*., 2005). In addition precipitation and flooding changes, indicating more frequent or intense low pressure systems, have been identified by various proxies (e.g. Bernardez *et al*., 2008, Benito *et al*., 2008). As in Chapter 4, the storminess reconstruction will be created by analysing the quantity and size of wind blown sand deposited on an ombrotrophic peat bog in Galicia.

A summary of the current understanding of Late Holocene climate in Spain, with a focus on Galicia, are presented in Figure 5.1. The results show some contradictory findings as well as some similarities. The period between 4000 and 1800 cal yr BP is inferred by the proxies as being a time with high precipitation and storminess, although the duration of this period varies between reconstructions (Figure 5.1 C-I). Following this, storminess and precipitation are thought to have been low between c.2000 and 1000 cal yr BP with some reconstructions suggesting an increase after 1000 cal yr BP (Figure 5.1 D, E, G and I). The temperature reconstructions shown in Figure 5.1 (A and B) have been verified against instrumental temperature data so are considered as reliable. The climate oscillated between warm and cold periods between 4000 and 3000 cal yr BP (Figure 5.1 A). After this there is less agreement between the records for the timings of cold and warm periods, until c.700 cal yr BP, when both reconstructions indicate cold temperatures. Therefore temperature, precipitation and storminess reconstructions indicate that there were centennial and millennial length variations through the Late Holocene. There are high resolution temperature and precipitation reconstructions but fewer high resolution reconstructions of storminess from this region, particularly from terrestrial archives, demonstrating the importance of this research.

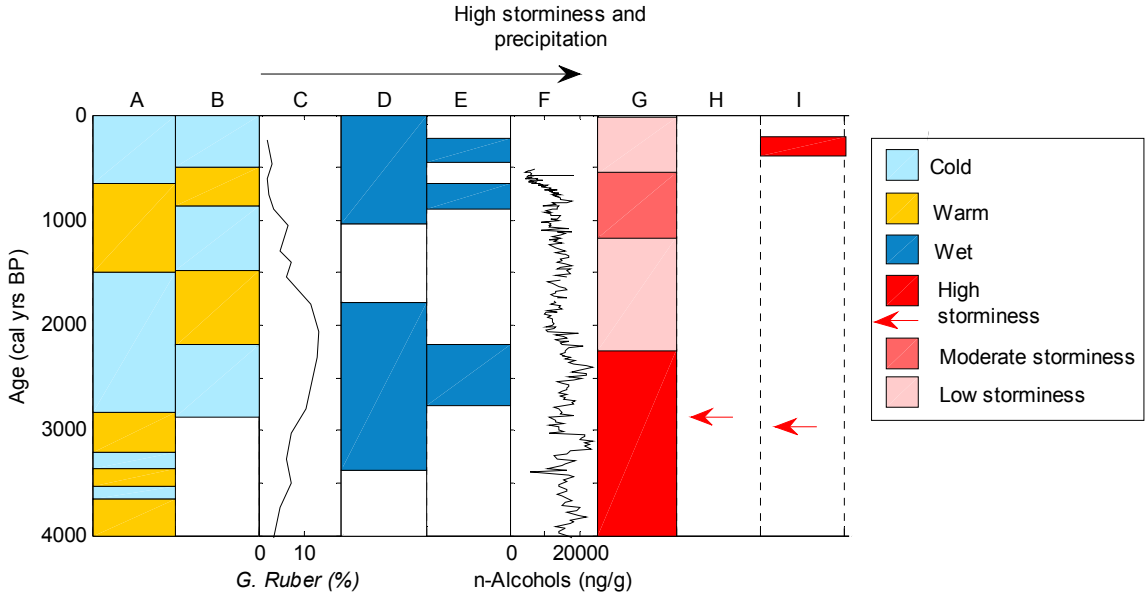

Figure 5.1: Summary diagram of reconstructed climate changes in Spain. A: Speleothem reconstruction of temperature from northern Spain (Martín-Chivelet *et al*., 2011). B: a pollen influx reconstruction of temperature from the Ría de Vigo estuary in Galicia (Desprat *et al*., 2003). C: *Globigerinoides ruber* foraminifera percentages from a core from the southeast Bay of Biscay, high values show greater strength of the Iberian Poleward Current resulting from negative NAO conditions (Mojtahid *et al*., 2013). D: high precipitation shown by a multiproxy study (based on lithostratigraphic and geochemical data) from marine cores from the Galicia Mud Patch capturing high terrigenous input (Bernárdez *et al*., 2008). E: paleoflood chronologies based on clusters of slackwater flood deposits from river basins in Spain (Benito *et al*., 2008). F: high precipitation shown by molecular biomarker (n-Alcohol) abundance as a proxy for terrestrial organic matter input from a marine core from the Ría de Muros, Galicia (Pena *et al*., 2010). G: storminess inferred from a multiproxy reconstruction of the strength of the hydrodynamic regime in the Ría de Vigo, Galicia (Martins *et al*., 2007). H: sandy facies interpreted as periodic stormy conditions from a marine core on the Galician continental shelf (González-Álvarez *et al*., 2005). I: storm deposits in Traba Lagoon, Galicia (Bao *et al*., 2007).

5.2. Study area

Pedrido Bog is an ombrotrophic raised bog situated in the Xistral Mountains of Galicia, in the northwest corner of Spain, at 43°27'1"N, 7°31'45"W and at an altitude of 770 m above sea level (Figure 5.2. and 5.3). The Pedrido Bog surface vegetation consists of *Calluna vulgaris, Eriophorum vaginatum, Erica makaiana, Molinia caerulea, Gentiana pneumonanthe, Potentilla erecta, Carex echinata, Carex sp, Sphagnum sp, Narthecium ossifragum, Parnassia palustris, Potamogeton and Succisa pratensis* and *Drosera rotundifolia*. The surrounding slopes have *Ilex aquifolium, Castanea sativa, Eucalyptus* and *Pinus pinaster* with *Pinus radiata* higher up (Pirita Oksanen, Bettina Stefanini, personal communication).

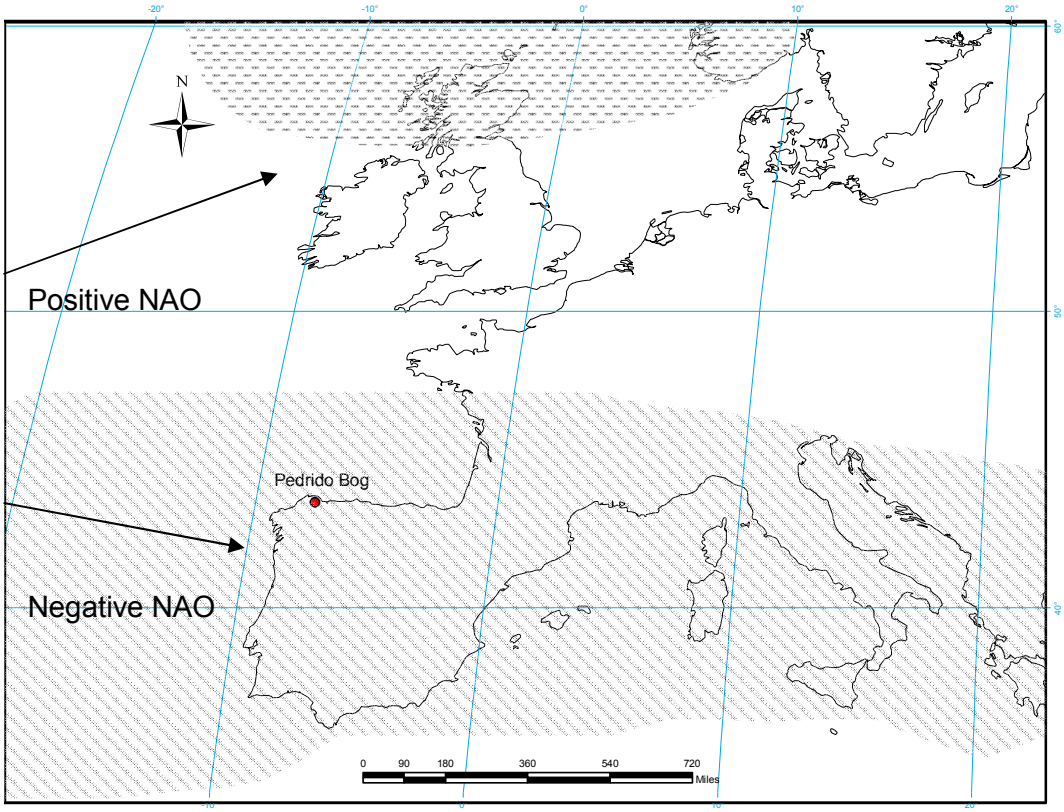

Figure 5.2: Location of Pedrido Bog in Galicia, northwest Spain. Shaded regions are the approximate areas influenced by increased winter cyclones during positive NAO (dashed area) and negative NAO (striped area) years as found by Andrade *et al*., (2008).

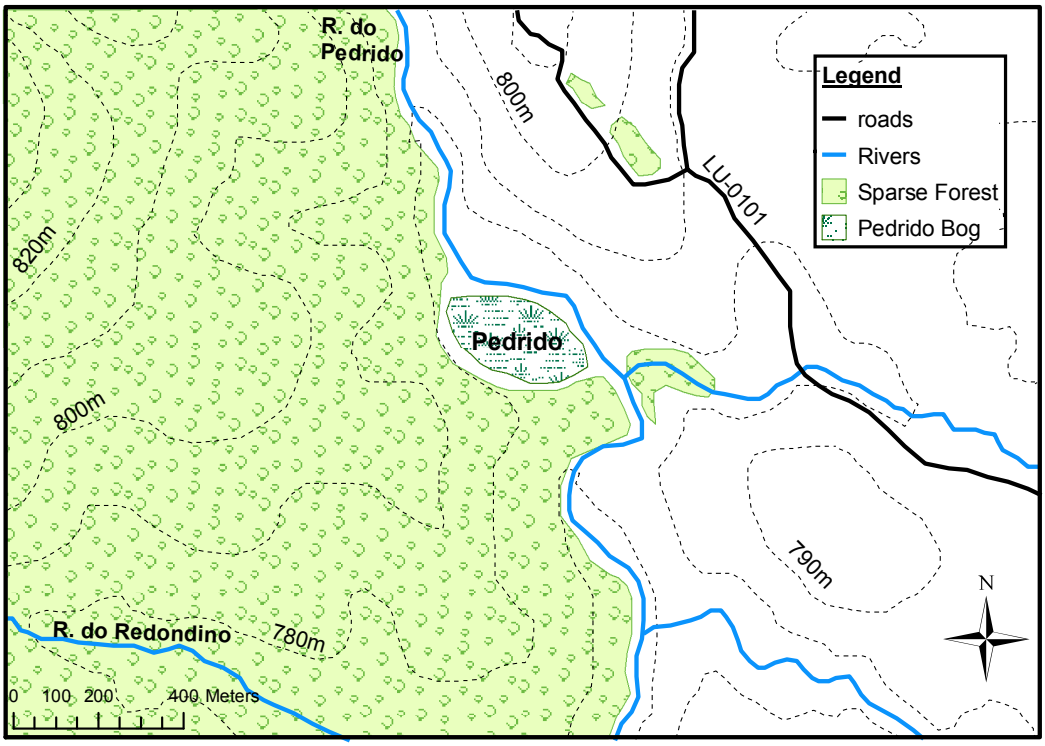

Figure 5.3: Site map of the ombrotrophic Pedrido bog (43°27'1"N, 7°31'45"W) situated in Galicia, northwest Spain in the Xistral Mountains at an altitude of 770 m.

The modern climate of Galicia is temperate and humid. The winter months have prevailing westerly and south-westerly winds caused by the passage of weather systems from the Atlantic, while the summer months have dry anti-cyclonic conditions and north or north-easterly winds, caused by the Azores high pressure being situated to the west (Penabad *et al*., 2008). The Xistral Mountains have an annual mean temperature range of 7.5-10 ºC while the annual mean precipitation in this area is reported to range from 1350-2000 mm/yr, with the highest precipitation and lowest temperatures at higher altitudes (Martinez-Cortizas *et al*., 1997; Fraga *et al*., 2008). As shown by the meteorological climate data from Santiago de Compostella, a town in central Galicia, the months of June-September are warm and dry, while the winter months are wetter and cooler (Figure 5.4.). The average monthly wind speeds show little variation through the year with a range of 10-12 knots (Figure 5.4.). These measurements were taken from 370 m above sea level, so Pedrido bog at an altitude of 770 m can be expected to have lower temperatures and higher precipitation than these measurements indicate.

The Xistral Mountains contain 80% of Galician peat bogs and these are the southernmost in Europe (Fraga *et al*., 2008; Díaz Varela *et al*., 2008). The environmental importance of the area has been recognised by inclusion in the Natura 2000 Network and it is the southernmost part of the Atlantic biogeographic region (Díaz Varela *et al*., 2008). Land-use is limited to free livestock grazing at higher altitudes, with wind farms constructed in recent years, while on lower slopes there is intensive agriculture and livestock grazing (Díaz Varela *et al*., 2008).

The investigation of climatic changes in the Holocene from Galicia is complicated by the long history of human activity here. Deforestation was widespread at low altitudes from 4000 cal yr BP (Santos *et al*., 2000) and charcoal concentrations indicate there was a gradual increase in deforestation up until 3000 cal yr BP (Kaal *et al*., 2011). After 3000 cal yr BP there is thought to have been an acceleration of environmental degradation (deforestation and pollution; Martínez-Cortizas *et al*., 2009) and more widespread grazing and agriculture (Sobrino *et al.,* 2005), although historical archives have indicated that before c.2080 cal yr BP there was weak human impact and little cultivation (Desprat *et al*., 2003; Valdés *et al*., 2001). The Roman occupation of the area resulted in agriculture at higher altitudes, as well as more settlement, mining and local deforestation between c.2080-1750 cal yr BP, however these changes were reversed between 1650-1150 cal yr BP (Santos *et al*., 2000; Desprat *et al*., 2003; Valdés *et al*., 2001; Mighall *et al.,* 2006; Martinez-Cortizas *et al.,* 2005). The population and human impact again increased from c.1350/1150 until 650 cal yr BP before decreasing due to disease at 650-450 cal yr BP (Mighall *et al.,* 2006; Martinez-Cortizas *et al.,* 2005; Desprat *et al*., 2003; Valdés *et al*., 2001). Therefore these human activities may have caused vegetation changes and sediment disturbance, and therefore influenced the quantity of sediment being blown during storms. Changes in the amount of sediment available for aeolian entrainment caused by human activities must be considered when interpreting reconstructions of storminess from this region that are based on sand deposits.

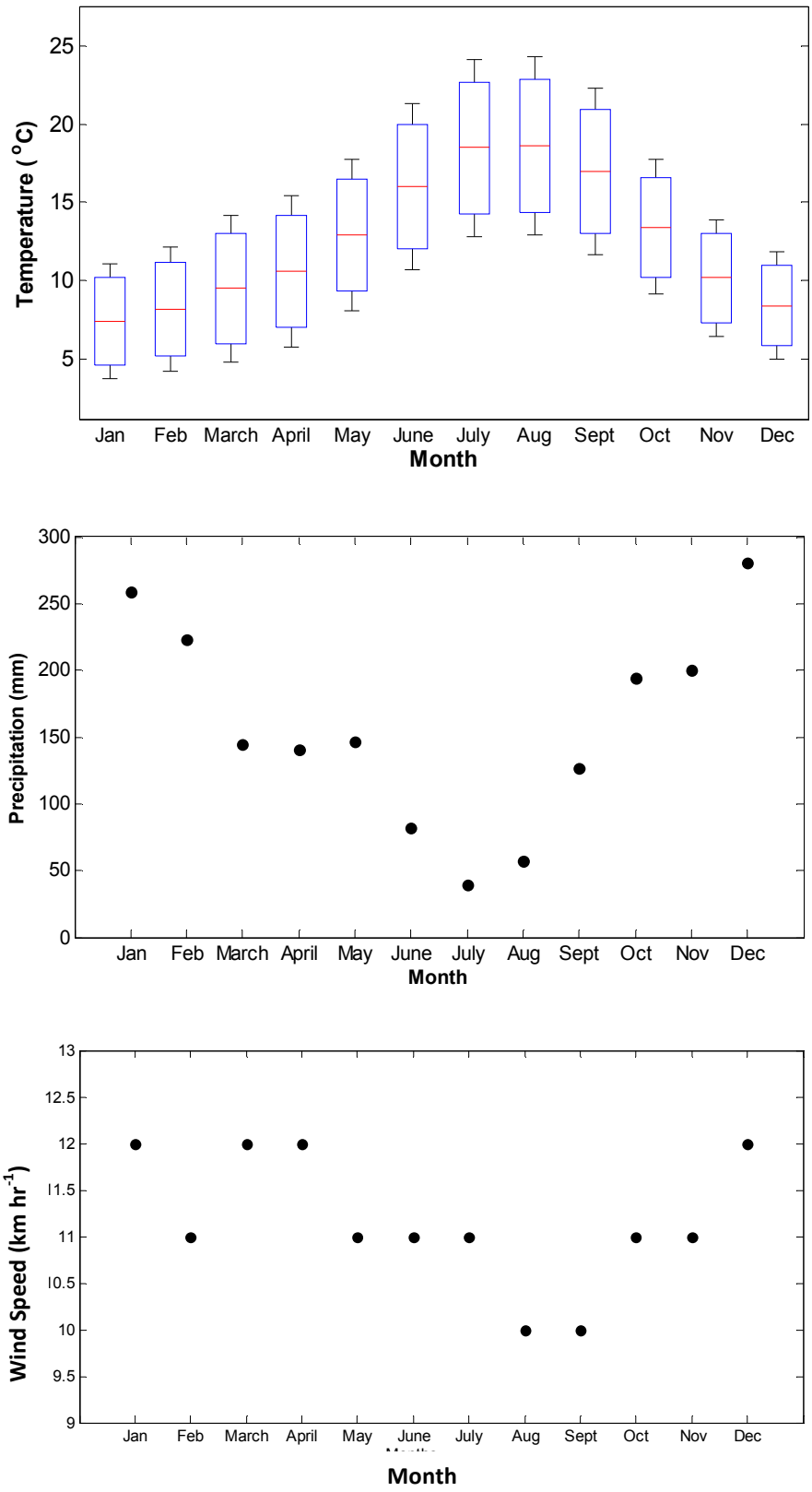

Figure 5.4: Climatological plots for Santiago de Compostela, Galicia. *Top:* Box plots of average monthly temperatures (1971-2000). *Middle:* Average monthly precipitation (1971-2000) (aemet, 2014). *Bottom:* Average monthly wind speed (1993-2013) (myweather2, 2014).

5.3. Methodology

Coring of Pedrido Bog was carried out in 2003 by Fraser Mitchell, Bettina Stefanini, Maarten Blaauw and Javier Maldonado as part of the ACCROTELM Project (EU FP5, Professor Fraser Mitchell, TCD). Two adjacent cores (core 1 and 2) were sampled using a Russian corer, and it was intended that overlapping segments between these would be used to reduce the effect of disturbance from the coring procedure. Core segments were wrapped securely in the field and stored in a cold store thereafter. As the peat was firm and undisturbed however, dating and initial analysis was only done on one core (Core 1), while sediment from core 2 was analysed in this research.

Of the two adjacent cores sampled from Pedrido Bog all dating and analyses were initially done on Core 1 prior to the start of this research, as part of the wider project. This included loss-on-ignition, pollen and charcoal analysis (which are considered in this chapter) as well as various proxies to determine bog surface wetness (macrofossils, non-pollen palynomorphs, bog pollen). The interpretation of the bog surface wetness proxies is complex and will be addressed in forthcoming research papers, so these will not be considered in this research. However the charcoal and tree pollen percentages will be considered, as these provide information on vegetation changes and human activity in the area surrounding the bog.

^{210}Pb and radiocarbon dating were carried out previously on core 1. The ^{210}Pb dating was carried out by Bettina Stefanini, who prepared samples following the methods of Flynn (1968) and Robbins (1978) before dating at the University of Gloucestershire. Sampling for radiocarbon dating was carried out by Bettina Stefanini, who sampled plant macrofossils (*Ericales* and *Cyperaceae*), which were AMS dated at the Centre for Isotope Research, Groningen University, in the Netherlands. Using these dates the chronology was recalculated, following the same methods of age-depth model calculation as in Chapter 4. The age-depth model was created using Bayesian analysis by OxCal version 4.2.3, which used the IntCal13 calibration curve (Bronk Ramsey, 2013; Reimer *et al*., 2009; Bronk Ramsey 2009a). The median of the 2-sigma age range was used to estimate the age for individual samples down the core.

As in Chapter 4 the sand-sized aeolian material within the peat was analysed and used as a proxy for storminess (see section 2.8 for detailed methods). Additionally the organic bulk density was estimated using the loss-on-ignition measurements (as explained in section 2.8.), which can indicate the amount of humification of the peat (Yu *et al.,* 2003; Björck and Clemmensen, 2004; Chambers *et al.,* 2011).

The previously measured pollen and charcoal results were of interest as a way of inferring whether sand input could be explained by land-use changes in the proximity of the bog. These analyses were carried out on core 1, prior to the sand content analysis, as part of a wider project. The full results and methods are in Stefanini *et al.* (in prep) and are summarised here. Pollen and charcoal analyses were carried out every 4 cm. Pollen was extracted using the method of Faegri and Iversen (1950) with a tablet of *Lycopodium* spores added to each sample to account for sample concentrations (Stockmarr, 1971). The charcoal (>125 μm) was extracted following the method of Mooney and Radford (2001) and the concentrations estimated as area (Mooney and Black, 2003), before being converted to charcoal accumulation rates. The low sampling resolution (every 4 cm) of the charcoal and pollen results mean that comparison with the higher resolution IR and coarse-fraction results is difficult, as the synchronicity of changes may be hidden by the discontinuous sampling of the pollen and charcoal samples. Nevertheless the pollen and charcoal analysis was used to show general vegetation changes and human activity in the region.

Finally, spectral analysis (as described in section 2.8.3.) was carried out on the medium (120-180 μm) sand weight results, which was first detrended using a polynomial fit to remove the nonlinear trend. This sand fraction was used rather than the coarse sand because this proxy was considered more sensitive to storminess, as the threshold for aeolian transport of the smaller sand grains is lower than that of coarse sand.

5.4. Results

The core analysed in this research (core 2) was taken from depths of 7-357 cm and is highly decomposed sedge and grass dominated peat. The organic bulk density results show the peat between 250-220 cm and 130-79 cm had a low density (i.e. poorly humified) and the core sections between 220 and 130 cm and above 70 cm were high density peat (well humified).

The age-depth model of core 2 was constrained using 8 ^{210}Pb dates and 27 radiocarbon dates (Tables 5.1 and 5.2), which allowed a highly constrained age model to be made, as shown in Figure 5.5. The core spans the Late Holocene from c.4600 cal yr BP to present. There was a slower peat accumulation rate at 4600-4200 and 3000-2000 cal yr BP and variations in the uppermost 20 cm, which is within the acrotelm. As the peat is well dated these variations can be accounted for (using the sand influx measure) to prevent peaks in sand content resulting from slower peat accumulation.

Table 5.1: ^{210}Pb dates, measured and calculated prior to the start of this project.

Sample depth	^{210}Pb Age (A.D)	Error (1σ)
1-2	2002	6
3-4	1995	4
5-6	1982	5
7-8	1963	6
9-10	1944	8
11-12	1920	13
13-14	1896	24
15-16	1825	96

Table 5.2: Radiocarbon dates and calibrations used in the age-depth model. Dates were analysed prior to the start of this research.

Sample Depth (Core 1)	Laboratory Code	Radiocarbon Age (^{14}C yr BP ± 1σ)	Median calibrated age (cal yr BP)
20-21	GrA-30387	360 ± 45	348
24-25	GrA-26807	370 ± 30	446
30-31	GrA-30464	540 ± 35	538
37-38	GrA-30454	665 ± 35	639
44-45	GrA-30466	795 ± 35	708
56-57	GrA-30467	945 ± 35	842
60-61	GrA-26809	940 ± 30	888
70-71	GrA-30402	1130 ± 50	1028
80-81	GrA-30468	1260 ± 35	1187
96-97	GrA-30459	1460 ± 35	1373
99-100	GrA-30460	1580 ± 35	1433
129-130	GrA-30455	1955 ± 35	1914
139-140	GrA-30410	2080 ± 50	2077
143-144	GrA-26854	2220 ± 40	2189
151-152	GrA-30406	2290 ± 50	2333
153-154	GrA-30408	2330 ± 50	2361
157-158	GrA-30403	2480 ± 50	2599
159-160	GrA-30409	2600 ± 50	2731
162-163	GrA-26811	2715 ± 35	2808
167-168	GrA-30448	2865 ± 40	2973
175-176	GrA-30449	3050 ± 40	3222
216-217	GrA-26800	3640 ± 45	3943
230-231	GrA-30404	3720 ± 50	4138
233-234	GrA-30487	3795 ± 35	4200
235-236	GrA-30450	3805 ± 40	4237
237-238	GrA-30452	3945 ± 40	4322
248-249	GrA-25192	4155 ± 40	4629

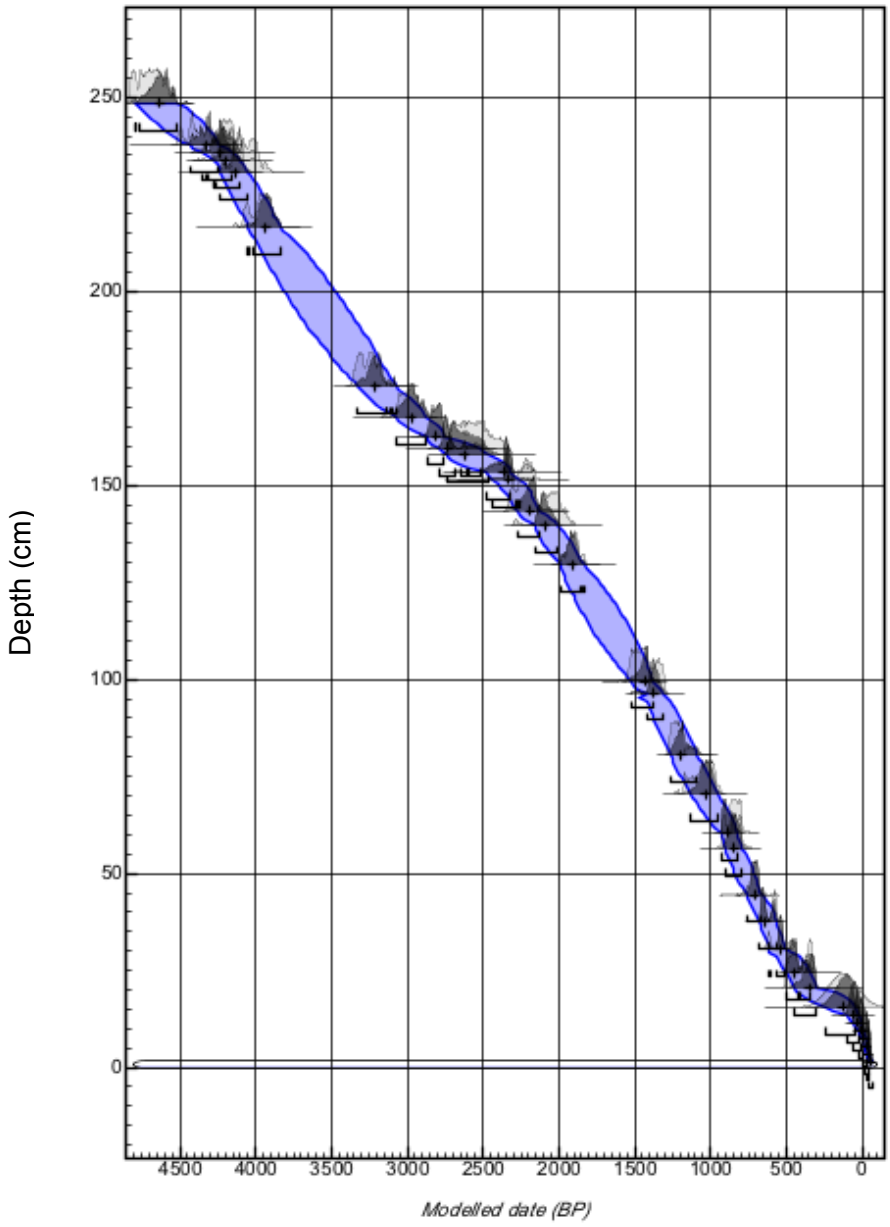

Figure 5.5: Age-depth model for Pedrido Bog. Modelled using Bayesian analysis by OxCal version 4.2.3, which used the IntCal13 calibration curve (Ramsey, 2013; Reimer *et al*., 2009; Ramsey 2009). Shaded section marks the 2-sigma calibrated age range.

The IR values along the core are between 2-5% of the dry peat weight, with peaks of 7 to 15%. The coarse-fraction weight results support that most of the IR peaks were the result of peaks in sand content. However the peak in the IR at c.900 cal yr BP does not occur as a peak in either sand fraction. As this is precisely at the top of a section of core it is thought that this peak is an artefact of the cores condition since being exhumed. It is not clear why this has occurred; potentially the core was contaminated or dried out. As sieving demonstrates that the peak in IR was not caused by sand >120 μm in size, it is therefore not considered as a potential peak in storminess hereafter.

Overall peaks seen in the IR, the coarse-fraction weights and the sand influx results indicate increased sand deposition onto the bog at 3900-3700, 3600-3500, 3400-3250, 3000-2700, 2600-2200, 2050-1850 and 400-0 cal yr BP. These suggest that the broad period from 3900-1800 cal yr BP had high sand input into the bog, and this was then followed by a period with reduced sand input. The influx results indicate that there were small variations between 1800 and 400 cal yr BP. The events at 3900-3700 and 400-0 cal yr BP were low magnitude events, while at 3400-3250 and 3000-2700 cal yr BP high magnitude events occurred.

The sand influx results reduce some of the peaks seen in the coarse-fraction weight results but increase others. For example the uppermost peak in the coarse-fraction weights (from c.400 cal yr BP to present) is reduced, suggesting it was partly the result of a slower accumulation rate. Another alteration is the period between 1800-500 cal yr BP: there are peaks that are more pronounced in the influx results than the weight values, which imply that a high accumulation rate during this time may be partly responsible for the low sand content. Small peaks occur in the sand influx at approximately 1350, 1000, 850 and 700 cal yr BP.

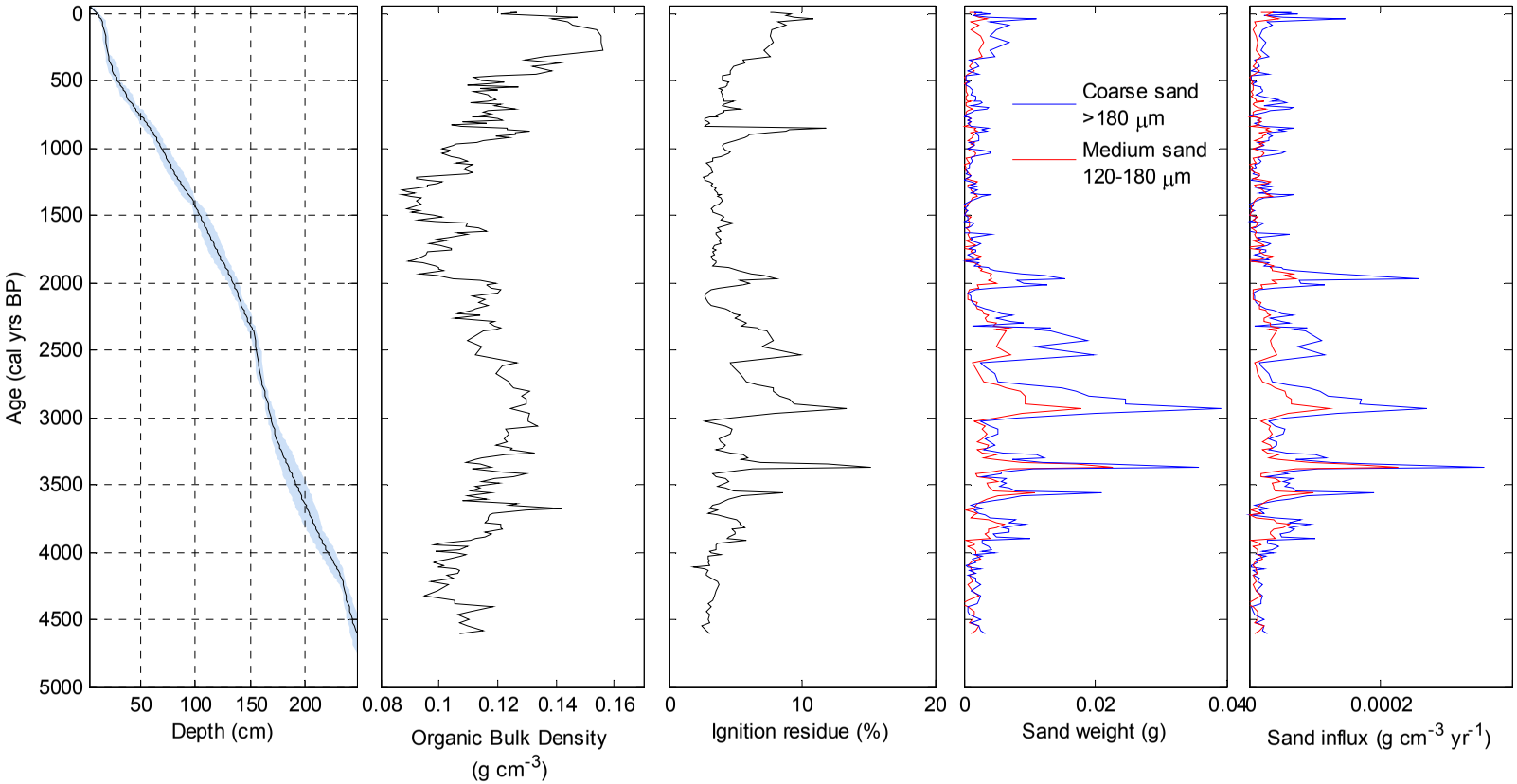

Figure 5.6: Results of sand content analysis plotted against age. From left: age-depth model with shaded area representing the 2-sigma error margin, organic bulk density, ignition residue, coarse-fraction weights and coarse-fraction influx.

The results of the Lomb-Scargle spectral analysis showed significant cycles of 2051 (range 1820-2325 years) and 513 years (490-540 years) (Figure 5.7). The Wavelet analysis indicates that these cycles have not been occurring throughout the Late Holocene: the cycle of c.512 was dominant between approximately 3600 and 2000 cal yr BP, while a cycle of ~220 years was significant between approximately 3800 and 2800 cal yr BP and present until 1800 cal yr BP (Figure 5.8.). The 2051 year cycle was considered insignificant based on the wavelet analysis.

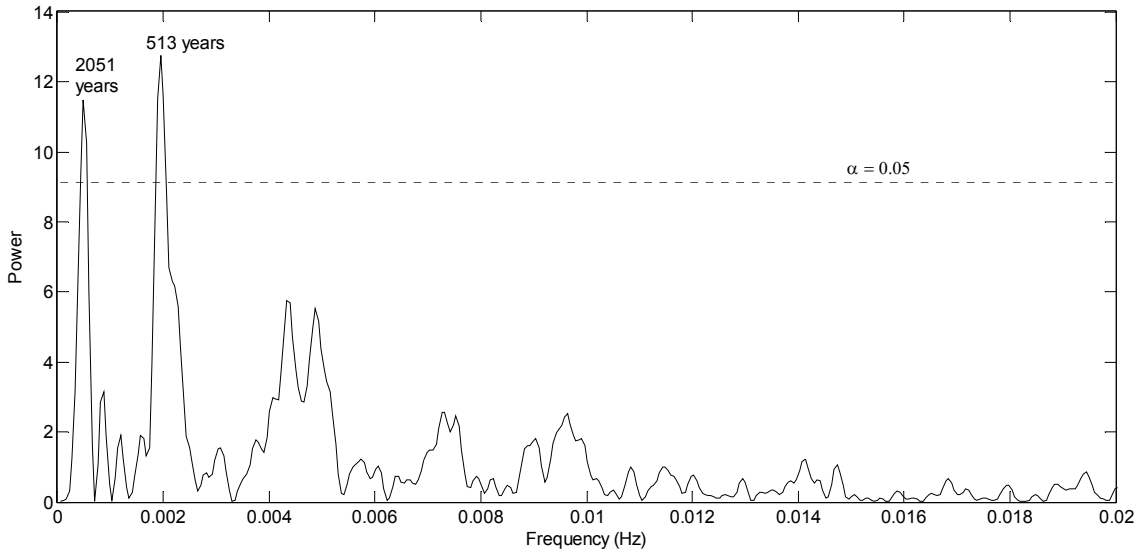

Figure 5.7: Lomb-Scargle spectral analysis of the medium sand content (120-180 μm fraction). The dashed line shows the 95% significance level.

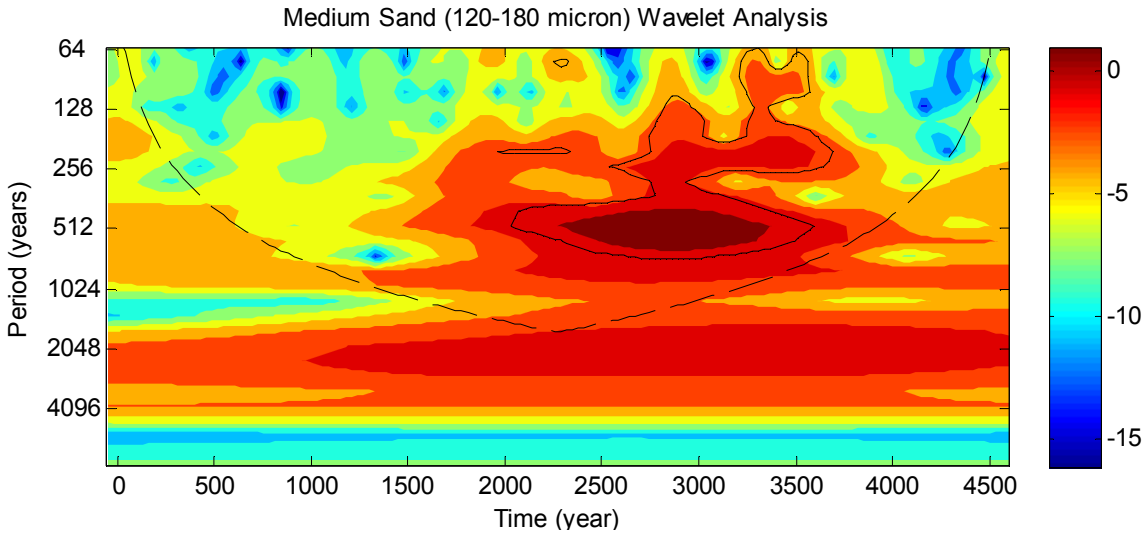

Figure 5.8: Wavelet power spectrum analysis of the medium sand content (120-180 µm fraction). Black line shows the 95th percent significance level. The dashed line shows the cone of influence: as the timeseries is finite in length, and therefore padded by zeros during analysis, the cycles outside the cone are likely to be underestimated. The colour bar shows the magnitude of the cycles, with high magnitude cycles shown by red colours.

The pollen analysis results are grouped with the aim of showing changes in tree cover. The most common types of tree pollen recorded include *Corylus*, *Alnus, Betula* and *Quercus*. Charcoal counts have been included to infer fire activity in the bog environs. The accumulation of tree pollen appears to have abruptly decreased at c.3500, 2750, 2300-2100, 1330-1200 and after 400 cal yr BP, with small decreases at c.4200, 3860-3700, 950 and 500 cal yr BP (Figure 5.9.). The low sampling resolution (every 4 cm) however means some of these intervals are the product of only 1-2 pollen samples and some decreases in tree pollen could be missed. The charcoal percentages suggest that there was moderately high accummulation at 4500-3600 cal yr BP before a reduction between 3600 and 1500 cal yr BP, with a peak at 3230 cal yr BP (Figure 5.9.). After 1500 cal yr BP charcoal deposition increased towards a maximum at 800 cal yr BP, with peaks at 1450 and 1200 cal yr BP. From approximately 700 cal yr BP to present the charcoal deposition was consistently low.

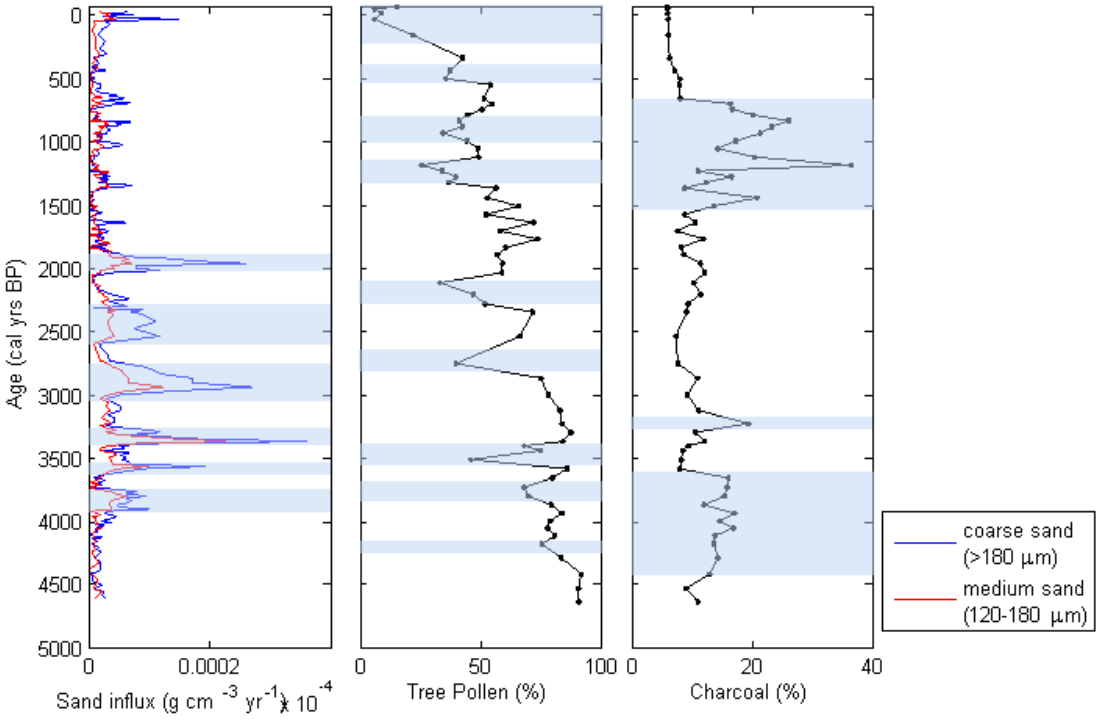

Figure 5.9: Comparison between (*from left*) sand influx results, combined tree pollen percentage and charcoal percentage. The shaded bars relate to (*from left*): peaks in sand influx, decreases in tree pollen and increases in >125 µm charcoal. The pollen and charcoal were measured on core 1 as part of the ACCROTELM project prior to the start of this research (as described in section 5.3).

5.5. Discussion

In this section possible human or climatic influences on Pedrido bog are discussed. In the first subsection there is a discussion of the human vs. climatic influences on vegetation, and in the second subsection the influence of climate (including temperature, storminess and the NAO) on sand deposition is investigated.

5.5.1. Vegetation influence

In this section two questions will be discussed: 1) Did vegetation decreases cause increased sand entrainment and deposition on Pedrido Bog? 2) Did vegetation decreases occur due to human or climatic changes? These will be answered by comparison between the sand influx and pollen results from Pedrido Bog (Figure 5.9), followed by comparison with regional human activities and climatic changes.

The sand content peaks at c. 3800, 3550 and 100 cal yr BP occur at the same time as tree pollen percentage decreases in the core (Figure 5.9.), so at these times deforestation in the area could have caused soil disturbance and an increase in the soil available for aeolian entrainment. The sand influx peaks at 2900 and 2500 cal yr BP occur immediately before tree pollen percentage decreases so are unrelated. The sand peaks at c. 3300 and 1900 cal yr BP occur when tree pollen is fairly high, indicating that these peaks are not the result of deforestation in the bog environs. Finally the occurrence of deforestation occurs without any influx of sand into the bog, for example decreases in tree pollen occur between 4400-4200 cal yr BP and particularly from 1400 to 800 cal yr BP but do not coincide with any increases in sediment influx. Overall there is some indication that vegetation changes caused enhanced sand deposition onto the bog, but there are also differences between the sand and pollen reconstructions.

The next question is whether changes in the vegetation were the result of human deforestation or climate deteriorations. The pollen and sand variations will first be compared with evidence of human activities from Galicia. Activities in the upland areas are known to have been agropastoral since at least 4000 cal yrs BP, with fire used as a tool to clear land for grazing and increase the

nutrients in soil (Kaal *et al*., 2011). The gradual decrease in tree pollen through the 4500 year reconstruction agrees with reconstructions suggesting weak or gradual human impact up until 3000-2000 cal yr BP but does not demonstrate the well documented acceleration after this time, resulting from Roman expansion from 2050-1750 cal yr BP (Desprat *et al*., 2003; Valdés *et al*., 2001; Kaal *et al*., 2011; Martínez-Cortizas *et al*., 2009; Muñoz Sobrino *et al* 2005). The tree pollen reconstruction in some ways reflects broad socio-economic changes in the region after this time. The population decreases at 1650-1150 cal yr BP and 650-450 cal yr BP (Desprat *et al*., 2003; Valdés *et al*., 2001) appear to be reflected in the tree pollen percentages as small increases, although there is some discrepancy in the timings. The population increase, settlement and deforestation thought to have occurred at 1350/1150 until 750 cal yr BP (Mighall *et al.,* 2006; Martínez-Cortizas *et al.,* 2005; Desprat *et al*., 2003; Valdés *et al*., 2001) coincided with two of the inferred decreases in tree cover and a large increase in charcoal deposition in the region. Therefore the historically known population changes, particularly since 2000 cal yr BP, are reflected in the level of deforestation indicated by the Pedrido tree pollen record.

The impact this may have had on the sand influx to the bog is unclear. One issue is that pollen and charcoal may represent regional signals, whereas sand deposition is likely to reflect local disturbances. The steady decrease in tree pollen is not mirrored by an increase in sand content, with the largest peaks in sand influx in the older part of the record when human activities would be expected to have been lower. Similarly the largest magnitude increases in charcoal occured at 1500-700 cal yr BP when sand content in the Pedrido Bog was low. Therefore as sand influxes occured at times when pollen and charcoal results suggest little human disturbance, and conversely reductions in tree pollen occurred without any increase of sand onto the bog, this supports that the Pedrido bog sand influx reconstruction is a climatic reconstruction. This contradicts the interpretation of previous research from the region that sediment deposition onto bogs was solely the result of human activities (Martinez-Cortizas *et al.,* 2005).

The above discussion contradicts that there is a causal link between decreased vegetation and increased sediment influx to the bog. However changes in vegetation could also have resulted from climatic variations (of

temperature and precipitation), which may explain the occasions when there were simultaneous increases in sand influx at times of reduced vegetation. As Galicia is a location with high precipitation, plants are limited by temperature rather than water availability, which has been suggested as an influence on vegetation density (Desprat *et al*., 2003). A study from Galicia has show that temperature changes of ~1 ºC cause changes in pollen influx during the instrumental period: this study goes on to infer, using reconstructed pollen influx, that in the last 3000 years temperatures were lower at 2900-2200 and 1500-1000 cal yr BP (Desprat *et al*., 2003; Figure 5.1 B). Although pollen influx hasn't been assessed in the Pedrido pollen reconstruction, these cold periods identified by Desprat *et al*., (2003) span the Pedrido Bog decreases in tree pollen, and support that these were the result of climatic rather than human vegetation changes. These cold events are supported by a marine record from the Ría de Vigo, Galicia, which indicates that there was a transition from warmer to cooler temperatures between 2925-1700 cal yr BP, during which time there were strong temperature fluctuations (Ãlvarez *et al*., 2005). As well as this a speleothem record from Galicia suggests that there were centennial cold events at c.3950, 3550, 3250 and 2850-2500 (Martin-Chivelet *et al*., 2011; Figure 5.1 A), which correspond to the tree pollen reductions in this time. The similar timings of these cold events in multiple records support that vegetation changes were the result of temperature changes..

As in the Outer Hebrides, the interactions between human activities and climate may cause most damage to the environment (Kaal *et al*., 2011; Martinez Cortizas *et al.,* 2009). It has been suggested that a climate deterioration after 1700 cal yrs BP reduced the ability of vegetation to regenerate in response to human disturbances such as fire, leading to enhanced erosion (Kaal *et al.,* 2011; Mighall *et al.,* 2006). However the lower sand content after 1800 cal yrs BP in the Pedrido reconstruction does not support that this was the case. Instead there may have been a similar environmental response to the abrupt cold events described above during the period 4000-2500 cal yrs BP (Martin-Chivelet *et al*., 2011), as these temperature decreases perhaps enhanced the human impacts on the environment. It has been suggested in this region that abrupt climate changes such as these were crucial for environmental degradation, as these not only increased the environmental fragility but also

caused humans to add pressure (Martinez Cortizas *et al*., 2009), for example reduced crop yields may have encouraged expansion of agricultural land. These studies have not suggested that storminess caused environmental degradation, however it is possible that flooding and wind-damage may have enhanced environmental degradation, causing past human societies in upland Galicia to adapt their land use practices, leading to greater sediment erosion.

To summarise, in the Pedrido Bog reconstruction some of the decreases in tree pollen occur at the same time as sand influxes. This could indicate that human deforestation was the cause of increased sand to the bog, by increasing the available sediment for aeolian entrainment. However as the largest peaks occur in the earliest part of the record, when human influence was likely to have been lowest, and sand content did not increase with decreasing forest cover towards the present, it seems that human deforestation was not the most important factor governing sand influx to the site. Instead it is considered that the long-term decrease in pollen was the result of regional, human deforestation, but that abrupt, centennial-duration tree-pollen declines were the result of climatic deteriorations, with sediment erosion possibly enhanced by the human response to these climate changes. This is supported by the study of Desprat *et al.* (2003), which has shown the influence of temperature on vegetation density in Galicia. Therefore sand influx peaks at c.3800, 3600, 3400, 2900, 2400 and 1900 cal yr BP are considered as resulting from higher storminess, sometimes accompanied by reduced temperatures.

5.5.2. Sand deposition: single or multiple storm events

A question when interpreting reconstructions of storminess are whether they reflect single, extreme storms or the cumulative result of multiple storms. The peaks in sand in the Pedrido reconstruction span between 3 and 10 cm, which indicates that they accumulated over decadal timescales and were the result of multiple storms. However there is the possibility that sand deposited in a single event could have been redistributed to deeper peat. The redistribution of sediment within peat has been investigated by looking at how tephra and ^{137}Cs are spread through peat, as these were deposited over short time periods, so are perhaps comparable to sand deposited by individual severe storms.

Some experiments have shown tephra can be redistributed within peat by up to 6 cm, with greater spreads on some experiments, although these experiments used the surface acrotelm where compression is minimal (Payne *et al*., 2005; Payne and Gehrels, 2010). On the other hand tephra analysis in compressed peat within the catotelm have described frequent tephra spreads of <5 cm (Dugmore and Newton, 1992) and another study found the spread of ^{137}Cs in a peat basin to be minimal, indicating negligible bioturbation (Tyler *et al*., 2001). As such the spread of sand through peat may be dependent on the bog, so these experiments do not help to determine whether individual severe storms or cumulative storms caused the sand peaks.

It can be observed that the events at 3900-3700, 3400-3250, 2600-2200, 2050-1850 and 400-0 cal yr BP have multiple peaks particularly in the >180 μm size fraction, so it is possible that each of these were caused by a new input of material. The depth where tephra is deposited within peat is usually where the peak tephra concentrations remain (Payne and Gehrels, 2010), which supports that these multiple sand peaks resulted from multiple storms. As the 1 cm samples span decades, it seems likely that multiple storms capable of transporting sand will have occurred in these periods. Therefore a tentative conclusion is that the reconstructed peaks in storminess were the result of multiple storms over decades and centuries rather than single storms, although based on the available results this cannot be considered certain.

5.5.3. Storminess, the NAO and sand deposition

Due to project limitiations multiple sites could not be cored in Galicia (as was done in the Outer Hebrides) to identify regional periods of sand influx. To address this, other literature has been reviewed to find loss-on-ignition results from similar bogs in this region. However only two records have been found with which to make a comparison, as ombrotrophic bogs are only present in the north of the area (Pontrevedra-Pombal *et al.,* 2006) and many studies do not show loss-on-ignition results. Martinez-Cortizas *et al*., (2005) analysed the ombrotrophic saddle mire Pena da Cadela and found some small peaks in sand content that coincide with peaks in the Pedrido reconstruction (at 3370, 3200, 2810, 2400, 1060 and 670 cal yrs BP and after 610 cal yrs BP) but others that

do not agree (at 1760 and 1180 cal yrs BP). The other ombrotrophic bog, Penido Vello, had increased inorganic material only after 660 cal yrs BP, which has been interpreted as resulting from recent human disturbance (Schellekens *et al*., 2011), as well as drying due to peat cutting (Martinez-Cortizas *et al.,* 1997). The similarity between the timings of peaks in the Pena da Cadela and Pedrido reconstructions support that these were the result of regional climate changes, however the sand content of both the Pena da Cadela and Penido Vello records are lower in the period 4000-2000 cal yrs BP than the Pedrido Bog record. This could be a result of different bog situations, for example Penido Vello is situated on a summit, which may have reduced the amount of aeolian material reaching and settling at this destination. On the other hand the sand influx to Pedrido Bog may have been amplified by human activities at certain times (see section 5.5.1). Further reconstructions from sites with similar localities to Pedrido Bog would further clarify regional climate changes.

To ascertain a climatic influence, the coarse fraction analysis results would ideally be correlated with instrumental data. However the low resolution of the sand content measurements, the short duration of instrumental data and the poor preservation of the upper peat means that this is not possible. Instead the Pedrido reconstruction is compared with the NAO reconstruction by Trouet *et al.* (2009), which extends back to 1050 A.D.. The medium sand weight has a (Spearmans) correlation of R = -0.49 (n=47) with the NAO reconstruction, which is significant at the 95% level. The reconstructions indicate that the positive NAO during the MCA (1050-550 cal yr BP) was accompanied by low storminess in the Pedrido reconstruction, with high storminess during the LIA (550-50 cal yr BP) when the NAO was more negative (Figure 5.10.). This is in agreement with the understanding of the NAO-storm relationship during the instrumental period, which indicates that the storm track crosses southern Europe during negative NAO periods (Hurrell and Van Loon, 1997; Zezere *et al.,* 2005).

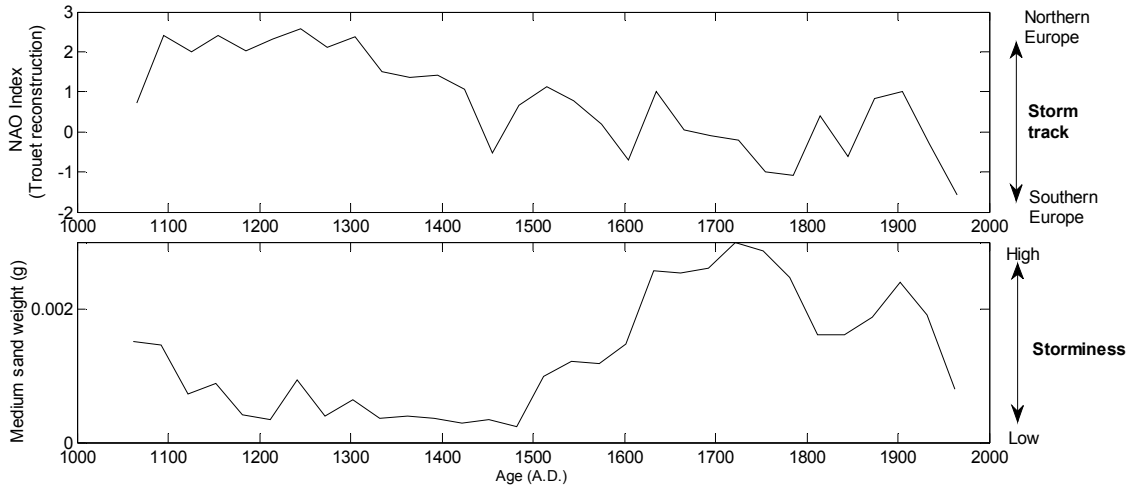

Figure 5.10: Comparison between the NAO reconstruction (Trouet *et al*., 2009) and the Pedrido Bog medium sand content (120-180 microns). Both reconstructions have been downsampled to a resolution of 30 years.

Comparison of the Pedrido Bog reconstruction with the longest NAO reconstruction by Olsen *et al.* (2012) also supports a consistent long-term NAO influence on storminess in northwest Spain (Figure 5.11). Between 4000-1800 cal yr BP there was a generally low NAO index, which coincides with higher storminess between 4000-1800 cal yr BP. Within this period there are peaks in storminess coinciding with extreme NAO minima at c.3350, 3000-2700 and 2500-2300 cal yr BP. The negative NAO event c.2100 cal yr BP occurs around 100 years before a storminess peak, which may be due to dating errors in one of the reconstructions. However the peaks in storminess at c.3800 and 3600 cal yr BP do not coincide with extremely low NAO anomalies. As a negative NAO index directs the storm track across southern Europe, the results here generally support that the Pedrido Bog storminess peaks were the result of dominant negative NAO conditions, as was observed during the instrumental period (Andrade *et al.*, 2008; Zezere *et al.,* 2005). After 1800 cal yr BP there was a more positive NAO and at this time storminess was greatly reduced in the Pedrido reconstruction. This supports that at this time the storm track was situated more frequently over northern Europe, as a result of positive NAO conditions. The influence of the NAO on storminess will be discussed further in Chapter 6, in combination with the results from the Outer Hebrides, which can allow changes in the storm track to be inferred.

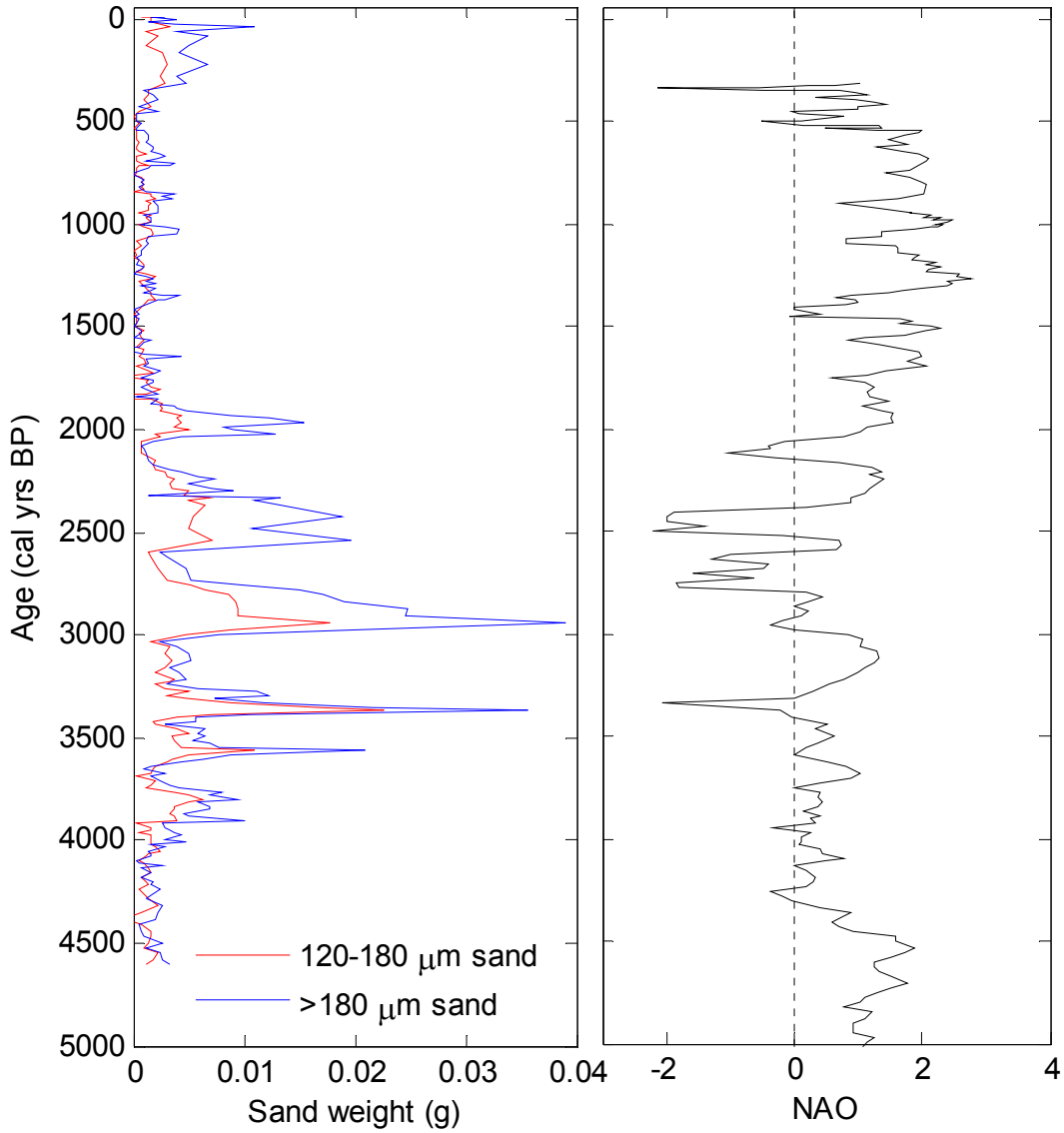

Figure 5.11: Comparison between the storminess reconstruction from Pedrido Bog and the NAO reconstruction by Olsen *et al.* (2012).

5.5.4. Comparison with Late Holocene Galician Climate

4000-1800 cal yr BP

In Galicia the reconstructed high storminess in the period 4000-1800 cal yr BP is supported by other proxies that appear to have identified high storminess and precipitation from the region during this time. These are summarised in Figure 5.12 alongside the Pedrido Bog reconstruction. Cores from the continental shelf off the northwest Iberian coast (called the Galicia Mud

Patch) have shown results that indicate a strong hydrodynamic regime caused by a prevalence of winter storms at 4800-2200 cal yr BP (Martins *et al*., 2007; Figure 5.12 G), which is approximately coincident with the higher storminess seen in the Pedrido reconstruction. Furthermore the largest peak in storminess inferred by the Pedrido record at c.3000-2700 cal yr BP is comparable with strong storm currents suggested at c.2850 cal yr BP as occuring in the Ría de Vigo (González -Alvarez *et al*., 2005; Figure 5.12 H).

The period 4000-1800 cal yr BP also appears to have been a time when precipitation was high in the northwest Iberian Peninsula. A record from the Galicia Mud Patch suggests that towards 3300 cal yr BP riverine inputs increased, which were then sustained between 3300-1700 cal yr BP (Bernardez *et al*., 2008; Figure 5.12 D). Similarly lake levels in the northeast Iberian Peninsula increased between 3800-2800 cal yr BP, before remaining high and fluctuating between 2600-1600 cal yr BP (Scussolini *et al*., 2011). A core from the Ría de Vigo, Galicia, suggests that from the start of the record at 2925 cal yr BP until 950 cal yr BP the marine environment was unstable with high terrestrial input (Diz *et al*., 2002), which implies precipitation remained high for 850 years after storminess decreased. Higher precipitation resulting in high terrestrial input has also been indicated by a Galician marine proxy reconstruction between c.4200 and 2100 cal yr BP (Pena *et al*., 2010; Figure 5.12 F). This has peaks at c.4100, 3800, 3200 and 2400 cal yr BP, which coincide with some but not all of the Pedrido Bog storm peaks. Furthermore higher precipitation has been inferred at c.2800 and c.2510-2200 cal yr BP by mercury concentrations in a peat bog (Martínez-Cortizas *et al*., 1999), and high river flood occurrence in the Atlantic regions of Spain has also been indicated between 2865-2350 cal yr BP (Benito *et al*., 2008 Figure 5.12 E). These latter precipitation reconstructions are around the same time as high storminess at 3000-2700 and 2600-2200 cal yr BP in the Pedrido reconstruction. Finally the Pedrido reconstruction is supported by a record from the Bay of Biscay, which has suggested that there were warm and humid conditions between 3500-1800 cal yr BP, interpreted as being the result of a negative NAO (Mojtahid *et al*., 2013; Figure 5.12 C). These proxies imply that the period of high storminess also had high precipitation associated with low-pressure systems bringing more rain as well as wind, which is in support of this being a period with frequent negative NAO events.

Post-1800 cal yr BP

From c.1800 cal yr BP the Pedrido reconstruction suggests that climate in this region became less stormy, with only low magnitude peaks in sand content (particularly sand influx) at 1370-1230, 1060-990, 960-850 and 740-620 cal yr BP. Although these peaks are small they are greater than the precision margins calculated for the sand fraction weights in Chapter 2, so can be treated as significant.

Lower storminess during this time is supported by evidence of a weak hydrodynamic regime on the Galicia Mud Patch between 2200-1200 cal yr BP (Martins *et al*., 2007; Figure 5.12 G) and cool, stable conditions since 1800 cal yr BP in the Bay of Biscay, which is synonymous with a positive NAO (Mojtahid *et al*., 2013) (Figure 5.12 C). The precipitation proxies are inconclusive; some precipitation proxies indicate that there was low river flow (of the Duoro and Miño rivers) from 1700-1200 cal yr BP in the northwest Iberian Peninsula (Bernardez *et al*., 2008; Figure 5.12 D), however the Ría de Vigo is thought to have had high river flow from 1700-580 cal yr BP (Ãlvarez *et al*., 2005) and high terrestrial input, suggesting high river flow, until 950 cal yr BP (Diz *et al*., 2002). There is a suggestion therefore that precipitation was high at a time when storminess was low, which implies that low pressure systems were not accompanied by as intense winds as earlier in the Late Holocene.

In the last millennium the MCA is suggested by the Pedrido reconstruction as a time when sand influx increased moderately between 1100-600 cal yr BP. This is at the same time as flooding and precipitation from the Galicia region may have increased: in Atlantic Spain proxy evidence provides evidence that there was increased precipitation and flooding from 960-790 cal yr BP (Benito *et al*., 2008; Figure 5.12 E) and 1000-800 cal yr BP (Thorndycraft and Benito, 2006). Documentary evidence showed a later wet period at 800-660 cal yr BP (Benito *et al*., 1996), while a peat bog mercury reconstruction of precipitation provides some evidence for an increase at 620-490 cal yr BP (Martínez-Cortizas *et al*., 1999), both of which fall within a broader period with high river flow suggested from 800-500 cal yr BP (Bernardez *et al*., 2008; Figure 5.12 D). These increases in precipitation are around the time the Pedrido sand influx results show three peaks, therefore the precipitation and storm

reconstructions suggest that low intensity storms may have occurred during the MCA.

The Pedrido reconstruction of storminess during the LIA is unclear, as the sand influx (which, as an expression of the sand receipt per year, takes into account changes in peat accumulation rate) indicates low storminess, but the IR and sand weight results (which do not account for changes in accumulation rate) show higher sand quantities. This means that the sand accumulation during the LIA may have been the result of slower peat formation rather than greater storminess. Regional evidence indicates that the LIA had high storminess: over-washed sand from Traba Lagoon may record a period of intense storminess between 270-190 cal yr BP (*1680-1760 A.D.*) (Bao *et al.*, 2007; Figure 5.12 I), which was the only over-washed sand in this record since 2900 cal yr BP. From a marine record however a weak hydrological regime has been suggested at 500-0 cal yr BP, which can be caused by persistent northerly winds (Martins *et al.*, 2007; Figure 5.12 G) and the Bay of Biscay reconstruction implies there was a small increase in storminess of lower magnitude than the high storminess before 1800 cal yr BP (Motjahid *et al.*, 2012, Figure 5.12 C). The Traba Lagoon over-wash deposits may show that a small number of intense storms occurred, while the marine records are more likely to capture the longer trends in climate, and these appear to show lower storminess. There is therefore evidence in support of the LIA having had high intensity but low frequency storms.

However precipitation proxies do not support this, instead indicating that the LIA was wet. There is evidence that the early part of the LIA had high precipitation, as shown by evidence that suggests increased flooding in Spain at 520-290 cal yr BP (Benito *et al.*, 2008; Figure 5.12 E) and 500-250 cal yr BP (Thorndycraft and Benito, 2006) and increased flooding in northern Portugal at 550-480 cal yr BP (Abrantes *et al.*, 2011). Other evidence supports that the whole LIA had high precipitation: documentary evidence from across Spain shows flooding from 450-100 cal yr BP (Benito *et al.*, 1996; Figure 5.12 E) and increased flooding of the river Douro (northern Portugal) from 550-50 cal yr BP (Martins *et al.*, 2012; Figure 5.12 G), while lake levels were higher in the northeast Iberian Peninsula between 570-100 cal yr BP (Scussolini *et al.*, 2011). Flooding occurs in Europe during periods with a succession of low pressure

systems (Benito *et al*., 2008) suggesting there was a high frequency of storms, however deforestation and afforestation can also increase or reduce flooding respectively (López -Moreno *et al*., 2006). Furthermore in central Spain flooding of the Tagus river has been linked to human activities over the last 1000 years (Vis *et al*., 2010), so there may be other explanations. Therefore, taking into account both the storminess and precipitation evidence from Galicia, it appears the LIA may have had an increase in the occurrence of low pressure systems, some of which were intense, which would in fact indicate that the sand weight and IR results are more reliable than the sand influx results. It is possible that the adjustment for changes in the accumulation rate obscured the increased sand deposition during the LIA.

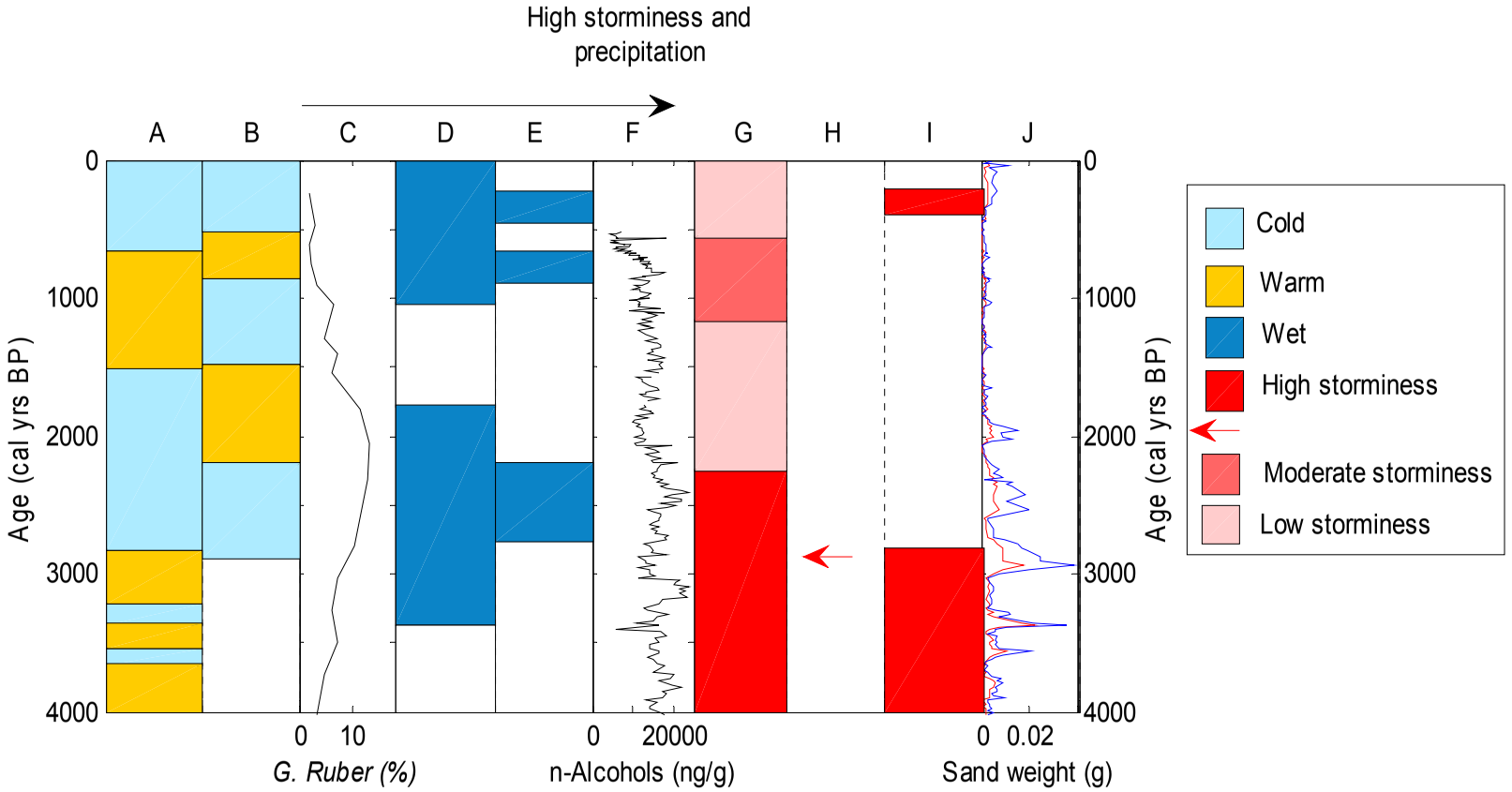

Figure 5.12: Summary diagram of reconstructed climate changes in Spain with results from this research. Reconstructions as in Figure 5.1. with the addition of J: sand weight results from Pedrido Bog, Galicia (*this research*).

5.5.5. Cycles in the Pedrido Record

The spectral analysis of the Pedrido Bog sand influx reconstruction (Figures 5.7 and 5.8) showed that between c.4000 and 1800 cal yr BP there was high variability, with cycles of c.510 and 220 years. After 1800 cal yr BP the cyclicity was reduced. A strong solar influence on storminess is supported by the cycles identified in the Pedrido reconstruction.

The longer cycle of 2050 years approaches the limits of cycles that can be identified in a reconstruction spanning 4500 years, as shown by it being considered insignificant in the wavelet analysis. This cycle had a range from 1820 to 2325 years, so it may have resulted from solar forcing, as a recognised solar cycle has a periodicity of 2100 years (Damon and Sonnett, 1991).

The cycle of 512 years in the Pedrido reconstruction also resembles a solar cycle of 512 years (Stuiver and Braziunas, 1993; Wanner *et al*., 2008; Vonmoos *et al*., 2006). This cycle has been identified in proxies of atmospheric circulation and solar irradiance prior to the Holocene (Mayewski *et al*., 1997) and linked with instabilities in the North Atlantic thermohaline circulation (Stuiver and Braziunas, 1993). A similar length cycle of c.550 years has also been identified in a proxy for North Atlantic Deep Water formation (Chapman and Shackleton, 2000). This supports a solar forcing on storminess, as well as a possible link with ocean circulation.

A solar cycle of ~220 years (the Suess or De Vries cycle) has been identified, and shown to have been particularly dominant during the period 3000-2000 cal yr BP (Stuiver and Braziunas, 1989; Knudsen *et al*., 2009; Wanner *et al*., 2008). The Suess 220-year cycle amplification has been identified between 3500-1800 cal yr BP in monsoon records from China and Turkey (Knudsen *et al*., 2012) and in proxy reconstructions of the ITCZ position from the Gulf of Mexico (Poore *et al*., 2003; 2004), which indicates that the solar variability was influencing circulation patterns globally. In the Pedrido Bog reconstruction this cycle is significant between 3800 and 2800 cal yr BP, and present but weaker until c.1800 cal yr BP (Figure 5.8). Therefore there is some similarity in the timings of amplified solar forcing and higher storminess in Spain.

The cycles identified here support that there is a solar influence on storminess, however there are many identified solar cycles, such as 1050-830, 350 and 300 year cycles (Stuiver and Braziunas, 1989; 1993) that are not present in the Pedrido reconstruction. Steinhilber *et al.* (2012) has suggested, using wavelet analysis, that since 4000 cal yr BP the largest magnitude solar variability was the 220 year Suess cycle between 3000-2000 cal yr BP. After this time a weaker cycle of c.130 years is thought to have occurred (Steinhilber *et al*., 2012). Therefore the presence of the 220-year cycle in the Pedrido reconstruction may have been the result of the strong amplitude of this solar cycle, as other solar cycles may not been strong enough forcings to alter the circulation patterns. The forcings on storminess will be discussed further in Chapter 6.

5.6. Conclusion

Late Holocene storminess in northwest Spain has been reconstructed by analysis of the sand content variations in Pedrido Bog, Galicia, which is a region sensitive to the NAO during the instrumental period. Some of the increases in storminess coincide with decreases in tree pollen: it is speculated that abrupt vegetation reductions are the result of periods with colder temperatures, based on comparisons with temperature proxies from northern Spain. These abrupt cold events and increases in storminess, may have slowed the recovery of vegetation following human disturbance and caused changes in land use that further destabilised the environment, providing greater sediment sources for aeolian erosion that enhanced the storminess signal in the reconstruction.

The 4500 year reconstruction indicates that the period from 4000-1800 cal yr BP had higher storminess in northwest Spain, with six peaks centred at 3900-3700, 3600-3500, 3400-3250, 3000-2700, 2600-2200, 2050-1850 and 400-0 cal yr BP. The broad period from 4000-1800 cal yr BP was a time when other reconstructions from the region indicate storminess and precipitation were increased. This period of higher storminess was a time with more frequent negative NAO events, indicating there was a southerly storm track position, while low storminess between 1800-400 cal yr BP supports that there was a positive NAO and a northerly storm track. Overall the reconstruction of Late Holocene storminess supports that there has been a consistent relationship between the NAO and storminess, at least over multi-centennial timescales. Cycles of 2050 and 510 years, and 220 years between 3800 and 1800 cal yr BP, indicate that solar variability could have a strong influence on storminess.

Chapter 6: The patterns and causes of European storminess during the Late Holocene

6.1. Introduction

In the previous results chapters the focus of the discussions was on the storminess reconstructions in relation to regional environmental and climatic changes. In this discussion chapter the reconstructions of storminess from the Outer Hebrides and Spain will be compared and contrasted with storminess reconstructions from across Europe, to investigate European-wide changes in the storm track and storm intensity over the Late Holocene. In sections 6.2, 6.3 and 6.4 of this chapter the reconstructions will be used to investigate the patterns of storminess in north and south Europe and how these relate to storm track changes, the NAO and climate deteriorations. As the previous results chapters were structured as papers they included short discussions on the causes of storminess. This will be investigated more fully in section 6.5, as here the results from each site can be combined. In section 6.6 the storminess reconstructions will be compared with the results from a coupled ocean-atmosphere model simulation forced by solar and volcanic variability and future changes in storminess will be discussed. Finally the projects limitations and suggested future research will be discussed in section 6.7.

6.2. Comparison of the storminess reconstructions

In this section the four storminess reconstructions from the Outer Hebrides and Galicia are compared (Figure 6.1), which addresses the first research question on the temporal patterns of storminess in northern and southern Europe. The results indicate that storminess was high in southern Europe between 4000-1800 cal yr BP, at the same time as storminess was low in northern Europe. It is notable however that between 3000 and 1800 cal yr BP the prominent increases in storminess shown by the Spanish Bog reconstruction coincide with smaller increases in storminess in the Hill Top Bog reconstruction. This therefore indicates simultaneous European-wide periods of increased storminess, but with the largest magnitude storms in southern Europe. After 1800 cal yr BP storminess decreased in the Pedrido Bog

reconstruction and after 1500 cal yr BP began increasing in the reconstructions from the Outer Hebrides bogs. Storminess peaked in the northern European reconstructions during the last 1000 cal yr BP, although inter-site differences mean that the timing of this maximum storminess is unclear. After 500 cal yr BP the Loch Hosta and Hill Top Bog reconstructions in particular support that there was increased storminess (Figure 6.1); and this increase is also possibly seen in the Struban Bog reconstruction within the age errors. Overall the comparison between the reconstructions indicates that there was high storminess in southern Europe between 4000 and 1800 cal yr BP, followed by an abrupt decrease, after which storminess appears to have gradually increased in northern Europe after 1500 cal yr BP.

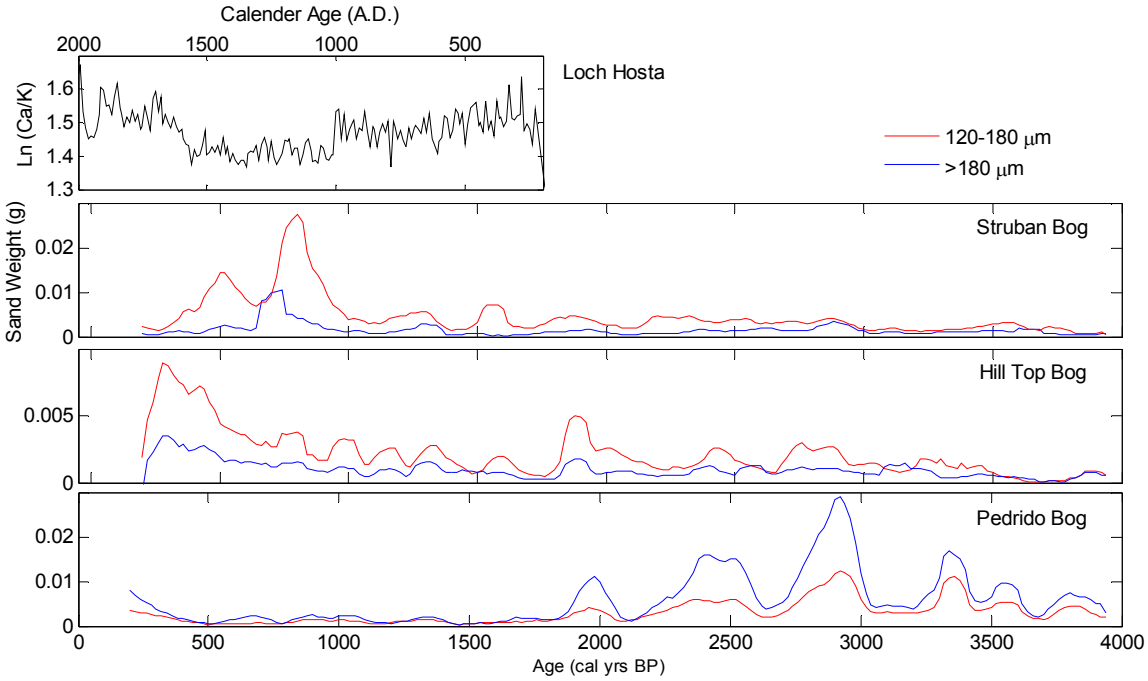

Figure 6.1: Comparison between the smoothed storminess reconstructions from northern Europe (Loch Hosta, Struban Bog and Hill Top Bog) and southern Europe (Pedrido Bog). Note: the Hill Top Bog reconstruction is on a different scale to the Pedrido Bog and Struban Bog reconstructions, due to low sand content.

The second research question sought to infer storm track changes by comparison between the reconstructions from northern and southern Europe. To do this a north-south storm track index has been created. To this end the Hill Top Bog, Struban Bog and Pedrido Bog reconstructions were first re-sampled to 20-year resolutions. This was done by interpolating the data to high (annual) resolutions, before smoothing to 20 years (so that each data point is the average of that 20-year period) and then down-sampling at the 20-year resolution. The results were smoothed to 100-years to remove decadal changes, which are more likely to be caused by intra-bog factors (as described in section 4.5.1.). The reconstructions were then normalised to units of standard deviation by subtracting the reconstructions mean value from each data point and then dividing by the standard deviation. To create the north-south index the average values of the two Outer Hebrides bog reconstructions was found for each 20-year period. The Pedrido Bog results were then subtracted from the averaged Outer Hebrides results to give the north-south index of storminess. Low and high values are used to infer when the storm track was across southern and northern Europe respectively. This index is shown in Figure 6.2. It supports that there was a transition from a southerly to northerly storm track starting at 3300 cal yr BP until approximately 900 cal yr BP.

Spectral analysis was carried out after detrending the index. As the data was evenly spaced, the Welch method of spectral analysis was carried out in Matlab using code from Trauth (2006), which is based on the original method of Welch (1967). The 95th percentile significance was calculated by 5000 iterations of the Welch method analysis on the randomly sorted data, before the 95th percentile of these results was calculated (Jones *et al.,* 2013). This analysis showed that there was a significant cycle of 394 years (Figure 6.3). Therefore cyclic changes in storminess appear to have persisted when the storm track was both in a southerly and northerly position, and may represent periods of increased storm intensity superimposed on broader storm track changes.

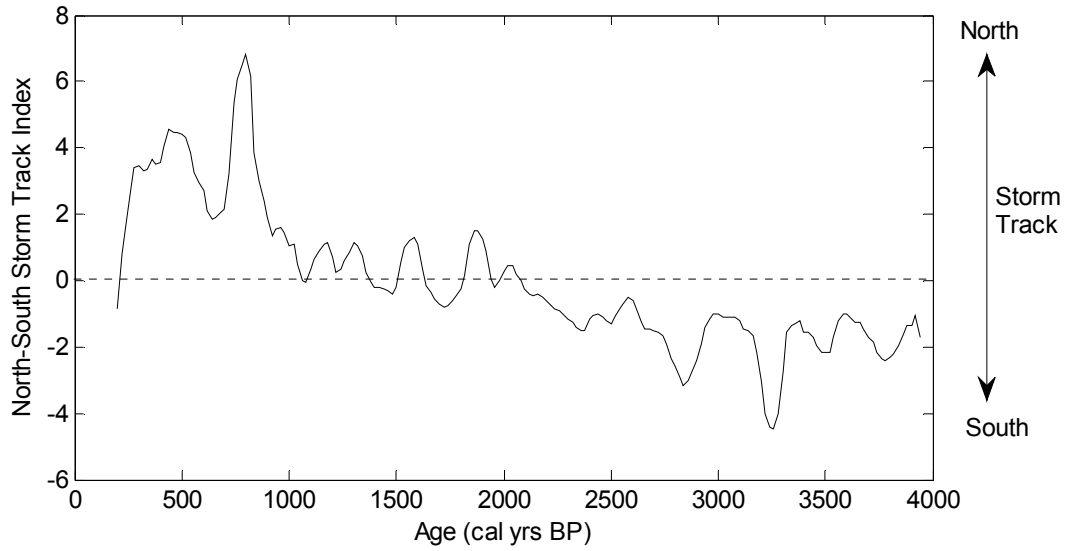

Figure 6.2: North-South Index of European storminess based on the difference between the averaged Outer Hebrides bog storminess reconstructions and the Galicia storminess reconstruction.

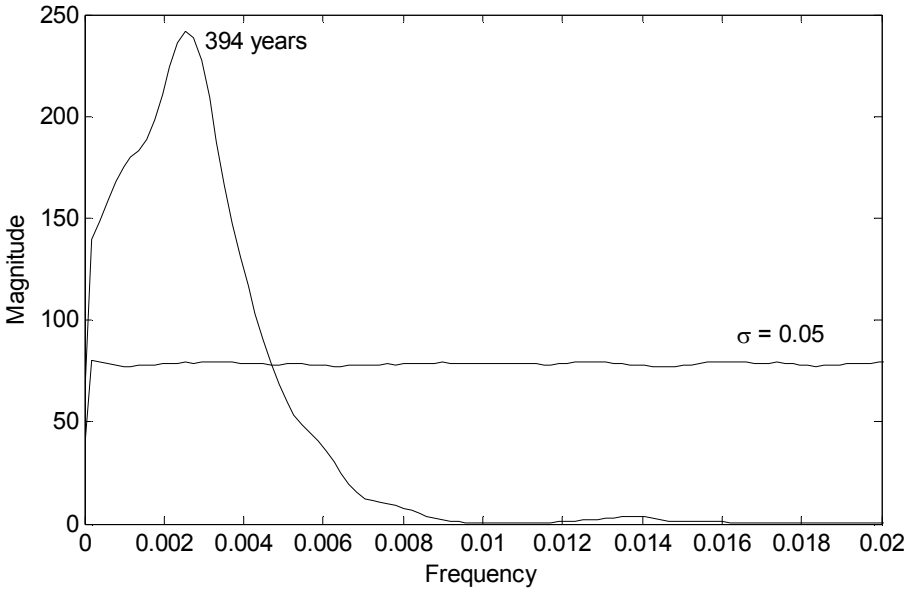

Figure 6.3: Welch method spectral analysis of the north-south index of storminess, including the 95% significance line.

6.3. Comparison with storm track reconstructions

In this section the results of this project are compared with reconstructions of storminess and storm track shifts from across Europe and the North Atlantic (Figure 6.4). The long-term storminess and storm track trends are compared with reconstructions of storm track changes in Europe (Figure 6.5). A southerly storm track around 4000-1800 cal yr BP has been suggested by a number of reconstructions. In northern Europe, Atlantic Water Inflow into the Norwegian Sea was low at this time, which is caused by reduced wind stress during negative NAO conditions (Giraudeau *et al*., 2010; Nilsen *et al*., 2003). The north-south index of westerlies from Norway, based on a transect of glacier precipitation reconstructions, indicates that between c.3500-2500 cal yr BP northern Norway had drier conditions than southern Norway and therefore that there was a southerly storm track (Bakke *et al*., 2008). Northwest of Iceland ocean proxies indicate an increasingly southward position of the polar front and decreasing storminess towards c.2000 cal yr BP (Andresen *et al*., 2005). High flooding in the southern Alps compared to the northern Alps between 4200-2400 cal yr BP has been used to infer that in this time the storm track was in a more southerly position (Wirth *et al*., 2013). In addition the expansions of glaciers in the Alps, and conversely the retreat of glaciers in Norway due to reduced precipitation (Nesje *et al*.,2001; Bakke *et al*., 2005; Schimmelpfennig *et al*., 2012; Ivy-Ochs *et al*., 2009) are indicative of a southerly storm track and outbreaks of cold polar air across Europe at this time. These reconstructions therefore point towards the storm track being across southern Europe between 4000 and 1800 cal yr BP.

However various studies in *northern* Europe have found evidence indicating high storminess at this time. In Britain dated alluvial units suggest that the period from 3940-1940 cal yr BP was a time with increased flooding (Macklin and Lewin, 2003). More detailed, subsequent research has proposed flooding peaks across Britain at c.3540, 2730 and 2280 cal yr BP (Johnstone *et al.,* 2006). In Ireland dune instability attributed to heightened storminess occurred at 3100-2400 cal yr BP (Wilson *et al*., 2004). In Sweden two reconstructions have suggested storminess and precipitation fluctuated between 2800-2200 cal yr BP (De Jong *et al*., 2006; Figure 6.5 C) and between c.3700-1500 cal yr BP (Snowball *et al*., 1999). Finally high latitude

reconstructions from the northern North Atlantic have indicated that there was a warm but unstable climate at 3800-2000 yrs BP (Moros *et al*., 2004). These reconstructions support that there was increased variability of storminess in northern Europe between approximately 4000-1800 cal yr BP, contradicting the suggestion that the storm track was positioned further south.

There is a body of evidence to suggest that instead of the storm track shifting south, meridional circulation patterns (a more meandering, weak polar vortex) may have caused greater climate variability between 3800-1800 cal yr BP. More meridional circulation of the atmosphere at this time has been suggested as a cause of the high sea salt and dust influx in Greenland (measured by the GISP2 reconstruction) between 3100-2400 cal yr BP (O'Brien *et al*., 1995) and the warmer and unstable conditions in the high latitudes of the North Atlantic (Moros *et al*., 2004). This can also explain the variable climate in northern Europe described above. The meridional circulation patterns would also have caused lower temperatures in the mid-latitudes due to the penetration of polar air further south. Few proxies exist to capture winter temperature, however an increase in minerogenic material to a Finnish lake between 4000 and 2000 cal yr BP has been interpreted as reflecting colder or longer winters (Ojalla *et al*., 2008), consistent with meridional circulation patterns. A similar situation may have occurred at the transition from the MCA to the LIA: reconstructed increased variability in winter temperatures in the Alps has been suggested as resulting from reduced zonal airflow that allowed other climate drivers such as the Siberian High pressure to dominate (De Jong *et al*., 2013). Therefore there is some evidence to suggest that the 4000-1800 cal yr BP period with high storminess in southern Europe was the result of meridional circulation patterns, as supported by circulation and temperature proxies elsewhere in Europe and the North Atlantic region.

After 1800 cal yr BP the storminess reconstructions indicate that there was a gradual northward shift in the storm track. This is supported by reconstructions from northern Europe that also suggest increasing storminess or precipitation. As shown in Figure 6.5, there is thought to have been increased flooding in the northern Alps (Wirth *et al*., 2013), higher reconstructed wind-driven Atlantic Water Inflow into the Norwegian Sea (Giraudeau *et al*., 2010), a more northerly storm track across Norway (Bakke *et al*., 2008), and increased

storminess (and a northward shifted polar front) northwest of Iceland (Andresen *et al*., 2005). In Sweden a record has suggested that storms and winter precipitation became more variable *after* 2500 cal yr BP (De Jong *et al*., 2009). Others have indicated high precipitation from 2000 cal yr BP onwards, thought to be the result of positive NAO conditions and stronger westerly winds (Andersson *et al*., 2010; Jonsson *et al*., 2010). Dated alluvial flooding units in the upland catchments of northern Britain provide evidence for increased flood events particularly between 2750 to 550 cal yr BP (Johnstone *et al*., 2006). These fit with the suggestion that the circumpolar vortex became more zonal after c.2500 cal yr BP (Bakke *et al*., 2008), meaning it was stronger, less meandering and shifted northwards (Walter and Graf, 2005; Barry and Chorley, 2010). Therefore after 1800 cal yr BP many reconstructions support that there was an increase in storminess in northern Europe, possibly due to zonal circulation patterns.

Other reconstructions have suggested different patterns of storminess during the Late Holocene, with multi-centennial cyclical variations rather than a long-term storm track shift. Cycles of 1500-1700 years have been identified in storminess reconstructions (Fletcher *et al*., 2013; Debret *et al*., 2007; O'Brien *et al*., 1995; Jackson *et al*., 2005; Pena *et al*., 2010; Turney *et al*., 2005; Sorrel *et al*., 2012; Yu, 2003). It is possible that the significant cycles of 1450 and 1330 years identified in the Struban Bog and Hill Top Bog reconstructions respectively correspond to these cycles. The c.390 year cycle present in the north-south storminess index, described in section 6.2, has also been identified as climate shifts of 300-400 years in Sweden (De Jong *et al*., 2007). Similarly cycles of 180, 220, 480 and 940 years have been identified in an NAO- and storm- sensitive Baltic Sea sea-level reconstruction spanning the mid-Holocene (Yu, 2003), and these resemble the identified c.230 year cycle (Loch Hosta and Pedrido Bog), 510 year cycle (Pedrido Bog) and c.900 year cycle (Loch Hosta, Pedrido Bog, Hill Top Bog) from this research. These appear to be cycles characteristic of storminess variability, although given the few reconstructions that have used spectral analysis, these are not widely recognised.

A compilation of northern European storm reconstructions proposed that in the Late Holocene widespread storminess occurred at 4500-3950, 3300-2400, 1900-1050 and 600-250 cal yr BP (Sorrel *et al*., 2012; Figure 6.5). The

Outer Hebrides peat bog storminess reconstructions do not show these prominent changes in storminess, aside from the period 600-250 cal yr BP, however the Loch Hosta reconstruction spanning the last 1800 years indicated increased storminess at 1750-900 and 400-50 cal yr BP, which support the timing of the most recent Sorrel *et al.* (2012) storm events. There is therefore a contradiction between reconstructions, with some suggesting that there were multi-centennial variations and others long-term trends. It is possible that each reconstruction is sensitive to different aspects of climate, such as extreme events or long-term climate. As the Outer Hebrides and Galicia are particularly sensitive to the NAO in the instrumental period (Andrade *et al*., 2008), these sites may have been dominated by this, while sites elsewhere may have been influenced by other factors.

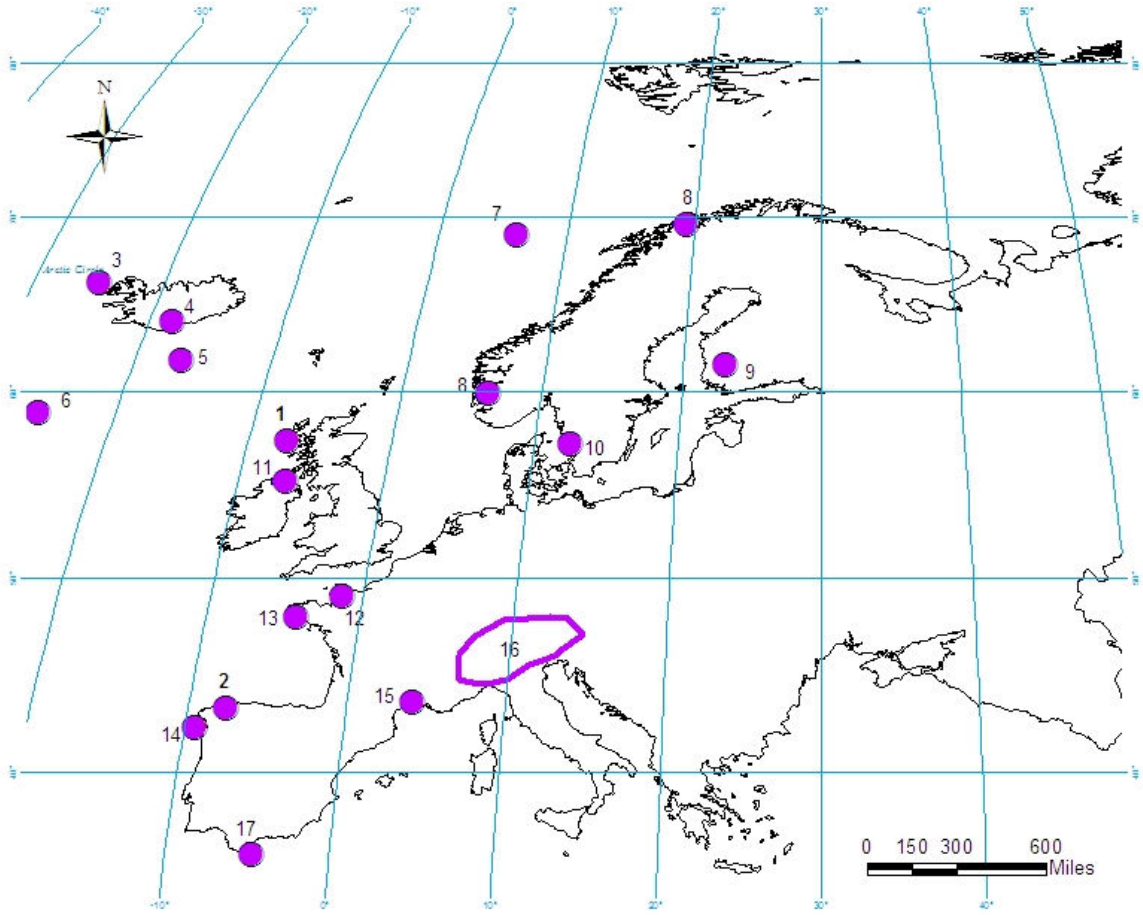

Site List

1: Outer Hebrides sites (*this study*)
2: Galician site (*this study*)
3: Iceland (Andresen *et al*., 2005)
4: Iceland (Jackson *et al*., 2004)
5: Subpolar Gyre, core RAPiD-12-1K (Thornalley *et al*., 2009)
6: Mid-Atlantic, core LO09-14 (Moros *et al*., 2004)
7: Norwegian Sea (Giraudeau *et al*., 2010)
8: Norway (Bakke *et al*., 2008)
9: Finland (Ojala *et al*., 2008)
10: Sweden (De Jong *et al*., 2006; 2007; 2009)
11: Ireland (Wilson *et al*., 2004)
12: Seine Estuary (basis of compilation of reconstructions by Sorrel *et al*., 2012)
13: Northern France (Van Vliet-Lanoë *et al*., 2014)
14: Galicia (Pena *et al*., 2010)
15: Southern France (Sabatier *et al*., 2011)
16: Alps (Wirth *et al*., 2013)
17: Western Mediterranean (Fletcher *et al*., 2012)

Figure 6.4: Map of the locations from which key storminess reconstructions have been created, as discussed in section 6.3.

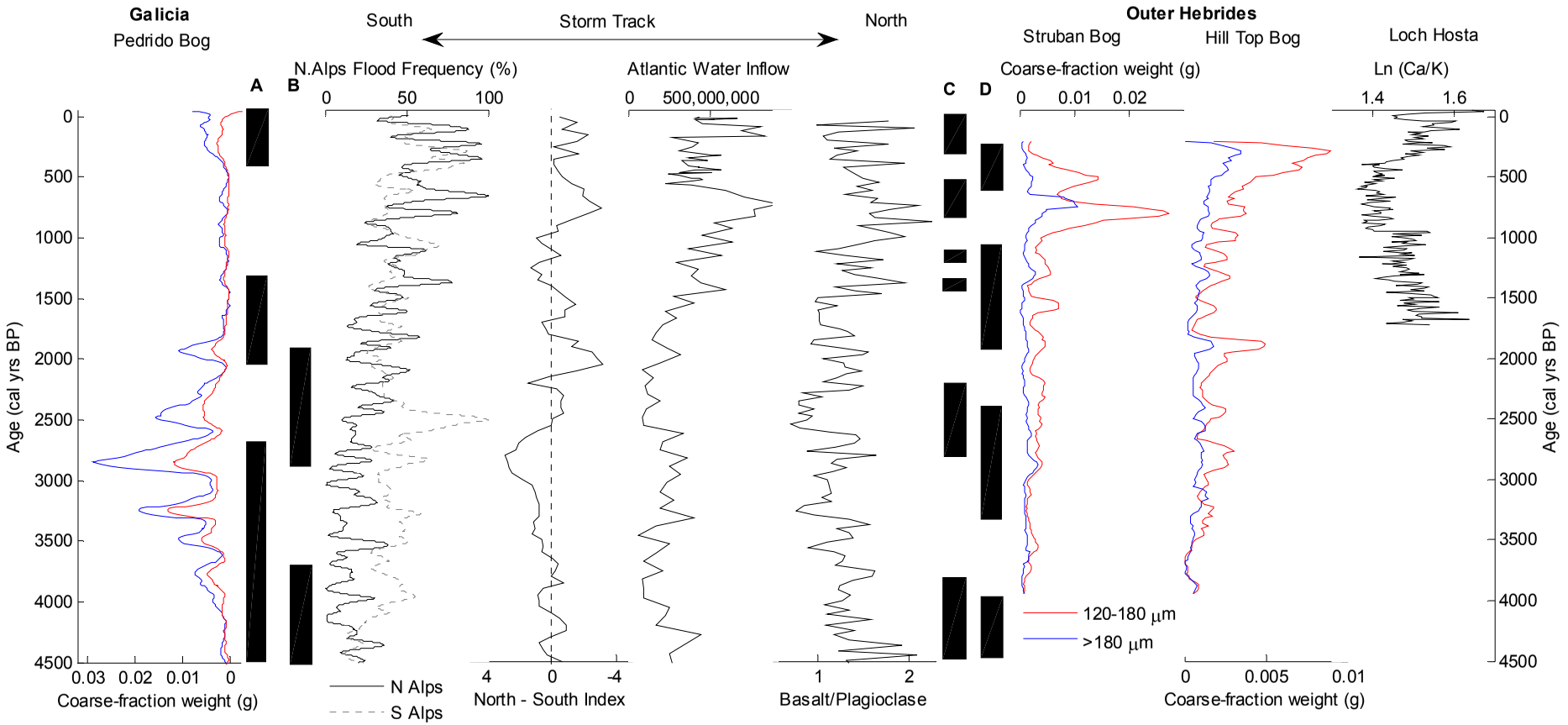

Figure 6.5: Comparison of storminess and storm track reconstructions. From left: Pedrido Bog reconstruction, A: lagoonal storminess reconstruction based on overwash deposits in a lagoon on French Mediterranean coast (Sabatier *et al.*, 2011), B: southerly storm track position based on Mediterranean forest pollen concentrations (Fletcher *et al.*, 2012), flood frequency from the northern and southern Alps based on combined flood proxies from multiple lakes (Wirth *et al.*, 2013), North-South Index of westerly airflow based on glacier mass balance reconstructions from Norway (Bakke *et al.*, 2008), reconstructed Atlantic Water Inflow into the Nordic Sea, with high inflow driven by a northerly storm track (Giraudeau *et al.*, 2010), marine storminess reconstruction from northwest Iceland, based on the basalt/plagioclase ratio, as storm-driven bottom currents transport more basaltic sediment resulting in high ratios (Andreson *et al.*, 2005), C: peat bog storminess reconstruction from the Halland coast, Sweden, based on Aeolain Sediment Influx measurements (De Jong *et al.*, 2006), D: compiled periods of high storminess in northern Europe, based primarily on sediments containing storm deposits from the Seine and Mont-St-Michel estuaries (Sorrel *et al.*, 2012), Struban Bog reconstruction, Hill Top Bog reconstruction and Loch Hosta reconstruction.

Multi-centennial variations in storm track position though the Holocene have also been suggested by a compilation of reconstructions from along a transect of western Europe (Fletcher *et al*., 2012; Figure 6.5 B). In this compilation reconstructed declines in forest vegetation in the western Mediterranean, caused by reduced precipitation, are contrasted with a transect of reconstructions of wind, precipitation and ocean circulation (Fletcher *et al*., 2012). The Mediterranean record shows higher forest pollen sums and therefore suggests higher precipitation at around 4500-3800 cal yr BP and around 3000-1800 cal yr BP, indicating the storm track was southwards during these times (Fletcher *et al*., 2012). High cyclonic activity is not indicated in the Pedrido record during the 4500-3800 cal yr BP interval, but does coincide with the period 3000-1800 cal yr BP. For the latter period Fletcher *et al*. (2012) showed that between 3000-1800 cal yr BP Icelandic winds are thought to have been weaker (Jackson *et al*., 2005) and there is evidence of increased erosion in the Middle Atlas Mountains, Morocco (Lamb *et al*., 1999). Additionally the period 3000-1800 cal yr BP is considered as a period with reduced stratification of the North Atlantic Current south of Iceland, indicating reduced subpolar gyre circulation that occurs when wind stress decreases during a negative NAO (Fletcher *et al*., 2012; Thornalley *et al*., 2009; Curry and McCartney, 2001). These support the findings of this research that at 3000-1800 cal yr BP the storm track was further south. On the other hand the inferred storminess shown by the Pedrido reconstruction increases at 3800 cal yr BP, around 500 years earlier than the precipitation increase suggested by the Fletcher *et al*. (2012) reconstruction. Furthermore during this time there were indications for a northerly storm track, as indicated by high storminess in Iceland (Jackson *et al*., 2005), a strong subpolar gyre (Thornalley *et al*., 2009) and reduced erosion in Morocco (Lamb *et al*., 1999; Fletcher *et al*. 2012). The high Galician storminess may have been caused by less pronounced southward excursions of the storm track, influencing northwest Spain but not the Mediterranean. Overall the Fletcher *et al*. (2012) reconstruction supports that the storm track was further south between 3000-1800 cal yr BP, but shows differences between 4500-3000 cal yr BP.

In summary the storminess reconstructions and north-south index formed as part of this research compare favourably with a number of storm track

reconstructions (Figure 6.5). It is suggested that these capture a shift from a southerly to northerly storm track around 1800 cal yr BP, which it is suggested was due to a transition from meridional to zonal circulation patterns. The storminess reconstructions of this research support pronounced long-term trends, rather than multi-centennial variations in storminess. The reason for this is unclear, but may be related to the high sensitivity of Galicia and the Outer Hebrides to the Atlantic climate and NAO, with other factors influencing storminess elsewhere.

6.4. Comparison with North Atlantic Oscillation reconstructions

The Late Holocene storminess reconstructions and the north-south storm track index will in this section be compared with reconstructions of the NAO (Figure 6.6). The weather of the Outer Hebrides and Galicia is highly influenced by the NAO during the instrumental period (e.g. Andrade *et al*., 2008), therefore comparison between the Late Holocene reconstructions of the NAO and storminess allow the long term NAO-storm relationship to be explored. This section addresses the third research question concerning the nature of the NAO-storminess relationship.

The reconstructed NAO and storminess indicated similar long-term trends. The NAO reconstruction by Olsen *et al.* (2012) has suggested that the period from 2000-550 cal yr BP had a predominantly positive NAO, while the period 4500-2000 cal yr BP had mostly negative NAO conditions (Olsen *et al*., 2012). Additionally opposite changes in sea surface temperatures for the north-east Atlantic and western subtropical Atlantic have been used to suggest a weakening of the NAO through the Early to Late Holocene (from positive to negative NAO) with a reversal at 2000 cal yr BP back to positive NAO conditions (Rimbu *et al*., 2003; Wanner *et al*., 2008). The high storminess in the Pedrido reconstruction between 4500-1800 cal yr BP supports the hypothesis that there was a prolonged period with low NAO conditions at this time, which directed the storm track across southern Europe. After 1500 cal yr BP storminess in the Outer Hebrides gradually increased, which corresponds to the period when the most positive NAO conditions are reconstructed, although the increase in storminess occurs gradually whereas the NAO transition is more

abrupt. A strong NAO influence is supported by the significant correlations between the NAO and storminess reconstructions (when linearly detrended), as shown in Table 6.1. Therefore the long-term trends proposed by the NAO and storm reconstructions may demonstrate that there have been persistent and large-magnitude shifts in atmospheric circulation through the Late Holocene and support the idea that there has been a consistent NAO-storminess relationship.

Table 6.1: Correlation between the North Atlantic Oscillation reconstruction (Olsen *et al*., 2012) and the storminess reconstructions. Bold correlations are significant above the 95% level. Correlations were carried out first on linearly detrended data and following this on data which had been detrended using a polynomial fit. This latter process removed the millenial trends in the data allowing comparison of the high frequency variability.

Site	Correlation (R) when linearly detrended	Correlation when nonlinearly detrended (R)	n
Hill Top Bog	**0.214**	**-0.373**	180
Struban Bog	**0.457**	**-0.154**	180
Pedrido Bog	**-0.528**	**-0.299**	209

When considering the NAO-storminess relationship at multi-decadal and centennial timescales the results are more varied. There is a similarity between some of the negative NAO events and increased storminess in Pedrido Bog between 3500 and 1800 cal yr BP, particularly in the timing of peaks c.2800 and 2400 cal yr BP (Figure 6.6). This supports the suggestion that negative NAO anomalies caused the storm track to cross southern Europe. However there is an offset between the timing of other negative NAO events and increased storminess, such as the storm peak at c.1900 cal yr BP that follows a negative NAO event c.2100 cal yr BP. The reason for this is unclear, it could potentially be a result of errors in the age-depth model of either reconstruction, or could be

the result of a time lag, for example storminess could increase during the transitions into periods of negative NAO. Nevertheless there is a significant negative correlation between the nonlinearly detrended NAO and Pedrido storminess reconstruction (Table 6.1), indicating that storminess increased in southern Europe during times of negative NAO at centennial timescales.

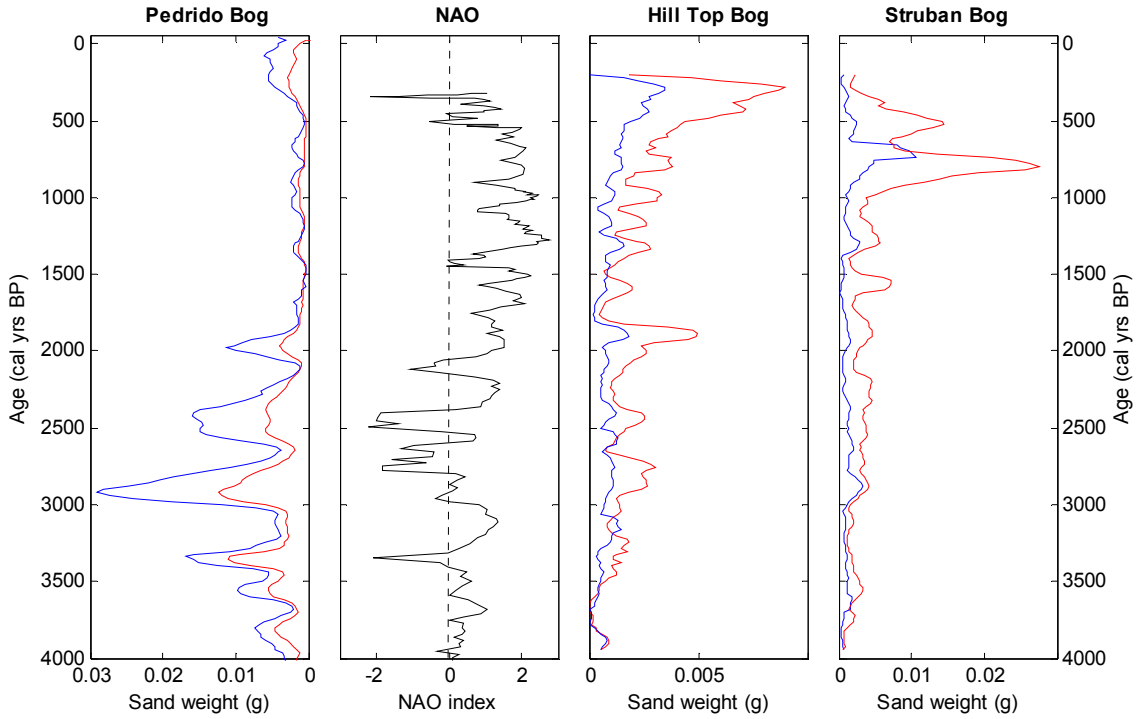

Figure 6.6: Comparison between the NAO reconstruction by Olsen *et al*., (2012) with the peat bog reconstructions of storminess from Pedrido Bog in Spain and Hill Top Bog and Struban Bog in the Outer Hebrides. Red lines are the 120-180 µm sand fraction and blue lines the >180 µm sand fraction.

The period after 1800 cal yr BP when the NAO was more positive was a period of increasing storminess in the Outer Hebrides, however the results indicate that at times there has been an inconsistent NAO-storm relationship (Figure 6.6). The centennial peaks observed in both storminess reconstructions after 1500 cal yr BP reflect some reconstructed positive NAO anomalies, for example at 1000 cal yrs BP, while other peaks, such as at 500 cal yrs BP correspond to negative NAO conditions. Likewise before 1800 cal yr BP the Hill Top Bog reconstruction in particular indicates that there were small increases in storminess at times of negative NAO. The nonlinearly detrended NAO and

storminess reconstructions from the Outer Hebrides (Table 6.1) also have a negative correlation, which suggests that, as in southern Europe, negative NAO events are associated with increased storminess. This contradiction between high northern European storminess and negative NAO conditions has been identified previously for the LIA period and suggested as being the result of intermittent, intense and rare storms during periods with frequent negative NAO anomalies (Trouet *et al*., 2012; Raible *et al*., 2007). Therefore in northern Europe increases in storminess appear to have been linked with negative NAO events through the Late Holocene, although the magnitude of the LIA storminess peak exceeds those earlier in the Late Holocene. Overall the long-term storminess trend supports that the NAO-storminess relationship through the Late Holocene was similar to that observed during the instrumental period. However, in both northern and southern Europe there is evidence that centennial increases in storminess are connected with negative NAO events.

An NAO influence on storminess can be inferred by identifying shared cycles in the storminess and NAO reconstructions, as summarised in Table 6.2. Struban Bog had no centennial cycles, however the Hill Top Bog reconstruction had cycles of 290 and 330 cal yr BP, which are similar to a ~300 year NAO cycle (Olsen *et al*., 2012), and indicates that this variation in storminess may have been driven by NAO variability. The Pedrido Bog and Loch Hosta reconstruction both show a cycle of c.220 years, which has not been identified as an NAO periodicity so may be showing storminess variability unrelated to the NAO. It is unclear whether the 390-year cycle observed in the north-south index is within the ~330 year band of variability seen in the NAO reconstruction, or if there is a different cause of what appears to be the dominant storminess cycle. As described in Chapter 3, high frequency cycles typical of the NAO were identified in the Loch Hosta reconstruction. For example, the cycle of 50-58 years was identified and is an NAO cycle (Glueck and Stockton, 2001; Luterbacher *et al*., 1999; Olsen *et al*., 2012; Wanner *et al*., 2001; Cook *et al*., 1998) and this was also identified by cross-spectral analysis between the Loch Hosta reconstruction and the Trouet *et al*. (2009) NAO reconstruction (Figure 3.10). Therefore the spectral analysis has shown that the NAO may have caused cycles of c.290-330 years observed in the peat bog reconstructions

(apart from Struban Bog) and decadal cycles identified in the Loch Hosta reconstruction.

Finally cross-spectral analysis between the NAO reconstruction (Olsen et al., 2012) and the peat bog reconstructions has been carried out to investigate the shared cycles, and therefore the NAO influence on storminess. The results were re-sampled to the 20 yr resolution and cross-spectral analysis was carried out using the same methods as described in section 2.8.3.. The results (Figure 6.7) show a cycle of 512 years is present in each of the Outer Hebrides bog reconstructions, which supports that the NAO influenced storminess at this periodicity. However a number of other cycles are identified which are not present in multiple sites, so it is possible that the sites are sensitive to storms from different directions (as discussed in Chapter 4), or different circulation patterns affecting north and south Europe.

In summary, the results indicate that during the Late Holocene there was a consistent NAO-storm relationship, with higher storminess in southern Europe when the NAO was generally low and higher storminess in northern Europe when the NAO was persistently positive. However when considering the centennial variations a different relationship is observed, with high storminess in both southern and northern Europe when there were periods with negative NAO. This pattern was present through the Late Holocene but was particularly evident during the LIA. These findings therefore suggest that storminess changes were caused by several interacting factors. The suggested long-term storm track shift from southern to northern Europe may have caused northern Europe to be increasingly influenced by high storminess during negative NAO events such as the LIA.

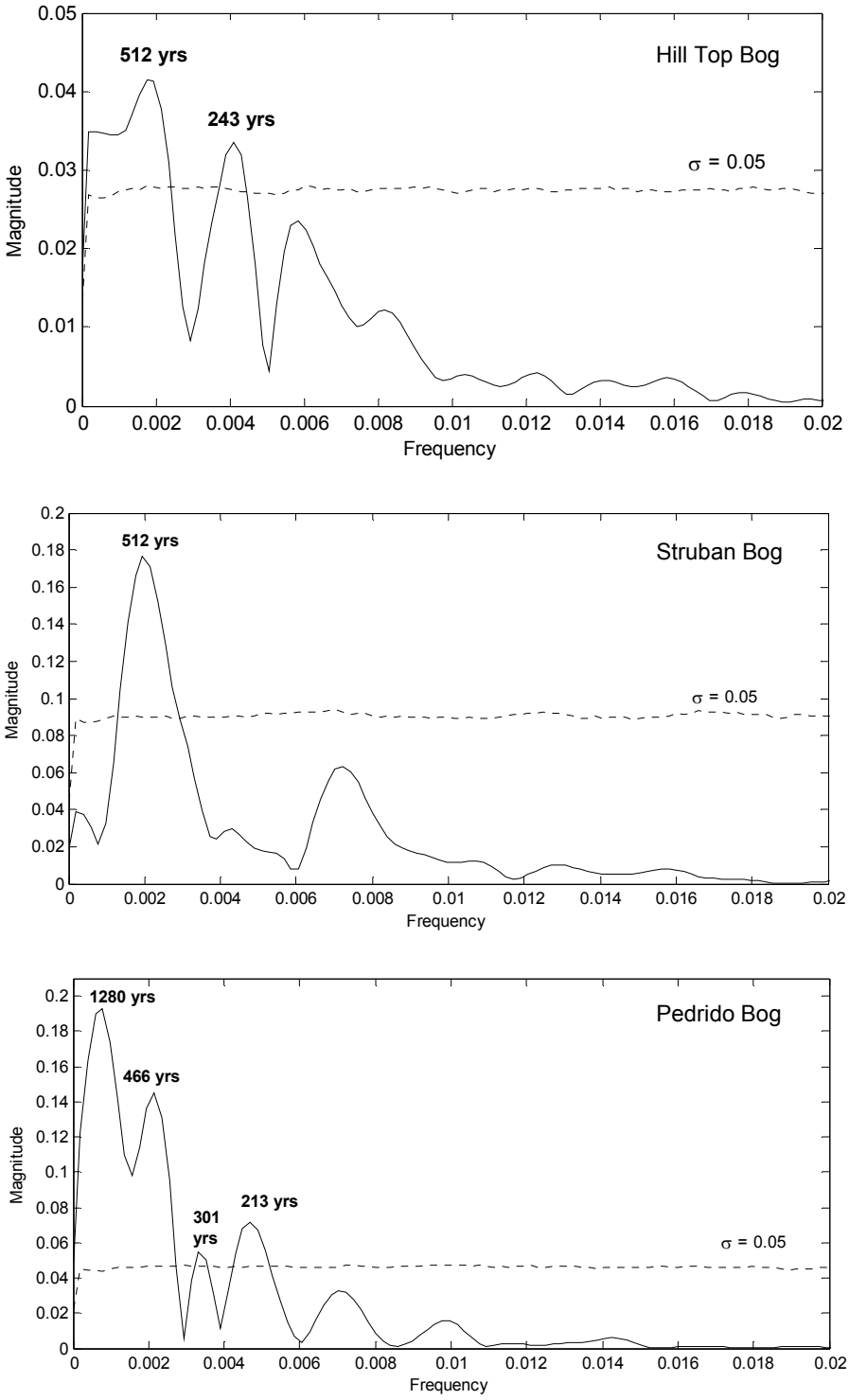

Figure 6.7: Cross-spectral analysis between the NAO reconstruction (Olsen *et al*., 2012) and the peat bog storminess reconstructions, using the method outlined in section 2.8.3. (Chatfield, 2004). The dashed lines indicate the 95% significance level.

Table 6.2: Summary of cycles present in the storminess reconstructions, the NAO and solar and oceanic forcings. The peak of the cycles are listed, with the range of frequencies spanned by this peak in brackets, where information was available. References are 1: Olsen *et al*., (2012) 2: Peristykh and Damon (2003), 3: Stuiver and Braziunas (1993), 4: Steinhilber *et al*., (2012), 5: Agnihotri *et al* (2002), 6: Bond *et al*., (1997), 7: Gray *et al*., (2004). 8: Chapman and Shackleton (2000) (Note: reference list is not exhaustive list).

Northern Europe			**Southern Europe**	**Forcings**		
Loch Hosta	*Struban Bog*	*Hill Top Bog*	*Pedrido Bog*	**NAO**	**Solar**	**Oceanic**
		2290 (2670-2040)	2050 (2325-1820)		c.2500[4], 2300[2]	
	1450 (1610-1230)	1330 (1460-1180)				1370 ± 500[6]
860	940 (1000-910)	890 (1000-870)			830-1050[3]	1000[8]
		730 (750-700)				
			510 (540-490)		512[3]	550[8]
		330			350[4]	
		290 (300-280)		~300[1]	300[4]	
250-200			220 years (*wavelet*)		220[3,4], 208[2]	
				~170[1]		
150-140					150[2]	
105-95					104[2]	60-100[7]
87-77					88[2], 77[5]	
58-50				50-70[1]	60[2], 53[5]	
20-16				~20 [1]	22[3], 11[3]	

6.5. Potential causes of variability in storminess, the storm track and the NAO

In this section comparisons between reconstructions and the results of the spectral analysis will be used to investigate the possible forcing mechanisms on storminess. This addresses the fourth research question on the causes of storminess variability. As the identification of cycles is used to infer the causes of storminess in the following sections, the cycles are summarised in Table 6.2. Forcings from orbital, solar, oceanic and volcanic changes will be assessed and discussed, before being synthesised into an explanation.

6.5.1. Orbital forcing

The shift at 1800 cal yr BP, from a southward storm track and frequently negative NAO, to a northward storm track and more positive NAO, could be the result of long-term changes in orbital forcing. This hypothesis has been invoked to explain latitudinal shifts in the storm track in the southern hemisphere, the position of the inter-tropical convergence zone and the Atlantic tropical cyclone track position during the Late Holocene (Haug *et al*., 2001; Gilli *et al*., 2005; Shulmeister *et al*., 2004; McCloskey and Knowles, 2009). In the northern hemisphere some palaeoclimate reconstructions, in particular precipitation reconstructions, have suggested that orbital forcing is a cause of the reconstructed long-term trends (Kirby *et al*., 2007; Czymzik *et al*., 2013; Moros *et al*., 2004; Kutzbach *et al*., 2014; Magny, 2013). As such in this section orbital forcing will be discussed as a potential cause of the inferred long-term storm track shift.

Orbital forcing changes the latitudinal insolation distribution, which has been described as one of the main factors influencing storm track position during the Holocene, as it controls the subtropical jet position and intensity, Hadley Cell circulation and the position of the subtropical highs (i.e. the Azores High) (Brayshaw *et al*., 2010; Flohn, 1984; McCloskey and Knowles, 2009). In the northern hemisphere from the Mid- to Late- Holocene December insolation increased steadily at 60ºN (Figure 6.8). As the poles receive no insolation during winter, increasing insolation in the mid-latitudes would steepen the

temperature gradient through the Late Holocene. Models forced by insolation have indicated that in the Mid-Holocene a lower insolation gradient caused weaker and northward shifted storm tracks (Rimbu *et al*., 2003; Brayshaw *et al*., 2010). Similarly modern observations of the influence of the latitudinal temperature gradient on the position of subtropical high pressures (i.e. Azores High) have shown that increasing gradients result in equatorward displacement of the subtropical high pressures (Flohn, 1984; McCloskey and Knowles, 2009). So by inference the increasingly steep insolation gradient during the Late Holocene may have caused stronger and southwards shifted storminess. However the high storminess in the Pedrido reconstruction at 3800-1800 cal yr BP and the suggested northward shift in the storm track through the Late Holocene is the reverse of the response indicated by these studies.

The patterns of storminess may also have been influenced by the general trends of increasing winter or decreasing summer insolation in the northern hemisphere, rather than the gradient, for example these have been suggested as causing precipitation variations in California and central Europe through the Holocene (Kirby *et al*., 2007; Czymzik *et al*., 2013; Magny, 2013). A model experiment has shown that periods with low winter insolation in the northern hemisphere have weaker and southward shifted mid-latitude westerlies (Kutzbach *et al*., 2014). Therefore the gradual increase in winter insolation through the Holocene would be expected to cause an increasingly northward-shifted storm track, which has been observed in this research. An insolation forcing behind the storm track transition is supported by Bakke *et al.* (2008), who suggested that the transition from reconstructed low to high precipitation in Norway from 4000-1500 cal yr BP was the result of increasing winter insolation. Therefore winter insolation changes may explain the long-term reconstructed northward storm track shift through the Late Holocene.

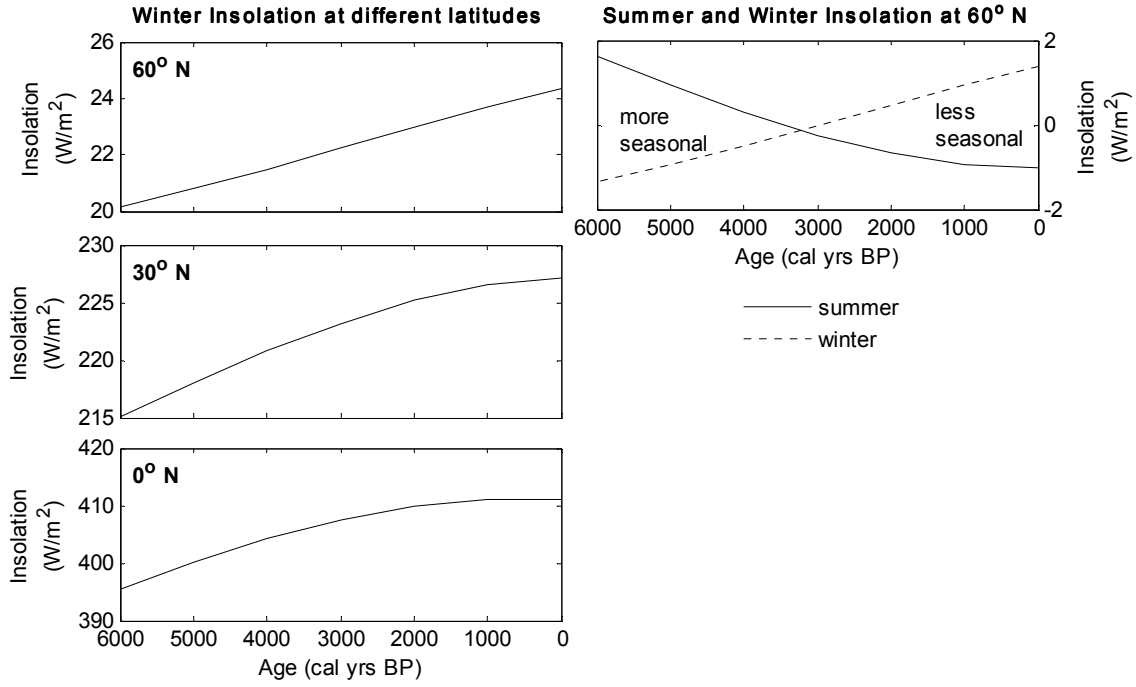

Figure 6.8: December Insolation at (*left column from top)* 60ºN, 30ºN, 0ºN and the seasonal insolation trends at 60ºN (*top right*). Data from Berger (1992) dataset, calculated using Berger and Loutre (1991).

6.5.2. Solar activity

Solar activity may have influenced the position of the storm track, the NAO and storm intensity during the Late Holocene over millennial, centennial and decadal timescales. A solar influence on storminess is supported by certain research (Sabatier *et al*., 2011; Wirth *et al*., 2013; De Jong *et al*., 2006) and contradicted by others (Sorrel *et al*., 2012; Fletcher *et al*., 2012), so the importance of this forcing is controversial.

Various studies have been carried out to assess the influence of solar changes on climate circulation and storms using modern observations, modelling and reconstructions of past changes. The mid-latitudes (40-50ºN) are highly influenced by solar changes, which influence the mean location of the polar fronts and therefore cyclonic activity (Gleisner and Thejll, 2003; Rumney, 1968). Most results indicate that solar minima are associated with negative NAO anomalies and southwardly displaced storm tracks (e.g. Ineson *et al*., 2011), for example during the Maunder Minimum (Shindell *et al*., 2001; Raible

et al., 2007; Lockwood *et al*., 2010). During solar minima reanalysis data and model results have shown a contraction and strengthening of the Ferrell Cells and therefore a strengthening and equatorward-shift of the atmospheric jets (Haigh *et al*., 2005; Gleisner and Thejll, 2003; Raible *et al*., 2007). Conversely solar maxima have been associated with widely higher humidity (Gleisner and Thejll, 2003), a positive NAO (Boberb and Lundstedt, 2002; Kuroda and Kodera, 2002) and more zonal (or westerly) airflow, as shown by models and instrumental data (Matthes *et al*., 2006; Huth *et al*., 2006). Model and reanalysis data have indicated that higher solar activity is also associated with weakening and expansion of the Ferrell Cells and therefore weaker and poleward shifted atmospheric jets (Haigh, 1996; Haigh *et al*., 2005; Gleisner and Thejll, 2003). Therefore contraction of the Ferrell Cells and stronger, southward shifted atmospheric jets during solar minima may have caused increased storminess in Europe.

Models have only recently become sufficiently advanced to integrate the influence of both UV radiation on the stratosphere and TSI on surface temperature (Gray *et al*., 2010). This means important processes influencing storm tracks involving the stratosphere are only recently being considered. For example, UV changes can cause sudden stratospheric warming events to occur, when heating of the stratosphere causes the circumpolar vortex to weaken, the effects of which descend to the troposphere and cause negative NAO circulation patterns (Baldwin and Dunkerton, 1999; Limpasuvan *et al*., 2004; Matthes *et al*., 2006; Gray *et al*., 2010; Kodera and Kuroda, 2002). A recent model simulation that includes a stratosphere sensitive to UV variations has indicated that solar minima cause negative NAO patterns and southward shifted storm tracks (Martin-Puertas *et al*., 2012).

Visual comparison of the storminess reconstructions with the TSI reconstruction (Steinhilber *et al*., 2012; Figure 6.9) in some ways support a solar forcing on storminess. The millennial-scale trend from high TSI between c.4000-2000 cal yr BP to lower TSI after this time reflects the changes observed in the peat bog storminess reconstructions. The period of generally high solar activity before 2000 cal yr BP had higher storminess in southern Europe; this contradicts the findings of the above literature which indicates that solar maxima have northerly storm tracks. Likewise the lower solar activity after 2000 cal yr

BP would be expected to result in southward, stronger atmospheric jets; however storminess increased in northern rather than southern Europe. There is also disagreement with the Olsen *et al.* (2012) NAO reconstruction, as this suggested that there was a generally lower NAO index before 2000 cal yr BP, but the high TSI reconstructioned for this time would be expected to cause positive NAO conditions (Boberb and Lundstedt, 2002; Kuroda and Kodera, 2002).

The comparison of the centennial changes shows abruptly low TSI events at c. 3400, 2700 and 2300 cal yr BP, around the times that there is thought to have been increased storminess in Galicia, and between 700 and 200 cal yr BP, which coincide with the inferred high storminess in the Outer Hebrides. On the other hand there are some offsets in the timings and some peaks in storminess, such as in the Struban Bog reconstruction at 800 cal yr BP, coincide with reconstructed solar maxima instead. It is possible that errors within each of the reconstructions caused the offset in timings, as palaeoclimatic reconstructions are subject to chronological uncertainty. A solar and wind reconstruction from Germany, based on the same varved sediment sequence (thus removing chronological issues), suggested that increased storminess occurred during the solar minimum c.2800 cal yr BP (Martin-Puertas *et al*., 2012). There is therefore some evidence that solar minima caused increased storminess in Europe over centennial timescales.

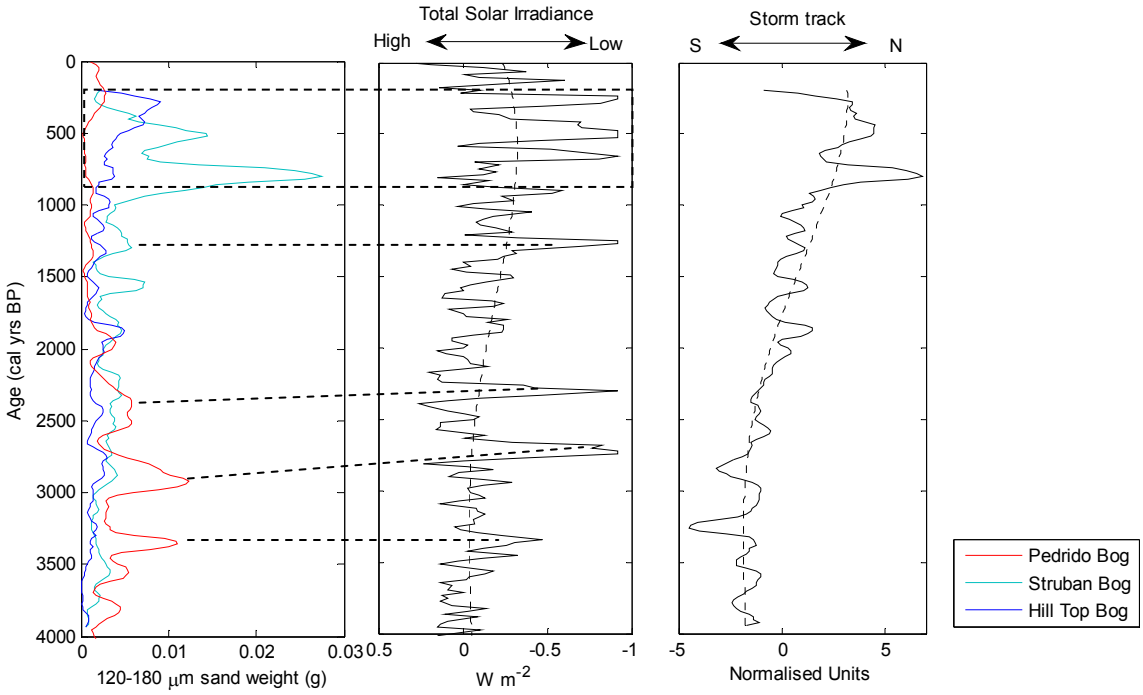

Figure 6.9: Comparison between the storminess reconstructions from this research (l*eft*), Total Solar Irradiance reconstruction (Steinhilber *et al*., 2012; *middle*) and north-south storm track index from this research (*right*). Dashed lines indicate the polynomial trends. Note: x-axis of centre figure is reversed. Thick dashed lines highlight comparisons discussed within the text.

The comparison of the Loch Hosta storminess reconstruction with the TSI reconstruction has some contrasting results (Figure 6.10). The reconstructed storminess since 1600 A.D. shows peaks coinciding with solar minima, at c.1700 A.D. and 1800-1900 A.D., however before this time there is less agreement between the two reconstructions. Therefore the forcings on the Loch Hosta reconstruction are equivocal as the similarities since 1600 A.D. may be coincidental and additional explanatory factors or forcings are required to account for the variability before 1600 A.D.

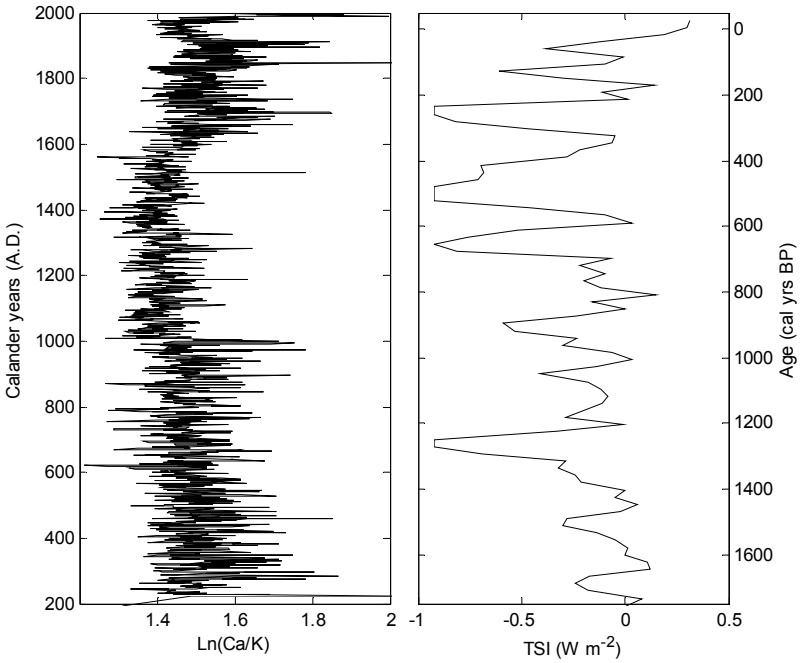

Figure 6.10: Comparison between the Loch Hosta storm reconstruction and reconstructed Total Solar Irradiance (Steinhilber *et al*., 2012).

The identification of solar cycles in climate data can be used as a means of attributing a solar forcing mechanism to the observed changes (Gray *et al*., 2010). Many solar cycles are present in the storminess reconstructions from this research, as illustrated in Table 6.2. To investigate this further cross-spectral analysis has been carried out between the reconstructions of storminess from this research and the NAO (Olsen *et al*., 2012) with the TSI reconstruction (Steinhilber *et al*., 2009), to assess shared spectral frequencies (using the methods described in section 2.8.3). The results show significant shared cycles, which indicate a solar forcing on storminess as well as the NAO at the given frequencies (Figures 6.11 and 6.12).

The Hallstadt cycle of c.2500 years (Steinhilber *et al*., 2012) is similar to the 2290 year cycle in Hill Top Bog record spectral analysis and is shown by the 2560 year cycle in the cross-spectral analysis with the Pedrido Bog reconstruction. Millennial forcing of storminess is also indicated by the cycles of 1024 and 1280 years in the cross-spectral analysis with the Outer Hebrides bog reconstructions. Shorter cycles of 890, 940 and 860 year cycles were identified in the spectral analysis of the Outer Hebrides reconstructions (Table 6.2.) and are similar to millennial solar cycles of 830-1050 years (Stuiver and Braziunas,

1993; Stuiver *et al*., 1995; Debret *et al*., 2007), although these were not shown by cross-spectral analysis. A 512 year solar cycle (Stuiver and Braziunas, 1993; Vonmoos *et al*., 2006) was identified in the spectral and cross-spectral analysis with the Pedrido Bog reconstruction, so is a cycle influencing southern Europe. Cycles between 300-370 years were present in cross-spectral analysis between TSI and the Outer Hebrides bog reconstructions, as well as with the NAO reconstruction (Figure 6.12), which suggests an influence on atmospheric circulation from the 350 and 300 year solar cycles (Stuiver and Braziunas, 1989; Turney *et al*., 2005; Steinhilber *et al*., 2012). Finally the Suess cycle of 220 years (Stuiver and Braziunas, 1989; Knudsen *et al*., 2009; Wanner *et al*., 2008; Steinhilber *et al*., 2012) was identified in the cross-spectral analysis with all the reconstructions aside from Hill Top Bog (Figure 6.11), as well as with the NAO reconstruction (Figure 6.12). Therefore the results of the spectral and cross-spectral analyses provides strong evidence that solar forcing is causing changes to atmospheric circulation patterns over multi-centennial timescales.

Overall, visual comparison of the TSI and storminess reconstructions gives some indication that low centennial-duration TSI events are connected with heightened storminess, in the Pedrido Bog between 3500-2000 cal yr BP and since 1000 cal yr BP in the Outer Hebrides. However there are offsets in the timings of solar minima with periods of increased storminess, which could be due to errors within each of the reconstructions. The presence of solar cycles within the reconstructions and particularly the cross-spectral analysis, support there is a solar influence on storminess. On the other hand the millenial trends observed in the storminess reconstruction cannot be explained by the long-term changes in solar activity, as these would have forced opposite storm track shifts to those indicated by the storminess reconstructions.

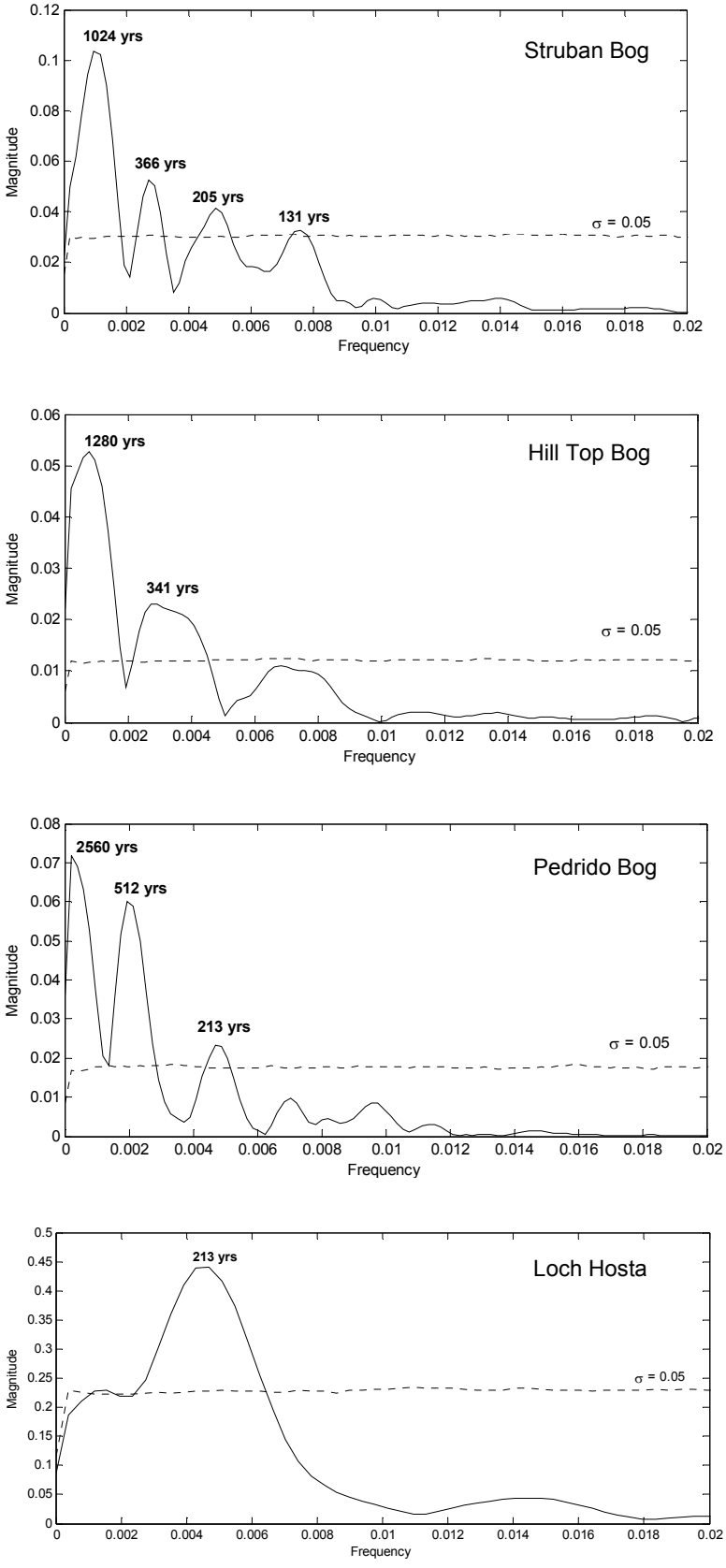

Figure 6.11: Cross-spectral analysis of the storminess reconstructions from this research with the Total Solar Irradiance reconstruction from Steinhilber *et al*. (2009) using the method outlined in section 2.8.3. (Chatfield, 2004). The dashed line indicates the 95% significance level.

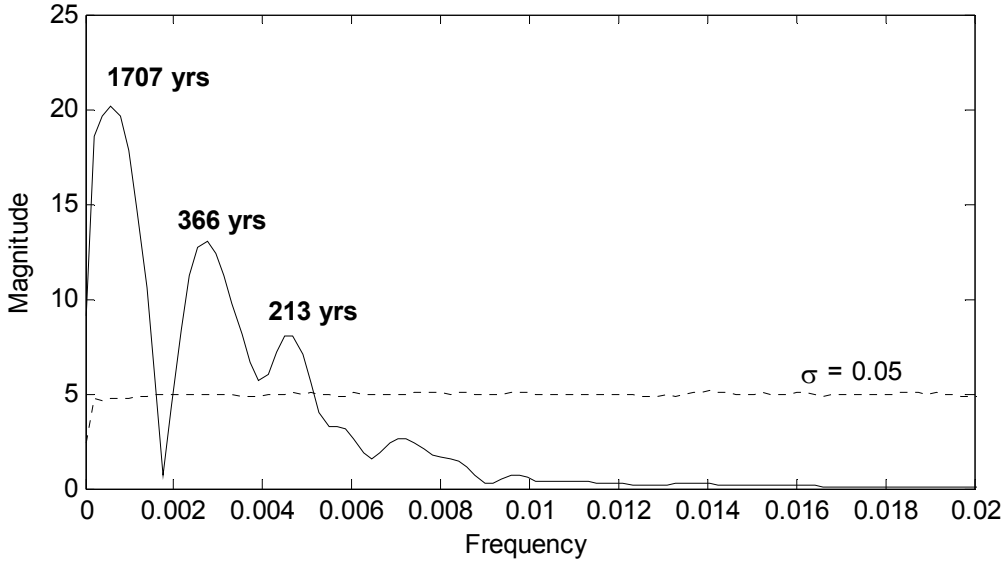

Figure 6.12: Cross-spectral analysis of NAO reconstruction (Olsen et al., 2012) and Total Solar Irradiance reconstruction from Steinhilber *et al*. (2009) using the method outlined in section 2.8.3. (Chatfield, 2004).. The dashed line indicates the 95% significance level.

6.5.3. Oceanic forcing

Ocean circulation proxies

Research has discussed the influence of oceanic changes on the storm track position. It has been suggested that the southerly penetration of cold water in the North Atlantic (caused by the weak ocean circulation) and increased sea ice at high latitudes may have at times increased the temperature gradient, which would shift the region of maximum temperature contrast southwards and with it the North Atlantic storm track (Sabatier *et al*., 2011; Bakke *et al*., 2008; Betts *et al*., 2004; Sorrel *et al*., 2012; Raible *et al*., 2007). Ocean temperatures may similarly influence the NAO index: a model driven by sea-surface temperatures was able to predict NAO changes reliably (Rodwell *et al*., 1999). However it is also considered that ocean circulation is in part driven by wind stress associated with the storm track position over the North Atlantic (e.g. Lohmann *et al*., 2009; Curry and McCartney, 2001), so separating the cause and effect is difficult.

Visual comparison shows that the two largest peaks in the Pedrido Bog storminess reconstruction were at c.3200 and 2800 cal yr BP; these coincide with times of increased ice-rafting in the North Atlantic (Bond *et al*., 2001) and the transition to weaker ocean circulation indicated by the Iceland-Scotland Overflow Water and subpolar gyre strength reconstructions (Bianchi and McCave, 1999; Thornalley *et al*., 2009; Figure 6.13). Comparison may also be made tentatively between the increased storminess after 1000 cal yr BP indicated by the Outer Hebrides reconstructions and the period of increased ice-rafting and minimally reduced Iceland-Scotland Overflow Water and subpolar gyre strength reconstructed during this time. Finally the periods of reconstructed high IRD and low Iceland-Scotland Overflow Water strength at c. 1600-1000 and 600-0 cal yr BP coincide with the periods of increased storminess indicated by the Loch Hosta reconstruction. Overall there appears to be some agreement at times between storminess and oceanic changes, however there are also asynchronous variations and peaks in storminess occur during times of both strong and weak ocean circulation. Therefore it is difficult to determine whether high storminess is forced by the ocean circulation changes and it is possible that the changes observed are unrelated.

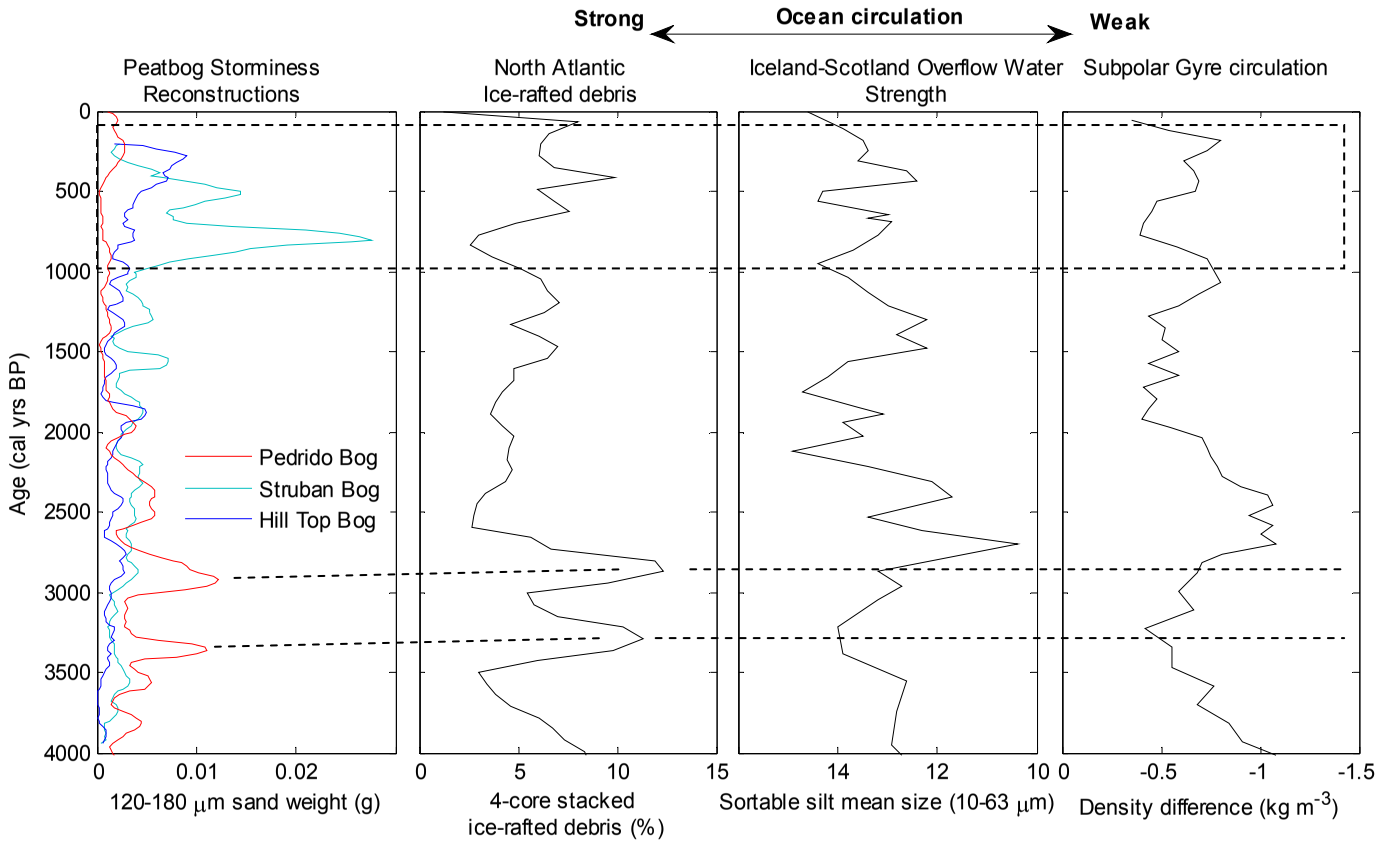

Figure 6.13. Comparison between reconstructions of storminess and ocean circulation. From left: peat bog storminess reconstructions from this study, stacked record of ice-rafted debris from 4 cores from the North Atlantic (Bond *et al.*, 2001); sortable silt particle size from a core sampled from the Gardar drift south of Iceland, representing the strength of the Iceland-Scotland Overflow Water (Bianchi and McCave, 1999); upper ocean density stratification from core RAPiD-12-IK as a proxy for subpolar gyre circulation (Thornalley *et al.*, 2009). Dashed lines show periods discussed in the text.

The cycles present within the storminess reconstructions give some suggestion that there is an oceanic forcing. A frequently identified cycle in North Atlantic proxy reconstructions is a c.1500 year cycle, which was first shown as a 1370 ± 500 year cycle in proxies of ice-rafting debris (Bond *et al*., 1997). It has since been identified in various proxy reconstructions of ocean circulation such as Iceland-Scotland Overflow Water strength (Bianchi and McCave, 1999) and sub-polar gyre strength (Thornalley *et al*., 2009). This cycle has also been identified in reconstructions of storminess from Europe and Greenland (Sorrel *et al*., 2012; Debret *et al*., 2007; Fletcher *et al*., 2012). In the Struban Bog and Hill Top Bog reconstructions similar cycles of 1330 and 1450 years (respectively) were identified (Table 6.2), however this cycle was not present in the other reconstructions. Cycles of 890 and 940 years in the Hill Top Bog and Struban Bog reconstructions respectively and a 510 year cycle in the Pedrido Bog reconstruction are similar to 1000 and 550 year cycles identified in reconstructions of North Atlantic Deep Water circulation (Chapman and Shackleton, 2000). There is therefore a possible oceanic influence on storminess in the Outer Hebrides, indicated by the cycles present.

To further investigate the ocean-atmosphere interaction, cross-spectral analysis has been carried out between the NAO reconstruction (Olsen et al., 2012) and storminess reconstructions with the ice-rafting debris reconstruction (Bond et al., 2001), following the methods described in section 2.8.3.. The results show that a c.1490 year cycle is present in cross spectral analysis of IRD with the NAO and the Hill Top Bog reconstructions (Figure 6.14 and 6.15), which supports a relationship between oceanic circulation and atmospheric circulation patterns. Additionally the c.1450 year cycle is not a feature of solar variability, supporting that this cycle is not the result of an external forcing (Debret *et al.,* 2007*)*. As there is evidence of both solar and oceanic forcing through the spectral and cross-spectral analysis, this is evidence that storminess is the result of a combination of forcings, which may vary in importance through time. This could explain why the visual comparison with the ocean circulation proxies did not provide strong results.

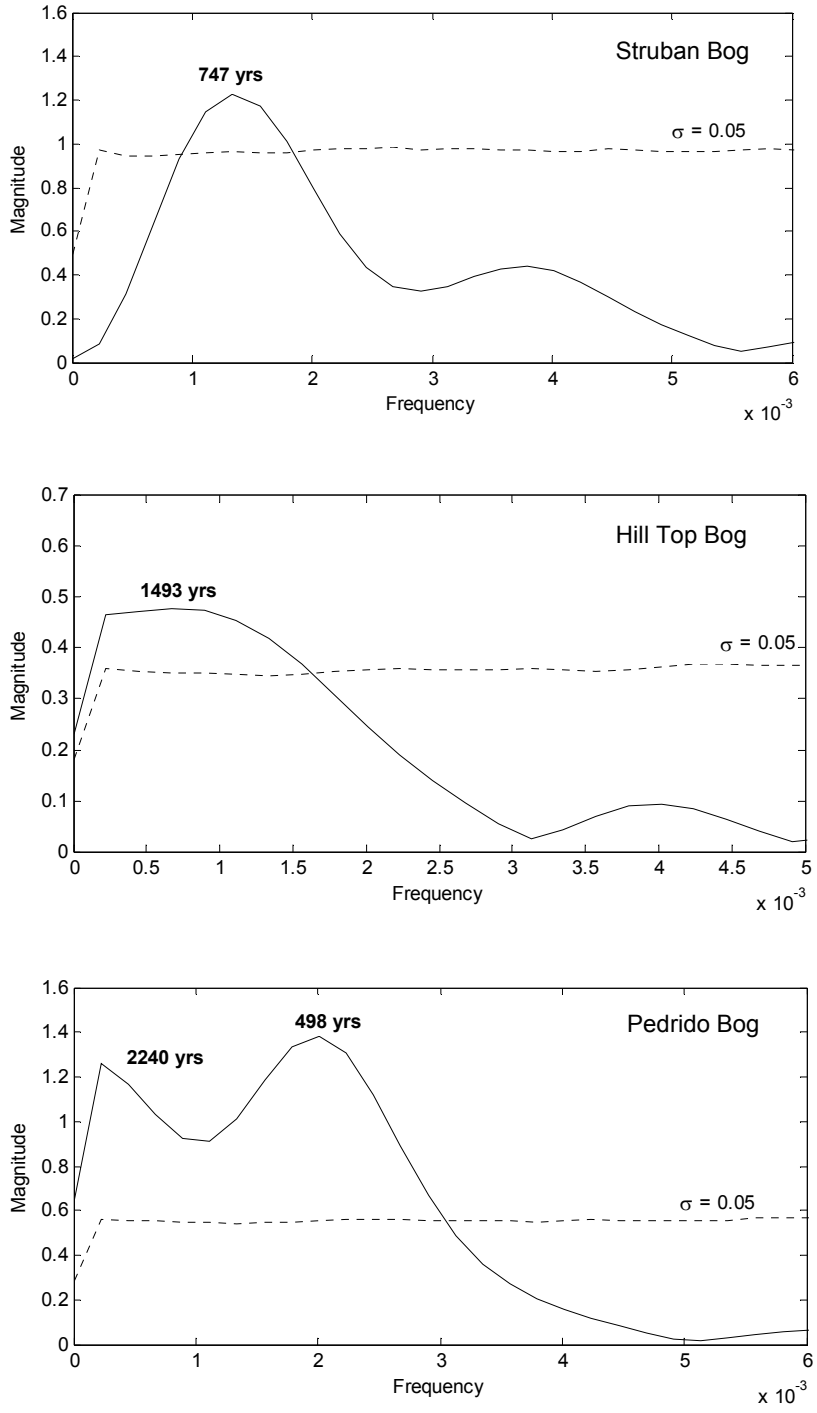

Figure 6.14: Cross-spectral analysis of the peat bog storminess reconstructions with the Ice-Rafting Debris reconstruction (Bond *et al*., 2001) calculated using the methods outlined in section 2.8.3 (Chatfield, 2004). The dashed lines indicate the 95% significance level.

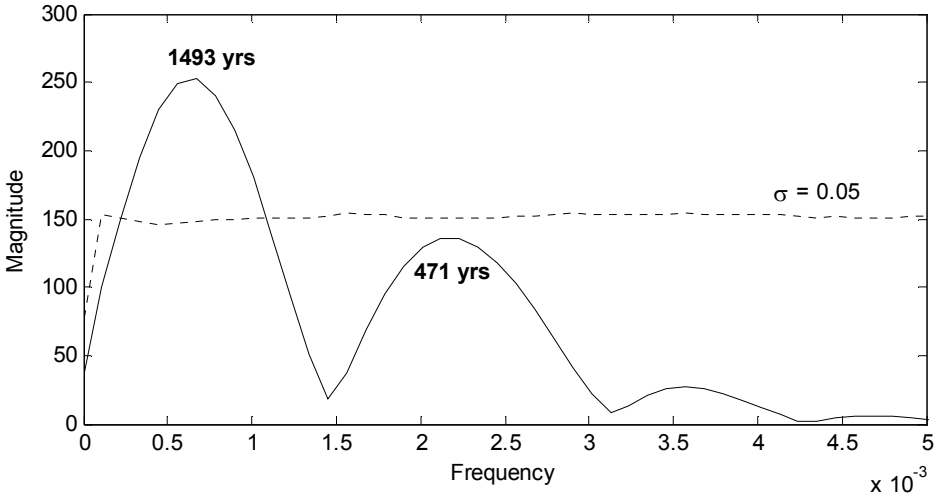

Figure 6.15: Cross-spectral analysis of NAO reconstruction (Olsen et al., 2012) with the Ice-Rafting Debris reconstruction (Bond *et al*., 2001), calculated using the methods outlined in section 2.8.3 (Chatfield, 2004). The dashed line indicates the 95% significance level.

Atlantic Multidecadal Oscillation

A different source of oceanic variability that may influence storminess in Europe is the Atlantic Multidecadal Oscillation (AMO), which is an internal mode of variability in the North Atlantic (Schlesinger and Ramankutty, 1994; Wei and Lohmann, 2012). Heat fluxes from the Atlantic Ocean to the atmosphere have been shown to occur at multidecadal timescales during the instrumental period, supporting that oceanic variation can drive the decadal climate variations (Gulev *et al*., 2013). Models also support that winter precipitation over areas of northern Europe, including the Outer Hebrides, increase as a result of positive AMO conditions (Knight *et al*., 2006). Therefore as the comparison with instrumental data indicated that the Loch Hosta reconstruction reflects precipitation changes (see Figure 3.9), it may be influenced by the AMO variability.

Visual comparison suggests higher storminess when the AMO was positive between 1640-1710 A.D. and 1850-1900 A.D. and lower storminess when the AMO was negative during the intervening time (Figure 6.16). However the relationship appears reversed during the twentieth century. The reconstruction of storminess by Van Vliet-Lanoë *et al.* (2014) has suggested

that the most severe storms in northern France occurred during negative NAO events, particularly during periods of positive AMO, when sea-surface temperatures were warm. This may have been due to increased cyclogenesis resulting from a steep vertical temperature gradient between the ocean and polar jet (Van Vliet-Lanoë *et al*., 2014; Betts *et al*., 2004). Therefore the greater similarity between the Loch Hosta storminess and AMO reconstructions before 1900 A.D. may have been the result of a predominantly low NAO during this time (Trouet *et al*., 2009), which in conjunction with the AMO caused multidecadal variability in storminess, by increasing the ocean-atmosphere temperature gradient and heat flux. Therefore it is speculated that the AMO is influencing storminess in the Outer Hebrides during periods with dominant negative NAO conditions.

An AMO influence on storminess is supported by cycles of 50-58 and 77-87 years in the Loch Hosta reconstruction, which are similar to those of the AMO. Furthermore cross-spectral analysis between the Loch Hosta and NAO reconstruction (Olsen *et al*., 2012) showed a cycle of 60 years (Figure 3.10), indicating that this cycle may have influenced the Loch Hosta storminess reconstruction through the NAO. Records and reconstructions of the AMO have shown cyclicity of 60-80 years, which has been connected with NAO variability and various climate variables including precipitation (Wanner *et al*., 2001; Higuchi *et al*., 1999; Enfield *et al*., 2001; Kerr, 2000; Gray *et al*., 2004; Knudsen *et al*., 2011; Knight *et al*., 2006). Cycles of 60-70 years have also been identified in reconstructed glacier fluctuations from the western French Alps, and attributed to AMO forcing of storminess and precipitation (Guyard *et al*., 2013). On the other hand there is a solar cycle of 60 years (Table 6.2), meaning it is possible that solar changes influenced both the oceanic and climatic changes.

In summary an oceanic influence is supported by the cycles present in the Outer Hebrides reconstructions and by visual comparison between reconstructions of ice-rafting and the AMO over some time periods. However asynchronous variability suggests that ocean forcing is not the sole driver of storminess, as similar timings may be coincidental and in fact both storminess and oceanic changes may be driven by the NAO as well as external factors like solar variability.

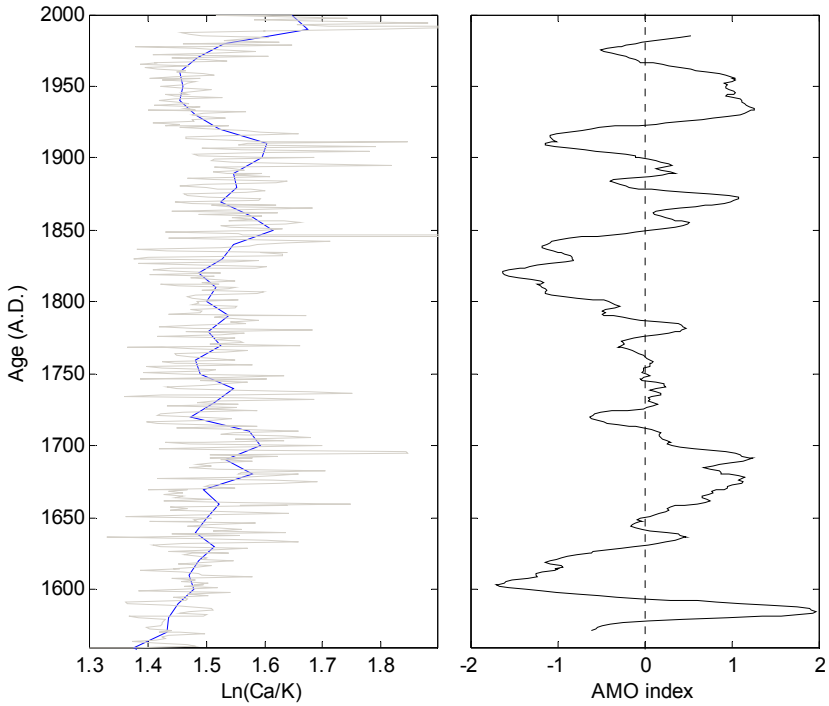

Figure 6.16.: Loch Hosta Ln(Ca/K) results (*left*) at annual (grey line) and 10-year (blue line) resolutions and Atlantic Multidecadal Oscillation reconstruction based on tree-ring chronologies from AMO-sensitive regions of America, Europe, the Middle East and north Africa (Gray *et al*., 2004).

6.5.4. Volcanic forcing

Volcanic eruptions can influence the atmospheric circulation patterns, so past eruptions may therefore have caused storminess changes in Europe. Research using observations and model simulations has indicated that large volcanic eruptions that add volcanic aerosols to the stratosphere lead to stronger circumpolar vortex circulation and positive NAO anomalies, associated with warmer and wetter conditions in northern Europe (Fischer *et al*., 2007; Stenchikov *et al*., 2006; Kodera, 1994, Jones *et al*., 2005). Therefore volcanic eruptions would be expected to coincide with peaks in storminess in the reconstructions from the Outer Hebrides in particular.

However visual comparison between the storminess reconstructions and proxies for volcanic eruptions (stratospheric aerosol optical depth and GISP2 sulphate measurements) do not support that there is a strong volcanic forcing on climate (Figures 6.17 and 6.18). The higher resolution Loch Hosta

reconstruction is more likely to have captured the effects of volcanic eruptions that typically only span a few years (Fischer *et al*., 2007) and there is potentially a correspondence between higher Aerosol Optical Depth's before 1000 A.D. and after c.1600 A.D. with higher storminess. There is less similarity between the volcanic forcing proxy and the peat bog storminess reconstructions (Figure 6.18), perhaps due to the multi-decadal resolution of these reconstructions. Only the peak in the Struban Bog reconstruction at c.800 cal yr BP coincides with a cluster of years with high sulphate concentrations. Therefore although higher storminess may have occurred at times with more frequent, large volcanic eruptions, the evidence is inconclusive.

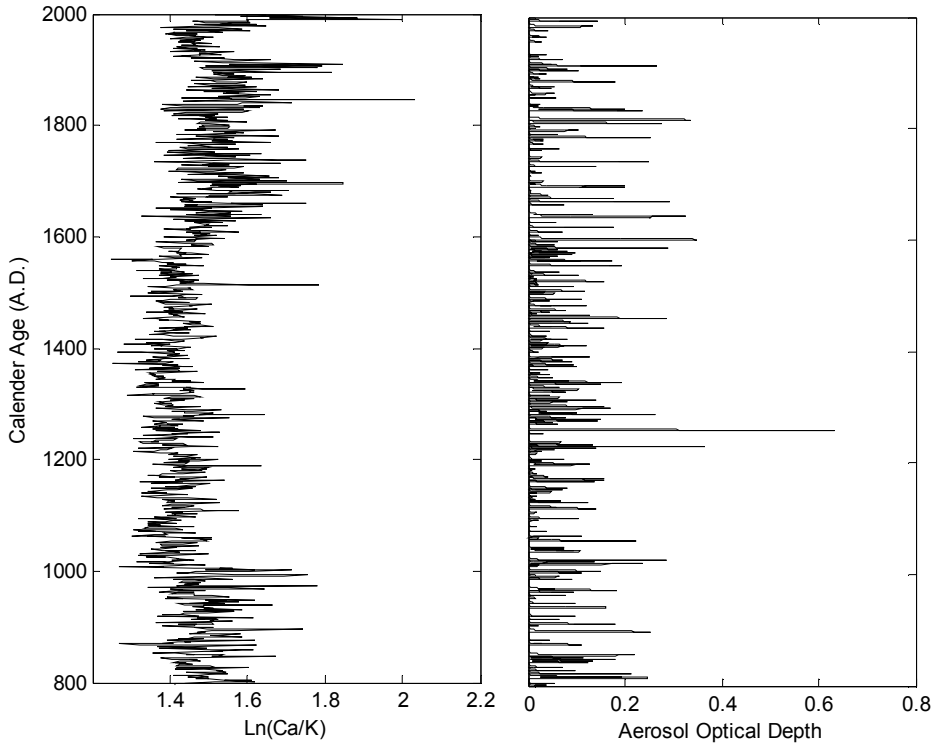

Figure 6.17: Loch Hosta Ln(Ca/K) reconstruction and reconstructed stratospheric aerosol optical depth for latitudes 30-90ºN, which is a proxy for volcanic activity (Crowley and Unterman, 2012)

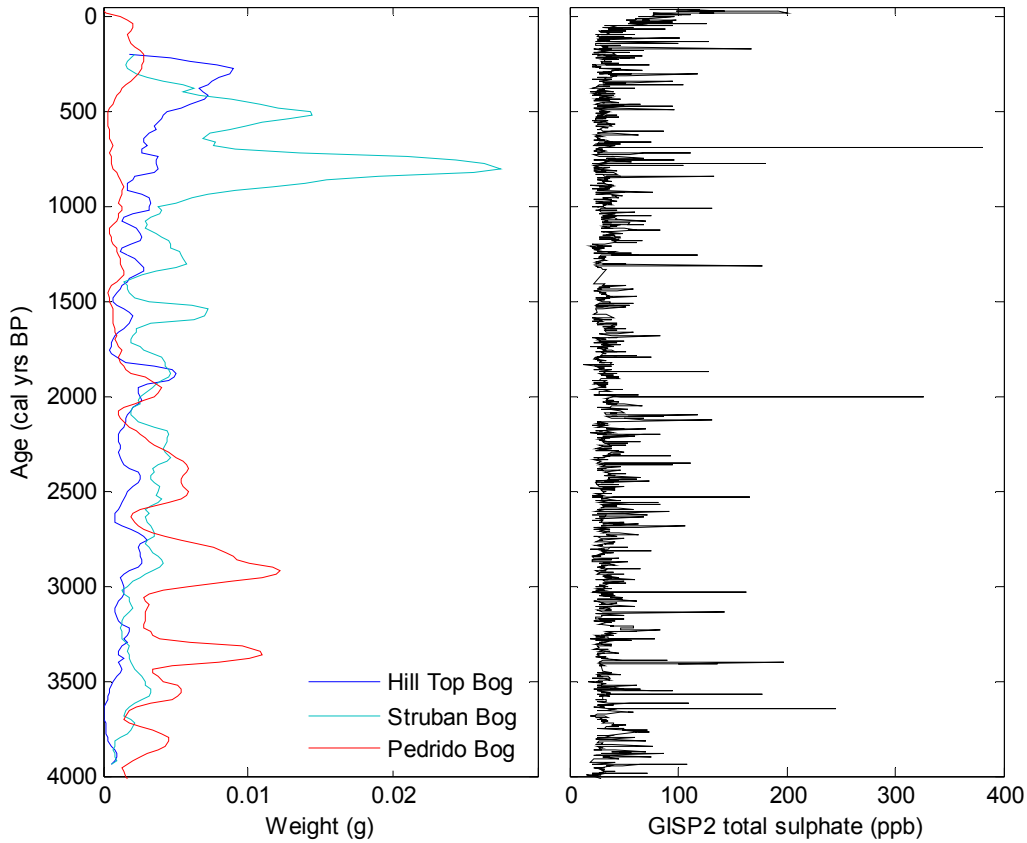

Figure 6.18: Peat bog storminess reconstructions from the Outer Hebrides and Galicia and total sulphate measurements from the GISP2 ice core considered as a proxy for past volcanic activity (data from website NOAA, 2014; Zielinski and Mershon, 1997; Zielinski *et al*., 1994; Hempel and Thyssen, 1992; Palais *et al*., 1992; Palais *et al*., 1991).

6.5.5. Integration of forcings

To untangle the forcings on storminess variability (both the millennial storm track transition and centennial peaks) the changes to the temperature gradient and therefore the circumpolar vortex and storm track will be considered. The temperature gradient between the mid- and high- latitudes drives the strength and wave pattern of the circumpolar vortex: a steeper (shallower) temperature gradient causes higher (lower) zonal wind velocities and therefore longer (shorter) wavelengths of the circumpolar vortex (Barry and Chorley, 2010; Lamb, 1995). This means that the strong vortex causes westerly winds that are stronger and displaced northwards and the weak vortex causes meridional winds, a southwardly displaced storm track and quasi-stationary

cyclones/anticyclones (Barry and Chorley, 2010; Lamb, 1995). Using this understanding, the changes to the temperature gradient from solar, orbital and oceanic forcings will be assessed and the resulting changes to the polar vortex, storminess and the storm track will be considered in this section.

The storm track shift at 1800 cal yr BP from southern to northern Europe may be explained by orbital and solar changes to the insolation distribution and latitudinal temperature gradient. As the high latitudes receive no solar radiation in winter, the temperature gradient would have been most influenced by solar insolation in the mid-latitudes. As the result of orbital changes the insolation increased by over 2 W m^{-2} at 60ºN from 4000 cal yr BP to present (Figure 6.8), therefore the latitudinal insolation gradient would have been increased. However the decreasing TSI trend was around 0.5 W m^{-2}, therefore this would have acted to reduce the latitudinal temperature gradient through the Holocene during winter. As the orbitally-driven insolation change is greater than the TSI change, it is considered that the orbital changes exerted a greater influence, so overall the latitudinal temperature gradient would have increased through the Late Holocene. This would have caused the circumpolar vortex to increase in strength through the Late Holocene, which could have resulted in fewer planetary waves, more zonal circulation and northwardly displaced storm tracks (Barry and Chorley, 2010; Lamb, 1995).

In terms of the storminess reconstructions the above explanation can account for higher storminess in Spain at 4000-1800 cal yr BP. The inferred meridional circulation patterns during this time were potentially associated with intensified and southwardly displaced storms, as the southward excursions of the jet stream cause large temperature differences between tropical and arctic air masses that foster cyclone formation (Van Vliet-Lanoë *et al*., 2014; Betts *et al*., 2004). Furthermore as explained in section 6.3, a more meridional circulation pattern before 2000 cal yr BP is indicated by higher, variable storminess in regions of northern Europe (Macklin and Lewin, 2003; Wilson *et al*., 2004; De Jong *et al*., 2006), unstable ocean conditions in the North Atlantic (Moros *et al*., 2004) and more sea-salt and dust delivery to the GISP2 drilling site (O'Brien *et al*., 1995).

The reconstructed increase in storminess in northern Europe after 1500 cal yr BP may be consistent with a stronger polar vortex. Reanalysis data has indicated that strong circumpolar vortex circulation causes strong westerly winds with high precipitation in northern Europe and low storminess in southern Europe (Walter and Graf, 2005; Graf and Walter, 2005), as well as positive NAO events (Baldwin and Dunkerton, 2001). Increasing polar vortex strength has been suggested as the cause of the northward storm track shift captured by the glacier-based north-south index from Norway (Bakke *et al*., 2008), which coincides with the storm track shift observed in the results of this study. On the other hand this transition may have been the result of a contracting polar vortex causing the pressure cells and storm tracks to be shifted northwards, as has been suggested by Wirth *et al*. (2013).

This interpretation of a transition from a shallow to steep temperature gradient, and weak to strong polar vortex, through the Late Holocene is somewhat supported by assessment of temperature reconstructions from high and low latitudes. The GISP2 temperature reconstruction (Figure 6.19) suggests a transition from warm to cold polar temperatures through the Late Holocene (Alley, 2004). Although this could be a result of the decreasing summer insolation (Figure 6.8; Berger and Loutre, 1991) it may also be the result of a stronger circumpolar vortex trapping cold air within the polar regions during winter (Chylek *et al*., 2004; Thompson and Wallace, 2000). The latter explanation for polar cooling supports that the circumpolar vortex has increased in strength through the Late Holocene. A reconstruction of atmospheric temperatures using multiple sites in Europe has also indicated that temperatures decreased in northern Europe and increased in southern Europe through the Late Holocene (Davis *et al*., 2003). Although this supports that the temperature gradient became steeper, caution is needed as the temperatures in Europe are influenced by the NAO and storms, so these patterns may in fact reflect the NAO negative-to-positive shift (Olsen *et al*., 2012). The issue of regional circulation patterns, as well as a bias towards summer temperature reconstructions, means that identification of temperature gradients is difficult.

The above changes explain the long-term storm track changes during the Late Holocene, however orbital changes cannot explain the decadal and centennial variability observed within the storminess reconstructions.

Furthermore in section 6.5.2 and 6.5.3 spectral and cross-spectral analysis indicated that solar forcing, and to a lesser extent oceanic forcing, play a role in storminess variability. The same mechanisms used to explain the orbitally-induced storminess changes can be used to explain the storminess peaks during intermittent solar minima. In winter solar minima would cause reduced temperatures in the mid-to-low latitudes, but radiation receipt of polar regions (during the polar night) would remain at zero – therefore it is considered that solar minima would cause a reduced latitudinal temperature gradient. As with orbital changes, the solar minima would therefore cause a weaker polar vortex and reduced zonal airflow, causing southwardly displaced storm tracks, quasi-stationary pressure cells and increased temperature contrasts (with more cyclogenesis) (Barry and Chorley, 2010; Van Vliet-Lanoë *et al*., 2014; Betts *et al*., 2004).

This above premise of changes to the latitudinal temperature gradient causing storm track shifts is somewhat supported by comparison of the storminess reconstructions with TSI reconstructions (Figure 6.19), although there are offsets in the timings of some events. High storminess in southern Europe appears to have occurred when there were solar minima at c. 3400, 2800 and 2400 cal yr BP and since 1000 cal yr BP in northern Europe. These periods of high storminess also coincide with global glacier advances (c.3500-2400 and after c.1400 cal yr BP) (Denton and Karlén, 1973) and increased precipitation in the Alps at 4200-2400, 1200-1000 and 500-100 cal yr BP (Wirth *et al*., 2013), which these authors have also suggested were due to solar changes. Furthermore the solar minima c.2800 cal yrs BP has been connected with higher storminess in Germany, which model results suggest was the result of stratospherically triggered circulation changes (Martin-Puertas *et al.,* 2012). A recent examples of solar minima is the Maunder Minimum (1645-1715 A.D.); during this period there were quasi-stationary pressure cells (associated with meridional circulation), persistent extremes of weather and high storminess (Lamb, 1979). Therefore it seems likely that solar minima caused increased storminess across southern Europe, in agreement with some previous research (Wirth *et al*., 2013; Bond *et al*., 2001; Lamb, 1979; Sabatier *et al*., 2011).

As well as solar variability it is possible that internal oceanic fluctuations caused the variations in storminess, although the evidence for this as a forcing

is weaker than that of solar forcing. A relationship is indicated by the Loch Hosta reconstruction in particular, which indicated higher storminess during some positive AMO phases and has cycles that resemble AMO cyclicity (Kerr, 2000; Gray *et al*., 2004; Wei and Lohmann, 2012). Warmer ocean temperatures (such as the positive AMO) have been suggested as a factor in increased cyclogenesis and storm intensity, based on a storm reconstruction, modelling experiments and reanalysis data (Van Vliet-Lanoë *et al*., 2014; Booth *et al*., 2012; Betts *et al*., 2004). Furthermore ice-rafting events coincide with some of the inferred storminess increases (Figure 6.19), albeit with much temporal variability. As explained, these may have been atmospherically forced by circulation changes (such as the NAO), but may also have caused a positive feedback, as sea-surface temperature gradients have been shown in the instrumental period to cause cyclogenesis (Betts *et al*., 2004). Therefore it is considered likely that oceanic changes are a feedback on storminess but also have internal oscillations that force storminess over multi-decadal timescales.

Finally, the low similarity between the storminess reconstructions and proxies for volcanic activity do not support that this is an important forcing over decadal timescales. However the peak in storminess at 800 cal yr BP in northern Europe correlated with a period of increased volcanicity, indicating that this event may have been the result of volcanic forcing. As this coincided with a solar maximum, it may show that volcanic forcing exceeded solar forcing.

In summary it is suggested that orbital forcing has driven the Late Holocene transition from high storminess in southern to northern Europe, by causing a northwards storm track shift and change from generally negative to positive NAO. These changes may have been caused by a gradual increase in the latitudinal insolation gradient in winter that encouraged a gradually stronger circumpolar vortex circulation and a storm track transition. The timing of storminess peaks in the reconstructions appear to be linked with solar variability and oceanic changes, as supported by spectral and cross-spectral analysis. It therefore is possible that storminess is the result of multiple forcing factors, which make direct comparisons complicated. Based on the results it is suggested that the dominant forcing on centennial storminess was solar changes, with solar minima bringing meridional circulation patterns, a negative NAO and intensified storms.

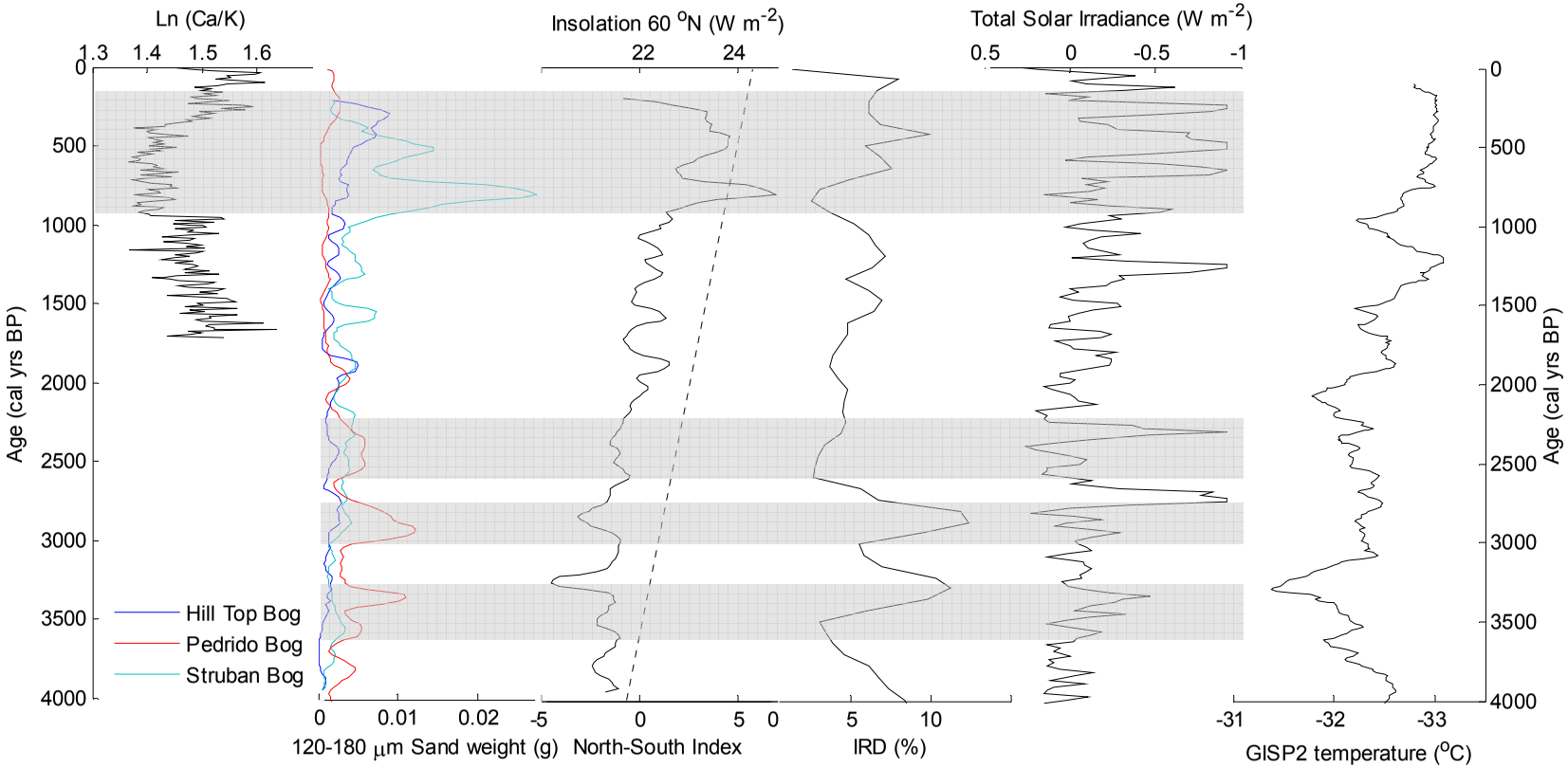

Figure 6.19: Comparison between reconstructions of storminess from this research and proxies discussed as forcings. From left: Loch Hosta Ln(Ca/K) storminess reconstruction, peat bog based storminess reconstructions from this study, North-South index of storm track position as described in section 6.2., winter insolation at 60ºN (Berger, 1992), stacked record of ice-rafted debris from 4 cores from the North Atlantic (Bond *et al*., 2001), Total Solar Irradiance (Steinhilber *et al*., 2012), GISP2 temperature reconstruction (Alley, 2004). Shaded sections illustrate comparisons discussed within the text.

6.6. Future predictions of storminess

6.6.1. Model comparison

An aim of palaeoclimatic research is to test whether climate models are able to reconstruct past climate changes, with the view that this then gives confidence in predictions of future climate change (Braconnot *et al*., 2012; González-Rouco *et al*., 2003). Here a coupled atmospheric-oceanic model reconstruction of average wind speed for the north west of Spain and the Outer Hebrides will be compared with the storminess reconstructions from this research. Only one model simulation will be used, which is not sufficient to fully explore this; however it is an example of the type of comparisons needed to make research into past climate applicable. In this research the results from 1000-1990 A.D. are compared with the 'Erik-the-red' simulation using the ECHO-G model (full name: 'European Centre Hamburg 4 – Hamburg Ocean Primitive Equation – G' model, identifier: ECHO-G version 4, T30 resolution). The ECHO-G model is an ocean-atmosphere coupled model combining the ECHAM4 atmospheric model (Roeckner *et al*., 1996) with the HOPE-G ocean model (Wolff *et al*., 1997; Legutke and Voss, 1999, González-Rouco *et al*., 2003; Von Storch *et al*., 2004). This model is forced by greenhouse gas concentrations, volcanic eruptions and solar variability (Crowley, 2000; González-Rouco *et al*., 2003) and the 'Erik-the-red' simulation shows the historically observed warming around 1100 A.D., coolings during solar minima (Spörer, Maunder and Dalton minima) and the recent anthropogenic warming (Von Storch *et al*., 2004).

The wind speed output, from the cells that included Galicia and the Outer Hebrides, was extracted and then compared with the reconstructed patterns of storminess from the bog reconstructions. As the Loch Hosta results had a strong correlation with precipitation, these results were similarly compared with the models precipitation output for the Outer Hebrides. There is low agreement between the modelled wind speeds and the storminess reconstructions (Figures 6.20 and 6.21). Both the Pedrido reconstruction and the Outer Hebrides bog reconstructions show multi-decadal and centennial trends in storminess, whereas the modelled wind speeds show no long-term trends. An exception to this is c.800 cal yr BP when the modelled Outer Hebrides storminess has three peaks in maximum wind speed that coincide with a peak in storminess in the

Struban Bog reconstruction. As explained in section 6.5.4, this peak coincides with a time with increased volcanic forcing, perhaps showing the models are able to capture the response of the climate to eruptions. The Loch Hosta reconstruction and the modelled precipitation patterns (Figure 6.22) have little resemblance, as the model does not show an increase in precipitation after 1600 A.D.. It must be acknowledged that the data resolutions are very different, with the modelled wind speed and precipitation showing annual resolution changes, while the sand influx values are the accumulation of sand transported by storms over decades. Furthermore there may not be a linear relationship between wind speed and sand transport. Nevertheless higher variability, extreme peaks or a trend to higher values would be expected in the model results at the times when sand influx was higher, if the results are in agreement. The findings, although basic, support that the ECHO-G model is not capturing the long-term variability, or magnitude, of the changes in windspeed or precipitation. This problem of overly high model stability and low magnitude responses has been previously observed for other time periods and contexts assessed by palaeoclimatic data (Valdes, 2011; Braconnot *et al*., 2012). Low variability was also found in a global assessment of storminess outcomes from several runs of the ECHAM4/HOPE-G model (Fischer-Bruns *et al*., 2005). The results therefore support that models may not predict large magnitude changes in future storminess.

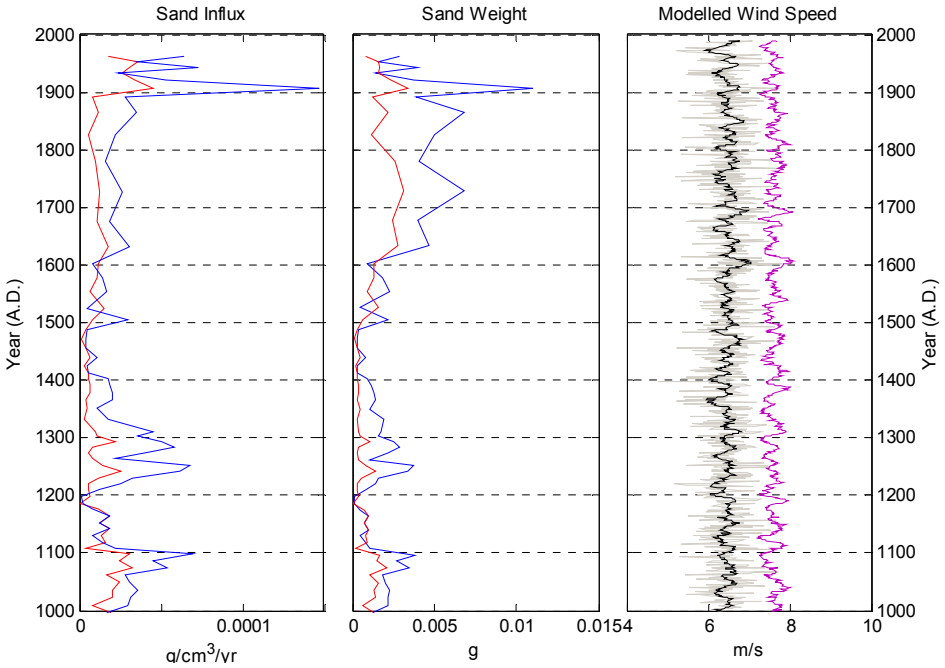

Figure 6.20: Comparison of the sand influx and weight results from Pedrido Bog (blue line = >180 µm sand, red line = 120-180 µm sand) with modelled winter (DJFM) 10m wind speed from cell including Galicia (43N, 7W) for the period 1000-1990 A.D.. Grey line = annual average wind speed, black line = 10-year smoothed average wind speed, purple line = 10-year smoothed maximum wind speed

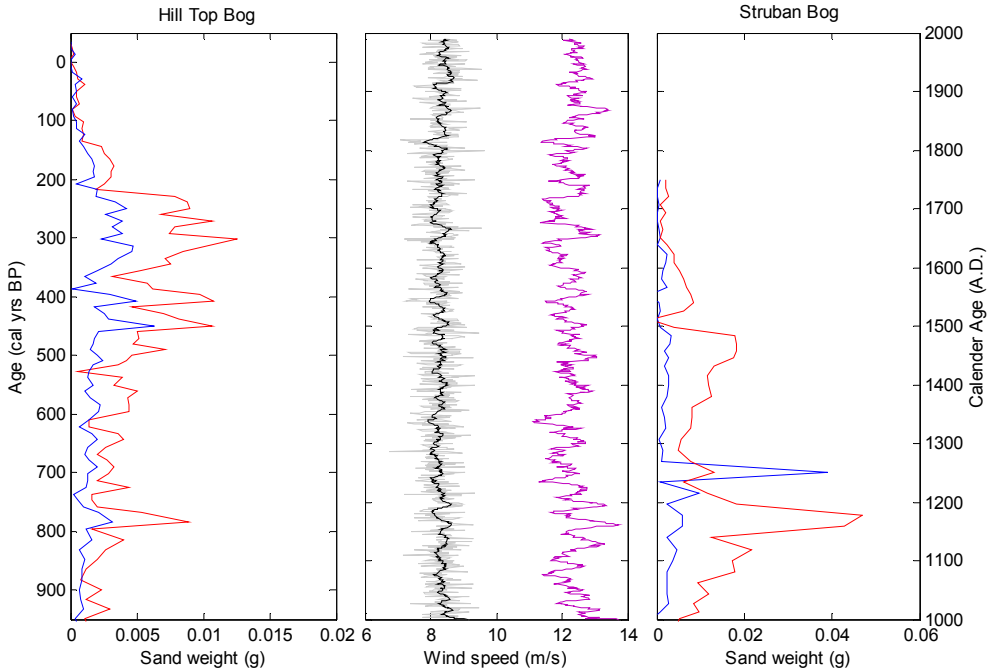

Figure 6.21: Comparison of the sand weight results from the Outer Hebrides Bogs (left: Hill Top Bog and right: Struban Bog) with the modelled average wind speed (centre). Line colours as in Figure 6.20.

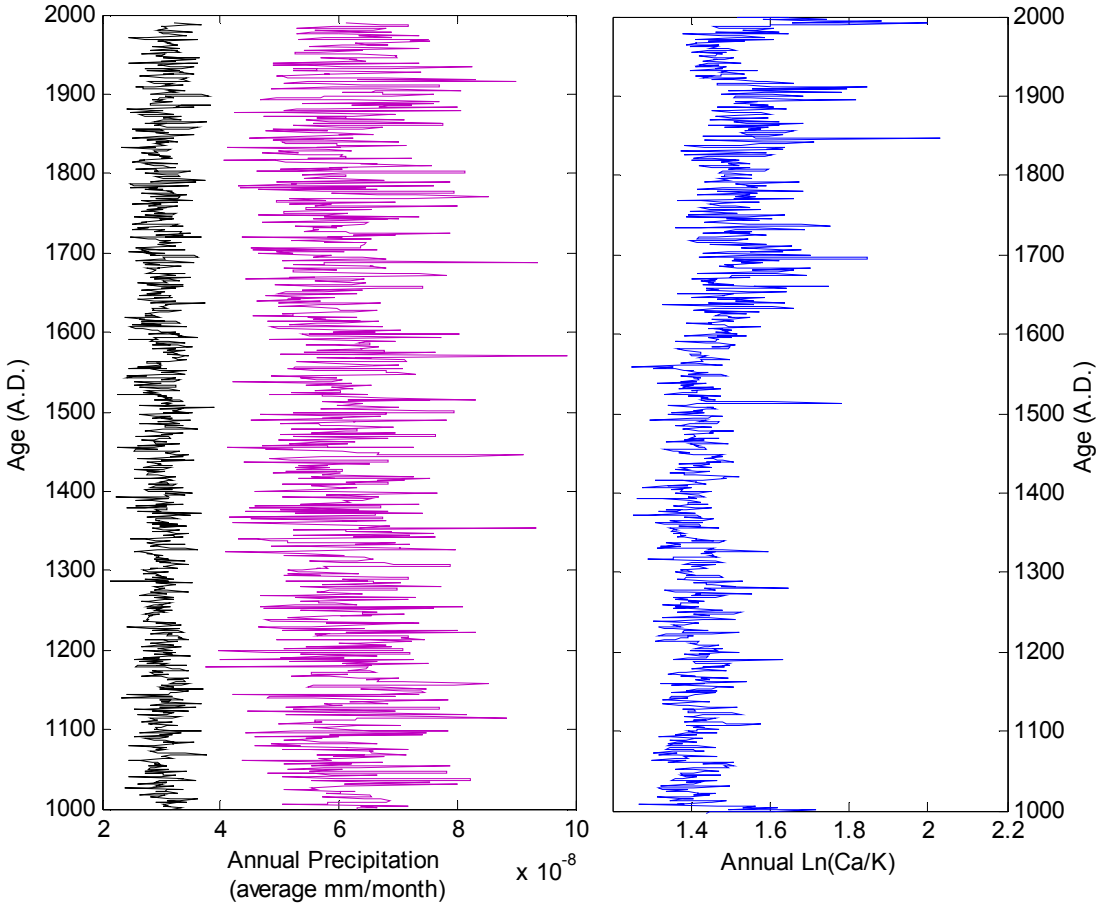

Figure 6.22: Comparison of the Ln(Ca/K) results from Loch Hosta with the modelled annual average (black line) and maximum (purple line) precipitation.

6.6.2. Future storminess and climate change

In section 6.5. it was argued that the dominant long-term control on storminess and storm track position is orbital forcing, which drives changes in the latitudinal temperature gradient. The increasing temperature gradient through the Late Holocene was driven by changes in insolation, which is thought to have caused a northward storm track shift (section 6.5.5.). As winter insolation in the northern hemisphere is predicted to continue to increase over the next 1000 years (Berger and Loutre, 1991), this indicates that the Late Holocene northward storm track shift may continue.

In addition to the orbital forcing, the findings of this research indicate that solar changes influence storminess. Solar minima are thought to cause greater storm intensity (as suggested in section 6.5.2.), due to a weakening of the temperature gradient (by low latitude cooling) causing more meridional

circulation that creates a negative NAO, steeper temperature contrasts and cyclogenesis. Currently there is an unusually prolonged and low solar minimum, which is projected to continue over the coming decades (Stocker *et al.*, 2013). Therefore solar minima may be expected to reduce the meridional temperature gradient during winter, slowing the polar vortex and causing more meridional, quasi-stationary circulation patterns.

On the other hand the influence of greenhouse gases will also have an effect on the temperature gradient and circulation patterns. The latest IPCC report states that the solar-induced radiation changes are small compared to the proposed radiative forcing from greenhouse gases (Stocker *et al*., 2013). Research has indicated that anomalous warming of the Arctic in recent decades has altered the temperature gradient, causing slower zonal winds and changes in the magnitude of the planetary waves, which has produced slow moving and persistent weather extremes (Francis and Vavrus, 2012). This is the same mechanism that is suggested here as occurring during solar minima in the Late Holocene, but with a different, anthropogenic cause. Furthermore the IPCC report indicates that changes to oceanic circulation may influence storminess particularly in northern Europe, through adjustments to the latitudinal temperature gradient (Stocker *et al*., 2013; Catto *et al.*, 2011; Woolings *et al.*, 2012). These predictions therefore show that multiple factors, and both oceanic and atmospheric temperature changes, may cause a change in storminess by adjusting the latitudinal temperature gradient.

Overall the orbital forcing in the future would be expected to strengthen the circumpolar vortex and cause more zonal and northerly storm track positions. However in the coming decades this may be counteracted by solar minima and greenhouse gas increases, both of which may reduce the latitudinal temperature gradient. This would be expected to cause more meridional circulation patterns and therefore heightened storminess in future.

Since the industrial revolution greenhouse gas concentrations in the atmosphere have increased, with global temperatures rising steeply since 1900 A.D. (Stocker *et al.,* 2013). Using storminess reconstructions the effect of this recent anthropogenic climate change can be observed and placed in the context of natural variability. Unfortunately the surface peat acrotelm was not

well preserved by coring and was not consolidated, meaning the peat bog reconstructions are not reliable during the last 100 years. However the Loch Hosta reconstruction correlated with instrumental measurements spanning the last c.120 years, so can be used to assess anthropogenic storminess changes. As shown in Figure 6.22, storminess was low between 1920 and 1970 A.D. before it steadily increased to a maximum in the 1990's A.D.. This maximum was the second highest in the Loch Hosta reconstruction, indicating the storms were of similar magnitude to those during the LIA; the most recent cool event of the Holocene c.1450 year cycle (Bond et al., 2001). This makes the recent storminess unusual, as it occurred during a warm climate period and the Loch Hosta reconstruction indicates that previous warm climates such as the MCA (950-1400 A.D.) had low storminess (Figure 6.22). Based on this assessment it is possible that during the late twentieth century storminess changes have begun to be anthropogenically enhanced.

The winter of 2013-14 may be analogous to climate extremes in the future, as there was an anomalous southward excursion of the storm track across America, which produced a persistent period of storminess affecting northern Europe. High storminess was caused by the temperature contrast between air-masses in the western Atlantic that accelerated the jet stream across the Atlantic and Europe, as well as anomalously warm ocean conditions in this region of cyclogenesis (Slingo *et al*., 2014). This demonstrates how heightened storminess can result from meridional and quasi-stationary circulation patterns as well as oceanic changes. A Met Office report on this could not prove that climate change was directly responsible (Slingo *et al*., 2014), however it is feasible that this winter weather was caused by a reduced temperature gradient as the result of Arctic warming (due to greenhouse gases) in combination with mid- and low- latitude cooling (due to solar minima).

6.7. Limitations and future research

In retrospect there are a number of limitations to the research; some of these were unavoidable and a result of limitations in available methods, whereas others could be investigated in future research. The nature of the reconstructions, particularly the lower resolution peat bog reconstructions, meant that it was unclear whether sand deposition reflected: seasonal climate changes (with possibly greater sand transport in dry summers rather than winter storms), storm frequency vs. intensity (multiple, low magnitude storms or few, extreme storms), locational factors (e.g. the influence of lakes as barriers to sand transport or variable distances of the sand sources) or vegetational changes (providing increased sand sources and caused by climatic changes or humans). These factors were addressed as far as was possible using available results and other research (e.g. pollen data and archaeological findings), however there are other potential solutions. Sand traps placed on the peat bogs, and analysed over a year or longer, may help to relate sand deposition with climate variables including wind speed and direction, precipitation and temperature. Alternatively current understanding of sand transport with wind speed and surface wetness (as briefly outlined in section 2.7.1) could be used to model sand transport inland, if forced by meterological wind, temperature and precipitation data, potentially with obstacles such as lakes added. Similarly lake dynamics could potentially be modelled to investigate the contributions of aeolian suspended sediment and inwashed material to the sediment in the centre of lakes during storms, again forced by meteorological data from the site. Process-based models such as LakeMab may be suitable for this purpose (Mooij *et al.,* 2010). These suggestions were beyond the time and financial limits of this research, but linking palaeoenvironmental and modelling approaches can provide a means of understanding and interpreting past changes (Anderson *et al.,* 2006).

Future research in this field would benefit from more high resolution storminess reconstructions from areas around the North Atlantic basin influenced by the NAO and North Atlantic storm track. Well distributed sites would help to account for possible spatial shifts of the NAO pressure cells over time (see section 1.3.2.), which is a limitation of this research, as with just two

study sites spatial shifts of the NAO (unrelated to the sign of the NAO index) cannot be identified. Furthermore regional syntheses of records would improve confidence that the observed results are due to climatic factors rather than local, possibly human, activities. In particular further reconstructions from southern Europe would be beneficial, as time and financial restraints prevented multiple sites being assessed in this project. In addition the reconstructions here are relatively short for assessing changes such as orbital and solar variability. For instance, it is possible that a comparison of longer reconstructions would show that the observed south-north storm track shift was not the result of orbital changes.

The discussion of the causes of storminess variability in this research has focused on *how* changes in the forcings resulted in storminess changes. As such the influence on the temperature gradient has been suggested frequently. Future research could therefore use temperature reconstructions from terrestrial proxies to reconstruct the latitudinal temperature gradients and then link these with storminess reconstructions that capture zonal or meridional circulation patterns. However these would need to be hemispheric averages, as regional circulation patterns like the NAO can influence some temperature reconstructions (e.g. Davis *et al.,* 2003), as was shown in section 6.5.5.

6.8. Chapter summary

In this chapter the results of storminess reconstructions from Galicia and the Outer Hebrides have been compared, integrated into a north-south storm track index and compared with other storminess and NAO reconstructions. These results, and others which capture storm track changes, indicate a transition from southerly to northerly storm track position through the Late Holocene. The period before 1800 cal yr BP appears to have had higher storminess in southern Europe at a time of reconstructed negative NAO (Olsen *et al*., 2012). Some reconstructions from high latitudes also indicate high and variable storminess at this time, which it is suggested was due to meridional circulation patterns. After c.1800 cal yr BP it is suggested that storminess gradually increased in northern Europe during a time with positive NAO (Olsen *et al*., 2012). These support a consistent NAO-storminess relationship during

the Late Holocene, however on centennial timescales negative NAO events appear to cause increased storminess in both northern and southern Europe.

The forcings on storminess from orbital, solar, oceanic and volcanic changes were considered. Overall the transition of the storm track from southern to northern Europe through the Late Holocene is thought to be due to gradual orbital changes and increased winter insolation in the low- and mid-latitudes. This is thought to have increased the meridional temperature gradient, causing a transition from meridional to zonal circulation, negative to positive NAO anomalies and a northward storm track shift. Superimposed on this long-term change were shorter variations in reconstructed storminess, which are thought to have been caused most often by solar minima. It is suggested that there was a reduced latitudinal temperature gradient and weaker and more meridional circulation of the circumpolar vortex, with the result that there was increased storminess (due to temperature contrasts between southward polar airmasses and subtropical air). These changes may have been associated with oceanic reorganisations that reinforced temperature contrasts and cyclogenesis. Internal variability such as the Atlantic Multidecadal Oscillation are likely to also have caused enhanced storminess at times. The forcing from volcanic eruptions appears minimal, at least at the age resolutions of the storminess reconstructions, aside from c.800 cal yr BP. With these forcings in mind the future storminess changes could depend on the balance between natural and anthropogenic forcing of the latitudinal temperature gradient: with orbital forcing encouraging northward storm tracks and a stronger circumpolar vortex (with more westerly airflow), but with solar forcing over the coming decades and greenhouse gases (with polar amplification of temperature) causing more meridional circulation and increased storminess.

Chapter 7: Conclusion

This research on Late Holocene storminess in Europe has had two main aims. The first was to create Late Holocene storminess reconstructions in Europe; as the Late Holocene patterns of storminess are unclear, with variations depending on the method used and the region studied. To address this aim two research questions were selected: 1) What are the patterns of storminess during the Late Holocene in northern and southern Europe? 2) Do the storminess reconstructions capture storm track changes or widespread storminess variations? The second aim was to assess the causes of storminess variability, in particular the role of the NAO. This was selected as the relationship between storminess and the NAO appears to have varied over the last 1000 years (Trouet *et al*., 2012; Dawson *et al*., 2002) and over longer timescales the causes of storminess variability are debated, with research supporting forcing from orbital (Bakke *et al*., 2008), solar (Sabatier *et al*., 2011; Wirth *et al*., 2013) and oceanic changes (Sorrel *et al*., 2012; Van Vliet-Lanoë *et al*., 2014; Fletcher *et al*., 2012). To address this aim two further research questions were selected: 3) What do the patterns of storminess and inferred storm track changes tell us about the storm-NAO relationship? 4) What do the results tell us about the causes of storminess variability?

As the relationship between storminess and the NAO was a key part of this research, the storminess reconstructions were made from two locations that have had a strong relationship between the NAO and storminess during the instrumental period (Andrade *et al.*, 2008; Trigo *et al.*, 2002; Pirazzoli *et al.*, 2010). To capture the periods when there was a southerly storm track caused by negative NAO events a storminess reconstruction was made from the Pedrido Bog site in Galicia (northwest Spain). To capture the periods when the storm track was in a northerly position, in association with dominant positive NAO anomalies, storminess reconstructions were made from three locations on the Outer Hebrides: Struban Bog (North Uist), Hill Top Bog (South Uist) and Loch Hosta (North Uist). Peat bog reconstructions were made in each location using measurements of sand content. As the bog sites are ombrotrophic in nature sand must have been deposited by aeolian transport and therefore can be used as a storminess proxy (Björck and Clemmensen, 2004; De Jong *et al*.,

2006). As lakes are influenced by both aeolian and fluvial inputs of sediments, the Loch Hosta reconstruction of storminess was the result of strong winds and high precipitation during storms.

The first research question, on the patterns of storminess in northern and southern Europe, was addressed by the results of the four reconstructions. The Struban Bog, Hill Top Bog and Pedrido Bog reconstructions all span the period since 4000 cal yr BP, thus allowing inference of storminess changes through the Late Holocene. The Loch Hosta reconstruction spanned the period since 1750 cal yr BP, and provides a precipitation-sensitive storminess reconstruction.

Two cores of sediment were sampled from Loch Hosta to make the storminess reconstruction (Chapter 3). This was made using ITRAX XRF core scanning technology, which was used to identify element changes that reflect sand content, with more traditional techniques (grain size analysis, C:N analysis and loss-on-ignition), instrumental data comparisons and element analysis of catchment sediments used to complement this interpretation. The Ln(Ca/K) results reflect influxes of shell sand into the lake, originating from both the catchment sediment and beach and machair sand. The Ln(Ca/K) of one core correlated strongly with instrumental precipitation and low pressure records, which is thought to be due to the proximity of the core to the lakes tributaries and therefore sediment deposition during storms. The reconstruction indicated that there was high storminess at 1750-950 cal yr BP and 350-50 cal yr BP.

The methodological limitations of high resolution ITRAX analysis were also investigated in Chapter 3, to establish how far sediment disturbances (e.g. from bioturbation) had degraded the ITRAX data. This was done by correlating the Ln(Ca/K) results with the instrumental data at different resolutions, to see at what resolution the maximum correlation occurred, and by identifying the highest frequency cycles present, as sediment disturbance would remove cyclical changes in the core. Furthermore as there was limited age-control, these analyses were carried out using a range of possible age-depth curves. Both the methods indicated that the optimum resolution of the ITRAX data in this lake was c.10 years, equivalent to 3-5 mm of sediment. However the sensitivity analysis showed that these results were dependent on the age-depth

model selection, for example the highest frequency cycle (c.20 years) was only present in the results using one of the tested age-depth models.

The Struban Bog and Hill Top Bog reconstructions (Chapter 4) were based on aeolian sand deposition, with two bogs used to reduce the likelihood that local human activities caused the sand peaks. Both reconstructions indicated that there was relatively low storminess until c.1500 cal yr BP followed by increasing storminess, with peaks particularly at c.900-700 and 500-200 cal yr BP. Storminess in the Outer Hebrides appears to have increased at c.3500, 2800, 2400, 1900, 1600, 1300-1100, 800 and 500 cal yrs BP. Transects of cores were analysed from across each bog to investigate the intra-bog variations in sand content. These cores were not dated however it was apparent that the trends were broadly similar between cores, but the low-magnitude, high frequency variations were different. As such only the centennial-scale changes in sand content were considered in the main cores. The inferred peaks in storminess at both sites reflected reconstructed storminess elsewhere in Scotland and northern Ireland. As there are differences in the magnitude of the peaks, it is considered that each reconstruction may be sensitive to storms from different directions, as a result of the environs of the bogs.

The Pedrido Bog reconstruction (Chapter 5) from southern Europe indicated that storminess was generally high between 4000-1800 cal yr BP, with six peaks during this time at 3900-3700, 3550-3450, 3300-3100, 2950-2650, 2550-2100 and 2000-1850 cal yr BP. After 1800 cal yr BP storminess appears to have decreased, although there may have been a small increase during the Little Ice Age, since 400 cal yr BP. That these peaks in sand were the result of anthropogenic deforestation and sediment disturbance was considered unlikely, as there were often asynchronous changes between tree-pollen declines and sand peaks, and the long-term decrease in tree pollen was not accompanied by an increase in sand influx. It was suggested instead that climatic deteriorations could have caused both peaks in storminess and abrupt vegetation declines in this highland area, the latter due to temperature drops and altered human activities. A climatic control was supported by a good correlation between the storminess reconstruction and NAO reconstructions (Trouet *et al*., 2009; Olsen *et al.,* 2012).

The second research question was: does comparison of the storminess reconstructions from northern and southern Europe reveal storm track changes or show synchronous storminess variability? In the discussion chapter (section 6.2) the results were compared and a north-south index was created using the peat bog reconstructions. High storminess indicated by the Pedrido Bog reconstruction coincided with low storminess suggested by the Outer Hebrides reconstructions until 1800 cal yr BP. During this time the peaks in reconstructed storminess in Galicia coincided with small increases in storminess in the Hill Top Bog reconstruction, that indicate there may have been simultaneous increases in storminess in northern and southern Europe. After 1500 cal yr BP the magnitude of storminess peaks in the Outer Hebridean reconstructions increased at a time of seemingly low storminess in the Pedrido reconstruction. These and the north-south index supported that the storm track was across southern Europe prior to c.1800 cal yr BP, before a northward shift towards northern Europe, particularly since 1500 cal yr BP. This shift has been mirrored in some storminess reconstructions from elsewhere in Europe, especially those that are sensitive to changes in the storm track (e.g. Bakke *et al*., 2008; Wirth *et al*., 2013; Giraudeau *et al*., 2010).

The third research question was: what do the patterns of storminess and inferred storm track changes tell us about the storm-NAO relationship? This was discussed in section 6.4. The above described storm track shift coincides with the transition from negative to positive NAO, which has recently been reconstructed (Olsen *et al*., 2013) and supports that during the Late Holocene there was a consistent relationship between the NAO and storminess. On the other hand, over centennial timescales storminess is suggested as increasing in both northern and southern Europe during negative NAO events. This has previously been suggested as occuring during the LIA as the result of a steepened temperature gradient causing storm intensification (e.g. Trouet *et al*., 2012; Raible *et al*., 2007). Finally the spectral analysis of the reconstructions showed some cycles that may have resulted from cyclicity of the NAO. The only Late Holocene NAO reconstruction has cycles of 300 and 170 years (Olsen *et al*., 2012); the 300 year cycle resembles the 290 and 330 year cycles in the Hill Top Bog reconstruction. The high resolution Loch Hosta reconstruction also showed cycles of 50-58 years, which are similar to cycles found in NAO

reconstructions, and cross-spectral analysis with the Trouet *et al.* (2009) NAO reconstruction had a significant 60-year cycle. These results therefore support that there has been an NAO influence on storminess over the Late Holocene.

The fourth research question was: what do the results tell us about the causes of storminess variability? This was discussed in section 6.5., where the influence from orbital, solar, oceanic and volcanic forcing on storminess was considered. The influence of each of these forcings on the latitudinal temperature gradient was assessed, as this drives the zonal or meridional nature of the circumpolar vortex and thus the storm track position and NAO index. It is considered that changes in the latitudinal insolation receipt caused by orbital changes can explain the inferred northward storm track shift through the Late Holocene, as also suggested by Bakke *et al*. (2008). Increasing winter insolation at low- and mid- latitudes could have gradually increased the latitudinal temperature gradient, resulting in stronger zonal airflow and northward storm tracks (Barry and Chorley, 2010; Lamb, 1995; Walter and Graf, 2005).

Superimposed on this long-term storm track shift are variations in storminess. Spectral analysis was carried out on each storminess reconstruction, as cycles can be a means of identifying the forcings behind climate variations (Gray *et al*., 2010). Many of the reconstructions had solar cycles. The Pedrido Bog in particular had cycles of 2050, 510 and 220 years, all of which are recognised in solar reconstructions (Stuiver and Braziunas, 1989; Steinhilber *et al*., 2012). Comparison with reconstructions of solar activity (Steinhilber *et al*., 2012) indicated that peaks in storminess in both the southern and northern Europe reconstructions often coincide with solar minima. Therefore reduced solar radiation during winter may have reduced the latitudinal temperature gradient, causing more meridional circulation patterns. These are associated with quasi-stationary pressure systems (causing persistent weather conditions) and southwardly displaced storm tracks, which not only cause storms to occur further south but also produce large temperature contrasts between airmasses that encourage cyclogenesis (Barry and Chorley, 2010; Lamb, 1995; Van Vliet-Lanoë *et al*., 2014; Betts *et al*., 2004).

The solar changes also coincide with some periods of reconstructed weaker North Atlantic circulation and southward shifts of polar water (Bond *et al*., 2001). It is speculated that the resulting increased temperature contrasts may have further increased cyclogenesis and storm intensity (Van Vliet-Lanoë *et al*., 2014; Betts *et al*., 2004). The forcing from the Atlantic Multidecadal Oscillation was indicated by the presence of 50-58 and 77-87 year cycles in the Loch Hosta reconstruction, as well as by visual comparison with an AMO reconstruction. Previous research suggests that positive AMO conditions (warm oceans) encourage cyclogenesis and more intense storms (Van Vliet-Lanoë *et al*., 2014; Betts *et al*., 2004; Knight *et al*., 2006) and this is supported by comparison with the Loch Hosta reconstruction, especially during the LIA period. Therefore this appears to be a mechanism of internal ocean variability (Wei and Lohmann, 2012) that influences storminess. Furthermore as the AMO is a multi-decadal cycle, it may have immediate implications for future storminess.

In summary: over millennial time-periods orbital forcing is suggested as causing a northward shift in storminess (more zonal airflow). Over decadal to centennial time-scales it is suggested that solar minima cause greater storminess across Europe, as reduced temperature gradients cause meridional circulation of the circumpolar vortex and negative NAO anomalies, causing southward storm track excursions and greater storm intensities. As well as this increased storminess appear influenced by variations in ocean temperature that cause temperature contrasts and therefore increased cyclogenesis.

In the future it has been predicted that global warming will cause more meridional and persistent circulation patterns, due to a reduced temperature gradient caused by amplified high latitude warming (Francis and Vavrus, 2013). This prediction is supported by the findings of this research, as speculated reductions in the temperature gradient during the Late Holocene that have occurred from natural forcings (solar minima) appear to have caused increased storminess in Europe. Therefore future changes to the temperature gradient may cause increased storminess in Europe, with more frequent stormy winters (such as that of 2013-2014).

Bibliography

Aagaard, T., Orford, J. and Murray, A. S. (2007) Environmental controls on coastal dune formation; Skallingen Spit, Denmark. *Geomorphology,* 83**:** 29-47.

aemet (2014) *Standard climate variables, Santiago de Compostela Aeropuerto*. Accessed 07/02/2014. <http://www.aemet.es/en/serviciosclimaticos/datosclimatologicos/valoresclimatologicos?l=1428&k=gal>

Abrantes, F. T., Rodrigues, T., Montanari, B., Santos, C., Witt, L., Lopes, C. and Voelker, A. H. (2011) Climate of the last millennium at the southern pole of the North Atlantic Oscillation: an inner-shelf sediment record of flooding and upwelling. *Climate Research,* 48**:** 261-280.

Agnihotri, R., Dutta, K., Bhushan, R. and Somayajulu, B. (2002) Evidence for solar forcing on the Indian monsoon during the last millennium. *Earth and Planetary Science Letters,* 198**:** 521-527.

Aguado, E. and Burt, J. (2013) *Understanding weather and climate,* Boston, Pearson.

Alexander, L. V., Tett, S. F. B. and Jonsson, T. (2005) Recent observed changes in severe storms over the United Kingdom and Iceland. *Geophysical Research Letters,* 32**:** L13704.

Alexander, M. A. and Deser, C. (1995) A Mechanism for the Recurrence of Wintertime Midlatitude SST Anomalies. *Journal of Physical Oceanography,* 25**:** 122-137.

Alexandersson, H., Schmith, T., Iden, K. and Tuomenvirta, H. (1998) Long-term variations of the storm climate over NW Europe. *The Global Atmosphere and Ocean System,* 6**:** 97-120.

Alexandersson, H., Tuomenvirta, H., Schmith, T. and Iden, K. (2000) Trends of storms in northwest Europe derived from an updated pressure data set. *Climate Research,* 14**:** 71-73.

Allan, M., Le Roux, G., Piotrowska, N., Beghin, J., Javaux, E., Court-Picon, M., Mattielli, N., Verheyden, S. and Fagel, N. (2013) Mid- and late Holocene dust deposition in western Europe: the Misten peat bog (Hautes Fagnes andndash; Belgium). *Climate of the Past,* 9**:** 2285-2298.

Allan, R., Tett, S. and Alexander, L. (2009) Fluctuations in autumn–winter severe storms over the British Isles: 1920 to present. *International Journal of Climatology,* 29**:** 357-371.

Alley, R. B. (2004) GISP2 ice core temperature and accumulation data. *IGBP PAGES/World Data Center for Paleoclimatology.* NOAA/NGDC Paleoclimatology Program.

Ãlvarez, M., Flores, J. A., Sierro, F. J., Diz, P., Francés, G., Pelejero, C. and Grimalt, J. (2005) Millennial surface water dynamics in the Ría de Vigo during the last 3000 years as revealed by coccoliths and molecular biomarkers. *Palaeogeography, Palaeoclimatology, Palaeoecology,* 218**:** 1-13.

Anderson, D., E. (1998) A reconstruction of Holocene climatic changes from peat bogs in north-west Scotland. *Boreas,* 27**:** 208-224.

Anderson, N. J., Bugmann, H., Dearing, J. A. and Gaillard, M.-J. (2006) Linking palaeoenvironmental data and models to understand the past and to predict the future. *Trends in Ecology and Evolution,* 21**:** 696-704.

Anderson, R. S. (1987) A theoretical model for aeolian impact ripples. *Sedimentology,* 34**,** 943-956.

Andersson, S., Rosqvist, G., Leng, M. J., Wastegård, S. and Blaauw, M. (2010) Late Holocene climate change in central Sweden inferred from lacustrine stable isotope data. *Journal of Quaternary Science,* 25**:** 1305-1316.

Andrade, C., Santos, J. O. A., Pinto, J. G. and Corte-Real, J. O. (2011) Large-scale atmospheric dynamics of the wet winter 2009-2010 and its impact on hydrology in Portugal. *Climate Research,* 46**:** 29-41.

Andrade, C., Trigo, R. M., Freitas, M. C., Gallego, M. C., Borges, P. and Ramos, A. M. (2008) Comparing historic records of storm frequency and the North Atlantic Oscillation (NAO) chronology for the Azores region. *Holocene,* 18**:** 745-754.

Andresen, C. S., Bond, G., Kuijpers, A., Knutz, P. C. and Björck, S. (2005) Holocene climate variability at multidecadal time scales detected by sedimentological indicators in a shelf core NW off Iceland. *Marine Geology,* 214**:** 323-338.

Angell, J. K. (2006) Changes in the 300-mb North Circumpolar Vortex, 1963-2001. *Journal of Climate,* 19: 2984-2994.

Angus, S. (1997) *The Outer Hebrides/The Shaping of the Islands,* England, The White Horse Press.

Angus, S., and Elliot, M. M. (1992) Erosion in Scottish Machair with particular reference to the Outer Hebrides. In Carter, R. W. G., Curtis, T. G. F., and Sheehy-Skeffington, M., J. (eds) *Coastal Dunes*. Balkema: 93-117.

Appenzeller, C., Schwander, J., Sommer, S. and Stocker, T. F. (1998) The North Atlantic Oscillation and its imprint on precipitation and ice accumulation in Greenland. *Geophysical Research Letters,* 25**:** 1939-1942.

Appleby, P. (2001) Chronostratigraphic techniques in recent sediments. In Last, W. And Smol, J. (eds) *Tracking environmental change using lake sediments, volume 1: basin analysis, coring and chronological techniques.* Kluwer Academic Publishers, Dordrecht: 171-203.

Appleby, P. G. and Oldfield, F. (1978) The calculation of lead-210 dates assuming a constant rate of supply of unsupported ^{210}Pb to the sediment. *CATENA,* 5**:** 1-8.

Arens, S. (1996) Rates of aeolian transport on a beach in a temperate humid climate. *Geomorphology,* 17**:** 3-18.

Ashmore, P., Brayshay, B., Edwards, K. J., Gilbertson, D., Grattan, J., Kent, M., Pratt, K. and Weaver, R. (2000) Allochthonous and autochthonous mire deposits, slope instability and palaeoenvironmental investigations in the Borve Valley, Barra, Outer Hebrides, Scotland. *The Holocene,* 10**:** 97-108.

Association of British Insurers (2003) The vulnerability of U.K. property to windstorm damage. London.

Bücher, A. and Lucas, C. (1984) Sédimentation éolienne intercontinentale, poussiéres sahariennes et géologie. *Bulletin des Centres de Recherches Exploration-Production Elf-Aquitaine,* 8**:** 151-165.

Bagnold, R. A. (1937) The Transport of Sand by Wind. *The Geographical Journal,* 89**:** 409-438.

Bahnson, H. (1972) Spor af muldflugt i keltisk jernalder pavist i hojmoseprofiler. *Danmarks Geologiska Undersogelse***:** 7-12.

Bakke, J., Lie, Ø., Dahl, S. O., Nesje, A. and Bjune, A. E. (2008) Strength and spatial patterns of the Holocene wintertime westerlies in the NE Atlantic region. *Global and Planetary Change,* 60**:** 28-41.

Baldwin, M. P. and Dunkerton, T. J. (1999) Propagation of the Arctic Oscillation from the stratosphere to the troposphere. *Journal of Geophysical. Research,* 104**:** 30937-30946.

Baldwin, M. P. and Dunkerton, T. J. (2001) Stratospheric Harbingers of Anomalous Weather Regimes. *Science,* 294**:** 581-584.

Bamber, R. N. (1982) Sodium hexametaphosphate as an aid in benthic sample sorting. *Marine Environmental Research,* 7**:** 251-255.

Bao, K., Xing, W., Yu, X., Zhao, H., Mclaughlin, N., Lu, X. and Wang, G. (2012) Recent atmospheric dust deposition in an ombrotrophic peat bog in Great Hinggan Mountain, Northeast China. *Science of the Total Environment,* 431**:** 33-45.

Bao, R., Alonso, A., Delgado, C. and Pagés, J. L. (2007) Identification of the main driving mechanisms in the evolution of a small coastal wetland (Traba, Galicia, NW Spain) since its origin 5700 cal yr BP. *Palaeogeography, Palaeoclimatology, Palaeoecology,* 247**:** 296-312.

Barnston, A. G. and Livezey, R. E. (1987) Classification, seasonality and persistence of low-frequency atmospheric circulation patterns. *Monthly Weather Review,* 115**:** 1083-1126.

Bärring, L. and Fortuniak, K. (2009) Multi-indices analysis of southern Scandinavian storminess 1780–2005 and links to interdecadal variations in the NW Europe – North Sea region. *International Journal of Climatology,* 29**:** 373-384.

Barry, R. G. and Chorley, R. J. (2010) *Atmosphere, weather and climate*, Routledge.

Bengtsson, L., Hellström, T. and Rakoczi, L. (1990) Redistribution of sediments in three Swedish lakes. *Hydrobiologia,* 192**:** 167-181.

Bengtsson, L., Hodges, K. I. and Roeckner, E. (2006) Storm tracks and climate change. *Journal of Climate,* 19**:** 3518-3543.

Benito, G., Machado, M. J. and Pérez-González, A. (1996) Climate change and flood sensitivity in Spain. *Geological Society, London, Special Publications,* 115**:** 85-98.

Benito, G., Thorndycraft, V., Rico, M., Sánchez-Moya, Y. and Sopeña, A. (2008) Palaeoflood and floodplain records from Spain: evidence for long-term climate variability and environmental changes. *Geomorphology,* 101**:** 68-77.

Bennett, K., Fossitt, J., Sharp, M. and Switsur, V. (1990) Holocene vegetational and environmental history at Loch Lang, South Uist, Western Isles, Scotland. *New Phytologist,* 114**:** 281-298.

Berger, A. and Loutre, M.-F. (1991) Insolation values for the climate of the last 10 million years. *Quaternary Science Reviews,* 10**:** 297-317.

Bernárdez, P., González-Álvarez, R., Francés, G., Prego, R., Bárcena, M. and Romero, O. E. (2008) Late Holocene history of the rainfall in the NW Iberian peninsula: Evidence from a marine record. *Journal of Marine Systems,* 72**:** 366-382.

Betts, N., Orford, J., White, D. and Graham, C. (2004) Storminess and surges in the south-western approaches of the eastern North Atlantic: the synoptic climatology of recent extreme coastal storms. *Marine Geology,* 210**:** 227-246.

Bianchi, G. and Mccave, I., N. (1999) Holocene periodicity in North Atlantic climate and deep-ocean flow south of Iceland. *Nature,* 397**:** 515-517.

Billeaud, I., Tessier, B. and Lesueur, P. (2009) Impacts of late Holocene rapid climate changes as recorded in a macrotidal coastal setting (Mont-Saint-Michel Bay, France). *Geology,* 37**:** 1031-1034.

Bindler, R., Klarqvist, M., Klaminder, J. and Förster, J. (2004) Does within-bog spatial variability of mercury and lead constrain reconstructions of absolute deposition rates from single peat records? The example of Store Mosse, Sweden. *Global Biogeochemical Cycles,* 18: GB3020.

Birse, E. L. (1971) *Assessment of Climatic Conditions in Scotland: The Bioclimatic Subregions Map and Explanatory Pamphlet*, Macaulay Institute for Soil Research.

Bjerknes, J. and Solberg, H. (1922) *Life cycle of cyclones and the polar front theory of atmospheric circulation*, Grondahl.

Björck, S. and Clemmensen, L., B. (2004) Aeolian sediment in raised bog deposits, Halland, SW Sweden: a new proxy record of Holocene winter storminess variation in Southern Scandinavia? *The Holocene,* 14**:** 677-688.

Blindheim, J., Borovkov, V., Hansen, B., Malmberg, S. A., Turrell, W. R. and Østerhus, S. (2000) Upper layer cooling and freshening in the Norwegian Sea in relation to atmospheric forcing. *Deep Sea Research Part I: Oceanographic Research Papers,* 47**:** 655-680.

Boberg, F. and Lundstedt, H. (2002) Solar wind variations related to fluctuations of the North Atlantic Oscillation. *Geophysical Research Letters,* 29 (15): 1718.

Bond, G., Kromer, B., Beer, J., Muscheler, R., Evans, M. N., Showers, W., Hoffmann, S., Lotti-Bond, R., Hajdas, I. and Bonani, G. (2001) Persistent Solar Influence on North Atlantic Climate During the Holocene. *Science,* 294**:** 2130-2136.

Bond, G., Showers, W., Cheseby, M., Lotti, R., Almasi, P., Demenocal, P., Priore, P., Cullen, H., Hajdas, I. and Bonani, G. (1997) A Pervasive

Millennial-Scale Cycle in North Atlantic Holocene and Glacial Climates. *Science,* 278**:** 1257-1266.

Boorman, L., A. (1993) Dry coastal ecosystems of Britain: dunes and shingle beaches. In Van Der Maarel, E. (Ed.) *Dry Coastal Ecosystems.* Amsterdam, Elsevier: 197-228.

Booth, J. F., Thompson, L., Patoux, J. R. M. and Kelly, K. A. (2012) Sensitivity of Midlatitude Storm Intensification to Perturbations in the Sea Surface Temperature near the Gulf Stream. *Monthly Weather Review,* 140**:** 1241-1256.

Boyd, J. M. and Boyd, I. L. (1990) *The Hebrides: a natural history*, Harper Collins.

Braconnot, P., Harrison, S. P., Kageyama, M., Bartlein, P. J., Masson-Delmotte, V., Abe-Ouchi, A., Otto-Bliesner, B. and Zhao, Y. (2012) Evaluation of climate models using palaeoclimatic data. *Nature Climate Change,* 2**:** 417-424.

Bragg, O. M. (2002) Hydrology of peat-forming wetlands in Scotland. *Science of the Total Environment,* 294**:** 111-129.

Brayshaw, D., Hoskins, B. and Black, E. (2010) Some physical drivers of changes in the winter storm tracks over the North Atlantic and Mediterranean during the Holocene. *Philosophical Transactions of the Royal Society A: Mathematical, Physical and Engineering Science,* 368**:** 5185-5223.

Bretherton, C. S. and Battisti, D. S. (2000) An interpretation of the results from atmospheric general circulation models forced by the time history of the observed sea surface temperature distribution. *Geophysical Research Letters,* 27**:** 767-770.

Canmore.rchams (2014). *North Uist, Loch Hosta, Baleloch*. Accessed 08/03/2014 <http://canmore.rcahms.gov.uk/en/site/10109/details/north+uist+loch+hosta+baleloch/>

Carr, P. (1993) *The Night of the Big Wind,* Belfast, White Row Press.

Cassou, C. (2010) The North Atlantic Oscillation: mechanisms and spatio-temporal variability. *Iceland in the central northern Atlantic: hotspots, sea currents and climate change.* Plouzane, France.

Cassou, C., Deser, C. and Alexander, M. A. (2007) Investigating the impact of reemerging sea surface temperature anomalies on the winter atmospheric circulation over the North Atlantic. *Journal of Climate,* 20**:** 3510-3526.

Cassou, C., Deser, C., Terray, L., Hurrell, J. W. and Drevillon, M. (2004a) Summer sea surface temperature conditions in the North Atlantic and their impact upon the atmospheric circulation in early winter. *Journal of Climate,* 17**:** 3349-3363.

Cassou, C., Terray, L., Hurrell, J. W. and Deser, C. (2004b) North Atlantic winter climate regimes: Spatial asymmetry, stationarity with time, and oceanic forcing. *Journal of Climate,* 17**:** 1055-1068.

Casty, C., Handorf, D. R., Raible, C., González-Rouco, J., Weisheimer, A., Xoplaki, E., Luterbacher, J., Dethloff, K. and Wanner, H. (2005) Recurrent climate winter regimes in reconstructed and modelled 500 hPa geopotential height fields over the North Atlantic/European sector 1659-1990. *Climate Dynamics,* 24**:** 809-822.

Cattaneo, A. and Steel, R. J. (2003) Transgressive deposits: a review of their variability. *Earth Science Reviews,* 62**:** 187-228.

Cattiaux, J., Vautard, R., Cassou, C., Yiou, P., Masson-Delmotte, V. and Codron, F. (2010) Winter 2010 in Europe: A cold extreme in a warming climate. *Geophysical Research Letters,* 37**,** 6: L20704.

Catto, J. L., Shaffrey, L. C. and Hodges, K. I. (2011) Northern Hemisphere extratropical cyclones in a warming climate in the HiGEM high-resolution climate model. *Journal of Climate,* 24**:** 5336-5352.

Chambers, F., Beilman, D. and Yu, Z. (2011) Methods for determining peat humification and for quantifying peat bulk density, organic matter and carbon content for palaeostudies of climate and peatland carbon dynamics. *Mires and Peat,* 7**:** 1-10.

Chapman, M. R. and Shackleton, N. J. (2000) Evidence of 550-year and 1000-year cyclicities in North Atlantic circulation patterns during the Holocene. *The Holocene,* 10**:** 287-291.

Charman, D. J. (2010) Centennial climate variability in the British Isles during the mid-late Holocene. *Quaternary Science Reviews,* 29**:** 1539-1554.

Charman, D. J., Caseldine, C., Baker, A., Gearey, B., Hatton, J. and Proctor, C. (2001) Paleohydrological Records from Peat Profiles and Speleothems in Sutherland, Northwest Scotland. *Quaternary Research,* 55**:** 223-234.

Chatfield, C. (2004) *The Analysis of Timeseries: An Introduction. ,* Florida, CRC Press.

Chepil, W. (1956) Influence of moisture on erodibility of soil by wind. *Soil Science Society of America Journal,* 20**:** 288-292.

Christensen, E. R. (1982) A model for radionuclides in sediments influenced by mixing and compaction. *Journal of Geophysical Research: Oceans,* 87**:** 566-572.

Chylek, P., Box, J. E. and Lesins, G. (2004) Global warming and the Greenland ice sheet. *Climatic Change,* 63**:** 201-221.

Clarke, M., Rendell, H., Tastet, J.-P., Clave, B. and Masse, L. (2002) Late-Holocene sand invasion and North Atlantic storminess along the Aquitaine Coast, southwest France. *The Holocene,* 12**:** 231-238.

Clarke, M. L. and Rendell, H. M. (2006) Effects of storminess, sand supply and the North Atlantic Oscillation on sand invasion and coastal dune accretion in western Portugal. *The Holocene,* 16**:** 341-355.

Clarke, M. L. and Rendell, H. M. (2009) The impact of North Atlantic storminess on western European coasts: A review. *Quaternary International,* 195**:** 31-41.

Clemmensen, L. B., Murray, A., Heinemeier, J. and De Jong, R. (2009) The evolution of Holocene coastal dunefields, Jutland, Denmark: A record of climate change over the past 5000 years. *Geomorphology,* 105**:** 303-313.

Climate Research Unit, University of East Anglia. (2004) *North Atlantic Oscillation data.* Accessed 10/01/14. <http://www.cru.uea.ac.uk/cru/data/nao/>

Coggins, A., Jennings, S. and Ebinghaus, R. (2006) Accumulation rates of the heavy metals lead, mercury and cadmium in ombrotrophic peat lands in the west of Ireland. *Atmospheric Environment,* 40**:** 260-278.

Cohen, J. and Barlow, M. (2005) The NAO, the AO, and global warming: How closely related? *Journal of Climate,* 18**:** 4498-4513.

Cook, E. R., D'arrigo, R. D. and Briffa, K. R. (1998) A reconstruction of the North Atlantic Oscillation using tree-ring chronologies from North America and Europe. *Holocene,* 8**:** 9-17.

Cook, E. R., D'arrigo, R. D. and Mann, M. E. (2002) A well-verified, multiproxy reconstruction of the winter North Atlantic Oscillation index since AD 1400. *Journal of Climate,* 15**:** 1754-1764.

Copard, K., Colin, C., Henderson, G., Scholten, J., Douville, E., Sicre, M.-A. and Frank, N. (2012) Late Holocene intermediate water variability in the northeastern Atlantic as recorded by deep-sea corals. *Earth and Planetary Science Letters,* 313**:** 34-44.

Costas, S., Jerez, S., Trigo, R. M., Goble, R. and Rebêlo, L. (2012) Sand invasion along the Portuguese coast forced by westerly shifts during cold climate events. *Quaternary Science Reviews,* 42**:** 15-28.

Croci-Maspoli, M., Schwierz, C. and Davies, H. (2007) Atmospheric blocking: space-time links to the NAO and PNA. *Climate Dynamics,* 29**:** 713-725.

Croudace, I. W., Rindby, A. and Rothwell, R. G. (2006) ITRAX: description and evaluation of a new multi-function X-ray core scanner. *Geological Society, London, Special Publications,* 267**:** 51-63.

Crowley, T. J. (2000) Causes of Climate Change Over the Past 1000 Years. *Science,* 289**,** 270-277.

Crowley, T. J. and Unterman, M. B. (2012) Technical details concerning development of a 1200-yr proxy index for global volcanism. *Earth System Science Data Discussions.,* 5**:** 1-28.

Cullen, H. M., D'arrigo, R. D., Cook, E. R. and Mann, M. E. (2001) Multiproxy reconstructions of the North Atlantic Oscillation. *Paleoceanography,* 16**:** 27-39.

Curry, R. G. and McCartney, M. S. (2001) Ocean gyre circulation changes associated with the North Atlantic Oscillation. *Journal of Physical Oceanography,* 31: 3374-3400.

Czymzik, M., Brauer, A., Dulski, P., Plessen, B., Naumann, R., Von Grafenstein, U. and Scheffler, R. (2013) Orbital and solar forcing of shifts in Mid-to Late Holocene flood intensity from varved sediments of pre-alpine Lake Ammersee (southern Germany). *Quaternary Science Reviews,* 61**:** 96-110.

D'arrigo, R. D., Cook, E. R., Jacoby, G. C. and Briffa, K. R. (1993) Nao and sea surface temperature signatures in tree-ring records from the North Atlantic sector. *Quaternary Science Reviews,* 12**:** 431-440.

D'odorico, P., Yoo, J. C. and Jaeger, S. (2002) Changing Seasons: An Effect of the North Atlantic Oscillation? *Journal of Climate,* 15**:** 435-445.

Damon, P. E. and Sonett, C. P. (1991) Solar and terrestrial components of the atmospheric C^{14} variation spectrum. *The Sun in Time.*

Davis, B., Brewer, S., Stevenson, A. and Guiot, J. (2003) The temperature of Europe during the Holocene reconstructed from pollen data. *Quaternary Science Reviews,* 22**:** 1701-1716.

Davis, R. E. and Benkovic, S. R. (1994) Spatial and temporal variations of the January circumpolar vortex over the northern hemisphere. *International Journal of Climatology,* 14**:** 415-428.

Davison, W. (1993) Iron and manganese in lakes. *Earth-Science Reviews*, 34: 119-163.

Dawson, A., Elliott, L., Noone, S., Hickey, K., Holt, T., Wadhams, P. and Foster, I. (2004) Historical storminess and climate 'see-saws' in North Atlantic region. *Marine Geology,* 210**:** 247-259.

Dawson, A. G., Dawson, S. and Ritchie, W. (2007) Historical climatology and coastal change associated with the “Great Storm” of January 2005, South Uist and Benbecula, Scottish Outer Hebrides. *Scottish Geographical Journal,* 123**:** 135-149.

Dawson, A. G., Elliott, L., Mayewski, P., Lockett, P., Noone, S., Hickey, K., Holt, T., Wadhams, P. and Foster, I. (2003) Late-Holocene North Atlantic climate 'seesaws', storminess changes and Greenland ice sheet (GISP2) palaeoclimates. *Holocene,* 13**:** 381-392.

Dawson, A. G., Hickey, K., Holt, T., Elliott, L., Dawson, S., Foster, I. D. L., Wadhams, P., Jonsdottir, I., Wilkinson, J., Mckenna, J., Davis, N. R. and Smith, D. E. (2002) Complex North Atlantic Oscillation (NAO) Index signal of historic North Atlantic storm-track changes. *The Holocene,* 12**:** 363-369.

De Jong, R., Björck, S., Björkman, L. and Clemmensen, L. B. (2006) Storminess variation during the last 6500 years as reconstructed from an ombrotrophic peat bog in Halland, southwest Sweden. *Journal of Quaternary Science,* 21**:** 905-919.

De Jong, R., Hammarlund, D. and Nesje, A. (2009) Late Holocene effective precipitation variations in the maritime regions of south-west Scandinavia. *Quaternary Science Reviews,* 28**:** 54-64.

De Jong, R., Kamenik, C. and Grosjean, M. (2013) Cold-season temperatures in the European Alps during the past millennium: variability, seasonality and recent trends. *Quaternary Science Reviews,* 82**:** 1-12.

De Jong, R., Schoning, K. and Björck, S. (2007) Increased aeolian activity during humidity shifts as recorded in a raised bog in south-west Sweden during the past 1700 years. *Climate of the Past,* 3**:** 411-422.

De Vleeschouwer, F., Le Roux, G. and Shotyk, W. (2010) Peat as an archive of atmospheric pollution and environmental change: A case study of lead in Europe. *The Holocene,* 51**:** 11-19.

Dean, W. E. (1974) Determination of carbonate and organic matter in calcareous sediments and sedimentary rocks by loss on ignition;

comparison with other methods. *Journal of Sedimentary Research,* 44**:** 242-248.

Debret, M., Bout-Roumazeilles, V., Grousset, F., Desmet, M., Mcmanus, J., Massei, N., Sebag, D., Petit, J.-R., Copard, Y. and Trentesaux, A. (2007) The origin of the 1500-year climate cycles in Holocene North Atlantic records. *Climate of the Past,* 3**:** 679-692.

Defoe, D. (1704) *The storm: a collection of the most remarkable casualties and disasters which happened in the late dreadful tempest both by sea and land*.

Denton, G. H. and Karlén, W. R. (1973) Holocene climatic variations - their pattern and possible cause. *Quaternary Research,* 3**:** 155-205.

Desprat, S. P., Sánchez Goñi, M. Ì. A. F. and Loutre, M.-F. (2003) Revealing climatic variability of the last three millennia in northwestern Iberia using pollen influx data. *Earth and Planetary Science Letters,* 213**:** 63-78.

Devoy, R. J. N., Delaney, C., Carter, R. W. G. and Jennings, S. C. (1996) Coastal Stratigraphies as Indicators of Environmental Changes upon European Atlantic Coasts in the Late Holocene. *Journal of Coastal Research,* 12**:** 564-588.

Dezileau, L., Sabatier, P., Blanchemanche, P., Joly, B., Swingedouw, D., Cassou, C., Castaings, J., Martinez, P. and Von Grafenstein, U. (2011) Intense storm activity during the Little Ice Age on the French Mediterranean coast. *Palaeogeography, Palaeoclimatology, Palaeoecology,* 299**:** 289-297.

Diaz, H. F., Trigo, R., Hughes, M. K., Mann, M. E., Xoplaki, E. and Barriopedro, D. (2011) Spatial and Temporal Characteristics of Climate in Medieval Times Revisited. *Bulletin of the American Meteorological Society,* 92: 1487-1500.

Díaz Varela, R., Ramil Rego, P., Calvo Iglesias, S. and Muñoz Sobrino, C. (2008) Automatic habitat classification methods based on satellite images: A practical assessment in the NW Iberia coastal mountains. *Environmental Monitoring and Assessment,* 144**:** 229-250.

Dittrich, M. and Obst, M. (2004) Are picoplankton responsible for calcite precipitation in lakes? *AMBIO: A Journal of the Human Environment,* 33**:** 559-564.

Diz, P., Francés, G., Pelejero, C., Grimalt, J. O. and Vilas, F. (2002) The last 3000 years in the Ría de Vigo (NW Iberian Margin): climatic and hydrographic signals. *The Holocene,* 12**,** 459-468.

Dugmore, A. J., Larsen, G. R. N. and Newton, A. J. (1995) Seven tephra isochrones in Scotland. *The Holocene,* 5**:** 257-266.

Dugmore, A. J. and Newton, A. J. (1992) Thin tephra layers in peat revealed by X-radiography. *Journal of Archaeological Science,* 19**:** 163-170.

Dylmer, C. V., Giraudeau, J., Eynaud, F., Husum, K. and De Vernal, A. (2013) Northward advection of Atlantic water in the eastern Nordic Seas over the last 3000 yr: a coccolith investigation of volume transport and surface water changes. *Climate of the Past,* 9**:** 1259-1295.

Ekman, V. W. (1905) On the influence of the earth's rotation on ocean currents. *Arkiv For Matematik, Astronomi och Fysik.,* 2**:** 1-53.

Enfield, D. B., Mestas-Nuñez, A. M. and Trimble, P. J. (2001) The Atlantic multidecadal oscillation and its relation to rainfall and river flows in the continental US. *Geophysical Research Letters,* 28**:** 2077-2080.

Esper, J., Frank, D., Büntgen, U., Verstege, A., Luterbacher, J. R. and Xoplaki, E. (2007) Long-term drought severity variations in Morocco. *Geophysical Research Letters,* 34: L17702.

Fábregas Valcarce, R., Martínez Cortizas, A., Blanco Chao, R. and Chesworth, W. (2003) Environmental change and social dynamics in the second-third millennium BC in NW Iberia. *Journal of Archaeological Science,* 30**:** 859-871.

Faegri, K. and Iversen, J. (1950) Text-book of modern pollen analysis. *GFF,* 72**:** 363-364.

Feser, F., Barcikowska, M., Krueger, O., Schenk, F., Weisse, R. and Xia, L. (2014). Storminess over the North Atlantic and northwestern Europe—A review. *Quarterly Journal of the Royal Meteorological Society*.

Fischer-Bruns, I., Von Storch, H., Gonzãlez-Rouco, J. and Zorita, E. (2005) Modelling the variability of midlatitude storm activity on decadal to century time scales. *Climate Dynamics,* 25**:** 461-476.

Fischer, E. M., Luterbacher, J., Zorita, E., Tett, S. F. B., Casty, C. and Wanner, H. (2007) European climate response to tropical volcanic eruptions over the last half millennium. *Geophysical Research Letters,* 34**:** L05707.

Fischer, H. and Mieding, B. (2005) A 1,000-year ice core record of interannual to multidecadal variations in atmospheric circulation over the North Atlantic. *Climate Dynamics,* 25**:** 65-74.

Fletcher, W. J., Debret, M. and Goni, M. F. S. (2013) Mid-Holocene emergence of a low-frequency millennial oscillation in western Mediterranean climate: Implications for past dynamics of the North Atlantic atmospheric westerlies. *The Holocene,* 23**:** 153-166.

Flohn, H. (1984) Climatic belts in the case of a unipolar glaciation. *Climatic Changes on a Yearly to Millennial Basis.* Springer.

Flynn, W. (1968) The determination of low levels of polonium-210 in environmental materials. *Analytica chimica acta,* 43**:** 221-227.

Forchhammer, M. C., Post, E. and Stenseth, N. C. H. R. (2002) North Atlantic Oscillation timing of long- and short-distance migration. *Journal of Animal Ecology,* 71**:** 1002-1014.

Fossitt, J. A. (1996) Late Quaternary vegetation history of the Western Isles of Scotland. *New Phytologist,* 132**:** 171-196.

Fraga, M., Romero-Pedreira, D., Souto, M., Castro, D. and Sahuquillo, E. (2008) Assessing the impact of wind farms on the plant diversity of blanket bogs in the Xistral Mountains (NW Spain). *Mire and Peat,* 4.

Francis, J. A. and Vavrus, S. J. (2012) Evidence linking Arctic amplification to extreme weather in mid-latitudes. *Geophysical Research Letters,* 39**:** L06801.

Frauenfeld, O. W. and Davis, R. E. (2003) Northern Hemisphere circumpolar vortex trends and climate change implications. *Journal of Geophysical Research: Atmospheres,* 108**:** 4423.

García, N., Gimeno, L., De La Torre, L., Nieto, R. and Añel, J. (2005) North Atlantic Oscillation (NAO) and precipitation in Galicia (Spain). *Atmósfera,* 18**:** 25-32.

Garrow, D. and Sturt, F. (2011) Grey waters bright with Neolithic argonauts? Maritime connections and the Mesolithic-Neolithic transition within the “western seaways” of Britain, c. 5000-3500 BC. *Antiquity,* 85**:** 59-72.

Giguet-Covex, C., Arnaud, F., Poulenard, J. R. M., Disnar, J.-R., Delhon, C., Francus, P., David, F., Enters, D., Rey, P.-J. R. M. and Delannoy, J.-J. (2011) Changes in erosion patterns during the Holocene in a currently treeless subalpine catchment inferred from lake sediment geochemistry (Lake Anterne, 2063 m a.s.l., NW French Alps): The role of climate and human activities. *The Holocene,* 21**:** 651-665.

Gilbertson, D. D., Schwenninger, J., Kemp, R. and Rhodes, E. (1999) Sand-drift and Soil Formation Along an Exposed North Atlantic Coastline: 14,000 Years of Diverse Geomorphological, Climatic and Human Impacts. *Journal of Archaeological Science,* 26**:** 439-469.

Gillette, D. A. (1981) Production of dust that may be carried great distances. *Desert dust: Origin, characteristics, and effect on man,* 186**:** 11-26.

Gilli, A., Ariztegui, D., Anselmetti, F. S., Mckenzie, J. A., Markgraf, V., Hajdas, I. and Mcculloch, R. D. (2005) Mid-Holocene strengthening of the southern westerlies in South America - sedimentological evidences from Lago Cardiel, Argentina (49ºS). *Global and Planetary Change,* 49**:** 75-93.

Giot, P.-R. (1998) La dune ancienne de la baie d'Audierne. *Norois,* 179**:** 487-494.

Giraudeau, J., Grelaud, M., Solignac, S., Andrews, J. T., Moros, M. and Jansen, E. (2010) Millennial-scale variability in Atlantic water advection to the Nordic Seas derived from Holocene coccolith concentration records. *Quaternary Science Reviews,* 29**:** 1276-1287.

Girs, A. (1974) Macro-Circulation Method of Long-Term Meteorological Forecasts. *Leningrad, Gidrometeoizdat,* 485.

Gleisner, H. and Thejll, P. (2003) Patterns of tropospheric response to solar variability. *Geophysical Research Letters,* 30: 1711.

Glentworth, R. (1979) Observations on the soils of the Outer Hebrides. *Proceedings of the Royal Society of Edinburgh Section B: Biological Sciences,* 77**:** 123-137.

Glueck, M. F. and Stockton, C. W. (2001) Reconstruction of the North Atlantic Oscillation, 1429-1983. *International Journal of Climatology,* 21**:** 1453-1465.

Goldberg, E. (1963) Geochronology with Pb210: Radioactive dating. *Conference proceedings.* Athens, IAEA.

González-Álvarez, R., Bernárdez, P., Pena, L. D., Francés, G., Prego, R., Diz, P. and Vilas, F. (2005) Paleoclimatic evolution of the Galician continental shelf (NW of Spain) during the last 3000 years: from a storm regime to present conditions. *Journal of Marine Systems,* 54**:** 245-260.

González -Rouco, J., Zorita, E., Cubasch, U., Von Storch, H., Fisher-Bruns, I., Valero, F., Montavez, J., Schlese, U. and Legutke, S. (2003) Simulating the climate since 1000 AD with the AOGCM ECHO-G. In Wilson, A. ed. *Solar Variability as an Input to the Earth's Environment Symposium,* Tatranská Lomnica, Slovak Republic , 23-28 June 2003. Noordwijk, 535: ESA Publications Division: 329-338.

González-Villanueva, R., Pérez-Arlucea, M., Alejo, I. and Goble, R. (2009) Climatic-related factors controlling the sedimentary architecture of a Barrier-Lagoon complex in the context of the Holocene transgression. *Journal of Coastal Research,* 56**:** 627-631.

Goudie, A. and Middleton, N. (2001) Saharan dust storms: nature and consequences. *Earth-Science Reviews,* 56**:** 179-204.

Goy, J. L., Zazo, C. and Dabrio, C. J. (2003) A beach-ridge progradation complex reflecting periodical sea-level and climate variability during the Holocene (Gulf of Almería, Western Mediterranean). *Geomorphology,* 50**:** 251-268.

Grötzner, A., Latif, M. and Barnett, T. P. (1998) A decadal climate cycle in the North Atlantic Ocean as simulated by the ECHO coupled GCM. *Journal of Climate,* 11**:** 831-847.

Graf, H. F. and Walter, K. (2005) Polar vortex controls coupling of North Atlantic Ocean and atmosphere. *Geophysical Research Letters,* 32: LO1704.

Graff, L. S. and Lacasce, J. (2012) Changes in the Extratropical Storm Tracks in Response to Changes in SST in an AGCM. *Journal of Climate,* 25**:** 1854-1870.

Grattan, J. and Charman, D.J. (1994) Non-climatic factors and the environmental impact of volcanic volatiles: implications of the Laki fissure eruption of AD 1783. *The Holocene*, 4: 101-106.

Grattan, J., Gilbertson, D. and Charman, D. (1999) *Modelling the impact of Icelandic volcanic eruptions upon the prehistoric societies and environment of northern and western Britain*. Geological Society, London, Special Publications, 161: 109-124.

Gray, L. J., Beer, J., Geller, M., Haigh, J., Lockwood, M., Matthes, K., Cubasch, U., Fleitmann, D., Harrison, G. and Hood, L. (2010) Solar influences on climate. *Reviews of Geophysics,* 48: RG4001.

Gray, S. T., Graumlich, L. J., Betancourt, J. L. and Pederson, G. T. (2004) A tree-ring based reconstruction of the Atlantic Multidecadal Oscillation since 1567 AD. *Geophysical Research Letters,* 31: L12205.

Greatbatch, R. J. (2000) The North Atlantic Oscillation. *Stochastic Environmental Research and Risk Assessment,* 14**:** 213-242.

Grenander, U. (1959) *Probability and Statistics: The Harald Cramér Volume*, Alqvist and Wiksell.

Guirguis, K., Gershunov, A., Schwartz, R. and Bennett, S. (2011) Recent warm and cold daily winter temperature extremes in the Northern Hemisphere. *Geophysical Research Letters,* 38**:** L17701.

Gulev, S. K., Latif, M., Keenlyside, N., Park, W. and Koltermann, K. P. (2013) North Atlantic Ocean control on surface heat flux on multidecadal timescales. *Nature,* 499**:** 464-467.

Guyard, H., Chapron, E., St-Onge, G., Anselmetti, F. S., Arnaud, F., Magand, O., Francus, P. and Mélières, M.-A. (2007) High-altitude varve records of abrupt environmental changes and mining activity over the last 4000 years in the Western French Alps (Lake Bramant, Grandes Rousses Massif). *Quaternary Science Reviews,* 26**:** 2644-2660.

Guyard, H., Chapron, E., St-Onge, G. and Labrie, J. (2013) Late-Holocene NAO and oceanic forcing on high-altitude proglacial sedimentation (Lake Bramant, Western French Alps). *The Holocene,* 23**:** 1163-1172.

Haigh, J. and Blackburn, M. (2006) Solar influences on dynamical coupling between the stratosphere and troposphere. *Space Science Reviews,* 125**:** 331-344.

Haigh, J. D. (1996) The impact of solar variability on climate. *Science,* 272**:** 981-984.

Haigh, J. D., Blackburn, M. and Day, R. (2005) The Response of Tropospheric Circulation to Perturbations in Lower-Stratospheric Temperature. *Journal of Climate,* 18**:** 3672-3685.

Hakanson, L. (1977) The influence of wind, fetch, and water depth on the distribution of sediments in Lake VÃ¤nern, Sweden. *Canadian Journal of Earth Sciences,* 14**:** 397-412.

Hall, A., Hansom, J., Williams, D. and Jarvis, J. (2006) Distribution, geomorphology and lithofacies of cliff-top storm deposits: examples from the high-energy coasts of Scotland and Ireland. *Marine Geology,* 232**:** 131-155.

Hall, V. A. and Pilcher, J. R. (2002) Late-Quaternary Icelandic tephras in Ireland and Great Britain: detection, characterization and usefulness. *The Holocene,* 12**:** 223-230.

Hanna, E., Caappelen, J., Allan, R., Jonsson, T., Le Blancq, F., Lillington, T. and Hickey, K. (2008) New insights into North European and North Atlantic surface pressure variability, storminess, and related climatic change since 1980. *Journal of Climate,* 21**:** 6739-6766.

Hansom, J. (2001) Coastal sensitivity to environmental change: a view from the beach. *CATENA,* 42**:** 291-305.

Hansom, J. D. and Hall, A. M. (2009) Magnitude and frequency of extra-tropical North Atlantic cyclones: A chronology from cliff-top storm deposits. *Quaternary International,* 195**:** 42-52.

Haslett, S. K. and Bryant, E. A. (2007) Reconnaissance of historic (post-AD 1000) high-energy deposits along the Atlantic coasts of southwest Britain, Ireland and Brittany, France. *Marine Geology,* 242**:** 207-220.

Hass, H. C. (1996) Northern Europe climate variations during late Holocene: evidence from marine Skagerrak. *Palaeogeography, Palaeoclimatology, Palaeoecology,* 123**:** 121-145.

Haug, G. H., Hughen, K. A., Sigman, D. M., Peterson, L. C. and Röhl, U. (2001) Southward Migration of the Intertropical Convergence Zone Through the Holocene. *Science,* 293**:** 1304-1308.

Hegerl, G. C., Crowley, T. J., Allen, M., Hyde, W. T., Pollack, H. N., Smerdon, J. and Zorita, E. (2007) Detection of Human Influence on a New, Validated 1500-Year Temperature Reconstruction. *Journal of Climate.* American Meteorological Society.

Hegerl, G. C., Crowley, T. J., Hyde, W. T. and Frame, D. J. (2006) Climate sensitivity constrained by temperature reconstructions over the past seven centuries. *Nature,* 440**:** 1029-1032.

Heiri, O., Lotter, A. F. and Lemcke, G. (2001) Loss on ignition as a method for estimating organic and carbonate content in sediments: reproducibility and comparability of results. *Journal of Paleolimnology,* 25**:** 101-110.

Hempel, L. and Thyssen, F. (1992) Deep radio echo soundings in the vicinity of GRIP and GISP2 drill sites, Greenland. *Polarforschung,* 62**:** 11-16.

Hendon, D., Charman, D. J. and Kent, M. (2001) Palaeohydrological records derived from testate amoebae analysis from peat lands in northern England: within-site variability, between-site comparability and palaeoclimatic implications. *The Holocene,* 11**:** 127-148.

Henley, C. (2003) The Outer Hebrides and the Hebridean world during the Neolithic: an island history. Unpublished PhD dissertation., Cardiff University.

Hewston, R. and Dorling, S. R. (2011) An analysis of observed daily maximum wind gusts in the UK. *Journal of Wind Engineering and Industrial Aerodynamics,* 99**:** 845-856.

Hickey, K. (1997) Documentary records of coastal storms in Scotland 1500-1991 A.D. . Coventry, Coventry University.

Higuchi, K., Huang, J. and Shabbar, A. (1999) A wavelet characterization of the North Atlantic oscillation variation and its relationship to the North Atlantic sea surface temperature. *International Journal of Climatology,* 19**:** 1119-1129.

Hilton, J., Lishman, J. and Allen, P. (1986) The dominant processes of sediment distribution and focusing in a small, eutrophic, monomictic lake. *Limnology and Oceanography,* 31**:** 125-133.

Hoerling, M. P., Hurrell, J. W. and Xu, T. Y. (2001) Tropical origins for recent North Atlantic climate change. *Science,* 292**:** 90-92.

Hotta, S., Kubota, S., Katori, S. and Horikawa, K. (1984) Sand transport by wind on a wet sand surface. *Coastal Engineering Proceedings,* 1: 1265-1281.

Hudson, G. (1991) The geomorphology and soils of the Outer Hebrides. In Pankhurst, R, J, and Mullin, J, M. (ed.) *Flora of the Outer Hebrides***,** London: Natural History Museum Publications: 19-27.

Hughes, M. and Diaz, H. (1994) Was there a medieval warm period, and if so, where and when? *Climatic Change,* 26**:** 109-142.

Hurrell, J. W. (1995) Decadal Trends in the North-Atlantic Oscillation - Regional Temperatures and Precipitation. *Science,* 269**:** 676-679.

Hurrell, J. W. (1996) Influence of variations in extratropical wintertime teleconnections on Northern Hemisphere temperature. *Geophysical Research Letters,* 23**:** 665-668.

Hurrell, J. W. and Deser, C. (2010) North Atlantic climate variability: The role of the North Atlantic Oscillation *Journal of Marine Systems,* 79**:** 231-244.

Hurrell, J. W., Kushnir, Y., Ottersen, G. and Visbeck, M. (2003) The North Atlantic Oscillation: climatic significance and environmental impact. *Geophysical Monograph Series,* 134.

Hurrell, J. W. and Vanloon, H. (1997) Decadal variations in climate associated with the north Atlantic oscillation. *Climatic Change,* 36**:** 301-326.

Huth, R., Pokorná, L., Bochníček, J. and Hejda, P. (2006) Solar cycle effects on modes of low-frequency circulation variability. *Journal of Geophysical Research: Atmospheres,* 111**:** D22107.

Ineson, S., Scaife, A. A., Knight, J., Manners, J., Dunstone, N., Gray, L. and Haigh, J. (2011) Solar forcing of winter climate variability in the Northern Hemisphere. *Nature Geoscience,* 4**:** 753-757.

Ivy-Ochs, S., Kerschner, H., Maisch, M., Christl, M., Kubik, P. W. and Schlüchter, C. (2009) Latest Pleistocene and Holocene glacier variations in the European Alps. *Quaternary Science Reviews,* 28**:** 2137-2149.

Jackson, M. G., Oskarsson, N., Trønnes, R. G., Mcmanus, J. F., Oppo, D. W., Grönvold, K., Hart, S. R. and Sachs, J. P. (2005) Holocene loess deposition in Iceland: Evidence for millennial-scale atmosphere-ocean coupling in the North Atlantic. *Geology,* 33**:** 509-512.

Janotta, A., Radtke, U., Czwielung, K. and Heidger, M. (1997) Luminescence dating (IRSL/TL) of lateglacial and holocene dune sands and sandy loesses near Bonn, Gifhorn and Diepholz (Germany). *Quaternary Science Reviews,* 16**:** 349-355.

Jones, G. S., Gregory, J. M., Stott, P. A., Tett, S. F. and Thorpe, R. B. (2005) An AOGCM simulation of the climate response to a volcanic super-eruption. *Climate Dynamics,* 25**:** 725-738.

Jones, P. D., Jonsson, T. and Wheeler, D. (1997) Extension to the North Atlantic Oscillation using early instrumental pressure observations from Gibraltar and south-west Iceland. *International Journal of Climatology,* 17**:** 1433-1450.

Jones, P. D. and Salmon, M. (2005) Preliminary reconstructions of the North Atlantic Oscillation and the Southern Oscillation Index from measures of wind strength and direction taken during the CLIWOC period. *Climatic Change,* 73**:** 131-154.

Jones, R. T., Reinhardt, L. J., Dearing, J. A., Crook, D., Chiverrell, R. C., Welsh, K. E. and Vergès, E. (2013) Detecting climatic signals in an anthropogenically disturbed catchment: The late-Holocene record from the Petit Lac d'Annecy, French Alps. *The Holocene* 23: 1329-1339.

Jonsson, C. E., Andersson, S., Rosqvist, G. C. and Leng, M. J. (2010) Reconstructing past atmospheric circulation changes using oxygen isotopes in lake sediments from Sweden. *Climates of the Past,* 6**:** 49-62.

Jordan, J. T., Smith, D. E., Dawson, S. and Dawson, A. G. (2010) Holocene relative sea-level changes in Harris, Outer Hebrides, Scotland, UK. *Journal of Quaternary Science,* 25**:** 115-134.

Kaal, J., Carrión Marco, Y., Asouti, E., Martãn Seijo, M., Martínez-Cortizas, A., Costa-Casais, M. and Criado-Boado, F. (2011) Long-term deforestation in NW Spain: linking the Holocene fire history to vegetation change and human activities. *Quaternary Science Reviews,* 30**:** 161-175.

Kaas, E., Li, T., S. and Schmith, T. (1996) Statistical hindcast of wind climatology in the North Atlantic and northwestern European region. *Climate Research,* 7**:** 97-110.

Kerr, R. A. (2000) A North Atlantic climate pacemaker for the centuries. *Science,* 288**:** 1984-1985.

Kilian, M. R., Van Der Plicht, J. and Van Geel, B. (1995) Dating raised bogs: New aspects of AMS 14C wiggle matching, a reservoir effect and climatic change. *Quaternary Science Reviews,* 14**:** 959-966.

Kinahan, G., H., Leonard, H. and Cruise, R., J. (1871) Memoirs of the geological survey of Ireland.

Kingston, D. G., Lawler, D. M. and Mcgregor, G. R. (2006) Linkages between atmospheric circulation, climate and streamflow in the northern North Atlantic: research prospects. *Progress in Physical Geography,* 30**:** 143-174.

Kirby, M. E., Lund, S. P., Anderson, M. A. and Bird, B. W. (2007) Insolation forcing of Holocene climate change in Southern California: a sediment study from Lake Elsinore. *Journal of Paleolimnology,* 38**:** 395-417.

Knight, J. R., Folland, C. K. and Scaife, A. A. (2006) Climate impacts of the Atlantic Multidecadal Oscillation. *Geophysical Research Letters,* 33**:** L17706.

Knudsen, K. L., Eiríksson, J. N. and Bartels-Jónsdóttir, H. B. R. (2012) Oceanographic changes through the last millennium off North Iceland: Temperature and salinity reconstructions based on foraminifera and stable isotopes. *Marine Micropaleontology,* 84-85**:** 54-73.

Knudsen, M. F., Jacobsen, B. H., Riisager, P., Olsen, J. and Seidenkrantz, M.-S. (2011) Evidence of Suess solar-cycle bursts in subtropical Holocene speleothem δ18O records. *The Holocene,* 22**:** 597-602.

Knudsen, M. F., Riisager, P., Jacobsen, B. H., Muscheler, R., Snowball, I. and Seidenkrantz, M. S. (2009) Taking the pulse of the Sun during the Holocene by joint analysis of 14C and 10Be. *Geophysical Research Letters,* 36: L16701.

Kodera, K. (1994) Influence of volcanic eruptions on the troposphere through stratospheric dynamical processes in the northern hemisphere winter. *Journal of Geophysical Research: Atmospheres,* 99**:** 1273-1282.

Kodera, K. and Kuroda, Y. (2002) Dynamical response to the solar cycle. *Journal of Geophysical Research: Atmospheres,* 107**:** 4749.

Kohfeld, K. E. and Harrison, S. P. (2000) How well can we simulate past climates? Evaluating the models using global palaeoenvironmental datasets. *Quaternary Science Reviews,* 19**:** 321-346.

Kok, J. F., Parteli, E. J., Michaels, T. I. and Karam, D. B. (2012) The physics of wind-blown sand and dust. *Reports on Progress in Physics,* 75**:** 106901.

Kotula, P. G., Keenan, M. R., and Michael, J. R. (2003) Automated Analysis of SEM X-Ray Spectral Images: A Powerful New Microanalysis Tool. *Microscopy and Microanalysis*, 9: 1-17.

Krantzberg, G. (1985) The influence of bioturbation on physical, chemical and biological parameters in aquatic environments: a review. *Environmental Pollution Series A, Ecological and Biological,* 39**:** 99-122.

Krichak, S. O. and Alpert, P. (2005) Decadal trends in the east Atlantic–west Russia pattern and Mediterranean precipitation. *International Journal of Climatology,* 25**:** 183-192.

Krumbein, W., E. (1979) Calcification by bacteria and algae. In: Trudinger, P. A. and Swaine, D. J. (eds.) *Biogeochemical cycling of mineral-forming elements*. Amsterdam, Elsevier.

Kuroda, Y. and Kodera, K. (2002) Effect of Solar Activity on the Polar-night Jet Oscillation in the Northern and Southern Hemisphere Winter. *Journal of the Meteorological Society of Japan,* 80**:** 973-984.

Kutzbach, J., Chen, G., Cheng, H., Edwards, R. and Liu, Z. (2014) Potential role of winter rainfall in explaining increased moisture in the Mediterranean and Middle East during periods of maximum orbitally-forced insolation seasonality. *Climate Dynamics,* 42**:** 1079-1095.

Kvamsto, N. G., Skeie, P. and Stephenson, D. B. (2004) Impact of Labrador sea-ice extent on the North Atlantic Oscillation. *International Journal of Climatology,* 24**:** 603-612.

Kylander, M. E., Ampel, L., Wohlfarth, B. and Veres, D. (2011) High-resolution X-ray fluorescence core scanning analysis of Les Echets (France) sedimentary sequence: new insights from chemical proxies. *Journal of Quaternary Science,* 26**:** 109-117.

López-Moreno, J., Vicente-Serrano, S., Morán-Tejeda, E., Lorenzo-Lacruz, J., Kenawy, A. and Beniston, M. (2011) Effects of the North Atlantic Oscillation (NAO) on combined temperature and precipitation winter modes in the Mediterranean mountains: Observed relationships and projections for the 21st century. *Global and Planetary Change,* 77**:** 62-76.

López-Moreno, J. I., Beguería, S. and García-Ruiz, J. M. A. (2006) Trends in high flows in the central Spanish Pyrenees: response to climatic factors or to land-use change? *Hydrological Sciences Journal,* 51**:** 1039-1050.

Lamb, F. (1991) *Historic Storms of the North Sea, British Isles and Northwest Europe.,* Great Britain, Cambridge University Press.

Lamb, H. (1967) *The Changing Climate,* London, Methuen and co. .

Lamb, H., H. (1995) *Climate, History and the Modern World,* London, Routledge.

Lamb, H., Roberts, N., Leng, M., Barker, P., Benkaddour, A. and Van Der Kaars, S. (1999) Lake evolution in a semi-arid montane environment: response to catchment change and hydroclimatic variation. *Journal of Paleolimnology,* 21**:** 325-343.

Lamb, H. H. (1965) The early medieval warm epoch and its sequel. *Palaeogeography, Palaeoclimatology, Palaeoecology,* 1**:** 13-37.

Lamb, H. H. (1979) Climatic variation and changes in the wind and ocean circulation: The Little Ice Age in the northeast Atlantic. *Quaternary Research,* 11**:** 1-20.

Lamb, H. H. (1984) Some studies of the Little Ice Age of recent centuries and its great storms. In: Mörner, N-A and Karlén (eds.) *Climatic changes on a yearly to millennial basis.* Springer, Netherlands: 309-329.

Lancaster, N. (1989) Late Quaternary paleoenvironments in the southwestern Kalahari. *Palaeogeography, Palaeoclimatology, Palaeoecology,* 70**:** 367-376.

Lancaster, N. and Baas, A. (1998) Influence of vegetation cover on sand transport by wind: field studies at Owens Lake, California. *Earth Surface Processes and Landforms,* 23**:** 69-82.

Langdon, P. G. and Barber, K. E. (2005) The climate of Scotland over the last 5000 years inferred from multiproxy peatland records: inter-site correlations and regional variability. *Journal of Quaternary Science,* 20**:** 549-566.

Lau, K. M. and Weng, H. (1995) Climate Signal Detection Using Wavelet Transform: How to Make a Time Series Sing. *Bulletin of the American Meteorological Society,* 76**:** 2391-2402.

Lawrence, C. R. and Neff, J. C. (2009) The contemporary physical and chemical flux of aeolian dust: A synthesis of direct measurements of dust deposition. *Chemical Geology,* 267**:** 46-63.

Le Roux, G. L., Laverret, E. and Shotyk, W. (2006) Fate of calcite, apatite and feldspars in an ombrotrophic peat bog, Black Forest, Germany. *Journal of the Geological Society,* 163**:** 641-646.

Lee, G. (1970) Factors affecting the transfer of materials between water and sediments.

Legutke, S. and Voss, R. (1999) *The Hamburg atmosphere-ocean coupled circulation model ECHO-G*, DKRZ.

Lehner, F., Raible, C. C. and Stocker, T. F. (2012) Testing the robustness of a precipitation proxy-based North Atlantic Oscillation reconstruction. *Quaternary Science Reviews,* 45**:** 85-94.

Leifeld, J., Gubler, L. and Grünig, A. (2011) Organic matter losses from temperate ombrotrophic peat lands: an evaluation of the ash residue method. *Plant and soil,* 341**:** 349-361.

Leng, M., Barnker, P., Greenwood, P., Roberts, N. and Reed, J. (2001) Oxygen isotope analysis of diatom silica and authigenic calcite from Lake Pinarbasi, Turkey. *Journal of Paleolimnology,* 25**:** 343-349.

Limpasuvan, V., Thompson, D. W. J. and Hartmann, D. L. (2004) The Life Cycle of the Northern Hemisphere Sudden Stratospheric Warmings. *Journal of Climate,* 17**:** 2584-2596.

Liu, K.-B. and Fearn, M. L. (1993) Lake-sediment record of late Holocene hurricane activities from coastal Alabama. *Geology,* 21**:** 793-796.

Lockwood, M. (2012) Solar Influence on Global and Regional Climates. *Surveys in Geophysics,* 33**:** 503-534.

Lockwood, M., Harrison, R. G., Woollings, T. and Solanki, S. K. (2010) Are cold winters in Europe associated with low solar activity? *Environmental Research Letters,* 5**:** 024001.

Lohmann, K., Drange, H. and Bentsen, M. (2009) Response of the North Atlantic subpolar gyre to persistent North Atlantic Oscillation-like forcing. *Climate Dynamics,* 32**:** 273-285.

Lomb, N. R. (1976) Least-squares frequency analysis of unequally spaced data. *Astrophysics and space science,* 39**:** 447-462.

Loutre, M.-F., Berger, A., Bretagnon, P. and Blanca, P. (1992) Astronomical frequencies for climate research at the decadal to century time scale. *Climate Dynamics,* 7**:** 181-194.

Löwemark, L., Chen, H. F., Yang, T. N., Kylander, M., Yu, E. F., Hsu, Y. W., Lee, T. Q., Song, S. R. and Jarvis, S. (2010) Normalizing XRF-scanner

data: A cautionary note on the interpretation of high-resolution records from organic-rich lakes. *Journal of Asian Earth Sciences,* 40**:** 1250-1256.

Lozano, I., Devoy, R. J. N., May, W. and Andersen, U. (2004) Storminess and vulnerability along the Atlantic coastlines of Europe: analysis of storm records and of a greenhouse gases induced climate scenario. *Marine Geology,* 210**:** 205-225.

Luterbacher, J., Xoplaki, E., Dietrich, D., Rickli, R., Jacobeit, J., Beck, C., Gyalistras, D., Schmutz, C. and Wanner, H. (2002) Reconstruction of sea level pressure fields over the Eastern North Atlantic and Europe back to 1500. *Climate Dynamics,* 18**:** 545-561.

Luterbacher, J., Rickli, R., Xoplaki, E., Tinguely, C., Beck, C., Pfister, C. and Wanner, H. (2001) The Late Maunder Minimum (1675-1715) - A Key Period for Studying Decadal Scale Climatic Change in Europe. *Climatic Change,* 49**:** 441-462.

Luterbacher, J., Schmutz, C., Gyalistras, D., Xoplaki, E. and Wanner, H. (1999) Reconstruction of monthly NAO and EU indices back to AD 1675. *Geophysical Research Letters,* 26**:** 2745-2748.

Mackereth, F. J. H. (1969) Short core sampler for subaqueous deposits. *Limnology and Oceanography,* 14:145-151.

Macklin, M. G. and Lewin, J. (2003) River sediments, great floods and centennial-scale Holocene climate change. *Journal of Quaternary Science,* 18**:** 101-105.

Magny, M. (2013) Orbital, ice-sheet, and possible solar forcing of Holocene lake-level fluctuations in west-central Europe: A comment on Bleicher. *The Holocene,* 23**:** 1202-1212.

Magny, M., De Beaulieu, J.-L., Drescher-Schneider, R., Vannière, B., Walter-Simonnet, A.-V. R., Miras, Y., Millet, L., Bossuet, G., Peyron, O.,

Brugiapaglia, E. and Leroux, A. L. (2007) Holocene climate changes in the central Mediterranean as recorded by lake-level fluctuations at Lake Accesa (Tuscany, Italy). *Quaternary Science Reviews,* 26**:** 1736-1758.

Mann, M. E., Zhang, Z., Rutherford, S., Bradley, R. S., Hughes, M. K., Shindell, D., Ammann, C., Faluvegi, G. and Ni, F. (2009) Global Signatures and Dynamical Origins of the Little Ice Age and Medieval Climate Anomaly. *Science,* 326**:** 1256-1260.

Marques, R., Zêzere, J., Trigo, R., Gaspar, J. and Trigo, I. (2008) Rainfall patterns and critical values associated with landslides in Povoação County (São Miguel Island, Azores): relationships with the North Atlantic Oscillation. *Hydrological Processes,* 22**:** 478-494.

Martin-Puertas, C., Matthes, K., Brauer, A., Muscheler, R., Hansen, F., Petrick, C., Aldahan, A., Possnert, G. and van Geel, B. (2012) Regional atmospheric circulation shifts induced by a grand solar minimum. *Nature Geoscience,* 5: 397-401.

Martínez-Cortizas, A., Costa-Casais, M. and López-Sáez, J. A. (2009) Environmental change in NW Iberia between 7000 and 500 cal BC. *Quaternary International,* 200**:** 77-89.

Martínez-Cortizas, A., Pontevedra-Pombal, X., García-Rodeja, E., Novoa-Munoz, J. and Shotyk, W. (1999) Mercury in a Spanish peat bog: archive of climate change and atmospheric metal deposition. *Science,* 284**:** 939-942.

Martãn-Chivelet, J., Muñoz-García, M. B. N., Edwards, R. L., Turrero, M. J. and Ortega, A. I. (2011) Land surface temperature changes in Northern Iberia since 4000 yr BP, based on $\delta^{13}C$ of speleothems. *Global and Planetary Change,* 77**:** 1-12.

Martínez-Cortizas, A., Mighall, T., Pombal, X. P., Munfoz, J. N., Varelal, E. P. and Rebolol, R. P. (2005) Linking changes in atmospheric dust

deposition, vegetation change and human activities in northwest Spain during the last 5300 years. *The Holocene,* 15**:** 698-706.

Martínez-Cortizas, A., Pontevedra-Pombal, X., Munoz, J. C. N. and Garcia-Rodeja, E. (1997) Four Thousand Years of Atmospheric Pb, Cd and Zn Deposition Recorded by the Ombrotrophic Peat Bog of Penido Vello (Northwestern Spain). *Water, Air, and Soil Pollution,* 100**:** 387-403.

Martinez Catalan, J., R., Garcia-Cortes, A. and Palacio Suarez-Valgrande, J. (2009) The Iberian Variscan Orogen. In: Garcia-Cortes, A. (Ed.) *Spanish Geological frameworks and geosites: An approach to Spanish geological heritage of international relevance.* Publications of the Geological Survey of Spain (IGME).

Martinez Catalan, J. R., Arenas, R. and Diez Balda, M. A. (2003) Large extensional structures developed during emplacement of a crystalline thrust sheet: the Mondonedo nappe (NW Spain). *Journal of Structural Geology,* 25**:** 1815-1839.

Martins, V., Figueira, R. C. L., França, E. J., Ferreira, P. A. D. L., Martins, P., Santos, J. F., Dias, J. O. A., Laut, L. L., Monge Soares, A. M. and Silva, E. F. D. (2012) Sedimentary processes on the NW Iberian Continental Shelf since the Little Ice Age. *Estuarine, Coastal and Shelf Science,* 102**:** 48-59.

Martins, V. N., Dubert, J. S., Jouanneau, J.-M., Weber, O., Da Silva, E. F., Patinha, C., Alveirinho Dias, J. O. M. and Rocha, F. (2007) A multiproxy approach of the Holocene evolution of shelf-slope circulation on the NW Iberian Continental Shelf. *Marine Geology,* 239**:** 1-18.

Marx, S. K., Kamber, B. S., Mcgowan, H. A. and Denholm, J. (2011) Holocene dust deposition rates in Australia's Murray-Darling Basin record the interplay between aridity and the position of the mid-latitude westerlies. *Quaternary Science Reviews,* 30**:** 3290-3305.

Masse, G., Rowland, S. J., Sicre, M.-A., Jacob, J., Jansen, E. and Belt, S. T. (2008) Abrupt climate changes for Iceland during the last millennium: evidence from high resolution sea ice reconstructions. *Earth and Planetary Science Letters,* 269**:** 565-569.

Matthes, K., Kuroda, Y., Kodera, K. and Langematz, U. (2006) Transfer of the solar signal from the stratosphere to the troposphere: Northern winter. *Journal of Geophysical Research: Atmospheres (1984-2012),* 111: DO6108.

Matthews, J. A. and Briffa, K. R. (2005) The "Little Ice Age": Re-evaluation of an evolving concept. *Geografiska Annaler: Series A, Physical Geography,* 87**:** 17-36.

Mauquoy, D., Engelkes, T., Groot, M. H. M., Markesteijn, F., Oudejans, M. G., Van Der Plicht, J. and Van Geel, B. (2002) High-resolution records of late-Holocene climate change and carbon accumulation in two north-west European ombrotrophic peat bogs. *Palaeogeography, Palaeoclimatology, Palaeoecology,* 186**:** 275-310.

Mayewski, P. A., Meeker, L. D., Twickler, M. S., Whitlow, S., Yang, Q., Lyons, W. B. and Prentice, M. (1997) Major features and forcing of high-latitude northern hemisphere atmospheric circulation using a 110,000-year-long glaciochemical series. *Journal of Geophysical Research: Oceans (1978-2012),* 102**:** 26345-26366.

Mayewski, P. A., Rohling, E. E., Curt Stager, J., Karlén, W. R., Maasch, K. A., David Meeker, L., Meyerson, E. A., Gasse, F., Van Kreveld, S., Holmgren, K., Lee-Thorp, J., Rosqvist, G., Rack, F., Staubwasser, M., Schneider, R. R. and Steig, E. J. (2004) Holocene climate variability. *Quaternary Research,* 62**:** 243-255.

Mayr, C., Wille, M., Haberzettl, T., Fey, M., Janssen, S., Lücke, A., Ohlendorf, C., Oliva, G., Schäbitz, F. and Schleser, G. H. (2007) Holocene variability

of the Southern Hemisphere westerlies in Argentinean Patagonia (52 S). *Quaternary Science Reviews,* 26**:** 579-584.

McCloskey, T. A. and Knowles, J. T. (2009) Migration of the tropical cyclone zone throughout the Holocene. *Hurricanes and Climate Change.* Springer.

McKenna-Neuman, C. and Nickling, W. (1989) A theoretical and wind tunnel investigation of the effect of capillary water on the entrainment of sediment by wind. *Canadian Journal of Soil Science,* 69**:** 79-96.

Meeker, L. D. and Mayewski, P. A. (2002) A 1400-year high-resolution record of atmospheric circulation over the North Atlantic and Asia. *The Holocene,* 12**:** 257-266.

Mehta, V. M., Suarez, M. J., Manganello, J. V. and Delworth, T. L. (2000) Oceanic influence on the North Atlantic Oscillation and associated northern hemisphere climate variations: 1959-1993. *Geophysical Research Letters,* 27**:** 121-124.

Met Office (2014) *Stornoway historic station data.* Accessed 10/08/13. <http://www.metoffice.gov.uk/pub/data/weather/uk/climate/stationdata/stornowaydata.txt>

Metcalfe, S. E., Jones, M. D., Davies, S. J., Noren, A. and Mackenzie, A. (2010) Climate variability over the last two millennia in the North American Monsoon region, recorded in laminated lake sediments from Laguna de Juanacatlán, Mexico. *The Holocene,* 20**:** 1195-1206.

Meyers, P. A. (1994) Preservation of elemental and isotopic source identification of sedimentary organic matter. *Chemical Geology,* 114**:** 289-302.

Michelangeli, P.-A., Vautard, R. and Legras, B. (1995) Weather Regimes: Recurrence and Quasi Stationarity. *Journal of the Atmospheric Sciences,* 52**:** 1237-1256.

Mighall, T., Martínez-Cortizas, A., Biester, H. and Turner, S. (2006) Proxy climate and vegetation changes during the last five millennia in NW Iberia: pollen and non-pollen palynomorph data from two ombrotrophic peat bogs in the North Western Iberian Peninsula. *Review of Palaeobotany and Palynology,* 141**:** 203-223.

Moisley, H. (1961) North Uist in 1799. *The Scottish Geographical Magazine,* 77**:** 89-92.

Mojtahid, M., Jorissen, F., Garcia, J., Schiebel, R., Michel, E., Eynaud, F., Gillet, H., Cremer, M., Diz Ferreiro, P. and Siccha, M. (2013) High resolution Holocene record in the southeastern Bay of Biscay: Global versus regional climate signals. *Palaeogeography, Palaeoclimatology, Palaeoecology,* 377**:** 28-44.

Mooij, W., Trolle, D., Jeppesen, E., Arhonditsis, G., Belolipetsky, P., Chitamwebwa, D. R., Degermendzhy, A., DeAngelis, D., De Senerpont Domis, L., Downing, A., Elliott, J. A., Fragoso, C., Jr., Gaedke, U., Genova, S., Gulati, R., Håkanson, L., Hamilton, D., Hipsey, M., t' Hoen, J., Hülsmann, S., Los, F. H., Makler-Pick, V., Petzoldt, T., Prokopkin, I., Rinke, K., Schep, S., Tominaga, K., Van Dam, A., Van Nes, E., Wells, S. and Janse, J. (2010) Challenges and opportunities for integrating lake ecosystem modelling approaches. *Aquatic Ecology* 44: 633-667.

Mooney, S. and Black, M. (2003) A simple and fast method for calculating the area of macroscopic charcoal isolated from sediments. *Quaternary Australasia,* 21**:** 18-21.

Mooney, S. and Radford, K. (2001) A simple and fast method for the quantification of microscopic charcoal in sediments. *Quaternary Australasia,* 19**:** 43-46.

Moore, G. and Renfrew, I. (2012) Cold European winters: interplay between the NAO and the East Atlantic mode. *Atmospheric Science Letters,* 13**:** 1-8.

Moore, P. D. (1987) Ecological and hydrological aspects of peat formation. *Geological Society, London, Special Publications,* 32**:** 7-15.

Moreno, A., Valero-Garcés, B., González-Sampériz, P. and Rico, M. (2008) Flood response to rainfall variability during the last 2000 years inferred from the Taravilla Lake record (Central Iberian Range, Spain). *Journal of Paleolimnology,* 40**:** 943-961.

Morlet, J. (1983) Sampling Theory and Wave Propagation. In Chen, C. H. (Ed.) *Issues in Acoustic Signal/ Image Processing and Recognition.* Springer Berlin Heidelberg.

Mörner, N.-A. (2010) Solar Minima, Earth's rotation and Little Ice Ages in the past and in the future: The North Atlantic-European case. *Global and Planetary Change,* 72**:** 282-293.

Moros, M., Emeis, K., Risebrobakken, B. R., Snowball, I., Kuijpers, A., Mcmanus, J. and Jansen, E. (2004) Sea surface temperatures and ice rafting in the Holocene North Atlantic: climate influences on northern Europe and Greenland. *Quaternary Science Reviews,* 23**:** 2113-2126.

Müller, B., Wang, Y., Dittrich, M., and Wehrli, B. (2003) Influence of organic carbon decomposition on calcite dissolution in surficial sediments of a freshwater lake. *Water Research*, 37: 4524-4532.

Myweather2 (2014) *Santiago de Compostela climate history.* Accessed 07/02/2014. <http://www.myweather2.com/City-Town/Spain/Santiago-De-Compostela/climate-profile.aspx>

Nesje, A., Lie, Ø. and Dahl, S. O. (2000) Is the North Atlantic Oscillation reflected in Scandinavian glacier mass balance records? *Journal of Quaternary Science,* 15**:** 587-601.

Nesje, A., Matthews, J. A., Dahl, S. O., Berrisford, M. S. and Andersson, C. (2001) Holocene glacier fluctuations of Flatebreen and winter-precipitation changes in the Jostedalsbreen region, western Norvay, based on glaciolacustrine sediment records. *The Holocene,* 11**:** 267-280.

Nilsen, J., Gao, Y., Drange, H., Furevik, T. and Bentsen, M. (2003) Simulated North Atlantic-Nordic Seas water mass exchanges in an isopycnic coordinate OGCM. *Geophysical Research Letters,* 30: 1536.

NOAA (2014) *Total sulphate measurements from the GISP2 ice core.* Accessed 17/06/2014. <ftp://ftp.ncdc.noaa.gov/pub/data/paleo/icecore/greenland/summit/gisp2/chemvolcano.txt>

Noren, A. J., Bierman, P. R., Steig, E. J., Lini, A. and Southon, J. (2002) Millennial-scale storminess variability in the northeastern United States during the Holocene epoch. *Nature,* 419**:** 821-824.

O'Brien, S. R., Mayewski, P. A., Meeker, L. D., Meese, D. A., Twickler, M. S. and Whitlow, S. I. (1995) Complexity of Holocene Climate as Reconstructed from a Greenland Ice Core. *Science,* 270**:** 1962-1964.

O'Hare, G., Sweeney, J. and Wilby, R. (2005) *Weather, Climate and Climate Change: Human Perspectives*, Pearson Education Limited, England.

Ojala, A. E., Alenius, T., Seppã, H. and Giesecke, T. (2008) Integrated varve and pollen-based temperature reconstruction from Finland: evidence for Holocene seasonal temperature patterns at high latitudes. *The Holocene,* 18**:** 529-538.

Oldfield, F., Battarbee, R. W., Boyle, J. F., Cameron, N. G., Davis, B., Evershed, R. P., Mcgovern, A. D., Jones, V. and Thompson, R. (2010) Terrestrial and aquatic ecosystem responses to late Holocene climate change recorded in the sediments of Lochan Uaine, Cairngorms, Scotland. *Quaternary Science Reviews,* 29**:** 1040-1054.

Olsen, J., Anderson, N. J. and Knudsen, M. F. (2012) Variability of the North Atlantic Oscillation over the past 5,200 years. *Nature Geoscience,* 5**:** 808-812.

Orvik, K. A., Skagseth, Ã. Y. and Mork, M. (2001) Atlantic inflow to the Nordic Seas: current structure and volume fluxes from moored current meters, VM-ADCP and SeaSoar-CTD observations, 1995-1999. *Deep Sea Research Part I: Oceanographic Research Papers,* 48**:** 937-957.

Ottersen, G., Planque, B., Belgrano, A., Post, E., Reid, P. and Stenseth, N. (2001) Ecological effects of the North Atlantic Oscillation. *Oecologia,* 128**:** 1-14.

Page, M. J., Trustrum, N. A., Orpin, A. R., Carter, L., Gomez, B., Cochran, U. A., Mildenhall, D. C., Rogers, K. M., Brackley, H. L., Palmer, A. S. and Northcote, L. (2009) Storm frequency and magnitude in response to Holocene climate variability, Lake Tutira, North-Eastern New Zealand. *Marine Geology,* 270**:** 30-44.

Palais, J., M., Germani, M., S and Zielinski, G., A. (1992) Interhemispheric transport of volcanic ash from a 1259 A.D. volcanic eruption to the Greenland and Antarctic ice sheets. *Geophysical Research Letters,* 19**:** 801-804.

Palais, J., M., Taylor, K., C, Mayewski, P. and Grootes, P. M. (1991) Volcanic ash from the 1362 A.D. Oraefajokull eruption (Iceland) in the Greenland ice sheet. *Geophysical Research Letters,* 18**:** 1241-1244.

Palmer, T., N. (1999) A Nonlinear Dynamical Perspective On Climate Prediction. *Journal Of Climate,* 12**:** 575-591.

Parris, A. S., Bierman, P. R., Noren, A. J., Prins, M. A. and Lini, A. (2010) Holocene paleostorms identified by particle size signatures in lake sediments from the northeastern United States. *Journal of Paleolimnology,* 43**:** 29-49.

Payne, R. and Gehrels, M. (2010) The formation of tephra layers in peat lands: An experimental approach. *CATENA,* 81**:** 12-23.

Payne, R. J., Kilfeather, A. A., Van Der Meer, J. J. and Blackford, J. J. (2005) Experiments on the taphonomy of tephra in peat. *Suo (Mires and Peat),* 56**:** 147-156.

Pearson, M. P., Chamberlain, A., Craig, O., Marshall, P., Mulville, J., Smith, H., Chenery, C., Collins, M., Cook, G. and Craig, G. (2005) Evidence for mummification in Bronze Age Britain. *Antiquity,* 79**:** 529-546.

Pena, L., Francés, G., Diz, P., Esparza, M., Grimalt, J. O., Nombela, M. and Alejo, I. (2010) Climate fluctuations during the Holocene in NW Iberia: high and low latitude linkages. *Continental Shelf Research,* 30**:** 1487-1496.

Penabad, E., Alvarez, I., Balseiro, C., Decastro, M., Gómez, B., Pérez-Muñuzuri, V. and Gómez-Gesteira, M. (2008) Comparative analysis between operational weather prediction models and QuikSCAT wind data near the Galician coast. *Journal of Marine Systems,* 72**:** 256-270.

Pennington, W., Tutin, T., G., Cambray, R., S. and Fisher, E., M. (1973) Observations on lake sediments using fallout ^{137}Cs as a tracer. *Nature Geoscience,* 242**:** 324-326.

Peristykh, A. N. and Damon, P. E. (2003) Persistence of the Gleissberg 88-year solar cycle over the last ~12,000 years: Evidence from cosmogenic

isotopes. *Journal of Geophysical Research: Space Physics (1978-2012),* 108**:** SSH 1-1-SSH 1-15.

Pinto, J. G. and Raible, C. C. (2012) Past and recent changes in the North Atlantic oscillation. *Wiley Interdisciplinary Reviews: Climate Change,* 3**:** 79-90.

Pinto, J. G., Ulbrich, U., Leckebusch, G. C., Spangehl, T., Reyers, M. and Zacharias, S. (2007) Changes in storm track and cyclone activity in three SRES ensemble experiments with the ECHAM5/MPI-OM1 GCM. *Climate Dynamics,* 29**:** 195-210.

Pinto, J. G., Zacharias, S., Fink, A. H., Leckebusch, G. C. and Ulbrich, U. (2009) Factors contributing to the development of extreme North Atlantic cyclones and their relationship with the NAO. *Climate Dynamics,* 32**:** 711-737.

Piotrowska, N., Blaauw, M., Mauquoy, D. and Chambers, F. (2011) Constructing deposition chronologies for peat deposits using radiocarbon dating. *Mires and Peat,* 7**:** 1-14.

Pirazzoli, P., Tomasin, A. and Ullmann, A. (2010) Recent changes in measured wind in the NE Atlantic and variability of correlation with NAO. *Annales Geophysicae,* 28**:** 1923-1934.

Pontevedra-Pombal, X., Nova Munoz, J., Garcia-Rodeja, A., Cortizas-Martinez, A., Marini, I., Marinez Cortiza, A., and Chesworth, W. (2006) Mountain mires from Galicia (NW Spain). In Martini, I, P. and Martinez Cortizas, A. (eds) *Peatlands evolution and records of environmental and climate changes*, Elsevier: 85-109.

Poore, R., Dowsett, H., Verardo, S. and Quinn, T. M. (2003) Millennial- to century- scale variability in Gulf of Mexico Holocene climate records. *Paleoceanography,* 18: 1048.

Poore, R., Quinn, T. and Verardo, S. (2004) Century-scale movement of the Atlantic Intertropical Convergence Zone linked to solar variability. *Geophysical Research Letters,* 31: L12214

Portis, D. H., Walsh, J. E., El Hamly, M. and Lamb, P. J. (2001) Seasonality of the North Atlantic Oscillation. *Journal of Climate,* 14**:** 2069-2078.

Press, W. H. and Rybicki, G. B. (1989) Fast algorithm for spectral analysis of unevenly sampled data. *The Astrophysical Journal,* 338**:** 277-280.

Proctor, C., Baker, A. and Barnes, W. (2002) A three thousand year record of North Atlantic climate. *Climate Dynamics,* 19**:** 449-454.

Proctor, C. J., Baker, A., Barnes, W. L. and Gilmour, M. A. (2000) A thousand year speleothem proxy record of North Atlantic climate from Scotland. *Climate Dynamics,* 16**:** 815-820.

Pye, K. (1990) Physical and human influences on coastal dune development between the Ribble and Mersey estuaries, northwest England.

Pye, K. and Neal, A. (1994) Coastal dune erosion at Formby Point, north Merseyside, England: causes and mechanisms. *Marine Geology,* 119**:** 39-56.

Raible, C., Yoshimori, M., Stocker, T. and Casty, C. (2007) Extreme midlatitude cyclones and their implications for precipitation and wind speed extremes in simulations of the Maunder Minimum versus present day conditions. *Climate Dynamics,* 28**:** 409-423.

Raible, C. C., Luksch, U., Fraedrich, K. and Voss, R. (2001) North Atlantic decadal regimes in a coupled GCM simulation. *Climate Dynamics,* 18**:** 321-330.

Ramsey, C. B. (2009) Bayesian analysis of radiocarbon dates. *Radiocarbon,* 51**:** 337-360.

Ramsey, C. B. and Lee, S. (2013) Recent and planned developments of the program OxCal. *Radiocarbon,* 55.

Reimer, P. J., Baillie, M. G. L., Bard, E., Bayliss, A., Beck, J. W., Blackwell, P. G., Ramsey, C. B., Buck, C. E., Burr, G. S., Edwards, R. L., Friedrich, M., Grootes, P. M., Guilderson, T. P., Hajdas, I., Heaton, T. J., Hogg, A. G., Hughen, K. A., Kaiser, K. F., Kromer, B., Mccormac, F. G., Manning, S. W., Reimer, R. W., Richards, D. A., Southon, J. R., Talamo, S., Turney, C. S. M., Van Der Plicht, J. and Weyhenmeyer, C. E. (2009) IntCal09 and Marine09 radiocarbon age calibration curves, 0-50,000 years cal BP. *Radiocarbon*, 51: 1111-1150.

Rimbu, N., Lohmann, G., Kim, J. H., Arz, H. W. and Schneider, R. (2003) Arctic/North Atlantic Oscillation signature in Holocene sea surface temperature trends as obtained from alkenone data. *Geophysical Research Letters,* 30: 1280.

Ritchie, J., C., Mchenry, J., R. and Gill, A., C. (1973) Dating recent reservoir sediments. *Limnology and Oceanography,* 18**:** 254-263.

Ritchie, W. (1966) The Post-Glacial Rise in Sea-Level and Coastal Changes in the Uists. *Transactions of the Institute of British Geographers***,** 39: 79-86.

Ritchie, W. (1985) Inter-tidal and sub-tidal organic deposits and sea level changes in the Uists, Outer Hebrides. *Scottish Journal of Geology,* 21**:** 161-176.

Ritchie, W. and Whittington, G. (1994) Non-synchronous aeolian sand movements in the Uists: The evidence of the intertidal organic and sand deposits at Cladach Mor, North Uist. *The Scottish Geographical Magazine,* 110**:** 40-46.

Robbins, J. A., Edgington, D. N. and Kemp, A. L. W. (1978) Comparative ^{210}Pb, ^{137}Cs, and pollen geochronologies of sediments from Lakes Ontario and Erie. *Quaternary Research,* 10**:** 256-278.

Robertson, A. W., Mechoso, C. R. and Kim, Y. J. (2000) The influence of Atlantic sea surface temperature anomalies on the North Atlantic oscillation. *Journal of Climate,* 13: 122-138.

Robinson, S. D. and Moore, T. R. (1999) Carbon and peat accumulation over the past 1200 years in a landscape with discontinuous permafrost, northwestern Canada. *Global Biogeochemical Cycles,* 13**:** 591-601.

Rodó, X., Baert, E. and Comín, F. A. (1997) Variations in seasonal rainfall in Southern Europe during the present century: relationships with the North Atlantic Oscillation and the El Niño-Southern Oscillation. *Climate Dynamics,* 13**:** 275-284.

Rodrigo, F. S., Pozo-Vazquez, D., Esteban-Parra, M. J. and Castro-Diez, Y. (2001) A reconstruction of the winter North Atlantic Oscillation index back to AD 1501 using, documentary data in southern Spain. *Journal of Geophysical Research-Atmospheres,* 106**:** 14805-14818.

Rodríguez-Ramírez, A., Ruiz, F., Cáceres, L. M., Rodríguez Vidal, J., Pino, R. and Muñoz, J. M. (2003) Analysis of the recent storm record in the southwestern Spanish coast: implications for littoral management. *The Science of The Total Environment,* 303**:** 189-201.

Rodwell, M. J., Rowell, D. P. and Folland, C. K. (1999) Oceanic forcing of the wintertime North Atlantic Oscillation and European climate. *Nature,* 398**:** 320-323.

Roeckner, E., Oberhuber, J.-M., Bacher, A., Christoph, M. and Kirchner, I. (1996) ENSO variability and atmospheric response in a global coupled atmosphere-ocean GCM. *Climate Dynamics,* 12**:** 737-754.

Rogers, J. C. (1984) The Association between the North Atlantic Oscillation and the Southern Oscillation in the Northern Hemisphere. *Monthly Weather Review,* 112**:** 1999-2015.

Rosenmeier, M. F., Brenner, M., Kenney, W. F., Whitmore, T. J. and Taylor, C. M. (2004) Recent eutrophication in the southern basin of Lake Petén Itzá, Guatemala: human impact on a large tropical lake. *Hydrobiologia,* 511**:** 161-172.

Rumney, G. R. (1968) Climatology and the World's Climates.

Sabatier, P., Dezileau, L., Briqueu, L., Colin, C. and Siani, G. (2010) Clay minerals and geochemistry record from northwest Mediterranean coastal lagoon sequence: Implications for paleostorm reconstruction. *Sedimentary Geology,* 228**:** 205-217.

Sabatier, P., Dezileau, L., Colin, C., Briqueu, L., Bouchette, F. D. R., Martinez, P., Siani, G., Raynal, O. and Von Grafenstein, U. (2012) 7000 years of paleostorm activity in the NW Mediterranean Sea in response to Holocene climate events. *Quaternary Research,* 77**:** 1-11.

Santos, J. O. A., Woollings, T. and Pinto, J. G. (2013) Are the Winters 2010 and 2012 Archetypes Exhibiting Extreme Opposite Behavior of the North Atlantic Jet Stream?*. *Monthly Weather Review,* 141**:** 3626-3640.

Santos, L., Bao, R. and Sanchez-Goni, M. S. N. (2001) Pollen record of the last 500 years from the Doninos coastal lagoon (NW Iberian Peninsula): Changes in the pollinic catchment size versus paleoecological interpretation. *Journal of Coastal Research***:** 705-713.

Santos, L., Romani, J. R. V. and Jalut, G. (2000) History of vegetation during the Holocene in the Courel and Queixa Sierras, Galicia, northwest Iberian Peninsula. *Journal of Quaternary Science,* 15**:** 621-632.

Scargle, J. D. (1982) Studies in astronomical time series analysis. II-Statistical aspects of spectral analysis of unevenly spaced data. *The Astrophysical Journal,* 263**:** 835-853.

Schellekens, J., Buurman, P., Fraga, I., and Martínez-Cortizas, A. (2011) Holocene vegetation and hydrologic changes inferred from molecular vegetation markers in peat, Penido Vello (Galicia, Spain). *Palaeogeography, Palaeoclimatology, Palaeoecology*, 299: 56-69.

Schimmelpfennig, I., Schaefer, J. M., Akçar, N., Ivy-Ochs, S., Finkel, R. C. and Schlüchter, C. (2012) Holocene glacier culminations in the Western Alps and their hemispheric relevance. *Geology,* 40**:** 891-894.

Schlesinger, M. E. and Ramankutty, N. (1994) An oscillation in the global climate system of period 65-70 years. *Nature,* 367**:** 723-726.

Schmith, T., Kaas, E. and Li, T. S. (1998) Northeast Atlantic winter storminess 1875–1995 re-analysed. *Climate Dynamics,* 14**:** 529-536.

Schmutz, C., Luterbacher, J., Gyalistras, D., Xoplaki, E. and Wanner, H. (2000) Can we trust proxy-based NAO index reconstructions? *Geophysical Research Letters,* 27**:** 1135-1138.

Schneider, U. and Schonwiese, C.-D. (1989) Some statistical characteristics of the El Nino/Southern Oscillation and North Atlantic Oscillation indices. *Atmosfera,* 2**:** 167-180.

Schulz, M. and Paul, A. (2002) Holocene climate variability on centennial-to-millennial time scales: 1. Climate records from the North-Atlantic realm. *Climate development and history of the North Atlantic realm.* Springer, Berlin: 41-54.

Schulz, M. and Stattegger, K. (1997) Spectrum: spectral analysis of unevenly spaced paleoclimatic time series. *Computers & Geosciences*, 23: 929-945.

Scussolini, P., Vegas-Vilarrúbia, T., Rull, V., Corella, J. P., Valero-Garcés, B. and Goma, J. (2011) Middle and late Holocene climate change and human impact inferred from diatoms, algae and aquatic macrophyte pollen in sediments from Lake Montcortés (NE Iberian Peninsula). *Journal of Paleolimnology,* 46**:** 369-385.

Seager, R., Kushnir, Y., Visbeck, M., Naik, N., Miller, J., Krahmann, G. and Cullen, H. (2000) Causes of Atlantic Ocean Climate Variability between 1958 and 1998. *Journal of Climate,* 13**:** 2845-2862.

SEPA (2011) *The National Flood Risk Assessment.* Scottish Environment Protection Agency, Stirling.

Serreze, M. C., Carse, F., Barry, R. G. and Rogers, J. C. (1997) Icelandic low cyclone activity: Climatological features, linkages with the NAG, and relationships with recent changes in the Northern Hemisphere circulation. *Journal of Climate,* 10**:** 453-464.

Sharples, N. and Pearson, M. P. (1999) Norse settlement in the Outer Hebrides. *Norwegian archaeological review,* 32**:** 41-62.

Shindell, D. T., Schmidt, G. A., Mann, M. E., Rind, D. and Waple, A. (2001) Solar forcing of regional climate change during the maunder minimum. *Science,* 294**:** 2149-2152.

Shindell, D. T., Schmidt, G. A., Miller, R. L. and Mann, M. E. (2003) Volcanic and solar forcing of climate change during the preindustrial era. *Journal of Climate,* 16**:** 4094-4107.

Shoelson, B. (2001) lombscargle.m. *MATLAB Central File Exchange.* Accessed 06/07/2014 <http://www.mathworks.co.uk/matlabcentral/fileexchange/993-lombscargle-m>

Shulmeister, J., Goodwin, I., Renwick, J., Harle, K., Armand, L., Mcglone, M., Cook, E., Dodson, J., Hesse, P. and Mayewski, P. (2004) The Southern Hemisphere westerlies in the Australasian sector over the last glacial cycle: a synthesis. *Quaternary International,* 118**:** 23-53.

Silliman, J. E., Meyers, P. A. and Bourbonniere, R. A. (1996) Record of postglacial organic matter delivery and burial in sediments of Lake Ontario. *Organic Geochemistry,* 24**:** 463-472.

Slingo, J., Belcher, S., Scaife, A., Mccarthy, M., Saulter, A., Mcbeath, K., Jenkins, A., Huntingford, C., Marsh, T. and Hannaford, J. (2014) *The recent storms and floods in the UK*. Met Office report. Accessed 25/06/14 <http://www.metoffice.gov.uk/media/pdf/n/i/Recent_Storms_Briefing_Final_07023.pdf>

Smith, D. and Fettes, D. (1979) The geological framework of the Outer Hebrides. *Proceedings of the Royal Society of Edinburgh. Section B. Biological Sciences,* 77**:** 75-83.

Snowball, I., Sandgren, P. and Petterson, G. (1999) The mineral magnetic properties of an annually laminated Holocene lake-sediment sequence in northern Sweden. *The Holocene,* 9**:** 353-362.

Sobrino, C. M., Ramil-Rego, P., Gómez-Orellana, L. and Varela, R. A. D. (2005) Palynological data on major Holocene climatic events in NW Iberia. *Boreas,* 34**:** 381-400.

Sommerville, A., Hansom, J., Housley, R. and Sanderson, D. (2007) Optically stimulated luminescence (OSL) dating of coastal aeolian sand accumulation in Sanday, Orkney Islands, Scotland. *The Holocene,* 17**:** 627-637.

Sommerville, A. A., Hansom, J. D., Sanderson, D. C. W. and Housley, R. A. (2003) Optically stimulated luminescence dating of large storm events in Northern Scotland. *Quaternary Science Reviews,* 22**:** 1085-1092.

Sorrel, P., Debret, M., Billeaud, I., Jaccard, S., Mcmanus, J. and Tessier, B. (2012) Persistent non-solar forcing of Holocene storm dynamics in coastal sedimentary archives. *Nature Geoscience,* 5**:** 892-896.

Sorrel, P., Tessier, B., Demory, F., Delsinne, N. and Mouazé, D. (2009) Evidence for millennial-scale climatic events in the sedimentary infilling of a macrotidal estuarine system, the Seine estuary (NW France). *Quaternary Science Reviews,* 28**:** 499-516.

Stabel, H. (1986) Calcite precipitation in Lake Constance: Chemical equilibrium sedimentation, and nucleation by algae. *Limnology and Oceanography,* 31**:** 1081-1093.

Stefanini, B. S. Oksanen, P. O. Corcoran, J. P. and Mitchell, F. G. J. (in prep.) Wiggle match dated multi proxy peat record tests cohesion of palaeoenvironmental reconstructions in north-west Spain; implications for ocean atmosphere linkages since the mid-Holocene.

Steinhilber, F., Abreu, J. A., Beer, J. R., Brunner, I., Christl, M., Fischer, H., Heikkilä, U., Kubik, P. W., Mann, M. and Mccracken, K. G. (2012) 9,400 years of cosmic radiation and solar activity from ice cores and tree rings. *Proceedings of the National Academy of Sciences,* 109**:** 5967-5971.

Stenchikov, G., Hamilton, K., Stouffer, R. J., Robock, A., Ramaswamy, V., Santer, B. and Graf, H. F. (2006) Arctic Oscillation response to volcanic eruptions in the IPCC AR4 climate models. *Journal of Geophysical Research: Atmospheres (1984-2012),* 111.

Stocker, T. F., Qin, D., Plattner, G.-K., Tignor, M., Allen, S. K., Boschung, J., Nauels, A., Xia, Y., Bex, V. and Midgley, P. M. (2013) Climate change 2013: The physical science basis. *Intergovernmental Panel on Climate Change, Working Group I Contribution to the IPCC Fifth Assessment Report (AR5),* Cambridge University Press, New York.

Stockmarr, J. (1971) Tablets with spores used in absolute pollen analysis. *Pollen et spores*.

Stuiver, M. and Braziunas, T. F. (1989) Atmospheric ^{14}C and century-scale solar oscillations. *Nature,* 338: 405-408.

Stuiver, M. and Braziunas, T. F. (1993) Sun, ocean, climate and atmospheric 14CO2: an evaluation of causal and spectral relationships. *The Holocene,* 3**:** 289-305.

Stuiver, M., Grootes, P. M. and Braziunas, T. F. (1995) The GISP2 $\delta^{18}O$ Climate Record of the Past 16,500 Years and the Role of the Sun, Ocean, and Volcanoes. *Quaternary Research,* 44**:** 341-354.

Taws, S. L., Marsh, R., Wells, N. C. and Hirschi, J. L. (2011) Re-emerging ocean temperature anomalies in late 2010 associated with a repeat negative NAO. *Geophysical Research Letters,* 38: L20601.

Telford, R., Heegaard, E. and Birks, H. (2004) All age-depth models are wrong: but how badly? *Quaternary Science Reviews,* 23**:** 1-5.

Thompson, D. W. J. and Wallace, J. M. (2000) Annular modes in the extratropical circulation. Part 1: month-to-month variability. *Journal of Climate,* 13**:** 1000-1016.

Thornalley, D. J., Elderfield, H. and Mccave, I. N. (2009) Holocene oscillations in temperature and salinity of the surface subpolar North Atlantic. *Nature,* 457**:** 711-714.

Thorndycraft, V. and Benito, G. (2006) The Holocene fluvial chronology of Spain: evidence from a newly compiled radiocarbon database. *Quaternary Science Reviews,* 25**:** 223-234.

Tisdall, E. W., Mcculloch, R. D., Sanderson, D. C. W., Simpson, I. A. and Woodward, N. L. (2013) Living with sand: A record of landscape change

and storminess during the Bronze and Iron Ages Orkney, Scotland. *Quaternary International*. 308-309: 205-215.

Torrence, C. and Compo, G. P. (1998) A practical guide to wavelet analysis. *Bulletin of the American Meteorological Society,* 79**:** 61-78. Software downloaded from: <http://paos.colorado.edu/research/wavelets>

Trauth, M. H. (2006) *MATLAB Recipes for Earth Sciences,* Berlin, Springer.

Trigo, I. (2006) Climatology and interannual variability of storm-tracks in the Euro-Atlantic sector: a comparison between ERA-40 and NCEP/NCAR reanalyses. *Climate Dynamics,* 26**:** 127-143.

Trigo, R. M., Osborn, T. J. and Corte-Real, J. O. M. (2002) The North Atlantic Oscillation influence on Europe: climate impacts and associated physical mechanisms. *Climate Research,* 20**,** 9-17.

Trigo, R. M., Pozo-Vázquez, D., Osborn, T. J., Castro-Díez, Y., Gámiz-Fortis, S. and Esteban-Parra, M. A. J. (2004) North Atlantic Oscillation influence on precipitation, river flow and water resources in the Iberian Peninsula. *International Journal of Climatology,* 24**:** 925-944.

Trouet, V., Esper, J., Graham, N. E., Baker, A., Scourse, J. D. and Frank, D. C. (2009) Persistent Positive North Atlantic Oscillation Mode Dominated the Medieval Climate Anomaly. *Science,* 324**:** 78-80.

Trouet, V., Scourse, J. D. and Raible, C. C. (2012) North Atlantic storminess and Atlantic Meridional Overturning Circulation during the last Millennium: Reconciling contradictory proxy records of NAO variability. *Global and Planetary Change,* 84-85**:** 48-55.

Turney, C., Baillie, M., Clemens, S., Brown, D., Palmer, J., Pilcher, J., Reimer, P. and Leuschner, H. H. (2005) Testing solar forcing of pervasive Holocene climate cycles. *Journal of Quaternary Science,* 20**:** 511-518.

Tyler, A. N., Carter, S., Davidson, D. A., Long, D. J. and Tipping, R. (2001) The extent and significance of bioturbation on ^{137}Cs distributions in upland soils. *CATENA,* 43**:** 81-99.

Valdes, P. (2011) Built for stability. *Nature Geoscience,* 4**:** 414-416.

Van Geel, B., Raspopov, O., Renssen, H., Van Der Plicht, J., Dergachev, V. and Meijer, H. (1999) The role of solar forcing upon climate change. *Quaternary Science Reviews,* 18**:** 331-338.

Van Loon, H. and Rogers, J. C. (1978) The Seesaw in Winter Temperatures between Greenland and Northern Europe. Part I: General Description. *Monthly Weather Review,* 106**:** 296-310.

Van Vliet-Lanoë, B., Penaud, A. L., Hénaff, A., Delacourt, C., Fernane, A., Goslin, J. R. M., Hallégouët, B. and Le Cornec, E. (2014) Middle-to late-Holocene storminess in Brittany (NW France): Part II-The chronology of events and climate forcing. *The Holocene,* 24**:** 434-453.

Vautard, R. (1990) Multiple weather regimes over the North Atlantic: analysis of precursors and successors. *Monthly Weather Review,* 118**:** 2056-2081.

Veretenenko, S. V. and Ogurtsov, M. G. (2012) Stratospheric circumpolar vortex as a link between solar activity and circulation of the lower atmosphere. *Geomagnetism and Aeronomy,* 52**:** 937-943.

Vespremeanu-Stroe, A., Constantinescu, S., Tatui, F. and Giosan, L. (2007) Multi-decadal evolution and North Atlantic Oscillation influences on the dynamics of the Danube delta shoreline. *Journal of Coastal Research,* Special Issue 50**:** 157-162.

Vicente-Serrano, S. M., Trigo, R. M., Lopez-Moreno, J., Liberato, M., Lorenzo-Lacruz, J., Begueria, S., Moran-Tejeda, E. and El Kenawy, A. (2011) Extreme winter precipitation in the Iberian Peninsula in 2010: anomalies, driving mechanisms and future projections. *Climate Research,* 46**:** 51-65.

Vis, G. J., Bohncke, S. J., Schneider, H., Kasse, C., Coenraads-Nederveen, S., Zuurbier, K. and Rozema, J. (2010) Holocene flooding history of the lower Tagus valley (Portugal). *Journal of Quaternary Science,* 25**:** 1222-1238.

Visbeck, M. H., Hurrell, J. W., Polvani, L. and Cullen, H. M. (2001) The North Atlantic Oscillation: Past, present, and future. *Proceedings of the National Academy of Sciences of the United States of America,* 98**:** 12876-12877.

Von Storch, H., Zorita, E., Jones, J. M., Dimitriev, Y., González-Rouco, F. and Tett, S. F. (2004) Reconstructing past climate from noisy data. *Science,* 306**:** 679-682.

Vonmoos, M., Beer, J. R. and Muscheler, R. (2006) Large variations in Holocene solar activity: Constraints from 10Be in the Greenland Ice Core Project ice core. *Journal of Geophysical Research: Space Physics (1978-2012),* 111: A10105.

Walker, G. T. and Bliss, E. (1932) World weather. *V. Mem. Roy. Meteor. Soc.,* 4**:** 53-84.

Walker, M. J. C. (1984) A pollen diagram from St Kilda, Outer Hebrides, Scotland *New Phytologist,* 97**:** 99-113.

Walter, K. and Graf, H.-F. (2005) The North Atlantic variability structure, storm tracks, and precipitation depending on the polar vortex strength. *Atmospheric Chemistry and Physics,* 5**:** 239-248.

Wang, X., Zwiers, F. W., Swail, V., Feng, Y. and Wan, H. (2009) Trends and variability of storminess in the NE Atlantic-European Region during 1874-2007 and their relationship to the North Atlantic Oscillation. *EGU General Assembly 2009.19-24 April 2009.* Geophysical Research Abstracts.

Wanner, H., Beer, J. R., Bütikofer, J., Crowley, T. J., Cubasch, U., Flückiger, J., Goosse, H., Grosjean, M., Joos, F., Kaplan, J. O., Küttel, M., Müller, S. A., Prentice, I. C., Solomina, O., Stocker, T. F., Tarasov, P., Wagner, M. and Widmann, M. (2008) Mid- to Late Holocene climate change: an overview. *Quaternary Science Reviews,* 27**:** 1791-1828.

Wanner, H., Brönnimann, S., Casty, C., Gyalistras, D., Luterbacher, J. R., Schmutz, C., Stephenson, D. and Xoplaki, E. (2001) North Atlantic Oscillation - Concepts And Studies. *Surveys in Geophysics,* 22**:** 321-381.

Wanner, H., Solomina, O., Grosjean, M., Ritz, S. P. and Jetel, M. T. (2011) Structure and origin of Holocene cold events. *Quaternary Science Reviews,* 30: 3109-3123.

WASA_Group (1998) Changing waves and storms in the Northeast Atlantic? *Bulletin of the American Meteorological Society,* 79**:** 741-760.

Wasson, R. J. and Nanninga, P. M. (1986) Estimating wind transport of sand on vegetated surfaces. *Earth Surface Processes and Landforms,* 11**:** 505-514.

Weaver, B. L. and Tarney, J. (1981) Lewisian gneiss geochemistry and Archaean crustal development models. *Earth and Planetary Science Letters,* 55**:** 171-180.

Wei, W. and Lohmann, G. (2012) Simulated Atlantic Multidecadal Oscillation during the Holocene. *Journal of Climate,* 25**:** 6989-7002.

Welch, P. D. (1967) The use of fast Fourier transform for the estimation of power spectra: A method based on time averaging over short, modified periodograms. *Audio and Electroacoustics, IEEE Transactions on,* 15**:** 70-73.

Weltje, G. J. and Tjallingii, R. (2008) Calibration of XRF core scanners for quantitative geochemical logging of sediment cores: Theory and application. *Earth and Planetary Science Letters,* 274**:** 423-438.

Wetzel, R. (1975) *Limnology*, Saunders, Philadelphia: 743.

Wheeler, D., Garcia-Herrera, R., Wilkinson, C. W. and Ward, C. (2010) Atmospheric circulation and storminess derived from Royal Navy logbooks: 1685 to 1750. *Climatic Change,* 101**:** 257-280.

White, D. S. and Miller, M. F. (2008) Benthic invertebrate activity in lakes: linking present and historical bioturbation patterns. *Aquatic Biology,* 2**:** 269-277.

Williams, D. M. and Hall, A. M. (2004) Cliff-top megaclast deposits of Ireland, a record of extreme waves in the North Atlantic - storms or tsunamis? *Marine Geology,* 206**:** 101-117.

Wilson, P. (2002) Holocene coastal dune development on the South Erradale peninsula, Wester Ross, Scotland. *Scottish Journal of Geology,* 38**:** 5-13.

Wilson, P., Mcgourty, J. and Bateman, M. D. (2004) Mid-to late-Holocene coastal dune event stratigraphy for the north coast of Northern Ireland. *The Holocene,* 14**:** 406-416.

Wirth, S. B., Glur, L., Gilli, A. and Anselmetti, F. S. (2013) Holocene flood frequency across the Central Alps - solar forcing and evidence for variations in North Atlantic atmospheric circulation. *Quaternary Science Reviews,* 80**:** 112-128.

Witak, M., Wachnicka, A., Kuijpers, A., Troelstra, S., Prins, M. A. and Witkowski, A. (2005) Holocene North Atlantic surface circulation and climatic variability: evidence from diatom records. *The Holocene,* 15**:** 85-96.

Wolf, J. (2007) Modelling of Waves and Set-up for the Storm of 11-12 January 2005. Liverpool, UK., Proudman Oceanographic Institute. (Proudman Oceanographic Laboratory, Report No. 181)

Wolff, J.-O., Maier-Reimer, E. and Legutke, S. (1997) The Hamburg ocean primitive equation model. *DKRZ technical report.*

Wolman, M. G. and Miller, J. P. (1960) Magnitude and frequency of forces in geomorphic processes. *The Journal of Geology***,** 68: 54-74.

Woollings, T., Gregory, J. M., Pinto, J. G., Reyers, M. and Brayshaw, D. J. (2012) Response of the North Atlantic storm track to climate change shaped by ocean-atmosphere coupling. *Nature Geoscience,* 5**:** 313-317.

Woollings, T., Hannachi, A., Hoskins, B. and Turner, A. (2010) A Regime View of the North Atlantic Oscillation and Its Response to Anthropogenic Forcing. *Journal of Climate,* 23**:** 1291-1307.

Yancheva, G., Nowaczyk, N. R., Mingram, J., Dulski, P., Schettler, G., Negendank, J. F. W., Liu, J., Sigman, D. M., Peterson, L. C. and Haug, G. H. (2007) Influence of the intertropical convergence zone on the East Asian monsoon. *Nature,* 445**:** 74-77.

Yiou, P. and Nogaj, M. (2004) Extreme climatic events and weather regimes over the North Atlantic: When and where? *Geophysical Research Letters,* 31: L07202.

Yu, K.-F., Zhao, J.-X., Shi, Q. and Meng, Q.-S. (2009) Reconstruction of storm/tsunami records over the last 4000 years using transported coral blocks and lagoon sediments in the southern South China Sea. *Quaternary International,* 195**:** 128-137.

Yu, Z., Campbell, I. D., Campbell, C., Vitt, D. H., Bond, G. C. and Apps, M. J. (2003) Carbon sequestration in western Canadian peat highly sensitive

to Holocene wet-dry climate cycles at millennial timescales. *The Holocene,* 13**:** 801-808.

Zaccone, C., Miano, T. and Shotyk, W. (2012) Interpreting the ash trend within ombrotrophic bog profiles: atmospheric dust depositions vs. mineralization processes. The Etang de la Gruère case study. *Plant and soil,* 353**:** 1-9.

Zezere, J. L., Trigo, R. M., Fragoso, M., Oliveira, S., C. and Garcia, R. (2008) Rainfall-triggered landslides in the Lisbon region over 2006 and relationships with the North Atlantic Oscillation. *Natural Hazards and Earth System Sciences,* 8**:** 483-499.

Zhou, S., Miller, A. J., Wang, J. and Angell, J. K. (2002) Downward-Propagating Temperature Anomalies in the Preconditioned Polar Stratosphere. *Journal of Climate,* 15**:** 781-792.

Zielinski, G., A. and Mershon, G., R. (1997) Paleoenvironmental implications of the insoluble microparticle record in the GISP2 (Greenland) ice core during the rapidly changing climate of the Pleistocene-Holocene transition. *Geological Society of America Bulletin,* 109**:** 547-559.

Zielinski, G. A., Fiacco, R., J, Mayewski, P., A, Meeker, L., D, Whitlow, S., I, Twickler, M., S, Germani, M., S, Endo, K. and Yasui, M. (1994) Climatic impact of the A.D. 1783 Asama (Japan) eruption was minimal: Evidence from the GISP2 ice core. *Geophysical Research Letters,* 21**:** 2365-2368.